

**INTEGRIN DYNAMICS AND PLATELET
MECHANOSENSING VIA SURFACE
RECEPTORS GPIb α AND INTEGRIN $\alpha_{IIb}\beta_3$**

A Dissertation
Presented to
The Academic Faculty

by

YUNFENG CHEN

In Partial Fulfillment
of the Requirements for the Degree
Doctor of Philosophy in the
Bioengineering Interdisciplinary Graduate Program
Department of Mechanical Engineering

Georgia Institute of Technology
August 2016

COPYRIGHT ©YUNFENG CHEN 2016

**INTEGRIN DYNAMICS AND PLATELET
MECHANOSENSING VIA SURFACE
RECEPTORS GPIIb α AND INTEGRIN $\alpha_{IIb}\beta_3$**

Approved by:

Dr. Cheng Zhu, Advisor

Wallace H. Coulter Department of

Biomedical Engineering

Georgia Institute of Technology

Emory University School of Medicine

Dr. Xiaoping Du

Department of Pharmacology

University of Illinois at Chicago

Dr. Renhao Li

Department of Pediatrics

Emory University School of Medicine

Dr. Larry V. McIntire

Wallace H. Coulter Department of

Biomedical Engineering

Georgia Institute of Technology

Emory University School of Medicine

Dr. Wilbur Lam

Wallace H. Coulter Department of

Biomedical Engineering

Georgia Institute of Technology

Date Approved: May 23rd, 2015

To my dearest family

I dedicate this thesis

to

My parents

陈晓明 (Xiaoming Chen) and 常晓岚 (Xiaolan Chang). I would not have been able to finish my Ph.D. career without your love, endless patience and steadiest supports.

My Fiancée

王蕾 (Lei Wang). You are the love of my life, and I am grateful to have you on my side, supporting and encouraging me and cheering me up through all the past six years of my Ph.D.

ACKNOWLEDGEMENTS

I wish to express my deepest gratitude to people who have given me support and guidance throughout my Ph.D. career. Without you all, I will never succeed in accomplishing my works.

I would first like to thank my advisor Dr. Cheng Zhu for creating a supportive and liberal research environment, allowing me to find my own path by “messing up things” a little bit. I look up to your rigorous attitude towards research, and your knowledge, wisdom and patience in guiding lost students. I understand that educating a student for six years is a huge and difficult project, and I really appreciate that you have put such a lot of effort, attention and time on me.

I would like to thank Dr. Lining Ju (Georgia Tech alumni, now affiliated to Heart Research Institute, Sydney, Australia), who acted as my Ph.D. mentor, my good buddy and my golden partner who built the BFP system (Chapter 2.6), provided valuable guidance on the design of the temperature controller (Chapter 2.10), equally contributed to the study of platelet GPIb mechanosensing (Chapter 4), worked together with me on the switch BFP assay (Chapter 2.9), and applied it to the study of platelet integrin intermediate state study (Chapter 5). He also facilitated the collaboration with Dr. Shaun Jackson lab (Heart Research Institute, Sydney, Australia) and hosted my visit to Jackson lab in 2016.

I want to express my appreciation to all the support from my committee members, Drs. Larry McIntire, Xiaoping Du, Renhao Li and Wilbur Lam. You have been

extremely kind and generous in helping me out and giving me guidance. Dr. Du have been generously providing reagents and coming up with great scientific ideas that prompted the projects to in depth. Dr. Lam and his lab members Dr. David Myer, Dr. Yongzhi Qiu, Yumiko Sakurai, Reginald Tran, Jordan Ciciliano and more are really kind to help me out by providing blood draw services for more than four years, for which I owe them a lot.

I want to thank all the contributions from my collaborators beside my committee members. Fangyuan Zhou (Georgia Tech), my good friend and my pal in platelet studies, who supported some of my projects with her expertise, and helped me make devices. Drs. Tanya Mayadas and Florencia Rosetti (Harvard Medical School), my collaborators in the study of lupus and MAC-1 (Chapter 7). Dr. Martin Schwartz (Yale University) and Dr. Hyun-jung Lee (Georgia Tech), who make valuable contributions to my integrin bending/unbending projects (Chapter 3). Dr. Jack Wei Chen, who pioneered the bending/unbending analysis of integrins (Chapter 3) and provided valuable advice on the manufacture of the temperature controller (Chapter 2.10). Dr. Lingzhou Xue, who supported the project of platelet GPIb mechanosensing with beautiful statistical analysis (Chapter 4). Dr. Vincent Fiore, who led the work of integrin $\alpha_5\beta_1$ tri-molecular catch-bond, and helped me on cells transfection. I would like to specially thank Dr. Peter Hinterdorfer (Johannes Kepler University Linz, Austria) and Dr. Shaun Jackson (Heart Research Institute, Sydney, Australia) and their lab members, who hosted my visit to their labs in 2014 and 2016 respectively, and offered me warm welcome and tremendous help in acquiring experimental data

and learning techniques and skills. Dr. Jackson's lab also helped me with precious reagents and guidance on optimizing the platelet isolation procedures, for which I would like to especially express my appreciation to Dr. Simone Schoenwaelder and Dr. Roxane Darbousset.

In addition, I want to thank Dr. Zaverio Ruggeri, Dr. Miguel Cruz, Dr. Barry Coller, Dr. Peter Newman, Dr. Jing-fei Dong and Dr. Heyu Ni for their timely support and joining in with reagents and ideas, enabling the projects to be carried out.

Sincere thanks to my lab colleagues, Dr. Baoyu Liu (alumni), Dr. Zhenhai Li (alumni), Kaitao Li, Prithiviraj Jothikumar, Billy Rittase and Chenghao Ge, for your helpful discussions and support.

TABLE OF CONTENTS

ACKNOWLEDGEMENTS	III
LIST OF TABLES	XII
LIST OF FIGURES	XIII
LIST OF ABBREVIATIONS	XVIII
SUMMARY	XX
CHAPTER 1: INTRODUCTION.....	1
1.1 Specific aims	1
1.2 Background and significance	6
1.2.1 Hemostasis and thrombosis	6
1.2.2 Platelets in shear-dependent hemostasis.....	7
1.2.3 GPIb α -IX-V and VWF	8
1.2.4 Integrin $\alpha_{IIb}\beta_3$ and its ligands.....	11
1.2.5 Integrin affinity and conformational changes.....	15
1.2.6 Platelet activation	17
1.2.7 Platelet mechano-signaling.....	19
1.2.8 Significance	22
CHAPTER 2: MATERIALS AND METHODS	23
2.1 Proteins and reagents.....	23

2.2 Functionalization of beads	26
2.3 Red blood cells	26
2.4 Platelets	26
2.5 Hybridoma cell lines	27
2.6 BFP experiments	27
2.6.1 System setup	27
2.6.2 Force spectroscopy assays and data analysis.....	30
2.6.2.1 Force-ramp assay	30
2.6.2.2 Force/distance clamp assay	31
2.6.2.3 Thermal fluctuation assay	32
2.6.2.4 Spring constant measurements.....	32
2.6.2.5 Fitting adhesion frequency to derive average number of bonds	34
2.6.2.6 Calculation of average effective affinity.....	35
2.6.2.7 Lifetime multi-state analysis.....	35
2.7 Measurement of molecular site density.....	36
2.8 Fluorescence BFP experiment.....	37
2.9 Switch BFP assay	37
2.10 Temperature controlling system for BFP	39
2.11 Statistical testing	41

CHAPTER 3: CHARACTERIZATION AND REGULATION OF INTEGRIN

AFFINITY AND CONFORMATIONAL STATES 43

3.1 Introduction	43
------------------------	----

3.2 Results	44
3.2.1 Integrin $\alpha_V\beta_3$ binding kinetics and bending/unbending conformational changes – a purified system study	44
3.2.1.1 $\alpha_V\beta_3$ –fibronectin binding forms a catch-bond in Mn^{2+} which is suppressed in Ca^{2+}/Mg^{2+}	44
3.2.1.2 Observing $\alpha_V\beta_3$ bending/unbending conformational change with BFP in a purified system.....	47
3.2.1.3 Mn^{2+} cation condition favors the extended conformation of $\alpha_V\beta_3$ while Ca^{2+}/Mg^{2+} favors the bent conformation.....	50
3.2.1.4 Bending/unbending conformational change of $\alpha_V\beta_3$ shortens/prolongs its lifetime in Mn^{2+} but has no effect in Ca^{2+}/Mg^{2+}	56
3.2.2 Observing ligand binding and bending/unbending conformational changes of cell surface integrin $\alpha_V\beta_3$ regulated by mutations, force and ligands.....	57
3.2.2.1 Force dependency of cell surface $\alpha_V\beta_3$ ligand binding and its regulation by functional mutations	57
3.2.2.2 Observation of integrin $\alpha_V\beta_3$ bending/unbending conformational change on cell surface and its regulation by functional mutations	61
3.2.2.3 Kinetics of integrin conformational changes and their regulation by force and mutations.....	64
3.2.2.4 Lack of effect of $\alpha_V\beta_3$ bent/extended conformation or bending/unbending on its ligand dissociation rate under force	67

3.2.2.5 Observation of fibrinogen-bound integrin $\alpha_V\beta_3$ bending/unbending conformational change.....	70
3.2.3 Observation of integrin $\alpha_V\beta_3$ bending/unbending conformational change by High-Speed Atomic Force Microscopy (HS-AFM).....	73
3.3 Discussion	76

CHAPTER 4: CHARACTERIZING GPIB-ALPHA-INITIATED PLATELET

MECHANOSENSING IN SINGLE MOLECULAR LEVEL 83

4.1 Introduction	83
4.2 Results	84
4.2.1 Fluorescence BFP setup for studying GPIb α -mediated Ca ²⁺ signaling	84
4.2.2 Identification of GPIb α -mediated Ca ²⁺ signaling types	85
4.2.3 The necessity of durable bonds in GPIb α -mediated mechanotransduction	87
4.2.4 A single durable bond mediating mechanism of GPIb α mechanotransduction.....	89
4.2.5 Cooperative unfolding of lucine-rich repeat domain (LRRD) and mechano-sensitive domain (MSD).....	90
4.2.6 Model for cooperativity between LRRD and MSD unfolding.....	94
4.2.7 LRRD unfolding strengthens signaling by prolonging the lifetime while MSD unfolding is key to determining Ca ²⁺ type.....	102
4.2.8 Perturbing cytoplasmic association of GPIb α with 14-3-3 ζ inhibits mechanoreception.....	104
4.3 Discussion	106

CHAPTER 5: GPIB-ALPHA MECHANOTRANSDUCTION PRIMES	
PLATELETS INTO AN INTERMEDIATE ACTIVATION STATE	110
5.1 Introduction	110
5.2 Results	112
5.2.1 Bidirectional signals drive multi-state transition of integrin $\alpha_{IIb}\beta_3$ on platelets.....	112
5.2.1.1 Single durable adhesion through GPIb α triggers platelet integrin up-regulation	112
5.2.1.2 GPIb α mechanotransduction primed platelet $\alpha_{IIb}\beta_3$ into an intermediate state	116
5.2.1.3 Progression and recession of the intermediate state	120
5.2.1.4 Identification of three bond dissociating states.....	122
5.2.1.5 Signaling pathway and integrin conformation of the intermediate and active states	127
5.2.1.6 Synergy of chemical inside-out and mechanical outside-in signaling realize a fourth, hyperactive state	133
5.2.2 GPIb α -triggered signal primes low-level P-selectin expression on platelet surface.....	135
5.2.3 GPIb α -triggered signal primes PS exposure in platelet outer membrane layer	137
5.3 Discussion	138
CHAPTER 6: CONCLUSIONS	147

6.1 Summary	147
6.2 Future Works	153
6.2.1 Type I Diabetes – a preliminary study in platelet biomechanical thrombosis	154
6.2.2 Type II Diabetes – a preliminary study in platelet biomechanical thrombosis	156
6.2.3 Summary	156
CHAPTER 7: MISCELLANEOUS PROJECTS.....	158
REFERENCES.....	160
VITA.....	185

LIST OF FIGURES

Chapter 1

Figure 1-1. A model of platelet adhesion cascade in blood flow.....	9
Figure 1-2. GPIb-V-IX complex and VWF.....	12
Figure 1-3. Structures of β_3 and β_1 integrins, fibrinogen and fibronectin.....	14
Figure 1-4. Sketches of the three global conformational changes that integrins may undergo	15
Figure 1-5. A map of platelet activation pathways	18

Chapter 2

Figure 2-1. BFP experiment setup	28
Figure 2-2. Introduction of BFP experiment	29
Figure 2-3. Illustration of the spring constant calculation and an exemplary BFP signature of the retraction phase.....	34
Figure 2-4. Switch BFP demonstration using platelet GPIb α and integrin α IIb β 3 inter-talk as an example.....	38
Figure 2-5. Electric circuit design sketch of the temperature controlling system	40

Chapter 3

Figure 3-1. BFP setup for studying recombinant $\alpha_V\beta_3$, specificity test results, and lifetime vs. force results of $\alpha_V\beta_3$ binding	45
--	----

Figure 3-2. BFP signatures of recombinant $\alpha_V\beta_3$ unbending and bending conformational changes in the clamping phase of a BFP signal.....	46
Figure 3-3. “Clamping force vs. displacement” of recombinant $\alpha_V\beta_3$ unbending and bending	48
Figure 3-4. Determining the molecular complex stiffness with a bent/extended integrin and the initial fractions of integrin populations in bent and extended conformations in Mn^{2+} and Ca^{2+}/Mg^{2+}	49
Figure 3-5. Recombinant integrin bending and unbending switching time $t_{sw\pm}$ and time-to-switch $t_{0\pm}$	54
Figure 3-6. Recombinant integrin post-bending and -unbending lifetime.....	56
Figure 3-7. BFP setup and binding kinetics results of cell surface $\alpha_V\beta_3$ binding to $FN_{III7-10}$	59
Figure 3-8. Characterization of the cell surface $\alpha_V\beta_3$ bending and unbending events	60
Figure 3-9. Determining the initial fractions of cell surface integrin subpopulations in bent and extended conformations	61
Figure 3-10. Analyzing the dynamics of the cell surface integrin conformational changes	68
Figure 3-11. Lack of effect of cell surface $\alpha_V\beta_3$ bending/unbending on its ligand dissociation rate under force	69

Figure 3-12. Observing bending/unbending conformational changes of fibrinogen-bound WT $\alpha_V\beta_3$ on cell surface.....	72
Figure 3-13. Imaging recombinant $\alpha_V\beta_3$ in bent and extended conformations using a HS-AFM.....	74
Figure 3-14. Imaging recombinant $\alpha_V\beta_3$ bending/unbending conformational changes using a HS-AFM	75
Figure 3-15. Integrin bistability model.....	81

Chapter 4

Figure 4-1. BFP analysis of ligand binding kinetics.....	85
Figure 4-2. Concurrent analysis of single-platelet Ca^{2+} flux and GPIb-mediated single-bond binding at 25 pN clamped force.....	86
Figure 4-3. Robust platelet Ca^{2+} signal requires sustained bonding on GPIb α	88
Figure 4-4. Quantitative correlation of GPIb α lifetime and platelet Ca^{2+} signaling.	90
Figure 4-5. Force regulated and ligand-dependent cooperative unfolding of GPIb α LRRD and MSD	92
Figure 4-6. LRRD unfolding prolongs VWF–GPIb α bond lifetime and facilitates MSD clamped unfolding	100
Figure 4-7. Correlation between GPIb α domain unfolding and Ca^{2+} triggering at 25 pN clamped force	103

Figure 4-8. The effect of 14-3-3 ζ blockade to platelet Ca ²⁺ signaling and a proposed model.....	104
Figure 4-9. Model of GPIb-mediated platelet mechanotransduction	107

Chapter 5

Figure 5-1. Identification of β_3 integrin up-regulation following GPIb α mechanotransduction	114
Figure 5-2. Characterization of platelet binding kinetics against FN _{III7-10} and fibrinogen	117
Figure 5-3. Platelet–FN and –Fg adhesion frequency after different treatments....	119
Figure 5-4. Progression and recession of intermediate state	121
Figure 5-5. Characterization and three-state model of $\alpha_{IIb}\beta_3$ -ligand bond dissociation under forces	125
Figure 5-6. Semi-log survival frequency vs. lifetime of platelet $\alpha_{IIb}\beta_3$ binding to FN _{III7-10} and fibrinogen under different forces	126
Figure 5-7. $\alpha_{IIb}\beta_3$ inside-out signaling pathway and conformational changes following up-regulation	130
Figure 5-8. $\alpha_{IIb}\beta_3$ outside-in mechanical signaling following ADP activation	133
Figure 5-9. Platelet P-selectin expression after different treatments.....	136
Figure 5-10. Platelet PS exposure after different treatments.....	138

Fig. 5-11. Shifts between multiple states of individual $\alpha_{IIb}\beta_3$ realized four
 populational states: inactive, intermediate, active and hyperactive..... 143

Fig. 5-12. Multi-dimensional model of platelet activation 145

Chapter 6

Figure 6-1. Hypothesized model of normal and defected hemostasis from humans
 that have WT and R1450E VWD MT plasma VWF..... 150

Figure 6-2. Adhesion and signaling abnormality of Type I diabetic GPIb α and
 $\alpha_{IIb}\beta_3$ 155

Figure 6-3. Adhesion and signaling abnormality of Type II diabetic GPIb α 156

LIST OF TABLES

Chapter 3

Table 3-1. Statistics of the recombinant $\alpha_V\beta_3$ binding to FN_{III7-10} lifetime events and bending/unbending conformational change events under different conditions . 52

Chapter 4

Table 4-1. Decision rules for and statistical summary of GPIb α domain unfolding in force-clamp experiment mode 96

Table 4-2. Evaluation of LRRD and MSD unfolding cooperativity 98

Table 4-3. MSD unfolding rates (k_u) and the fraction (w_1) and off-rates (k_1, k_2) of GPIb α binding to A1WT or A1R1450E under different forces 101

Chapter 5

Table 5-1. Goodness-of-fit of one-, two- or three-state model fitting to the survival frequency vs. lifetime of platelet $\alpha_{IIb}\beta_3$ binding to FN_{III7-10} and fibrinogen under different forces 127

Table 5-2, parameters of fast-, intermediate- and slow-dissociating states of platelet $\alpha_{IIb}\beta_3$ binding to FN_{III7-10} or Fg, fitted by Bell's model 129

LIST OF ABBREVIATIONS

A.a.	Amino Acid
Ab	Antibody
ACD	acid-citrate-dextrose
ADP	Adenosine diphosphate
BFP	Biomembrane force probe
BSA	Bovine serum albumin
CHO	Chinese hamster ovary
ECM	Extracellular matrix
fBFP	Fluorescence biomembrane force probe
Fg	Fibrinogen
FITC	Fluorescein isothiocyanate
FN	Fibronectin
FN _{III7-10}	Fibronectin, type III domain, module 7-10
GOF	Gain-of-function
GPIb α	Glycoprotein Ib α
H-T buffer	Hepes-Tyrode's buffer
HSA	Human serum albumin
K_a	Affinity
k_{off}	Off-rate
k_{on}	On-rate
LRR	Lucine Rich Repeat

LOF	Loss-of-function
MSD	mechano-sensitive domain
MT	Mutant
nm	Nano-meter
RGD	Arginine-Glycine-Aspartic Acid
PE	Phycoerythrin
PS	Phosphatidylserine
PWB	Platelet washing buffer
VWD	von Willebrand disease
VWF	von Willebrand factor
WT	Wild type

SUMMARY

Cells sense the mechanical environment, actively or passively, through membrane embedded proteins named mechano-receptors. The binding force is generated once the mechano-receptor engages its immobilized ligand. The received mechanical signal propagates along the structure of the receptor and across the membrane, which is often accompanied and realized by local or global conformation changes of the receptor. Usually through allosteric mechanisms, which are not fully understood, this signal is converted into intracellular chemical signals – a procedure termed mechanotransduction – which then generates an elaborate response that mediates cell survival, proliferation, differentiation, migration and other physiological or pathological functions, thereby completes the whole mechanosensing process.

Integrins form a superfamily of adhesion mechano-receptors. Their mechanotransduction functions are realized by the various conformational changes, which enables bidirectional transduction of signaling, and the regulation of integrin binding kinetics. On platelet surface, multiple types of integrins are expressed, including $\alpha_{IIb}\beta_3$, $\alpha_V\beta_3$, $\alpha_5\beta_1$, $\alpha_M\beta_2$ and more. They enable platelet communication with the adjacent extracellular matrix and cells by binding to their respective counterparts, which involves probably subsequent conformational changes. Thus, studying the binding kinetics and molecular dynamics of integrins enables deep inspection of the linkage between their molecular structure and physiological functions.

The mechanosensing of platelets play a critical role in the proceeding hemostasis and thrombosis, especially in the arterial environments where shear forces become large, and soluble stimulating molecules can be easily dissipated by high-speed flow. In this context, two mechano-receptors - GPIb α and integrin $\alpha_{IIb}\beta_3$ - mediate the early and mid-stages of platelet adhesion and activation through mechanotransduction. The mechanosensing involves a cascade of molecular and cellular reactions in response to the force, which finally realize: 1) enhanced binding capacity of the receptors; and 2) signal transduction that leads to the activation of platelets via intracellular signaling. However, how platelets distinguish mechanical signals received from GPIb α and integrin $\alpha_{IIb}\beta_3$ and respond accordingly and precisely largely remain unknown.

In this thesis, I describe my Ph.D. researches on integrin dynamics and platelet GPIb α and integrin $\alpha_{IIb}\beta_3$ mechanosensing. I put myself in the shoes of an engineer, and regarded the platelet and its receptors as delicate machinery to addressed four questions: 1) how integrin conformational changes are associated with its binding kinetics and activities; 2) how is the mechanical signals in different waveforms deciphered and converted into corresponding chemical signals by platelets, and what is the required mechanical signal for GPIb α and integrin $\alpha_{IIb}\beta_3$ mechanosensing? 3) what is the underlying molecular mechanisms for the signal to propagate through the cell membrane and realize mechanical-to-chemical transfer? and 4) what is the difference in the results of GPIb α and integrin $\alpha_{IIb}\beta_3$ mechanosensing as compared to platelet activation by soluble stimulus? My studies were carried out surrounding the

above questions, which brought us new biomechanical insights on integrin dynamics and platelets adhesion and signaling:

- 1) Integrin conformational dynamics and binding kinetics: using a cutting-edge force spectroscopy, biomembrane force probe (BFP), it was discovered that integrin $\alpha_V\beta_3$ undergoes bending and unbending conformational changes in a dynamic fashion. This process does not require energetic or signaling support from a cell. The probability, rate and speed of these bending and unbending conformational changes are regulated by mechanical force, ligand, integrin genotype, cation and purified/cellular environment. In somewhat disagreement to conventional perspective that unbending is associated with integrin activation, force-enabled $\alpha_V\beta_3$ unbending does not reinforce the strength of its binding in the physiological $\text{Ca}^{2+}/\text{Mg}^{2+}$, but does in Mn^{2+} .
- 2) GPIIb α -mediated mechanotransduction: Using an upgraded, fluorescence-enabled BFP which manipulated a single human platelet, we showed the ability of a single GPIIb α -VWF-A1 binding event to trigger platelet intracellular Ca^{2+} flux. A positive correlation was found between the binding duration (lifetime) and the intensity of the Ca^{2+} signal, so that the signaling is stronger triggered by WT VWF-A1 (A1WT) at higher forces because of its catch-bond behavior, but weaker by a Von Willibrand disease (VWD) mutant R1450E which manifest a slip-bond. This suggests a new concept about VWD: signaling deficiency. Unfolding of two domains of the GPIIb α structure, lucine-rich-repeat (LRRD) and mechanosensitive (MSD) domains, mediates

the signal transduction in that, LRRD unfolding prolongs the binding lifetime and analogously enhances signaling intensity, whereas MSD unfolding digitally affects the fluxed Ca^{2+} type. Abolishment the binding of a cytoplasmic molecule 14-3-3 ζ to GPIb complex depleted most of the α -type Ca^{2+} . The strong correlation between mechanical force, structural conformational changes and molecular association of GPIb α , and the amplitude and type of the resulted Ca^{2+} signal suggested that GPIb together with its functionally adjacent molecules form a molecular mechanosensor.

- 3) GPIb α -triggered platelet activation: I invented a new dual-BFP approach that studies the adhesion molecules' inter-talk on platelet surface. It was found that the mechanotransduction of GPIb α leads to an intermediate level of integrin $\alpha_{\text{IIb}}\beta_3$ activation, P-selectin expression and phosphatidylserine exposure as compared to ADP and thrombin, two soluble platelet activators, which suggests that GPIb α triggers platelets into an intermediate activation state. The intermediate up-regulation of $\alpha_{\text{IIb}}\beta_3$ is unstable and transient, but is important in that it opens the pathway of integrin mechanotransduction mediated outside-in signaling, so that the $\alpha_{\text{IIb}}\beta_3$ can be further activated through repeated binding and pulling of ligand. This defines cooperation between integrin inside-out and outside-in mechano-signaling. On the other hand, ADP-activated $\alpha_{\text{IIb}}\beta_3$ can also be further activated via outside-in mechano-signaling to a hyperactive state. Overall, my study discovered a four-stage regulation of platelet $\alpha_{\text{IIb}}\beta_3$ by bidirectional signaling.

These studies altogether accomplished a step forward in the field of biomechanics and biophysics, and provide mechanistic insights in platelet physiology and mechanobiology. The technical innovations I made including micro-space temperature controlling, which allows BFP experiments to be done in a physiological thermal environment, and dual BFP, which can study inter-talk of heterogeneous receptors on the same cell during mechanosensing, should facilitate the future development of single-cell mechanobiology.

Finally, I extended my research to tentatively investigate atherothrombosis in type I and II diabetes. I found that platelet hyperreactivity in diabetes is closely associated with enhanced adhesive capacity and exaggerated mechano-signaling of GPIIb α and integrin $\alpha_{IIb}\beta_3$. These results imply the medical importance of my research, and reveal the advantages of single-cell biomechanics in disease studies and diagnostics.

CHAPTER 1: INTRODUCTION

1.1 Specific aims

Platelets are a key player in both hemostasis (the physiological process of blood cessation after blood vessel injuries) and thrombosis (pathological blood clotting). Upon a vascular injury, the platelets adhere to the sub-endothelium and attach to each other, so as to form an aggregation to block the injury site and stop the bleeding. Meanwhile, the adhesion of platelets through surface adhesion receptors triggers signals in a force-dependent fashion, which is transmitted into the cell and stimulates platelet activation, a process termed platelet mechanosensing. Specifically, two platelet receptors - GPIb α and integrin $\alpha_{IIb}\beta_3$ - mediate the early to mid-stages of platelet adhesion and activation, especially in the arterial environments and under pathological conditions where shear rates are high. Glycoprotein Ib α (GPIb α) is a major part of the GPIb α -V-IX complex that constitutes the receptor for von Willebrand factor (VWF). Its binding to VWF at the A1 domain (VWF-A1) enables rolling (translocation) of platelets on the sites of vascular injury. Integrin $\alpha_{IIb}\beta_3$, also known as glycoprotein IIb/IIIa, allows for platelet stable adhesion to VWF on the surface of sub-endothelium and promotes the expansion of the platelet aggregates by cross-linking via ligands like soluble fibrinogen and fibronectin. Both GPIb α and $\alpha_{IIb}\beta_3$ has been reported to trigger outside-in platelet-activating signals under forces via ligation, which suggests that both molecules are involved in the platelet mechanosensing. In my Ph.D. works, I studied platelet surface GPIb α and $\alpha_{IIb}\beta_3$ in

the context of adhesion and signaling. The goal is to figure out the respective mechanisms of GPIb α - and $\alpha_{IIb}\beta_3$ -mediated platelet mechanosensing and their physiological and pathological importance in the context of platelet functioning. I conducted single-molecular level experiments with a fluorescence biomembrane force probe (fBFP) to systematically correlate mechanically dependent GPIb α and $\alpha_{IIb}\beta_3$ ligation with readouts of platelet activation including platelet intracellular Ca²⁺ signal, integrin up-regulation, P-selectin expression, phosphatidylserine (PS) scrambling on the plasma membrane. Following three aims were formed:

Aim 1: Characterize integrin binding affinity regulation and bending/unbending conformational changes.

Integrins are a family of adhesion molecules that are able to adopt multiple conformational states, which allows regulation of their affinity in ligands binding. Under this aim I used purified $\alpha_V\beta_3$ – another β_3 integrin that has a high structural similarity to $\alpha_{IIb}\beta_3$ – to gain insights in its molecular basis for dynamically transitioning between multiple affinity states and conformational states, which were hypothesized to be determined by the flexible structure and affected by the environmental conditions. We used a BFP and a HS-AFM to conduct the experiments in the following steps:

- i) Use a BFP to analyze the single-bond lifetime of $\alpha_V\beta_3$ -fibronectin interaction in two cation conditions: Ca²⁺/Mg²⁺ (physiological-mimicking) and Mn²⁺ (artificially

activating). Also, study the impact of WOW-1, an antibody that specifically blocks the binding of activated $\alpha_V\beta_3$, on the binding kinetics.

ii) Use a BFP to observe the bending/unbending conformational changes of $\alpha_V\beta_3$ under a tensile force. The conformational changes were characterized by the bending/unbending distance, time-to-bend/extend and switch time under all forces. Results from $\text{Ca}^{2+}/\text{Mg}^{2+}$ and Mn^{2+} were compared to render the impact of integrin activation to the conformation regulation. The lifetime-after-bend/extend was collected to reflect how the bending/unbending of the integrin affects its binding capacity.

iii) Use a HS-AFM to observe the bending/unbending conformational changes of $\alpha_V\beta_3$ under zero-force. By seeding the integrin molecules onto a mica surface and scanning with a super-sensitive cantilever tip, HS-AFM allows real-time imaging of a single integrin with high temporal and spacial resolutions, and for the first time directly revealed the dynamic integrin conformational changes. Parameters collected from this section, including the bending/unbending distance, time-to-bend/extend and switch time were used as an extrapolation of the BFP results at zero-force, which is in benign agreement with the BFP results.

Besides, another integrin, $\alpha_M\beta_2$ (MAC-1), was also used in a collaborative lupus-associated project that measures its conformation and binding, and the impacts of mutations.

Considering that integrin adhesion and conformation could be used as solid readouts of integrin activity, the research in this aim provide critical fundamentals for the following studies and add significance to the overall thesis.

Aim 2: Investigate the GPIb α -mediated platelet mechanotransduction.

GPIb α is the primary adhesion receptor that enables initial platelet recruitment to the vascular injury site by binding to immobilized VWF multimers. This binding also initiates a platelet signaling that leads to transient intracellular Ca²⁺ flux and $\alpha_{IIb}\beta_3$ up-regulation. The studies under this aim intended to correlate GPIb α adhesion to its mediated platelet signaling. Several key questions were addressed:

i) In GPIb α mechanotransduction, what attributes are meaningful in the input mechanical signal in the sense that they can be distinguished by the platelet and affect the output chemical signal? To answer this question, we consider the GPIb signaling pathway as fine machinery, which receives certain input signals and precisely produces corresponding output signals. fBFP was used in this study. By manipulating the GPIb α binding on a single-molecular level and using intraplatelet Ca²⁺ flux as readout of signaling, it was discovered that GPIb α triggers outside-in signaling in a force-, bond duration (lifetime)- and ligand- dependent manner. Among them, durable force pulling is indispensable for activating signaling, while in the presence of lifetime, force amplitude positively correlates with signaling strength.

ii) How is the GPIb α mechanotransduction realized in the molecular level? Specifically, how could a molecule complex read the information contained in a

mechanical stimulation and translates it into a chemical signal? Of note, previous publications have suggested that certain domains of GPIb α may act as a signal transducer. In our investigation, we discovered that the unfolding of GPIb α mechano-sensitive domain (MSD), and the direct binding of a cytoplasmic molecule, 14-3-3 ζ , to the tail of GPIb α and GPIb β mediate the transduction of GPIb signaling.

Aim 3: Investigate the downstream consequence of GPIb α -mediated platelet mechanotransduction.

What is the physiological significance of GPIb α mechanotransduction? GPIb α signaling has been suggested to be trivial as compared to GPIV, another receptor that mediates initial platelet recruitment and signaling. However, scientific evidences also show that lack of GPIb α signaling results in drastic hemostatic deficiency *in vitro* and *in vivo*. In this section I studied the platelet activation consequence of GPIb α -mediated mechano-signaling. Using a BFP, we found that GPIb α mechanotransduction leads to several critical signs of platelet activation, which defines a new activation state of platelets:

1) Integrin $\alpha_{IIb}\beta_3$ up-regulation. The activation of $\alpha_{IIb}\beta_3$ by GPIb α signaling has been observed and acknowledged for long, but no work has quantified this activation in a single molecular level. Integrins could adopt multiple ligand binding states. For example, $\alpha_L\beta_2$ possesses at least three dissociation rate states. Based on functional studies, people conventionally believe that $\alpha_{IIb}\beta_3$ only possesses two states, an inactive state and an activated state. Surprisingly, our investigation discovered a new

intermediate state that exists in $\alpha_{\text{IIb}}\beta_3$, which is not simply realized by the mixture of the two conventionally acknowledged states, but has its independent molecular conformation, ligand binding affinity and regulatory mechanisms. The $\alpha_{\text{IIb}}\beta_3$ up-regulation by GPIb α signaling, ADP or thrombin stimulation is realized by the shift of the equilibrium among all three states to different extent, which realizes varied overall binding capacities.

2) P-selectin expression. The expression of P-selectin following GPIb α mechanotransduction is an unexpected discovery, because GPIb α signaling is conventionally believed trivial and not powerful enough to trigger α -granule release. What is more puzzling is that the binding strength of the expressed P-selectin decayed over time, suggesting this process might be reversible.

3) Phosphatidylserine (PS) exposure. The PS exposure has been shown to strongly rely on the action of shear force onto platelets. Agreeing with that, force pulling on GPIb α could trigger PS exposure.

1.2 Background and significance

1.2.1. Hemostasis and thrombosis

The primary physiological role of platelets is to facilitate hemostasis, namely, to prevent hemorrhage after injury by preserving vascular integrity¹⁻³. Upon sub-endothelium exposure due to blood vessel injury, circulating platelets embark on a cascade of well-coordinated events including adhesion and aggregation on the exposed sub-endothelium and ultimately result in stable thrombus formation to repair

the damaged blood vessel and stop bleeding. Thrombosis describes the formation of a blood clot (thrombus) inside a blood vessel, obstructing the flow of blood through the circulatory system. It occurs either together with hemostasis as triggered by a vascular injury and bleeding, or independent of injuries under certain pathological conditions. Certain diseases including diabetes, obesity and hypertension have high risks of severe thrombosis, which produces thrombus's that are significantly large enough to reduce the blood flow to a tissue or even completely occlude the whole blood vessel. This may lead to myocardial infarction and ischemic stroke, claiming one in each four deaths worldwide. As the two sides of the coin, platelets play a critical role in hemostasis, but also contribute significantly to pathological thrombosis^{2,4,5}.

1.2.2. Platelets in shear-dependent hemostasis

In the early and mid-stages of hemostasis, multiple receptor-ligand interactions function to recruit and attach platelet onto the injury site (Fig. 1-1). The early stage adhesion is mediated by the platelet receptors GPVI and GPIb-IX-V in parallel (Fig. 1-1). Depending on the amplitude of the shear force in the blood vessel, one or the other of them will play a primary role^{6,7}. In veins and small arteries where blood flow is relatively slow ($< 500 \text{ s}^{-1}$), the initiation of platelet recruitment cascade majorly mediated by GPVI-collagen interaction, which realizes stable adhesion at low forces⁶. However, under high shear rates ($> 800 \text{ s}^{-1}$), which are usually present in arteries and arterioles or at pathological situations such as restricted lumen in atherosclerosis, GPVI-collagen interaction becomes too weak to resist the high shear force. Instead,

the adhesive interaction between platelet surface GPIb α -IX-V and the collagen- and endothelium-bound VWF strings enables platelet rolling (translocation) on the exposed sub-endothelium^{6,8}. Both the GPIb-VWF interaction and GPVI-collagen interaction trigger outside-in signaling across the cell membrane, inducing downstream activation effects like cytoplasmic Ca²⁺ intensity increase and integrins activation⁹⁻¹¹. This activation promotes multiple integrins from a non-adhesive low-affinity state to a high-affinity state, which becomes able to mediate firm arrestment and aggregation^{10,11}.

1.2.3. GPIb-IX-V and VWF

The GPIb-IX-V complex is composed of four glycoproteins - GPIb α , GPIb β , GPIX, and GPV with a ratio of 2:4:2:1 (Fig. 1-2 A)^{12,13}. GPIb α is covalently connected with the two GPIb β s with a disulfide bond at the membrane-proximal end of the ectodomain, while GPIX and GPV are noncovalently associated with the complex¹⁴. By interacting with sub-endothelium-bound VWF through its major ligand-binding subunit GPIb α , it enables slow rolling of platelets on the surface of injured arteries and the initiation of platelet activation. This interaction also transmits mechano-signal that activates integrin $\alpha_{Ib}\beta_3$.

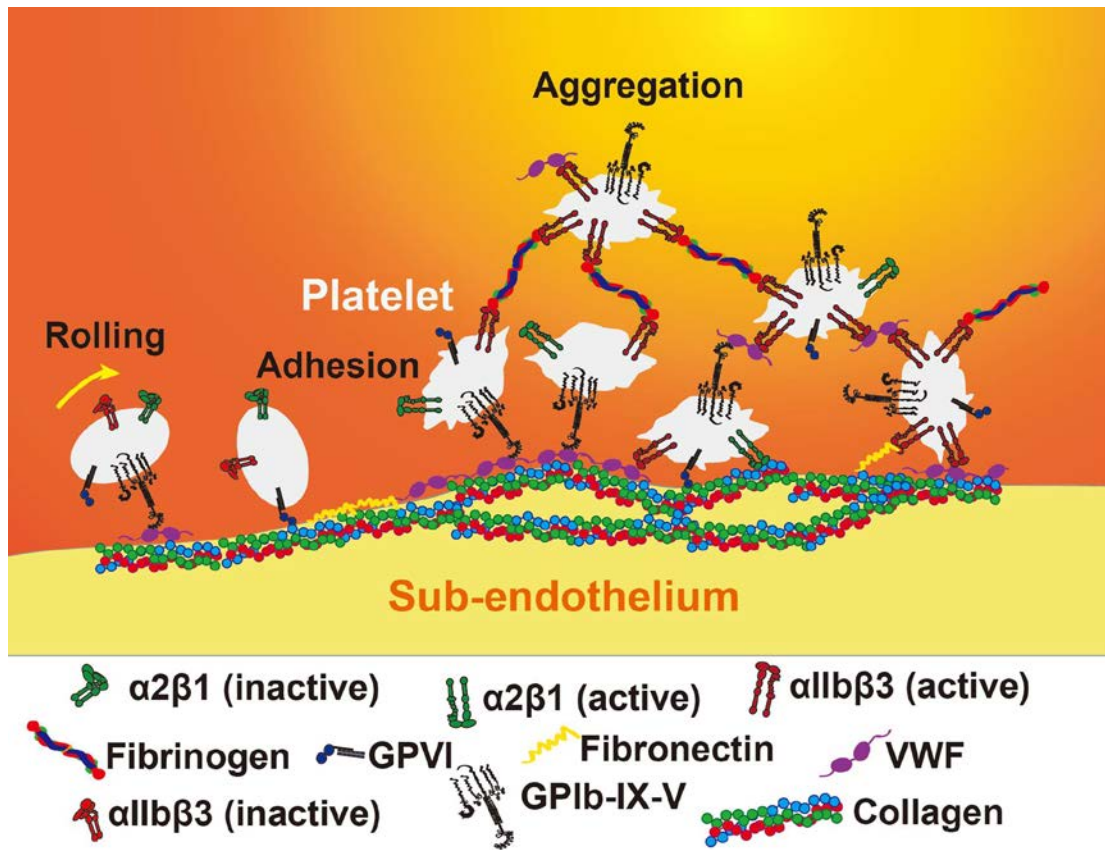


Figure 1-1. A model of primary hemostasis in blood flow. Platelets are firstly recruited through the specific interactions of GPVI and fibrillar collagen as well as GPIb-IX-V complex and collagen-bound VWF. Stable platelet adhesion occurs through the binding of platelet GPVI to fibrillar collagen⁶. These early stage adhesions stimulate platelets to undergo a series of biochemical changes that induce integrins activation, leading to their high affinity interactions with adhesion proteins, which include $\alpha_2\beta_1$ -collagen interaction⁶, $\alpha_5\beta_1$ -fibronectin interaction (not shown in this illustration)¹⁵, $\alpha_V\beta_3$ -fibronectin/fibrinogen/VWF interactions (not shown in this illustration)¹⁵, and most importantly, the interactions between $\alpha_{IIb}\beta_3$ and fibronectin, fibrinogen and VWF¹⁵. These adhesive interactions are indispensable in the ability of platelets to form stable aggregates with other activated platelets and promote thrombus growth.

GPIb α is a 145 kDa membrane surface protein that is composed of an ectodomain (489 amino acids (a.a.)), a transmembrane domain (21 a.a.) and a cytoplasmic domain (100 a.a.). Its ectodomain includes a Lucine Rich Repeat domain (LRRD) which contains the binding site for its ligand VWF-A1, and a long stalk (macroglycopeptide) that connects it to the transmembrane domain (Figure 1-2 B)¹⁶. Lack of GPIb α causes a congenital bleeding disorder – Bernard-Soulier syndrome, as well as severe defects

in both hemostasis and arterial thrombosis mouse models, claiming its indispensability in platelet function^{17,18}. GPIb β is a transmembrane protein much shorter than GPIb α with 121 extracellular, 25 transmembrane and 34 cytoplasmic amino acids, which are comparable to GPIX. No ligand binding site is found on the ectodomain of GPIb β and GPIX, and no evidence has directly shown their functionality in the cell behavior. It is postulated that GPIb β facilitates GPIb-IX-V mechano-signaling by juxtamembrane domain motional change^{16,19}. Nonetheless, their absence causes complete elimination or severe reduction of GPIb α expression on platelet surface, which results in phenotypes of Bernard-Soulier syndromes¹⁴. This indicates that GPIb α forms a complex with GPIb β and GPIX before expressed on cell surface.

VWF is a disulfide bonded multimeric glycoprotein that circulates in the blood stream. It is secreted by both endothelial cells and activated platelets. Its multimerization is realized by disulfide bond linkage on both termini homogeneously in an N-N and C-C manner. Endothelial cells initially secrete ultralarge forms of VWF (ULVWF), which are hyperactive and has exaggerated capacity in binding to platelet GPIb α . ULVWF is quickly cleaved by the plasma protease ADAMTS13 at the A2 domain to yield smaller and less active plasma VWF (pVWF) (Fig. 1-2 C), whose molecular weight typically exceeds 1,000 kDa²⁰. Each monomer of VWF consists of a number of functional domains, of which the A1 domain binds to both GPIb α and collagen, the A3 domain only binds to collagen, and the C1 domain binds to β_3 integrins (Fig. 1-2 C). In the platelet recruitment cascade, VWF acts as an

essential cross-linker between platelets and the sub-endothelium by interacting with GPIb α and β_3 integrins on platelet surface and interacting with collagen on the sub-endothelium or endothelial cells adjacent to the injury site^{6,8,21}.

The behavior of adhesions is mainly determined by kinetics (on-/off-rate constants) of its receptor-ligand systems. The binding between GPIb α and VWF-A1 features fast on-rate (k_{on}) and off-rate (k_{off}), resulting in rapid bond formation, but also rapid breaks. Because of its relatively low affinity (as calculated by $K_a = k_{on} / k_{off}$), this binding does not support firm adhesion but translocation on the sub-endothelium²²⁻²⁴; nonetheless, it is the only adhesion capable of slowing the platelets down while resisting the high shear forces in the arteries by inactive discoid platelets⁶.

1.2.4. Integrin $\alpha_{IIb}\beta_3$ and its ligands

Integrin, cadherin, selectin and Ig CAM superfamily are the four adhesion receptor families in human. They play central roles in cellular interactions with neighboring cells and the extracellular matrix²⁵. Members of the integrin family primarily act as receptors for extracellular matrix (ECM) proteins^{15,25,26}, but could also form adhesions with hetero-species cells^{15,27-30}. Each integrin is a heterodimer composed of an α and a β subunit; each subunit has a large extracellular domain, a single membrane spanning region, and a short cytoplasmic domain (except for the β_4 subunit)^{25,31}. The integrin receptor family of vertebrates includes at least 18 distinct α subunits and 8 β subunits, which creates a total of 24 different combinations that have been identified to date at the protein level^{15,32}. Among them, platelets constantly

express integrins $\alpha_V\beta_3$, $\alpha_2\beta_1$, $\alpha_6\beta_1$, $\alpha_5\beta_1$, and most abundantly, $\alpha_{IIb}\beta_3$ on their surface³³⁻³⁷. In addition, activated but not resting platelets have been reported to express $\alpha_L\beta_2$ (LFA-1) and $\alpha_L\beta_2$ (Mac-1), two integrins that mainly function in the adhesion and migration of leukocytes i.e. monocytes and neutrophils³⁸.

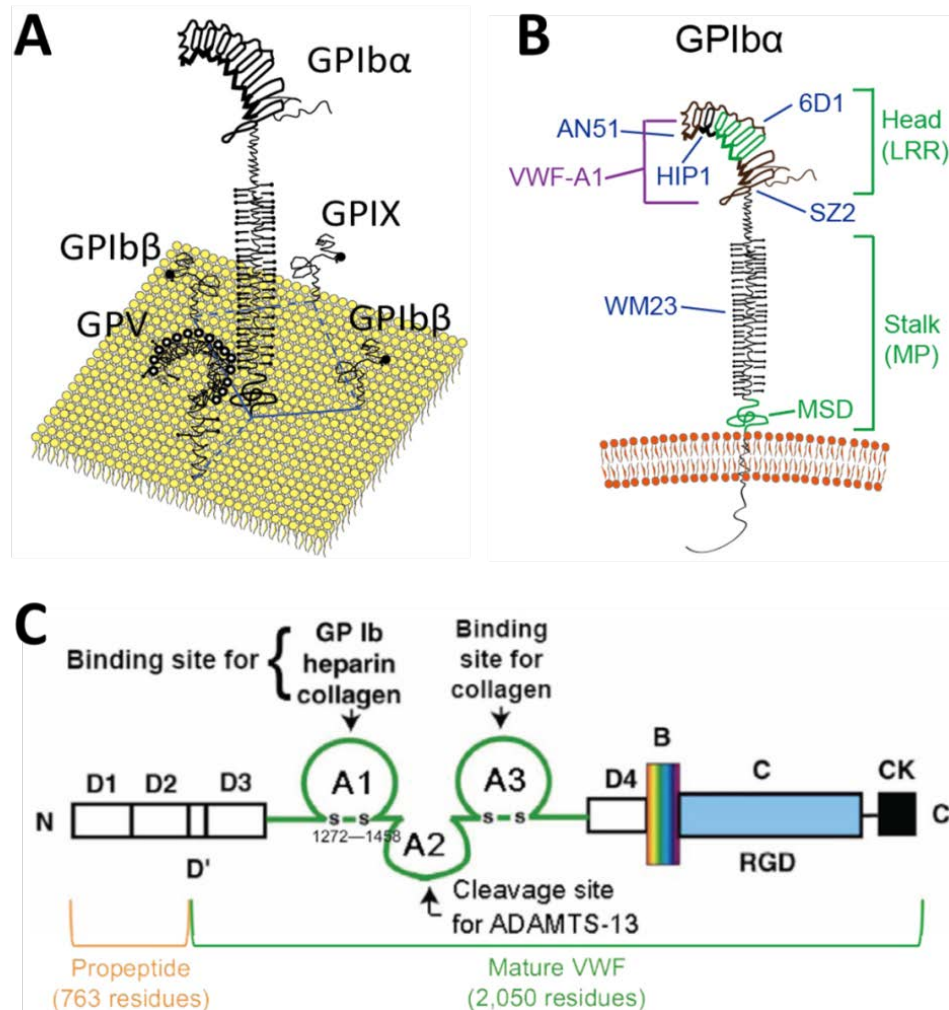


Figure 1-2. GPIb-V-IX complex and VWF. (A) Scheme of the GPIb α -V-IX complex arrangement on a cell membrane surface. GPIb-IX-V complex is composed of four glycoproteins - GPIb α , GPIb β , GPIX, and GPV. Solid blue lines indicate interactions between the members; dashed blue lines indicate potential interactions. (B) Scheme of a GPIb α inserted into a membrane bilayer. The binding epitopes for VWF-A1 and antibodies are indicated on the protein structure. The portions of the ectodomain that correspond to LRR and MP are indicated by green square brackets. (C) Domain organization of a VWF monomer. VWF contain a triplicate repeat sequence of A domains in the central portion of the 2,050-residue mature subunit (D'-D3-A1-A2-A3-D4-B-C).

Integrin $\alpha_{IIb}\beta_3$ (also known as glycoprotein IIb/IIIa, GPIIb/IIIa) is found mainly on platelets, which composes of an integrin α_{IIb} subunit and an integrin β_3 subunit (Fig. 1-3). Like other β_3 integrins and all β_1 integrins, $\alpha_{IIb}\beta_3$ is in lack of an αI domain at the top of its α subunit β -propeller domain, which can be seen in all β_2 integrins, and its epitope for ligand binding resides in between of the β -propeller and βI domain. Other than VWF, its ligands also include plasma proteins fibrinogen and fibronectin¹⁵. On inactive and discoid platelets, it remains in a low-affinity state which barely binds to its ligands. Upon activation, it becomes highly adhesive and plays a dominant role in platelet firm arrest and aggregation³⁹. $\alpha_{IIb}\beta_3$ could be activated by both inside-out signaling, which involves binding of talin and kindlin to the β_3 cytoplasmic domain and the separation of the α_{IIb} and β_3 at the transmembrane and cytoplasmic domains, and outside-in signaling, which requires ligation of an agonist at its headpiece and the downward signal transmission in a structurally allosteric fashion^{36,40-44}. The primed $\alpha_{IIb}\beta_3$ can also be suppressed by certain anti-platelet agents (e.g., Rap1 and PI3 kinase inhibitors)⁴⁵. Evidence has been found that $\alpha_{IIb}\beta_3$ activation/inactivation accompanies global conformational changes of its own structure^{41,46-48}. The activity of $\alpha_{IIb}\beta_3$ also mediates heterotypic cell-cell interactions of other cell species like tumor and endothelial cells⁴⁹.

Fibrinogen is the primary ligand of $\alpha_{IIb}\beta_3$ in the process of platelet aggregation. It exists in the blood stream, and is secreted by activated platelets. It has a dimerized structure, containing two sets of intertwine of three chains (α , β and γ). Each monomeric fraction of fibrinogen bears three sites for integrin binding: two RGD

sequences in the A α chain which applies to the binding of $\alpha_{IIb}\beta_3$, $\alpha_V\beta_3$ and $\alpha_5\beta_1$, and one AGDV sequence in the C-terminus of γ chain which is specific for $\alpha_{IIb}\beta_3$ ⁵⁰. The symmetric structure of fibrinogen with multiple binding sites together with a molecular length of ~50 nm makes it perfect glue to crosslink platelets to form an aggregate.

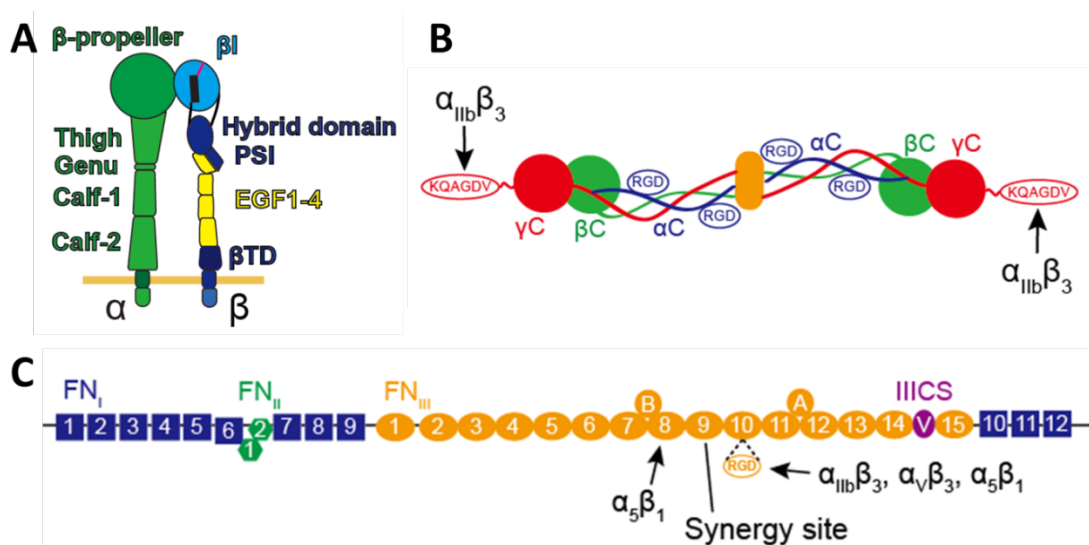


Figure 1-3. Structures of β_3 and β_1 integrins (A), fibrinogen (B) and fibronectin (C). (A) the extracellular fraction of α subunit is composed of β -propeller, thigh, genu, calf-1 and calf-2, while that of β subunit is composed of β_I , hybrid domain, PSI, EGF1, EGF2, EGF3, EGF4 and β TD (all indicated). (B) One fibrinogen molecule is made up from two sets of α , β and γ chains. The epitopes for integrin binding (RGD and AGDV a.a. sequences) are indicated. (C) Each fibronectin contains four classes of domains (FN_I, FN_{II}, FN_{III} and III CS). The 8th, 9th and 10th module of FN_{III} (FN_{III8-10}) bear all the epitopes that are important for interacting with integrins (all indicated).

Fibronectin is a glycoprotein of the extracellular matrix with a molecular length of ~15 nm. Just like fibrinogen, it exists both in the blood stream and the α -granules of platelets. Fibronectin is a physiological ligand for multiple integrins, which, except for hemostasis, also plays a critical role in the cell-ECM interactions and focal adhesion. Specifically, FN_{III10} contains the RGD sequence^{26,51,52}; FN_{III9} bears a

synergy site that reinforces the $\alpha_5\beta_1$ -FN_{III10} interaction, but seems to have no effect to the anchorage of β_3 integrins (Fig. 1-3 C)⁵³. Fibronectin binds to fibrinogen at the A α 221–391 region only when the fibrinogen is converted by thrombin to fibrin⁵⁴. During platelets aggregation, blood plasma fibronectin molecules attach to the activated platelets on the aggregate surface, and act as a cross-linker to attract more inactive platelets^{55,56}.

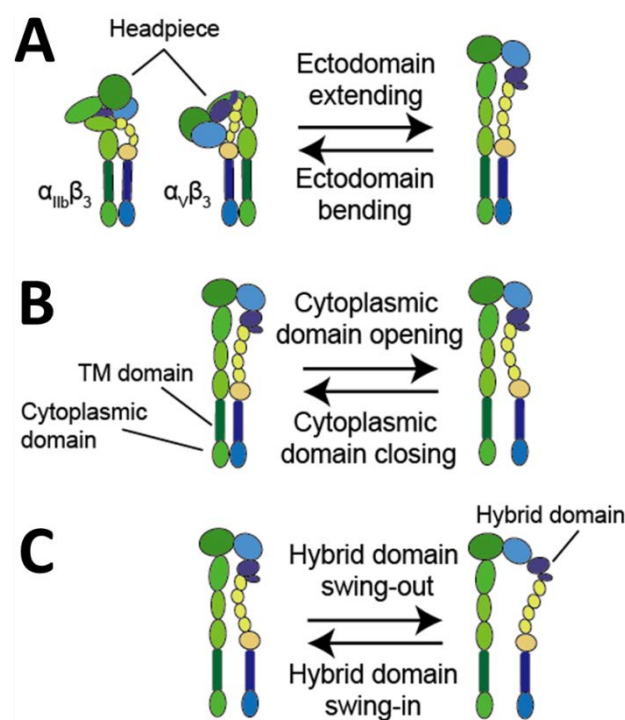


Figure 1-4. Sketches of the three global conformational changes that integrins may undergo: ectodomain bending/extending (A), cytoplasmic domain closing/opening (B) and hybrid domain swing-in/out (C).

1.2.5. Integrin affinity and conformational changes

Integrins adopt different functional states under different conditions. In the inactive state, integrins have extremely low affinities for ligand binding, which will be drastically up-regulated upon activation. So far, this multi-affinity property have been verified in integrin $\alpha_5\beta_1$, $\alpha_L\beta_2$ (LFA-1), and $\alpha_{IIB}\beta_3$ in single molecular level^{26,29,57,58}.

In the meanwhile, owing to the flexible molecular structure, integrins adopt multiple global conformations, including a bent /extended ectodomain, a closed/opened tail and swing-in/out of the β chain hybrid domain, which were observed by EM^{47,59,60}, crystallography⁵⁹, and antibody mapping^{61,62} (Fig. 1-4). In these studies, the integrin conformation was strongly affected by the cation conditions, talin-head binding and certain activating antibodies which all affect integrin binding capacity, indicating that integrin conformation has strong correlation with function. Among them, talin recruitment is one of the two major physiological manners of cell surface integrin activation, which docks in between of the integrin transmembrane domains and causes tail unclasping via steric effects, and in turn results in extodomain extension by allosteric effects^{40,46}. In parallel, a pulling force through ligand binding also induces integrin activation and conformational changes via allosteric effects. A recent research from our lab observed and characterized integrin LFA-1 ectodomain bending/unbending conformational change in real-time, which for the first time revealed this process in a dynamic manner and confirmed that: 1) integrins under bent or extended conformations have diverse binding affinities and 2) force breaks the bending/unbending equilibrium and facilitates extension⁶³. However, the mechanistic details of integrin conformational change are still missing, among which two intriguing questions are raised: 1) can integrins undergo conformational change without support from the cell, and 2) how do force and cell signaling trigger integrin conformational change respectively. To answer these questions, the proposed project

will characterize the real-time bending/unbending behavior of integrins in cell-free and cell-surface systems.

1.2.6. Platelet activation

Platelets can be activated through multiple signaling pathways:

1) Mechano-signaling pathways: the activation of platelets via mechano-signaling relies on the surface receptor molecules. According to current views, the primary receptors that initiate mechano-signaling are GPIb α and GPVI. Through binding to their respective ligand (VWF and collagen) against force (see Section 1.2.2), GPIb α transduces intracellular signals that activate integrin $\alpha_{IIb}\beta_3$, while GPVI activates integrin $\alpha_2\beta_1$, both involving the release/mobilization of the intracellular calcium storage (Fig. 1-5). Activated integrins adopt high-affinity association with their ligands, and initiate a secondary nonetheless stronger wave of mechano-signaling that leads to activation of other integrins (for example, $\alpha_{IIb}\beta_3$ adhesion is a sufficient and necessary pre-requisite for activating $\alpha_2\beta_1$ ⁶⁴), platelet cytoskeletal deformation, α - and dense-granule release and more².

2) Chemo-signaling pathways: these include activation pathways by soluble agonists. The engagement of ADP (with receptors P₂Y₁ and P₂Y₁₂)^{65,66} and thrombin (with PAR1 and PAR4)⁶⁷ both trigger strong activation, including integrin up-regulation, cytoskeletal remodeling, granule release, degranulation and cell death^{2,5,68}.

Several hallmarks of platelet activation are well-accepted by the field:

1) The activation of $\alpha_{IIb}\beta_3$ is a sign of platelet deriving strong adhesiveness and the capacity to mediate firm attachment and crosslinking. It can be detected by active $\alpha_{IIb}\beta_3$ specific antibody PAC-1⁴³, or the binding strength against ligands like fibrinogen and fibronectin. Similarly, the activation of other integrins like $\alpha_V\beta_3$ and $\alpha_5\beta_1$ is also informative on the platelet activation extent.

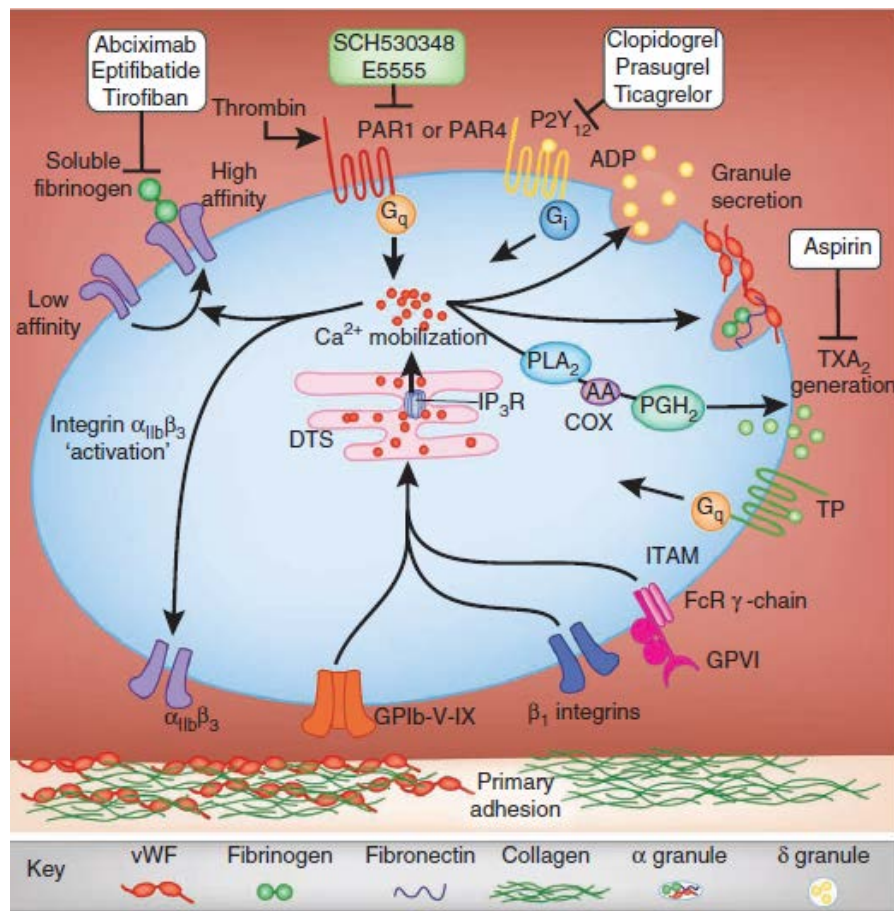


Figure 1-5. A map of platelet activation pathways. Adapted and modified from (Jackson, 2011)².

2) The α - and dense-granule releases are realized only when platelets are substantially activated. Among the released substances, P-selectin is an easily detectable subject since it will be expressed on the platelet surface instead of released to the extracellular environment⁶⁹. It adds an additional platelet-endothelium

interaction by binding to PSGL-1, and also allows crosstalk between platelets and leukocytes.

3) Phosphatidylserine (PS) exposure. Phospholipids in the platelet membrane have PS enriched in the inner leaflet but not in the outer leaflet. During platelet activation, cytoplasmic Ca^{2+} intensity increases induces lipid scrambling, by which the PS are exposed in the outer leaflet^{70,71}. This allows blood coagulation factors to be recruited to the platelet surface and convert pro-thrombin into thrombin^{72,73}, the importance of which is implicated by the lipid scrambling deficiency in Scott syndrome^{74,75}. It is argued in previous studies that GPVI is the major receptor that, upon binding to collagen under flow, induces PS exposure, while GPIIb α and $\alpha_{\text{IIb}}\beta_3$ only facilitate this process⁷⁶.

1.2.7. Platelet mechano-signaling

Mechano-signaling is a process that cells rely on to sense the mechanical environment and react. In adhesion-mediated mechano-signaling, a specific adhesion receptor-ligand interaction is required. It is initiated by the cell-surface receptors binding to the ligand on an opposing surface (of a cell or extracellular matrix), followed by a tensile force exerted on to the receptor-ligand complex, which could be either an external force like flow shear stress or produced by the cell body deformation. The force acts onto the receptor as a mechanical signal, which is transduced across the membrane and converted into a chemical signal. After reaching the cytoplasm, the signal induces a series of intracellular signaling events, finally

resulting in certain mechanical and/or chemical reactions of the cell. A mechano-signaling process can be divided into four steps, taking GPIb α an example: 1) mechanopresentation: the receptor binding domain A1 is exposed by structural changes in VWF induced by elongational flow and collagen immobilization⁷⁷; 2) mechanoreception: GPIb α receives the force signal via engaging A1 to tether the platelet against shear stress; 3) mechanotransmission: force is propagated from the A1-binding GPIb N-terminal leucine rich repeat domain (LRRD) through the mucin-like macroglycopetide (MP) stalk region and the juxtamembrane mechanosensitive domain (MSD) across the membrane to the supporting structures inside the platelet⁷⁸; 4) mechanotransduction: force induces mechanical and biochemical changes, eliciting intraplatelet Ca²⁺ mobilization and integrin activation⁹⁻¹¹. Of these, the previous three have been substantially studied, while the investigations on mechanotransduction in platelet molecules are still in their infancy. Intriguingly, how the binding kinetics manipulates signaling, and how this manipulation is realized by merely several cooperative molecules? This shapes up the central question of this thesis.

Many platelet receptors are involved in mechano-signaling. The proposed project only focuses on two: GPIb α and $\alpha_{IIb}\beta_3$. GPIb α is the primary mechano-receptor during platelet activation, which is further amplified by soluble agonists (e.g., adenosine diphosphate (ADP) and thromboxane A2 (TXA2)) released during the primary activation⁷⁹. Signaling through GPIb α via binding to VWF-A1 can activate $\alpha_{IIb}\beta_3$ independently of other receptors, in which Ca²⁺ plays an important role⁹. GPIb α

mediates transient Ca^{2+} concentration elevations released from the intracellular storage, which are designated as type α/β Ca^{2+} based on the pattern: type α Ca^{2+} manifest a sharp onset and a quick fading, while type β is smoother. Type α/β signals could be derived independently by GPIIb/IIIa interacting with VWF-A1¹⁰. Inhibition of the first stage Ca^{2+} release from intracellular storage by membrane permeable Ca^{2+} chelators prevents platelet firm adhesion, suggesting that Ca^{2+} is an obligatory signaling molecule on the pathway to $\alpha_{\text{IIb}}\beta_3$ activation^{10,11,80,81}.

Activated integrin $\alpha_{\text{IIb}}\beta_3$ initiates outside-in signaling when binding to its ligands, which triggers a secondary but more robust and sustained Ca^{2+} signal (type γ), and induces phosphorylation of downstream kinases (including Akt and FAK) and platelet spreading^{10,82,83}.

Previous studies have given beautiful mechanistic answers to many mechano-signaling systems in human cells, for example hair cells, in which force induces lateral motion of the hair along the cell membrane and controls the open/closing of ion channels⁸⁴⁻⁸⁷. In the platelet system, however, mechano-sensing remains poorly studied, probably due to the limitations in techniques: in previous studies, the activation of platelets in mechano-signaling is detected in low spatial and temporal resolution, and the mechanical stimulation cannot be well-controlled. With our unique technique Biomembrane Force Probe (BFP)^{88,89}, we will be able to control receptor-ligand bond formation to single-molecular level and characterize multiple aspects of platelet activation with high spatial and temporal resolution, which makes it

a perfect weapon for observing platelet mechano-triggering. The technical details of BFP will be introduced later in the corresponding section.

1.2.8. Significance

The outcome of this project will provide knowledge about mechanical and kinetic regulation of platelet signaling and activation by platelet adhesion, and thus advance our understanding on hemostasis and blood coagulation on molecular level. Overall, this research has scientific and clinical significance.

CHAPTER 2: MATERIALS AND METHODS

2.1 Proteins and reagents

Recombinant WT and MTs R1450E, R1306Q and V1279I monomeric VWF 1238-A1 (residues 1238–1471) was a generous gift from Dr. Miguel A. Cruz (Department of Medicine, Baylor College of Medicine, Houston TX) and was generated by E.coli as previously described⁹⁰. Recombinant WT and MT I1309V monomeric VWF 1208-A1 (residues A0742-17/21) and dimeric VWF 1208-A1 (residues A0742-17/21) were generously provided by Dr. Zaverio Ruggeri (The Scripps Research Institute, La Jolla, CA). GFP-lact-C2 and anti-GPIIb α antibody WM23 were gifts from Dr. Renhao Li (Emory University, Atlanta, GA). Human plasma fibrinogen and VWF were generous gifts from Dr. Shaun Jackson (The University of Sydney, Australia). Hexa-His tagged recombinant $\alpha_V\beta_3$ ectodomain was a gift from Dr. Junichi Takagi, Osaka University, Japan⁴⁷. Biotinylated fibronectin module III, domain 7-10 (FN_{III7-10}) and 9-10 (FN_{III9-10}) were generous gifts from Dr. Andres Garcia (Georgia Tech). Antibodies 10E5 (anti- $\alpha_{IIb}\beta_3$) and 7E3 (anti- β_3) were generous gifts from Dr. Barry Coller (Rockefeller University, New York, NY). The antibodies AP3 and AP5 were generous gifts from Dr. Peter Newman (Blood Center of Wisconsin). The antibody 6D1 (anti-GPIIb α) was a gift from Dr. Michael Berndt (University of Curtings, WA, Australia). Peptides mP6, Ser mP6, mP13, Ser mP13, MP α C and MPcsC were provided by Dr. Xiaoping Du (UIC, Chicago, Illinois).

CBRM1/29, CBRLFA1/2 and CBRLFA1/7 were a generous gift from Dr. Timothy Springer (Children's Hospital, Harvard University, Boston, MA).

All commercialized reagents purchased from companies are listed below:

Reagents	Company	Antibody	Antigen	Company
MAL-PEG3 500-NHS	JenKem, Plano, TX	AK2	GPIb α	Abcam, Cambridge, MA
Biotin-PEG 3500-NHS	JenKem, Plano, TX	AN51	GPIb α	EMD Millipore, Billerica, MA
Nystatin	Sigma-Aldrich , St. Louis, MO	Anti-ICAM -1-PE	ICAM-1	eBioscience, San Diego, CA
3-Mercapto propyltrimet hoxysilane (MPTMS)	Uct Specialties, llc, Bristol, PA	JON/A	α I II β 3 (mouse)	EMFRET Analytics GmbH & Co. KG, GERMANY
Borosilicate Glass beads	Distrilab Particle Technology, RC Leusden, The Netherlands	LS-B3174	GPIb β	Lifespan Biosciences, Seattle, WA
Streptavidin -Maleimide	Sigma-Aldrich , St. Louis, MO	LIBS-2	β 3 integrins	EMD Millipore, Billerica, MA
BSA	Sigma-Aldrich , St. Louis, MO	anti-Penta His antibody	Penta Histidine	Qiagen, Venlo, Netherlands
Fura2-AM	Life Technologies, Grand Island, NY	LM609	α V β 3	EMD Millipore, Billerica, MA

Dimethyl sulfoxide (DMSO)	Sigma-Aldrich, St. Louis, MO	Anti-Mac-1-PE	Mac-1	Biolegend, San Diego, CA
Quantibrite PE Beads	BD Biosciences, San Jose, CA	HFN 7.1	Fibronectin	Abcam, Cambridge, MA
Human ICAM-1Fc	R&D, Minneapolis, MN	PAC-1	α IIb β 3	BD Biosciences, San Jose, CA
human placenta type III collagen	Sigma-Aldrich, St. Louis, MO	PAC-1-FITC	α IIb β 3	BD Biosciences, San Jose, CA
ADP	Sigma-Aldrich, St. Louis, MO	AK4	P-selectin	Biolegend, San Diego, CA
Apyrase	Sigma-Aldrich, St. Louis, MO	HIP1	GPIb α	Biolegend, San Diego, CA
BAPTA	Sigma-Aldrich, St. Louis, MO	SZ2	GPIb α	Santa Cruz Biotechnology, Dallas, Texas
Cholesterol Oxidase	Sigma-Aldrich, St. Louis, MO			
F-127	Life Technologies, Grand Island, NY			
Theophylline	Sigma-Aldrich, St. Louis, MO			
Thrombin	Sigma-Aldrich, St. Louis, MO			

2.2 Functionalization of beads

The functionalization of beads by proteins was described in previous literature in detail⁹¹. In general, glass beads were first incubated with MPTMS (Section 2.1) to be thiolated. MAL-PEG3500-NHS linker was used to mix with the protein of interest and then the thiolated glass beads so as to link a certain protein onto the bead surface. Streptavidin (SA)–Maleimide (Section 2.1) was used to incubate with thiolated glass beads to derive SA beads. For proteins (segments) that were already biotinylated, they were simply incubated with SA beads to attach onto the beads surface. All beads after incubation were washed with and resuspended in phosphate buffer (27.6 g/L NaPhosphate monobasic ($\text{NaH}_2\text{PO}_4 \cdot \text{H}_2\text{O}$), 28.4 g/L Anhy. NaPhosphate dibasic (Na_2HPO_4)) and stored in 4°C.

2.3 Red blood cells

The preparation of RBCs was described in previous literature in detail. In general, 8-10 μl of blood was obtained from finger prick abiding an Institutional Review Board approved protocol, and RBCs were purified by centrifugation and then incubated with Biotin-PEG3500-NHS linker (Section 2.1) solution. Biotinylated RBCs were incubated with nystatin (Section 2.1) to be swollen to the desired osmolarity.

2.4 Platelets

To obtain fresh discoid human platelets, whole blood was drawn slowly from a healthy donor's vein to fill in a 3ml syringe preloaded with 0.43ml ACD buffer (6.25

g sodium citrate, 3.1 g citric acid anhydrous, 3.4 g D-glucose in 250 ml H₂O, pH 6.7). The whole blood was centrifuged at 300g for 10min without brake at 37 °C . Platelet-rich plasma was extracted, diluted by platelet washing buffer (PWB, 4.3 mM K₂HPO₄, 4.3 mM Na₂HPO₄, 24.3 mM NaH₂PO₄, 113 mM NaCl, 5.5 mM D-Glucose, 10 mM Theophylline, 0.5% bovine serum albumin (BSA), pH 6.5) with a 1:2 ratio, and centrifuged at 900g for another 10 min. The platelet pellet was finally resuspended into HEPES-Tyrode buffer (134 mM NaCl, 12 mM NaHCO₃, 2.9 mM KCl, 0.34 mM sodium phosphate monobasic, 5 mM HEPES, and 5 mM glucose, 1% BSA, pH 7.4) for BFP experiments. For the Ca²⁺ imaging experiments, isolated platelets were incubated with Fura2-AM (Section 2.1) at 30 μM for 30 min.

2.5 Cell lines

CHO cell lines and Jurkat cell lines expressing MAC-1 and FcγRIIA are provided by Dr. Tanya Mayadas lab (Harvard Medical School) by cell transfection techniques.

Mouse lung endothelial cells expressing human integrin α_vβ₃ were provided by Dr. Martin Schwarz lab (Yale University).

2.6 BFP experiments

2.6.1 System setup

The procedure of BFP experiments were described in detail in a previous paper⁹¹. Generally speaking, a BFP system is built up by an inverted microscope, an experimental chamber, three micropipette manipulators with a piezo-mover

supporting one of them (target), and three water reservoir systems. The experimental chamber was made up by two parallel pieces of coverglass, in the gap between which is experimental buffer filled. Three micropipettes are respectively mounted onto the three manipulators and inserted into the experimental buffer (Fig. 2-1A,B), which are respectively connected with the three water reservoir systems. By adjusting the reservoir height, one can control the inner pressure of the micropipettes so as to aspirate or blow away items. RBCs, probes beads and target cells/beads are separately injected into the experimental buffer at different areas.

Among the three micropipettes, the probe pipette aspirates a RBC, the helper pipette aspirates a probe bead and the target pipette aspirates a target cell/bead (Fig. 2-1B).

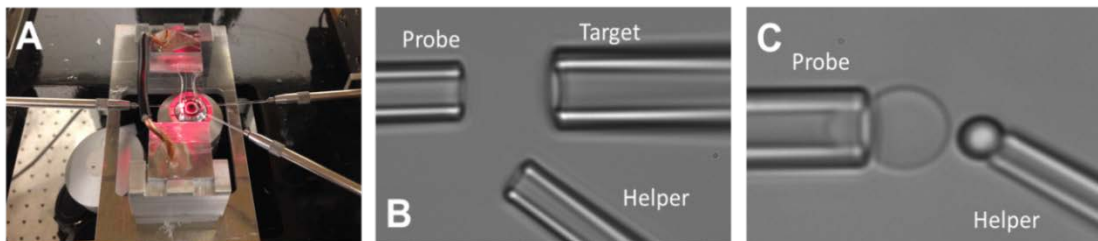


Figure 2-1. BFP experiment setup. Photo of the BFP chamber and micropipette setup (A), the placement of the three pipettes under the microscope (B) and a demonstration of the probe pipette grabbing a RBC and the helper pipette grabbing a glass bead (C). Adapted from (Chen et al, 2015)⁹¹

BFP uses this micropipette-aspirated biotinylated RBC as a force transducer (Fig. 2-2 A). On the apex of the RBC is a glass probe bead attached via SA-biotin interaction (Fig. 2-2 A). The placement of the probe bead onto the RBC is realized by the helper pipette (Fig. 2-1 C). The probe bead is also functionalized by certain ligand(s) to suit experimental purpose (Figure 2-1 A insert, using T-cell receptor and

peptide:MHC as an example, the bead is coated with peptide:MHC). Another opposing micropipette grabs a target cell/bead that expresses/immobilizes the receptor under investigation (Fig. 2-2 A insert, T-cell receptor).

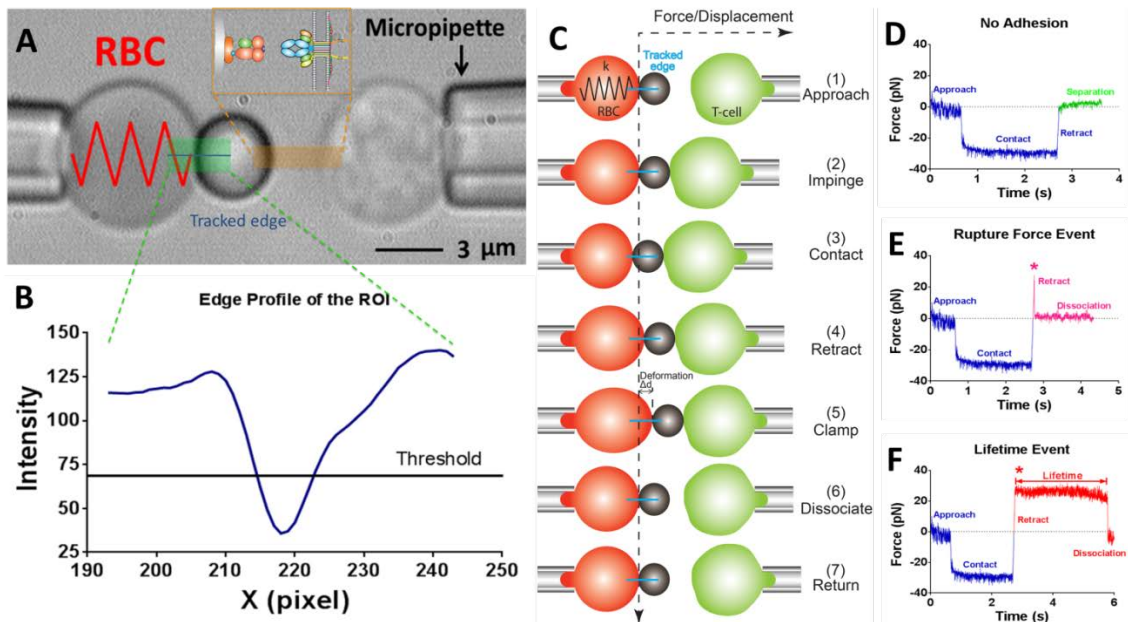


Figure 2-2. Introduction of BFP experiment. Take T-cell receptor and peptide:MHC interaction as an example, modified from (Chen 2015)⁹¹. (A) The BFP photomicrograph. A bead was attached to the apex of a micropipette-aspirated red blood cell (RBC, left) to form a force probe. The probe was aligned against a T-cell (target cell, right) aspirated by an opposing micropipette. Insert: BFP functionalization. The probe bead was pre-coated with peptide:MHC. The T-cell expressed T-cell receptor. (B) The intensity profile of the bead edge in (A). The ROI region in the x-direction is plotted as x-axis (in pixel number) and the light intensity (in gray scale value) averaged by binning 30 pixels along the y-direction. (C) The deflection of the RBC and the position of the bead and the target (T-cell) in a test cycle of force clamp assay. The vertical and horizontal dashed lines indicate the zero-force position of the RBC apex and the time course, respectively. The line edge tracker of the RBC deformation is shown in blue in each panel. The same yet less steps are adopted in adhesion frequency assay (which lacks the steps of “clamp” and “dissociate”) and thermal fluctuation assay (which lacks the step of “dissociate”). (D-F) Exemplary time-force raw data curves of a no-adhesion event (D), a rupture force event (E) and a lifetime event (F).

The interface between the probe bead and the RBC is tracked (Fig. 2-2 B). By judging from the deformation of the RBC, one can derive the force exerted onto it.

During the experiment, the target cell/bead is driven by a piezo movement to repeatedly contact with the probe bead, hold for a certain time and retract (Fig. 2-2 C). If the bead detaches from the cell surface readily, it indicates no adhesion, while an adhesion event would be manifested by a tensile force signal (Fig. 2-2 D-F)⁹¹.

2.6.2 Force spectroscopy assays and data analysis

In BFP, several experimental modes (assays) can be chosen to suit different purposes:

2.6.2.1 Force-ramp assay

Force-ramp assay ruptures all bonds without holding, which enables the collection of each bond's ramping and rupture signature. The characteristics of this signature, like the slope, rupture force and sometimes the existence of kinks, contain much information about this bond, which will be discussed in detail in later sections.

Force-ramp assay is sometimes simplified to adhesion frequency assay, which does not calibrate the force but simply record the probability of adhesion over touches (Fig. 2-2 E)⁹².

By counting the probability of adhesion in repeated touches (termed adhesion frequency) under a whole range of contact time, one can plot the "adhesion frequency vs. contact time"⁹². If only one association mode exists between the receptor and ligand, this plot should adopt a hyperbolic shape. A 2-D kinetics model was deduced previously to fit this data, which, together with the information of the probe's and

target's site densities (see Section 2.7), is able to quantitatively calculate the binding kinetics parameters including the on-rate, off-rate and thus the affinity of this interaction^{92,93} by using the Equation 2-1:

$$P_a = 1 - \exp\{-A_c m_r m_l K_a [1 - \exp(-k_{off} t)]\} \quad (\text{Equation 2-1})$$

in which P_a is the adhesion frequency, A_c is the contact area between the probe and the target. m_r and m_l are the site densities of the receptor and the ligand, respectively. K_a and k_{off} are the two-dimensional affinity and off-rate, respectively, in the absence of force, and t is the contact time.

However, if more than one association modes exist, the above model does not apply, and more complicated analysis will be required.

2.6.2.2 Force/distance clamp assay

Force/distance clamp assay clamps the tensile force at a certain level, and measures the bond lifetime in single molecular level (Fig. 2-2 F)^{29,91}. The molecular site densities of the probe/target pair are titrated to ensure infrequent adhesion, which guarantees most probably single-molecular interactions between the two surfaces²⁹.

The average clamping force and lifetime are extracted from each lifetime event. Plotting an “average lifetime vs. force” curve is one common way to present force/distance clamp assay result, which is produced by binning the lifetime data pool into different clamping force regimes (commonly 5-10 pN in width). The curve

reflects the binding strength under force, given that the lifetime is the reciprocal of the off-rate.

2.6.2.3 Thermal fluctuation assay

Thermal fluctuation assay pauses the retraction phase of the BFP cycle at 0 pN, so that the probe and target surfaces loosely contact with each other. The oscillation of the signal is measured and the decrease and increase of the thermal fluctuation level are distinguished, which is a measure of the bond formation and dissociation in single molecular level^{89,91,94}. The rationale of this assay is that when the probe bead is free of binding with an opposing surface, it has more freedom of motion, and thus has a higher level of thermal fluctuation, whereas once a bond forms, the bead's position will be better constrained⁹⁴.

The time lengths of each interval with high and low thermal fluctuation level were collected, which reflect the off- and on-state of the bond association, respectively. The time length of the former is an indicator of on-rate, while the latter an indicator of off-rate under zero-force.

2.6.2.4 Spring constant measurements

In the BFP rupture-force signature (Figure 2-2E) or the lifetime event signature (Fig. 2-2 F), the retraction phase data can be used to derive the overall spring constant of the biological system with all elements in series. In the compressive force fraction (negative to zero force), the biological system includes the RBC, the probe bead

(which is regarded as a rigid body and neglected) and the target bead/cell (Fig. 2-3 A), while in the tensile force fraction (zero to positive force), the molecular complex in association between the two surfaces will also be taken into consideration (Fig. 2-3 B). This is because when the force is compressive, the molecular complex will lay horizontally between the two opposing surfaces and avoid being compressed, while under tensile force they will be stretched due to the separation of the two surfaces and elongate. Thus, we have:

$$\begin{aligned} \frac{1}{Slope_1} &= \frac{1}{k_{target}} + \frac{1}{k_{RBC}} \\ \frac{1}{Slope_2} &= \frac{1}{k_{target}} + \frac{1}{k_{mol}} + \frac{1}{k_{RBC}} \end{aligned} \quad \text{(Equation 2-2)}$$

Which is also shown in Fig. 2-3 A,B. In Equation 2-2, k_{target} , k_{mol} , and k_{RBC} are respectively the spring constants of the target bead/cell, the molecular complex and the RBC. $Slope_1$ and $Slope_2$ are the overall spring constant of the system in the compressive and tensile force fractions of retraction, which are derived from the BFP signals. Shown in Fig. 2-3 C is an example of the BFP retraction phase signal signature. The insert is the original signal, while in the main figure the x-axis “Time” is converted to “Displacement” by multiplying it with the pre-set retraction rate, v_{ret} , which by default is 3333.33 nm/s. After conversion, we are able to derive the relationship between the force increase and the extension of the overall system, which reflects the rigidness of the system, in other words, the spring constant. The linear fitting slopes of the compressive and tensile force fractions are respectively $Slope_1$ and $Slope_2$.

From Equation 2-2, we are able to calculate the spring constant of the target bead/cell and the molecular complex:

$$k_{target} = 1/\left(\frac{1}{Slope_1} - \frac{1}{k_{RBC}}\right)$$

$$k_{mol} = 1/\left(\frac{1}{Slope_2} - \frac{1}{Slope_1}\right)$$

(Equation 2-3)

If the target is a bead, which we can regard as a rigid body considering its much higher stiffness when compared to cells and molecules, $k_{target} \rightarrow \infty$. So the Equation 2-2 can be simplified to:

$$\frac{1}{Slope_2} = \frac{1}{k_{mol}} + \frac{1}{k_{RBC}}$$

Thus,

$$k_{mol} = 1/\left(\frac{1}{Slope_2} - \frac{1}{k_{RBC}}\right)$$

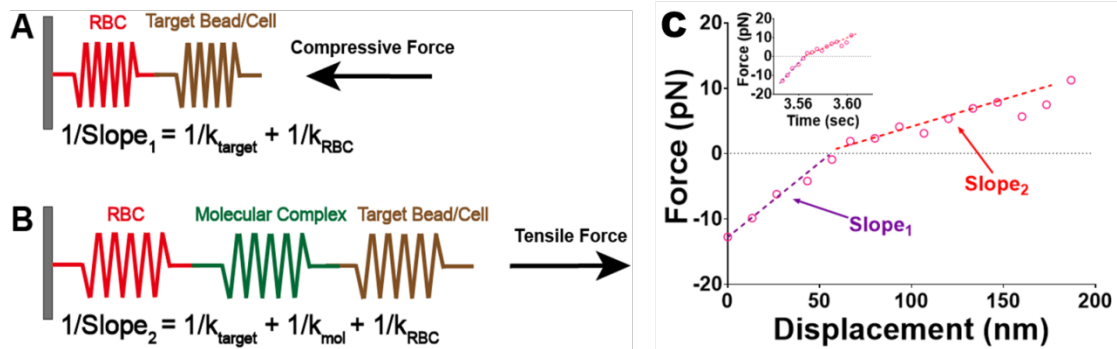


Figure 2-3. Illustration of the spring constant calculation under a compressive and tensile force (A,B) and an exemplary BFP signature of the retraction phase that shows the slope different in the compressive and tensile force fractions (C). In Panel C, the “Force vs. Time” signal (insert) was converted to “Force vs. Displacement”, so that the linear fitting slopes directly reflect the spring constant of the biological systems. The Slope₁ and Slope₂ in Panel C correspond to the terms with the same names in Panels A and B.

2.6.2.5 Fitting adhesion frequency to derive average number of bonds

The average number of receptor-ligand bonds formed during each cell-bead contact, $\langle n \rangle$, is derived as^{92,95}:

$$P_{a,max} = 1 - \exp(-\langle n \rangle) \quad (\text{Equation 2-4})$$

Assuming a single homogeneous population for both the receptors and ligands.

If more than one receptor population is involved:

$$P_{a,max} = 1 - \exp(-\langle n \rangle_{total}) \quad (\text{Equation 2-5})$$

where $\langle n \rangle_{total}$ is the total average number of bonds.

2.6.2.6 Calculation of average effective affinity

Continuing from Section 2.6.2.5, remember the definition:

$$\langle n \rangle = m_r m_l A_c \langle K_a \rangle = m_r m_l \langle A_c K_a \rangle,$$

in which m_r , m_l and $\langle K_a \rangle$ are respectively the receptor and ligand site density and average effective affinity. Thus:

$$\langle A_c K_a \rangle = \frac{\langle n \rangle}{m_l m_r} \quad (\text{Equation 2-6})$$

2.6.2.7 Lifetime multi-state analysis

The multi-state analysis assumes that the collected lifetime events under a certain force f are from a mixture of multiple receptor-ligand binding states with different dissociation rates under force. The survival frequency of lifetime t , defined as the

fraction of lifetime events longer than t , were fitted with the multi-state model that assumes superposition of exponential decays ²⁹:

$$\ln(\text{Survival frequency}) = \ln\{\sum_{i=1}^n w_i \exp[k_i(f) * t]\} \quad (\text{Equation 2-7})$$

in which t is lifetime, w_i and k_i are the fraction and off-rate of the i th state, respectively. The sum of all w_i equals to 1. Two-state ($n = 2$) and three-state ($n = 3$) models were tested.

The derived off-rates of each state were then plotted against force, which was fitted to the Bell's model – the average lifetime of single-state binding decays exponentially with force ⁹⁶:

$$k(f) = k_0 \exp(af/k_B T) \quad (\text{Equation 2-8})$$

in which f is force, k_0 is the off-rate under zero-force, a is the reactive compliance, k_B is Boltzmann constant, and T is absolute temperature.

2.7 Measurement of molecular site density

The deduction of 2-D binding kinetics parameters from BFP results need the information regarding the molecular site densities of the target cell/bead and probe bead (Section 2.6.2.1).

To measure the molecular site density, the cells or beads are incubated with a fluorescently tagged monoclonal antibody against the molecule of interest at 10 μ g/ml at room temperature for 30 minutes and washed for 3 times. The fluorescent

intensities of the cells or beads are measured by a BD LSR flow cytometer (BD Biosciences), and compared to standard calibration beads (Section 2.1) to determine the total number of molecules per cell or bead. Then the site density is calculated by dividing total number of molecules per cell or bead to the cell or bead surface area^{27,92}. The surface area was calculated from the radii measured with a customized LabView (National Instrument) program.

2.8 Fluorescence BFP experiment

The Fluorescence BFP (fBFP) experiment adds in the concurrent intracellular Ca^{2+} monitoring of the target cell. This is realized by pre-loading the cell with Fura2-AM, a fluorescent Ca^{2+} indicator, exciting this indicator with 340/380 nm wavelength light and detecting the emission signal via a fluorescence camera. The emission intensity triggered by 340 nm light indicates the Ca^{2+} -bound Fura2 concentration, while that triggered by 380 nm indicates free Fura2 concentration. A 340/380 intensity ratio reflects the Ca^{2+} concentration.

During an fBFP experiment, a regular BFP experiment is performed, while the alternating fluorescence images were produced in a ~ 1 Hz frequency⁹¹.

The data analysis of the fluorescence results is based on a customized Labview program, which reviews the images frame by frame, and calculates the intensity ratio between the two channels automatically.

2.9 Switch BFP assay

Cell surface receptor cross-talk and cooperativity is always an important and intriguing problem in cell biology and biomechanics, for example, GPIba and integrin $\alpha_{IIb}\beta_3$ on platelets, or selectins and β_3 integrins on neutrophils. In these systems, the ligand engagement with the first receptor initiates a mechano-signaling into the cell, which then leads to the activation of the second receptor in a time scale of tens of seconds or a couple of minutes. Studying receptor cross-talk has the difficulty due to the fact that it requires the sequential presentation of two sets of ligands that potentially interact with two receptor systems, which in most systems cannot be fulfilled.

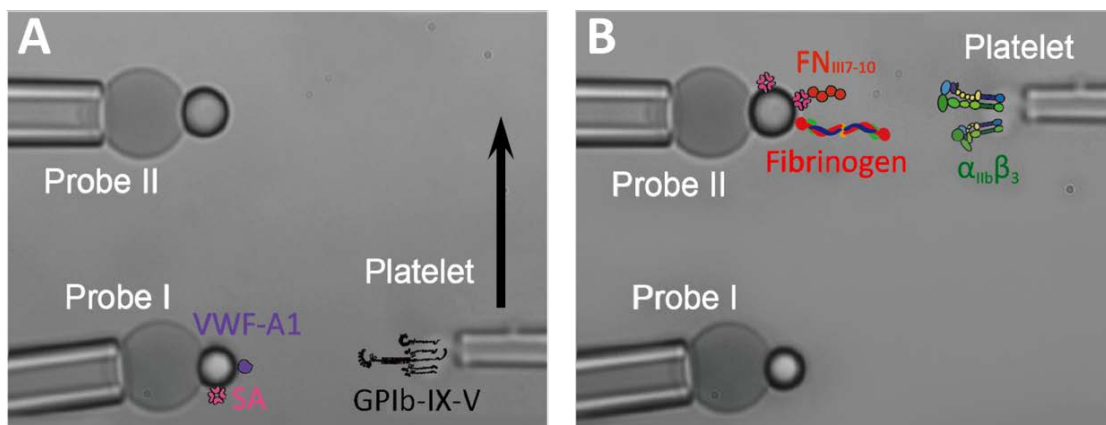


Figure 2-4. Switch BFP demonstration using platelet GPIba and integrin $\alpha_{IIb}\beta_3$ inter-talk as an example. (A) Switch BFP setup before switch. The platelet was aligned with and driven to repeated touch Probe I that presented VWF-A1, until a lifetime event was observed. Then the platelet aspirating pipette will be moved upward. (B) Switch BFP setup after switch. The platelet was aligned with and driven to repeated touch Probe II that presented FN_{III7-10} or fibrinogen to test $\alpha_{IIb}\beta_3$ integrin activity.

The switch BFP concept was first described in Dr. Lining Ju's thesis, attaching two ligand bearing beads onto one RBC probe. The switch mechanism was realized by manual rotation. The limitations of this method are low throughput and high failure rate. The new switch BFP technique was designed and built by myself with the help

of my colleague, Ms. Zhou Yuan. Besides the original probe pipette, a second pipette was added into the system that is able to realize sequential interrogation of the cell surface. With the capability of almost seamlessly sequentially presenting two sets of ligands to a single cell, it is a powerful tool to study cell surface receptor cross-talk.

Normally, only one force probe will be needed to fulfill the experiment. However, the switch assay which observes the inter-talk between cell surface receptors requires the addition of a second probe. In a switch assay, the added probe will act as Probe I, which is in charge of priming the signal-initiating mechano-receptor, e.g., GPIb α , by providing ligand for association (Fig. 2-4A). The original force probe acts as Probe II, which interrogates the platelet for signaling readouts, e.g., $\alpha_{IIb}\beta_3$ up-regulation (Fig. 2-4B). During the experiment, the platelet will first be aligned and repeatedly touch with Probe I for GPIb α -ligand engagement (Fig. 2-4A). Once the mechanotransduction is triggered, the platelet-aspirating micropipette will be moved upward to start interrogation by Probe II (Fig. 2-4B). The switch time, defined as the interval between the platelet interacting with Probe I and with Probe II, could be as short as ~30 seconds.

2.10 Temperature controlling system for BFP

The temperature controlling system was the second add-on of the BFP system designed and realized by myself. It enables *in vitro* BFP experiments under a physiological mimicking temperature, which is important in cell signaling studies,

considering that many cell signals could only be triggered under physiological temperature.

This temperature controlling system integrates a commercial temperature controller, Fuji PXR Temperature Controller (Part No.: PXR3-NAY1-4V0A1), and is composed of two electric circuits: the heating circuit and the controlling circuit, which are linked through a reed relay (Fig. 2-5). The system takes advantage of heat-electricity effect to heat up the experimental chamber, and to realize that, the top coverglass will have to be replaced by a piece of conductive glass (resistance: 240Ω).

In the heating circuit, heating of the conductive glass is via the heat effect of the currency flowing through the conductive glass provided by an 18V DC power supply. Since the resistance is distributed in the glass evenly, heat is also evenly generated all over the glass surface, which assures a relatively uniform temperature distribution throughout the glass covering area. One 500Ω rheostat is used as an adjustment of the heating speed, and also reduces overshooting during controlling.

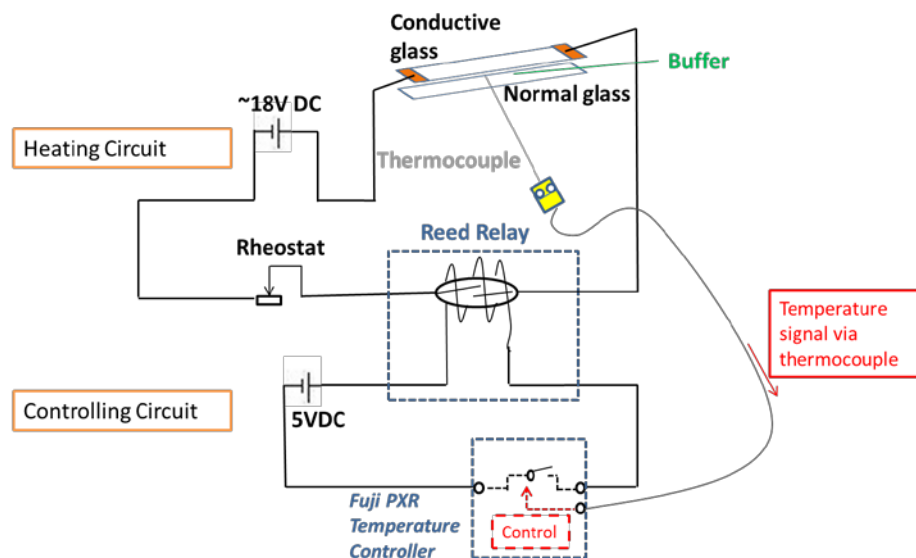


Figure 2-5. Electric circuit design sketch of the temperature controlling system

For the controlling circuit, a reed relay is used to link the heating circuit and the controlling circuit, whose operational voltage is 5V. The probe tip of the thermocouple sticks inside the buffer to sense the local temperature. The Fuji PXR Temperature Controller provides a PID loop control, which is the center of the controlling mechanism. Tolerating lower and higher limits are preset on the Fuji PXR Temperature Controller. Based on the current and historical temperature data, it is able to give feedback and manipulate the “on” and “off” state of its inner passage. When the temperature inside the chamber is lower than the tolerating lower limit, the inner passage will be set as “on”, which ensures the connectivity of the controlling circuit. With currency flowing through the electromagnet inside the reed relay, it sets the magnetic switch as “on”, which ensures the connectivity of the heating circuit and heat-up of the conductive glass. After the temperature probed by the thermal couple is higher than the tolerating higher limit, the inner passage will be set as “off”, which cut off the controlling circuit. With no currency flowing through the electromagnet inside the reed relay, it set the magnetic switch as “off”, which cut off the heating circuit. The heating power stops working and the conductive glass and the whole chamber begin to cool down.

With this temperature controlling system, the experimental temperature environment can be maintained relatively stable within 1°C.

2.11 Statistical testing

All data are mean \pm SEM. The statistical significance of the differences between two sets of data was determined by Student's t test. For group analysis, two-way ANOVA was used. If significant differences were shown, the data were subjected to Tukey's test for multiple comparisons, with $p < 0.05$ considered significant.

CHAPTER 3: CHARACTERIZATION AND REGULATION OF INTEGRIN AFFINITY AND CONFORMATIONAL STATES

3.1 Introduction

Due to their flexible multi-domain structure, integrins can adopt multiple global conformational states, each of which corresponding to certain activity. Ectodomain extension, tailpiece separation (unclasping of the transmembrane and cytoplasmic domains) and hybrid domain swing-out are generally believed to be associated with integrin activation, in other words, a higher binding capacity⁹⁷. This has been supported by the use of soluble integrin activators, like activating cations (e.g., Mn^{2+}), certain activating antibodies, talin head domain and ligand-mimicking peptide binding^{40,43,47,60,97,98}. The introduction of functional mutations also resulted in outnumbering of certain conformations as compared to wild-type (WT)⁹⁹. For example, cells expressing β_3 mutation D723R which causes the tail separation, showed significantly higher integrin activation and more pronounced outside-in signaling^{100,101}. L138I, another β_3 mutation that locks the integrin in the extended state, showed high affinity binding to ligands and higher efficiency in both outside-in and inside-out signaling^{101,102}. In parallel, supported by a MD simulation work on $\alpha_V\beta_3$, a pulling force through ligand binding may also induce integrin conformational changes via mechanical effects¹⁰³. Indeed, two recent works from our lab which characterized single integrin $\alpha_L\beta_2$ (LFA-1) binding kinetics and ectodomain bending/unbending

conformational changes, for the first time demonstrated a dual role of the mechanical force to concurrently up-regulate the integrin binding capacity and facilitate integrin extension^{29,63}. These works broke the previous bottleneck in this field which only had access to static images but no dynamic process. Meanwhile, it raised more questions, like whether this could occur independent of cell surface environment, and how mutations and different ligands may regulate this. Surrounding these questions, I studied the affinity and conformational states of two integrins, $\alpha_V\beta_3$ and $\alpha_M\beta_2$.

3.2 Results

3.2.1 Integrin $\alpha_V\beta_3$ binding kinetics and bending/unbending conformational changes – a purified system study

In this project, the conformational dynamics and binding activities of integrin $\alpha_V\beta_3$ was characterized by BFP in real-time, both in a cell-free system and on cell surface.

3.2.1.1 $\alpha_V\beta_3$ -fibronectin binding forms a catch-bond in Mn^{2+} which is suppressed in Ca^{2+}/Mg^{2+}

A biotinylated fragment of fibronectin, module III, domain 7-10 (FN_{III7-10}) was used as a substitute of the full-length protein, which contains both the integrin-binding RGD sequence in domain 10 and the synergy site in domain 9 (Fig. 1-3 C). The FN_{III7-10} was immobilized on SA beads via SA-biotin interaction to make the probe beads (Fig. 3-1A,B).

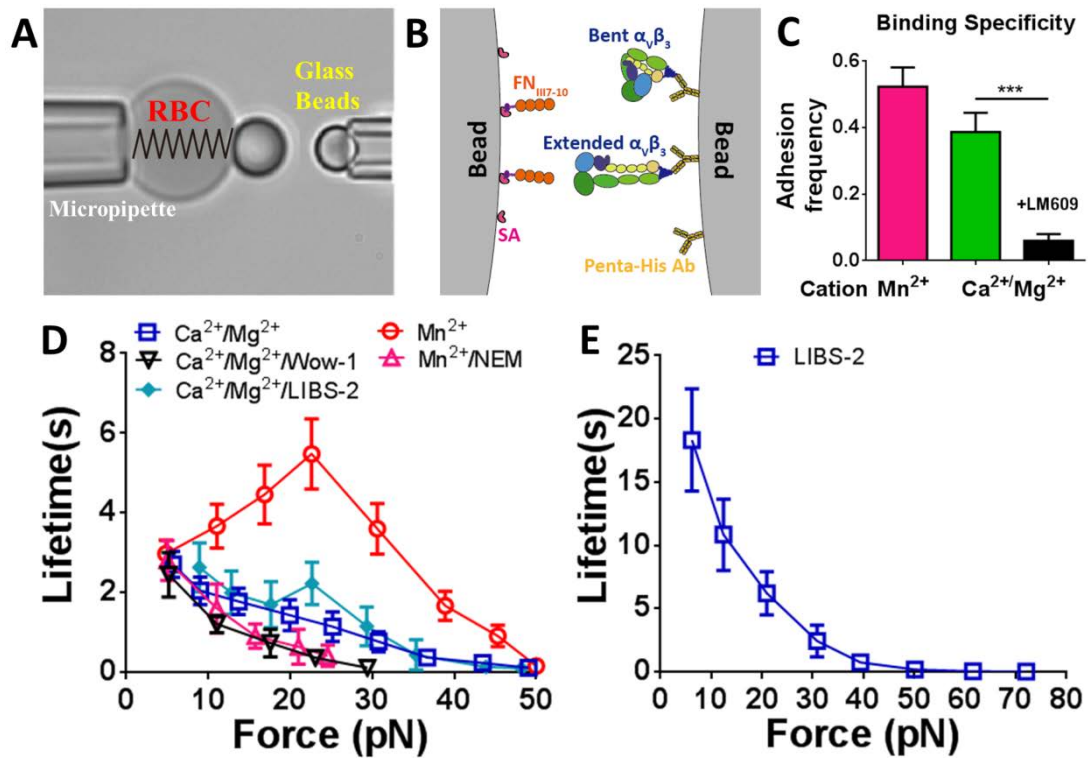


Figure 3-1. BFP setup for studying recombinant $\alpha_v\beta_3$ (A,B), specificity test results (C), and lifetime vs. force results of $\alpha_v\beta_3$ binding to fibronectin (D) and antibodies LIBS-2 (E). Error bar: SEM.

On the target beads, anti-pentahistidine antibody was immobilized following covalent linking protocol. A recombinant $\alpha_v\beta_3$ ectodomain construct clasped at the tail with a hexahistidine tag at the β_3 C-terminus⁴⁷ was then coated on via antibody-antigen interaction (Fig. 3-1 A,B).

In the initial specificity testing, the beads coating densities were not titrated to be around 20%. In both 2mM Mn^{2+} , a prevailingly used artificial integrin activation environment, and 1mM $Ca^{2+}/1mM Mg^{2+}$ conditions, robust level of adhesion exhibited between the two spheres. Addition of LM609, a $\alpha_v\beta_3$ blocking antibody, eliminated most of the binding, confirming that the adhesion was mainly contributed by $\alpha_v\beta_3$ -FN_{III7-10} interaction (Fig. 3-1 C).

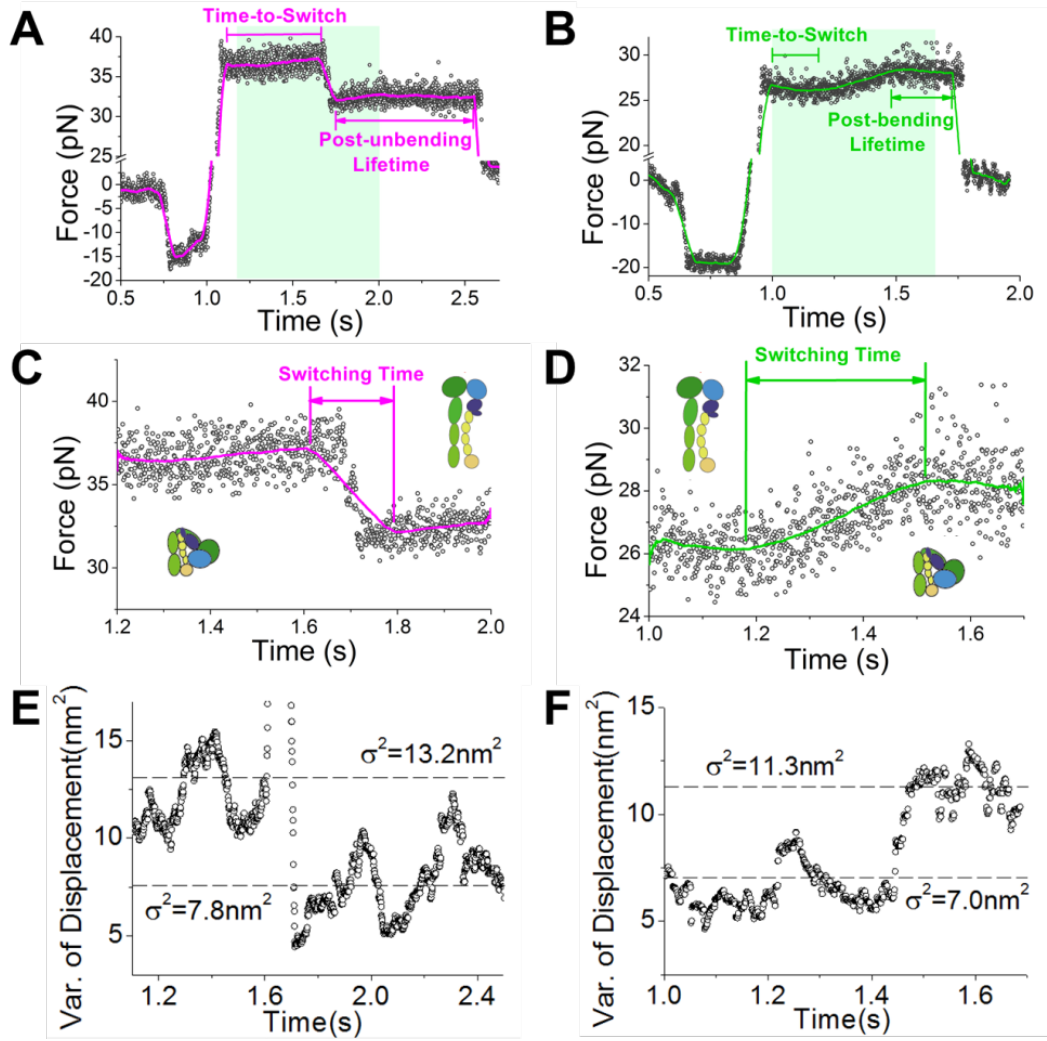


Figure 3-2. BFP signatures of recombinant $\alpha_v\beta_3$ unbending (A,C,E) and bending (B,D,F) conformational changes in the clamping phase of a BFP signal. (A-D) Representative force vs. time data points showing a putative integrin unbending (A, C), and bending (B, D) event. A higher force resolution was obtained by smoothing the raw data using the Savitzky-Golay method (curves). Force changes (Δf), switching time (t_{sw}), time-to-switch (t_0) and post unbending/bending lifetime (t_1) are indicated. (A,B) The overall signals of BFP cycles that contains an integrin unbending (A) or bending (B) event. (C,D) The zoom-in views of the BFP signal within the cyan-shaded time windows indicated in panel (A) or (B), which include the conformational changes of interest. The putative integrin global conformations were depicted by the cartoons before and after the said changes. (E,F) 100-point sliding variance of the displacement in (C) and (D) versus time. A decrease (E) or increase (F) in the thermal fluctuation (indicated by the values of σ^2 and dashed lines) followed integrin unbending (I) or bending (J), indicating the stiffening or softening of the integrin molecule, respectively.

Then the beads coating densities were titrated for lifetime measurements. The lifetime curve in Mn^{2+} manifested a clear catch-bond behavior in the force regime of

~5-~22 pN, with a gradual increase of lifetime along the increment of force. Over ~25 pN, the curve transitioned to slip-bond, so that the lifetime dropped while force increased, and finally approached zero around 50 pN (Fig. 3-1 D). In $\text{Ca}^{2+}/\text{Mg}^{2+}$, the lifetime curve originated from similar amplitude to Mn^{2+} at force close to zero; however, the catch-bond behavior was well suppressed and instead the lifetime curve showed a “slip bond” signature. This caused a significant downward shift of the lifetime in most forces. Especially, at 22 pN where the Mn^{2+} curve peaks, the lifetime in $\text{Ca}^{2+}/\text{Mg}^{2+}$ is shortened by ~3-fold. The above data was consistent with the well-known role of Mn^{2+} as an integrin activator. Moreover, unlike integrin $\alpha_L\beta_2$ which consistently manifests a “catch-slip” signature in $\text{Ca}^{2+}/\text{Mg}^{2+}$, Mn^{2+} and $\text{Mg}^{2+}/\text{EGTA}^{29}$, $\alpha_V\beta_3$ lifetime manifest different signatures in different cation conditions.

Catch-bond behavior was discovered on multiple receptors, like T-cell receptor¹⁰⁴, selectin¹⁰⁵, cadherin¹⁰⁶ and several integrins^{26,29,30}. It is regarded as a mechanism to resist force-induced bond dissociation. Catch-bond formation in integrin family is often related to the allosteric effect of integrin conformations. Thus, the abovementioned lifetime difference between the two cation conditions may suggest their preference of a certain conformation.

3.2.1.2 Observing $\alpha_V\beta_3$ bending and unbending conformational changes with BFP in a purified system

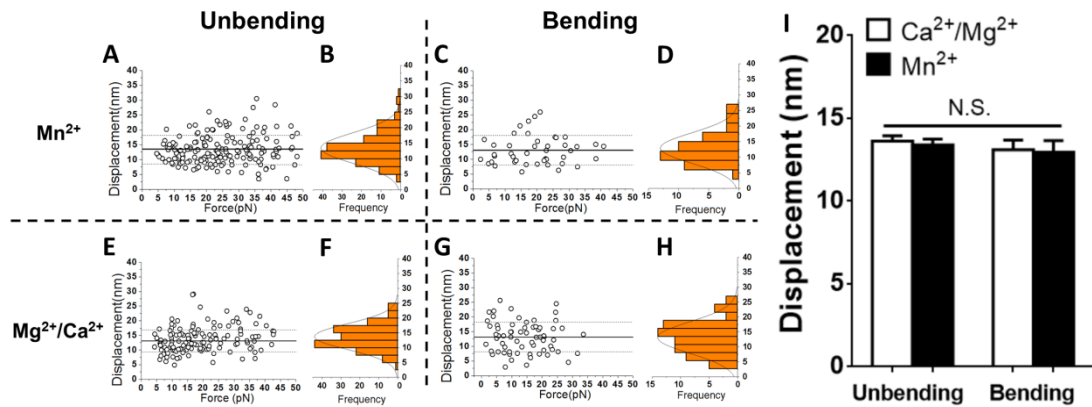


Figure 3-3. “Clamping force vs. displacement” scatter plots of recombinant $\alpha_V\beta_3$ unbending and bending events (A,C,E,G), and the distribution (B,D,F,H) and means \pm SEM (I) of the displacements in Mn^{2+} or Ca^{2+}/Mg^{2+} .

In distance/force clamp assay which holds the target bead at a fixed position, an integrin unbending event is signified by a concurrent decrease of force and thermal fluctuation level (Fig. 3-2 A,C,E), while bending by a concurrent increase of force and thermal fluctuation level (Fig. 3-2 B,D,F)⁶³. The rationale of this judgment is as following:

1) The distance between the probe micropipette tip and the target bead is fixed during the clamping phase, which is filled in by the serial linkage of RBC, probe bead and $\alpha_V\beta_3$ -FN_{III7-10} molecular complex. When the integrin extends, it claims more molecular length (Fig. 3-2 C insert), which causes the RBC to deform to engage less length, and that will be exhibited in the BFP signal as force decrease. Vice versa, when the integrin bends and claims less molecular length (Fig. 3-2D insert), RBC will be elongated.

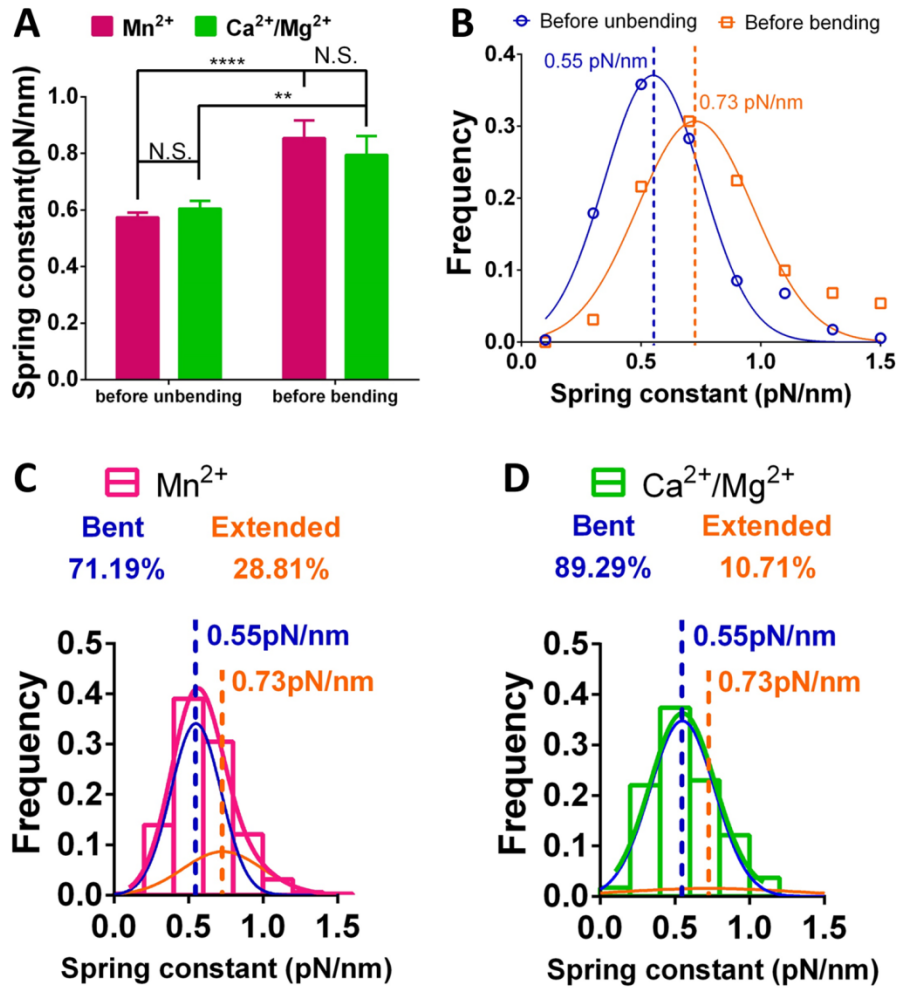


Figure 3-4. Determining the molecular complex stiffness with a bent/extended integrin and the initial fractions of integrin populations in bent and extended conformations in Mn²⁺ and Ca²⁺/Mg²⁺. (A) Mean \pm SEM of spring constants of the molecular complex (k_{mol}) prior to unbending (filled bars) or bending (empty bars) of the indicated integrin. * = $p < 0.05$, assessed by unpaired, two-tailed Student's t -test. (B) Data (points) and Gaussian fits (curves) of k_{mol} distributions of measured from the ramping phase of BFP cycles with lifetime events during which integrin unbending (blue) or bending (orange) was observed in the clamping phase. The means of the two Gaussian distributions were indicated by dashed lines with the values annotated. Data from Mn²⁺ and Ca²⁺/Mg²⁺ were pooled together. (C,D) Histograms (bars) and dual Gaussian fits (blue and orange curves were fits to the two sub-populations; color-matched curves were fits to the whole populations) of k_{mol} for $\alpha_v\beta_3$ pulled by FN_{III7-10} in Mn²⁺ (C) and Ca²⁺/Mg²⁺ (D). The calculated fractions of bent and extended sub-populations returned from the dual Gaussian fitting were indicated in each panel.

2) The integrin molecular stiffness is associated with the conformation. When the integrin is in the bent conformation, it is more flexible and softer, so that the thermal fluctuation will be less constrained, which results in a larger variation in the signal

(Fig. 3-2 E first half, 3-2 F second half). On the other hand, in the extended state the integrin becomes stiffer and thus the thermal fluctuation is better constrained (Fig. 3-2 E second half, 3-2 F first half). This difference in the molecular stiffness will be testified and confirmed via experiment results and analysis below.

In a bending/unbending signature, the force increase/drop divided by the RBC spring constant gives the integrin conformational change displacement. That is, how far the integrin headpiece is pulled away from proximity to the bead surface (unbending), or how far the headpiece pulls back (bending). Both unbending and bending occurred under all clamping forces where lifetimes are measurable, and the displacements all follow Gaussian distributions (Fig. 3-3 A-H). The average displacement (~13 nm) is indifferent to the clamping force or cation condition, and is comparable between unbending and bending events (Fig. 3-3 I).

As controls, LIBS-2 were coated on the bead surface and interrogate the integrin. The epitope of LIBS-2 resides in the β TD domain, which is in close proximity to the membrane¹⁰⁷ (Fig. 1-3), and thus should not be able to detect bending/unbending which only involve the headpiece movement. In agreement to that, LIBS-2 did not detect any bending or unbending events despite the long lifetimes (Table 3-1; Fig. 3-1 E).

3.2.1.3 Mn^{2+} cation condition favors the extended conformation of $\alpha_V\beta_3$ while Ca^{2+}/Mg^{2+} favors the bent conformation

Occurrence probability is defined as the chance of an extended/bent integrin undergoing bending/unbending conformational changes during the time window of BFP force-clamping phase. It reflects how frequent/easy the conformational changes could happen, which is a gauge of the energy barrier that needs to be overcome. In order to derive that information, the fractions of integrin in bent and extended conformations before ligand binding need to be known. Previous works have utilized EM imaging technologies to visualize the static images of different integrin conformations^{46,60,108}. In our system, the spring constant of the molecular complex was used to distinguish the conformations. As discussed in a previous publication, the $\alpha_L\beta_2$ integrin's spring constant depends on whether it resides in the bent (softer) or extended (stiffer) conformation⁶³.

Based on Section 2.6.2.4, we are able to measure the spring constant of the molecular complex, which assuming single receptor-ligand interaction, is the serial linkage of an integrin, an immobilizing antibody, a covalent linker, a FN_{III7-10} and a SA. Among these, the integrin is the only molecule in the complex that could contribute to changes in the spring constant. The spring constant of the molecular complex which later exhibited an unbending/bending conformational change event were measured. The rationale of distinguishing its conformational in the retraction phase is that, if it underwent unbending in the force-clamped phase, then in the retraction phase it has to adopt a bent conformation; while if it underwent bending in the force-clamped phase, then in the retraction phase it has to adopt an extended conformation. The bent and extended integrins induced a significant difference in the

overall spring constant of the molecular complex, which is softer with the integrin bent and stiffer with it extended (Fig. 3-4 A). Since the cation condition did not affect the spring constant (Fig. 3-4 A), we combined the spring constant data from both cation conditions and binned them to derive a column plot of “frequency vs. spring constant”. By assuming that the spring constant obeys a Gaussian distribution, we separately fit the data of bent and extended integrin group and then derived the mean spring constant to be 0.55 and 0.73 pN/nm respectively (Fig. 3-4 B).

Table 3-1. Statistics of the recombinant $\alpha_v\beta_3$ binding to FN_{III7-10} lifetime events and bending/unbending conformational change events under different conditions

Surface	Bead coated with	Condition/Mutation	#Lifetime events	Bent fraction	Extended fraction	Unbending		Bending	
						#Events	Probability	#Events	Probability
Bead	FN _{III7-10}	Mn ²⁺	1424	0.7119	0.2881	195	19.23%	43	10.48%
		Ca ²⁺ /Mg ²⁺	1847	0.8929	0.1071	164	9.14%	70	34.08%
		Mn ²⁺ /NEM	106	1	0	8	7.55%	0	N.A.
		Ca ²⁺ /Mg ²⁺ /WOW-1	310	0.889	0.111	21	6.77%	3	8.72%
		Ca ²⁺ /Mg ²⁺ /LIBS-2	183	0.203	0.797	5	13.46%	0	0%
	LIBS-2	Ca ²⁺ /Mg ²⁺	186	0	1	0	0%	0	0%
Cell	FN _{III7-10}	WT	1203	55.79%	44.21%	151	22.50%	59	11.09%
		D723R	1252	13.95%	86.05%	83	47.52%	3	0.28%
		L138I	1685	23.53%	76.47%	87	21.94%	4	0.31%
	Fg		1384			120	15.54%	49	8.01%
	LIBS-2	WT	350	55.79%	44.21%	0	0.00%	0	0.00%
	AP3		371			19	9.18%	4	2.44%

Following that, the spring constants of the molecular complex under Mn²⁺ condition were calculated and collected from no-conformational-change lifetime events (n = 200), and fit with a double-Gaussian distribution, with the two means pre-set as 0.55 and 0.73 pN/nm. Based on the fitting result, the fractions of bent and extended integrins under Mn²⁺ condition were respectively 71.19% and 28.81% (Fig. 3-4 C). Similarly, the fractions under Ca²⁺/Mg²⁺ condition were calculated to be 89.29% and 10.71% (Fig. 3-4 D).

Under Mn^{2+} condition, a total of 1424 lifetime events (including those with bending/unbending conformational changes) were collected, which based on the fraction calculation, were from 1014 bent and 410 extended integrins (Table 3-1). In all lifetime events, 195 exhibited unbending conformational changes, which yielded an occurrence probability of $195 / 1014 = 19.23\%$. Similarly, the occurrence probability of bending was calculated to be 10.48%. Under $\text{Ca}^{2+}/\text{Mg}^{2+}$ condition, only 9.14% of the bent integrins underwent unbending, while as many as 34.08% of the extended integrins underwent bending (Table 3-1).

The fact that a higher fraction of the integrin population adopts an extended conformation in Mn^{2+} than $\text{Ca}^{2+}/\text{Mg}^{2+}$ in the solution, and that under force the integrin has a higher unbending occurrence probability but a lower bending occurrence probability in Mn^{2+} , both indicated that Mn^{2+} favors the extended conformation of $\alpha_v\beta_3$.

In a soluble form, the β_3 antibody WOW-1 functionally blocks the active form of the integrin, while LIBS-2 facilitates the ectodomain extension^{107,109}. The addition of soluble WOW-1 did not change the fraction of the bent/extended integrins available for $\text{FN}_{\text{III7-10}}$ binding (Table 3-1), but narrowed the force regime of the integrin lifetime curve to 0-30 pN and shortened the lifetime in the force regime of > 15 pN (Fig. 3-1). The probabilities of bending and unbending during interrogation were both lowered (Table 1), probably due to the shortened lifetime which constrained the time window for detection (Fig. 3-1). In comparison with WOW-1, soluble LIBS-2 brought

most of the integrins to an extended conformation and eliminated all bending events (Table 3-1). About 13.5% of the bent integrins underwent unbending during interrogation, the fraction of which slightly higher than in the absence of LIBS-2, probably due to the prolonged lifetime around 25 pN (Fig. 3-1D).

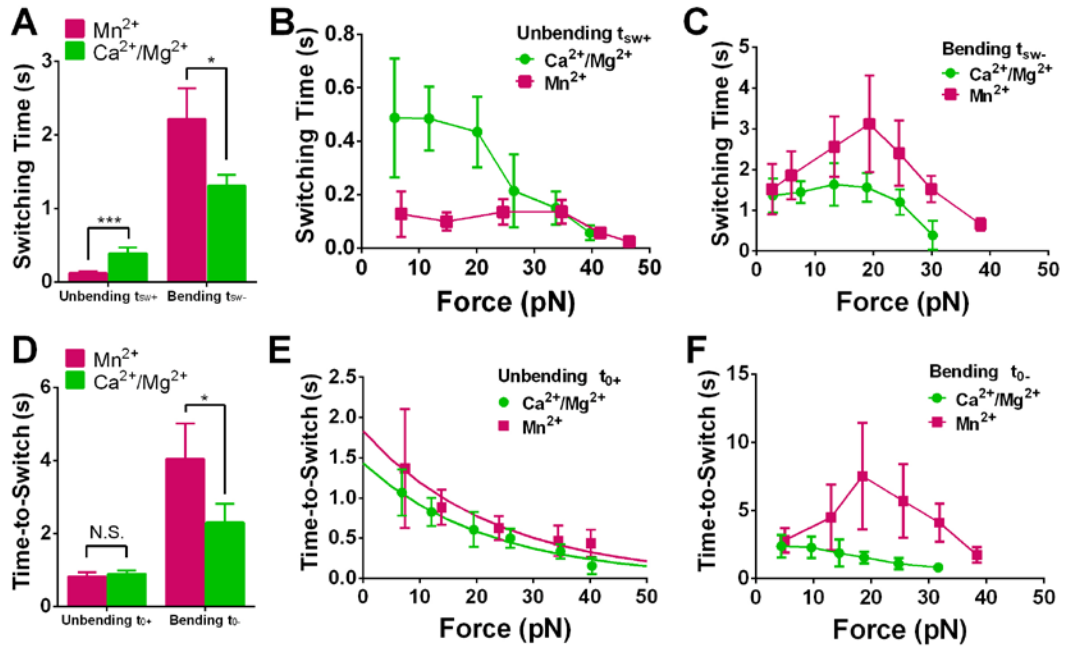


Figure 3-5. Recombinant integrin bending and unbending switching time $t_{sw\pm}$ (A-C) and time-to-switch $t_{0\pm}$ (D-F) in Mn^{2+} (magenta) and Ca^{2+}/Mg^{2+} (green). A and D averaged the data over all forces, while B, C, E, F plot the data against clamping force. Error bars: SEM.

Two parameters from the BFP signatures characterize the conformational change dynamic processes: time-to-switch ($t_{0\pm}$, defined in Fig. 3-2 A,B) and switching time ($t_{sw\pm}$, defined in Fig. 3-2 C,D), which gauge the underlying energy to be overcome. In both cation conditions, bending requires a longer t_0 and t_{sw} than unbending (Fig. 3-5 A,D). Compared to the physiological Ca^{2+}/Mg^{2+} condition, Mn^{2+} shortened the unbending t_{sw+} and did not affect the t_{0+} , but prolongs the t_{0-} and t_{sw-} of bending (Fig. 3-5 A,D). Plotting them against different clamping forces revealed that the above

observations generalize under most forces (Fig. 3-5 B,C,E,F). Moreover, both t_{0+} and t_{sw+} of unbending monotonically decreased as the clamping force increased, which was reasonable considering that the direction of force aligns with the extension of the integrin, so that a higher force provides more energy to help overcome the energy well for unbending (Fig. 3-5 B,E). On the contrary, the clamping force works on the opposite direction than bending so that bending should adopt a slower kinetics under high forces. This was consistent with the bending data under lower forces, but show discrepancy under higher forces, probably due to the constraint of the binding lifetime length, which prevented the detection of extremely slow conformational changes (Fig. 3-5 C,F). In support of this, the bending t_{0-} and t_{sw-} are comparable to the values of bond lifetimes (compare Fig. 3-5 C,F and Fig. 3-6 B,C).

The fact that the bending requires a longer t_0 and t_{sw} than unbending was in agreement with that bending occurred less frequently than unbending in Mn^{2+} (Table 3-1, 10.48% vs. 19.23%), but seems to disagree with the higher frequency of bending in Ca^{2+}/Mg^{2+} (Table 3-1, 34.08% vs. 9.14%). This suggested that more complicated mechanisms may exist to affect the occurrence of integrin conformational changes. One reasonably hypothesized possibility is that, a subpopulation of the bent integrin is “locked” in the presence of Ca^{2+}/Mg^{2+} , so that they are unable to undergo unbending even under forces. The inertness of this subpopulation counteracted on the high frequency of the active subpopulation and compromised the overall probability of unbending.

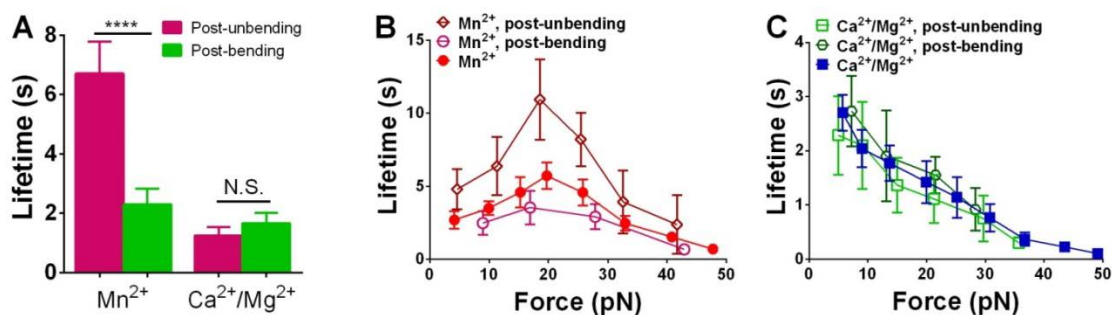


Figure 3-6. Recombinant integrin post-bending and -unbending lifetime, averaged over all forces (A), and “lifetime vs. force” curves in comparison with the lifetime curves without bending/unbending in Mn²⁺ (B) and Ca²⁺/Mg²⁺ (C).

3.2.1.4 Bending/unbending conformational change of $\alpha_V\beta_3$ shortens/prolongs its lifetime in Mn²⁺ but has no effect in Ca²⁺/Mg²⁺

How the integrin conformational changes regulate its binding capacity is an intriguing and important question to ask, which underlies the allosteric effects in integrin and acts in part as the mechanism of integrin outside-in and inside-out signaling on cells’ surface.

Of each integrin-FN_{III7-10} lifetime event in which a bending or unbending event was observed, the fraction of lifetime after bending/unbending was collected and respectively termed as post-bending and post-unbending lifetime. Results from cell surface LFA-1 have indicated that the bent/extended conformation of the integrin has a strong impact to the ligation bond kinetics⁶³. In $\alpha_V\beta_3$ system under the Mn²⁺ cation condition, a somewhat similar behavior was observed. The post-unbending lifetime was much longer than post-bending under all forces; the lifetime collected from events without bending/unbending, which based on the spring constant analysis result was from a mixed population of bent and extended integrins (Fig. 3-4 C), manifested

a lifetime level in between of post-bending and post-unbending (Fig. 3-6 A,B). Interesting, all three curves showed a catch-slip-bond behavior. The forces under which the lifetime curve peaks were similar among all three (17-20 pN), whereas their peak values were drastically distinct, being 10.9, 5.7 and 3.6 seconds for the post-unbending, average, and post-bending lifetime respectively (Fig. 3-6 B).

Different than in Mn^{2+} , in Ca^{2+}/Mg^{2+} the post-unbending and post-bending lifetimes were comparable and both curves overlapped well with the lifetime curve without bending/unbending, manifesting slip-bond behaviors (Fig. 3-6 A,C). This strongly suggested that in such a physiological cation condition, the integrin adopting a bent or unbending conformation does not affect its binding lifetime. This conclusion contradicts with the conventional view that the integrin ectodomain extension is a sign of integrin activation which is accompanied by an up-regulation of binding capacity. However, to be noted, the integrin extension under this circumstance was only in the presence of ligand engagement and force pulling through the ligand (outside-in signaling), which cannot represent the scenario where the integrin is regulated from the cytoplasmic terminus (inside-out signaling).

3.2.2 Observing ligand binding and bending/unbending conformational changes of cell surface integrin $\alpha_V\beta_3$ regulated by mutations, force and ligands

3.2.2.1 Force dependency of cell surface $\alpha_V\beta_3$ ligand binding and its regulation by functional mutations

To study the behaviors of $\alpha_v\beta_3$ on cell surface and compare with the purified system results, mouse lung endothelial cells (mLECs) were transfected with three types of human $\alpha_v\beta_3$ (WT, D723R, L138I) and tested in BFP experiments (Fig. 3-7 A). Again, FN_{III7-10}-coated beads was used. Experiments were only performed in the physiological cation condition of 1mM $\text{Ca}^{2+}/\text{Mg}^{2+}$, and Mn^{2+} was not used considering its toxicity to cells.

D723R is a point mutation in the cytoplasmic tail of β_3 subunit (Fig. 3-7 B)⁸². It destabilizes the TMD (transmembrane domain)-tail interactions between α - and β -subunits and causes tail separation. By doing so, it shifts the equilibrium of integrin activity towards activation. L138I, on the other hand, resides in the β I-domain of β_3 subunit, and promotes ectodomain extension and activates the integrin (Fig. 3-7 B)¹⁰¹.

All three cell lines expressing WT, D723R and L138I integrins resulted in high frequencies when binding to FN_{III7-10} (Fig. 3-7 C). Non-transfected cells against FN_{III7-10} and WT integrin transfected cells against SA both exhibited an adhesion frequency of ~5%, which confirmed the binding specificity of the integrin and the ligand respectively (Fig. 3-7 C). For all experiments following that, the binding frequencies of the three transfected cell lines were titrated by shortening the cell-bead contact time to ~20%, which ensured predominantly single-molecular interactions.

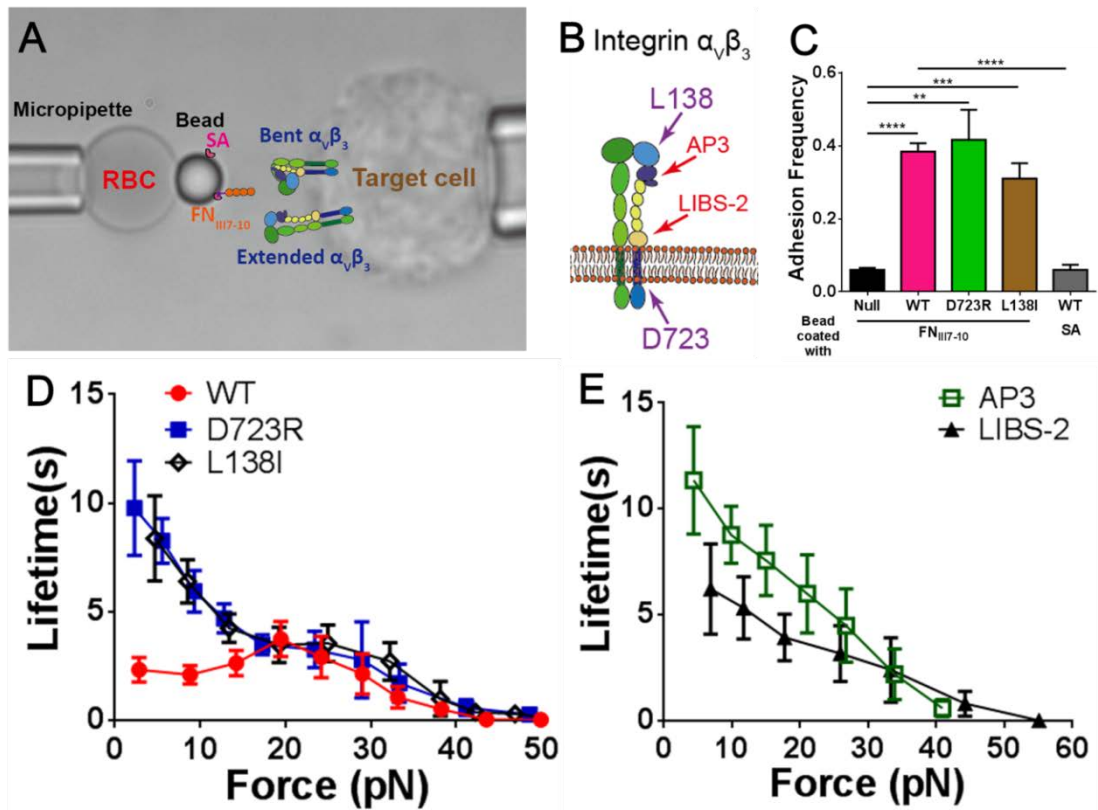


Figure 3-7. BFP setup and binding kinetics results of cell surface $\alpha_v\beta_3$ binding to FN_{III7-10}. (A) BFP setup for studying cell surface $\alpha_v\beta_3$. FN_{III7-10} acts as the interrogating ligand, and a mLEC expressing human integrin $\alpha_v\beta_3$ acts as the target cell. (C) Sketch of a $\alpha_v\beta_3$ integrin with the residue D723 and L138 and the binding epitope of AP3 and LIBS-2 indicated. (D) Specificity test results. (E) Lifetime vs. force curves of WT, D723R and L138I $\alpha_v\beta_3$ binding to FN_{III7-10}. (F) Lifetime vs. force curves of WT $\alpha_v\beta_3$ binding to AP3 and LIBS-2. Error bars: SEM.

The “lifetime vs. force” curve of WT $\alpha_v\beta_3$ manifested a “slip-catch-slip” triphasic trend that resembled the “GPIIb α -VWFA1” binding lifetime published before (Fig. 3-7 E)⁸⁸. This suggested an activating role of force, which was more prominent when the force was larger so that the “slip” trend of the integrin was converted to “catch”, ensuring enduring binding. This trend change was not observed in the purified system under the same condition (Fig. 3-1 D), probably due to the structural difference of the recombinant integrin that constrained certain conformational changes like tail separation and in turn restricted the activation. In sharp contrast to

WT, the D723R and L138I $\alpha_v\beta_3$ resulted in highly similar “slip-bond” lifetime curves, which overlapped with WT at forces higher than 20 pN but split at lower forces, and reached as high as 10 s when the force approached zero (Fig. 3-7 E). As controls, WT integrin binding to two antibodies, AP3 and LIBS-2 both manifested slip-bonds (Fig. 3-7 F).

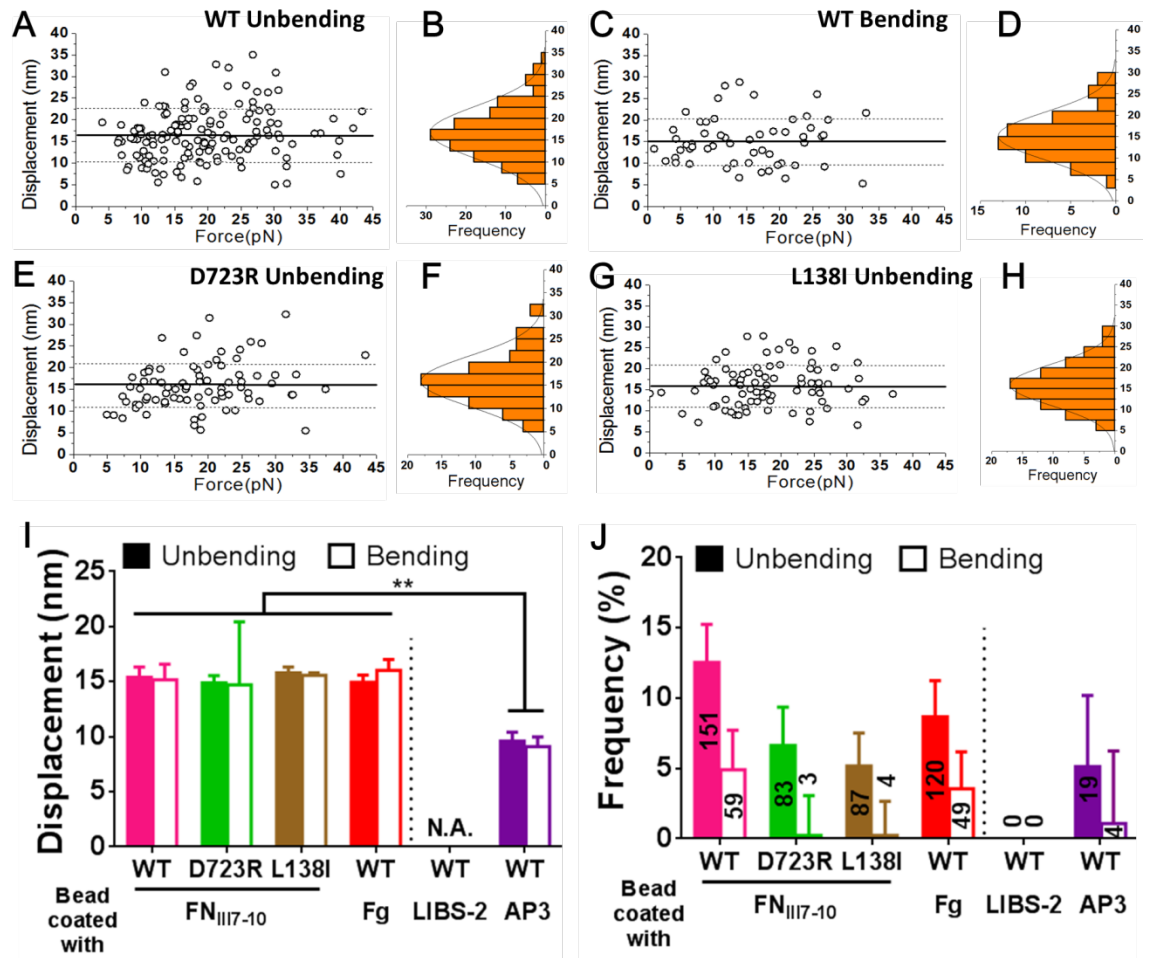


Figure 3-8. Characterization of the cell surface $\alpha_v\beta_3$ bending and unbending events. (A,C,E,G) Scatter plots of displacements ($= \Delta f / k_{BFP}$ where the Δf measurement was shown in Fig. 2, A and B and $k_{BFP} = 0.3$ pN/nm is the preset spring constant of the RBC) vs. pre-switch force of unbending (A,E,G) and bending (C) events of WT (A,C), D723R (E) and L138I (G) $\alpha_v\beta_3$ pulled via an engaged FN_{III7-10}. Mean \pm SD of displacements are shown as solid and dashed lines. (B,D,F,H) Histograms (bars) and Gaussian fits (curves) of the data from A, C, E, and G. (I,J) Displacement (I, means \pm SEM) and frequency (J, error bar = SEM estimated by the binomial distribution of events whose numbers are indicated) of unbending (filled bar) and bending (empty bar) of indicated $\alpha_v\beta_3$ pulled by different ligands (FN_{III7-10},

Fg)/antibodies (LIBS-2, AP3). ** = $p < 0.01$, assessed by unpaired, two-tailed Student's *t*-test. N.A. = not applicable due to lack of data.

3.2.2.2 Observation of integrin $\alpha_V\beta_3$ bending/unbending conformational change on cell surface and its regulation by functional mutations

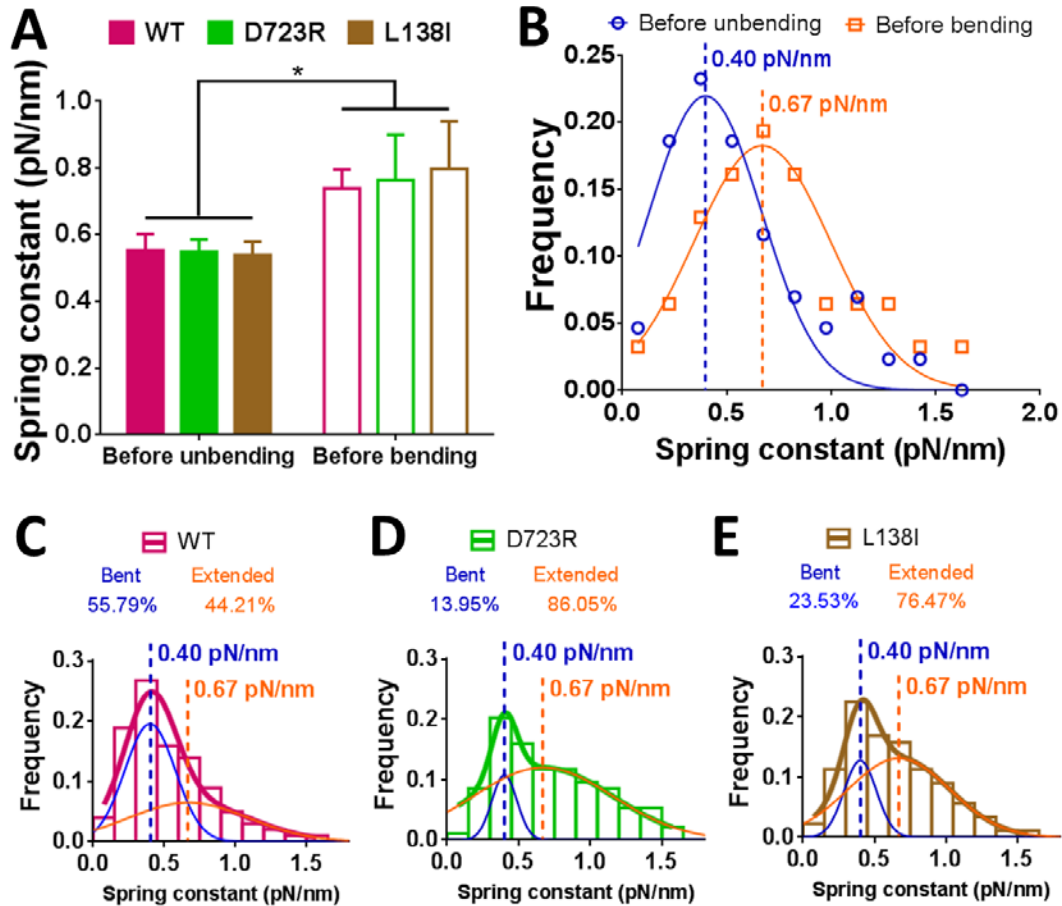


Figure 3-9. Determining the initial fractions of cell surface integrin subpopulations in bent and extended conformations. (A) Mean \pm SEM of spring constants of the molecular complex (k_{mol}) prior to unbending (filled bars) or bending (empty bars) of the indicated integrin. * = $p < 0.05$, assessed by unpaired, two-tailed Student's *t*-test. (B) Data (points) and Gaussian fits (curves) of k_{mol} distributions of measured from the ramping phase of BFP cycles with lifetime events during which integrin unbending (blue) or bending (orange) was observed in the clamping phase. The means of the two Gaussian distributions were indicated by dashed lines with the values annotated. Data from WT, D723R and L138I were pooled together, assuming that the two mutations had negligible effects in the integrin stiffness, as suggested by panel (A). (C-E) Histograms (bars) and dual Gaussian fits (blue and orange curves were fits to the two sub-populations; color-matched curves were fits to the whole populations) of k_{mol} for WT (C), D723R (D) and L138I (E) $\alpha_V\beta_3$ pulled by FN_{III7-10}. The calculated fractions of bent and extended sub-populations returned from the dual Gaussian fitting were indicated in each panel.

Similar to purified system results, both bending and unbending events were observed from cell surface integrins for all three genotypes (Table 3-1).

The displacements of WT $\alpha_V\beta_3$ bending events and WT, D723R and L138I unbending events were plotted against the clamping forces under which the conformational change occurred. To note, the bending of D723R and L138I $\alpha_V\beta_3$ occurred extremely rarely (Table 3-1), and thus could not be plotted in this way. From the scatter plots it could be seen that integrin unbending evenly occurred under all clamping forces except for the low and high extremes, while bending favored lower clamping forces (Fig. 3-8 A,C,E,G). The displacements of these four analyzable conditions all followed Gaussian distributions, which agreed with the purified system results (Fig. 3-8 B,D,F,H). The average displacements of WT, D723R and L138I bending and unbending were all ~15 nm (Fig 3-8 I), which were indifferent to the integrin genotype or the direction of the conformational change, and ~2 nm longer than the purified system displacements (Fig. 3-3 I), probably because of the structural difference between the recombinant and cell-expressed integrin molecules.

The frequency of observing unbending was much higher than bending in all three integrin genotypes, especially the two GOF MTs, where bending events were extremely rare (Fig. 3-8 J).

Based on Section 2.6.2.4, the molecular complex stiffness before unbending and before bending was collected, which were indifferent to the genotype of the integrin (Fig. 3-9 A). Considering that, the stiffness of before unbending and before bending

subpopulations from all three genotypes were pooled together, each of which was well fitted by a Gaussian distribution (Fig. 3-9 B, blue curve and orange curve). The means of the two fits, 0.40 and 0.67 pN/nm, were the average spring constant of the molecular complex upon the integrin being bent and extended, respectively.

Further fitting using these two average spring constants showed that the fractions of bent and extended populations of WT $\alpha_v\beta_3$ were 55.79% and 44.21% (Fig. 3-9 C), respectively, which by calculation resulted in probabilities of unbending and bending under force to be 22.50% and 11.09% (Table 3-1). The two GOF MTs had most of the integrins in the extended conformation before force pulling (Fig. 3-9 D,E). By calculation, the occurrence probabilities of unbending/bending events were 47.52/0.28% (D723R) and 21.94/0.31% (L138I) (Table 3-1). Compared to WT, these results indicated that both mutations strongly facilitate the extension of the integrin and impede bending. To note, because the lifetime length determines the time window of observing the conformational changes, the differences between WT, D723R and L138I lifetimes may also partially contribute to the abovementioned probability differences.

When the bent and extended conformations of the integrin reach equilibrium in a dynamic fashion, the following equation should be valid: (Extended fraction) *

(Unbending rate) = (Bent fraction) * (Bending rate). Thus:

$$\frac{(\text{Extended fraction})}{(\text{Bent fraction})} = \frac{(\text{Bending rate})}{(\text{Unbending rate})} \quad (\text{Equation 3-1})$$

In the scenario of force pulling through BFP manipulation, because the external force exerted onto the molecular complex was in the direction of integrin extension, it is reasonable to hypothesize that force facilitates unbending while inhibits bending, and thus shifts the conformation equilibrium towards extension. To test this hypothesis, the fractions of extended and bent integrin subpopulations under force were estimated. Because the lifetimes of bent and extended integrins are comparable (discussed in Section 3.2.2.4), $(\text{Probability of unbending}) / (\text{Probability of bending}) = (\text{Unbending rate}) / (\text{Bending rate})$. Thus, $(\text{Extended fraction}) / (\text{Bent fraction}) = (\text{Probability of unbending}) / (\text{Probability of bending})$. Based on this equation and the Probabilities of unbending/bending in Table 1, we are able to derive the equilibrium state of WT (33.03% bent, 66.97% extended), D723R (0.59% bent, 99.41% extended) and L138I (1.39% bent, 98.61% extended) under force. Comparing these numbers with those under zero-force (Table 1, Bent fraction and Extended fraction) revealed that the equilibrium was drastically shifted towards the extended state under force regulation.

3.2.2.3 Kinetics of integrin conformational changes and their regulation by force and mutations

The shifts of the bent and extended integrin population fractions following the introduction of the mutations D723R and L138I to the integrin, as well as the differences in the bending and unbending occurrence frequencies between the WT and MTs clearly indicated that the two mutations D723R and L138I realized a more

stable state for the extended conformation while disrupting the stability of the bent conformation as compared to WT.

To derive more details in the underlying mechanisms of how the two mutations shift the equilibrium between the bent and extended conformations, the time-to-switch (t_0) and switching time (t_{SW}) of the bending and unbending events were collected. Similar to results from the purified system, WT bending t_0 and t_{SW} were both much longer than unbending, which held true under all clamping forces (Fig. 3-10 A-D). This is probably due to the force pulling on the integrin, which facilitates unbending and inhibits bending. The mutants D723R and L138I both caused a drastic decrease of the unbending t_{sw} , so that their averages were much smaller than the WT, and both curves were rotated counterclockwise around ~ 32 pN where all three curves converged at ~ 0 s. However, only D723R shortened the t_{0+} , while L138I had negligible effects (Fig. 3-10 B,D). This indicated that both D723R and L138I substantially accelerated integrin unbending, but only D723R destabilized the bent conformation. This discovery should partially account for the shifted equilibrium between the bent and unbending integrin populations that existed in the scenario of both mutations.

Because the force imposed onto the integrin through ligand binding was towards the direction of integrin extension, it provides a positive/negative work to the integrin during unbending/bending. This means that the force should affect the kinetics of integrin bending/unbending, in the way that a higher force accelerates and stabilizes

the unbending but decelerates and destabilizes bending. Agreeing with that, the unbending t_{sw+} and t_{0+} of all three genotypes monotonically decreases along with force increase, which is consistent with the previously reported cell surface integrin $\alpha_L\beta_2$ conformational changes. Interestingly, the WT bending t_{sw-} and t_{0-} first increased and then decreased along with force instead of monotonically increasing (Fig. 3-10 C,D). This is probably due to the constraint of the integrin-ligand bond lifetime: the bending or unbending events being observable in the BFP system require them to occur prior to the dissociation of the bond. Thus, those bending events that occurred slowly may not be recorded. This constraining effect becomes more influential when the kinetics of the conformational changes were comparable or slower than the binding kinetics. Indeed, the $\alpha_V\beta_3$ -FN_{III7-10} lifetime (Fig. 3-10 E) was at the same scale as t_{sw-} and t_{0-} under all forces. More importantly, the average lifetime vs. force curve also manifested a catch-slip bond behavior, with the “catch” regime to be 0 - ~20 pN, consistent with the t_{sw-} and t_{0-} vs. force curves.

In the previous section, tensile force was shown to shift the conformation equilibrium towards extension. However, whether this was sensitive to the level of force was not clear. Because Unbending/Bending t_0 is the reciprocal of Unbending/Bending rate, Equation 3-1 can be converted to:

$$\frac{(\text{Extended fraction})}{(\text{Bent fraction})} = \frac{(\text{Unbending } t_0)}{(\text{Bending } t_0)} \quad \text{Equation 3-2}$$

showing that the ratio of time-to-extend to time-to-bend can directly reflect the equilibrium between extended and bent conformation. Thus, the ratio of WT $\alpha_V\beta_3$

time-to-extend to time-to-bend vs. clamping force was calculated, which exhibited an obvious force-dependency (Fig. 3-10 F, filled circles). The zero-force ratio was calculated by the ratio of the extended to bent integrin sub-populations estimated from Fig. 3-9 E according to Equation 3-2, which exhibited a smooth extrapolation from the points under force (Fig. 3-10 F, open circle). Under all forces, the ratio of time-to-extend to time-to-bend monotonically decreased with force increase, indicating that the conformation equilibrium was gradually shifted towards extension (Fig. 3-10F).

3.2.2.4 Lack of effect of $\alpha_V\beta_3$ bent/extended conformation or bending/unbending on its ligand dissociation rate under force

In the purified system, in $\text{Ca}^{2+}/\text{Mg}^{2+}$ the WT integrin lifetime was not affected by the bending or unbending conformational change (Fig. 3-6 C). Consistent with that, in the cell-surface system, the WT post-bending and post-unbending lifetimes appeared to be comparable (Fig. 3-11 A). By segregating the lifetime events into different force regimes, the post-bending and post-unbending lifetimes were shown to nearly overlap under all forces, which also aligned well with the average lifetime curve derived from measurements not containing bending/unbending events (Fig. 3-11 B). Similarly, the post-unbending lifetime curve of the two MTs, D723R and L138I, also overlapped with their respective average lifetime curve (Fig. 3-11 C,D).

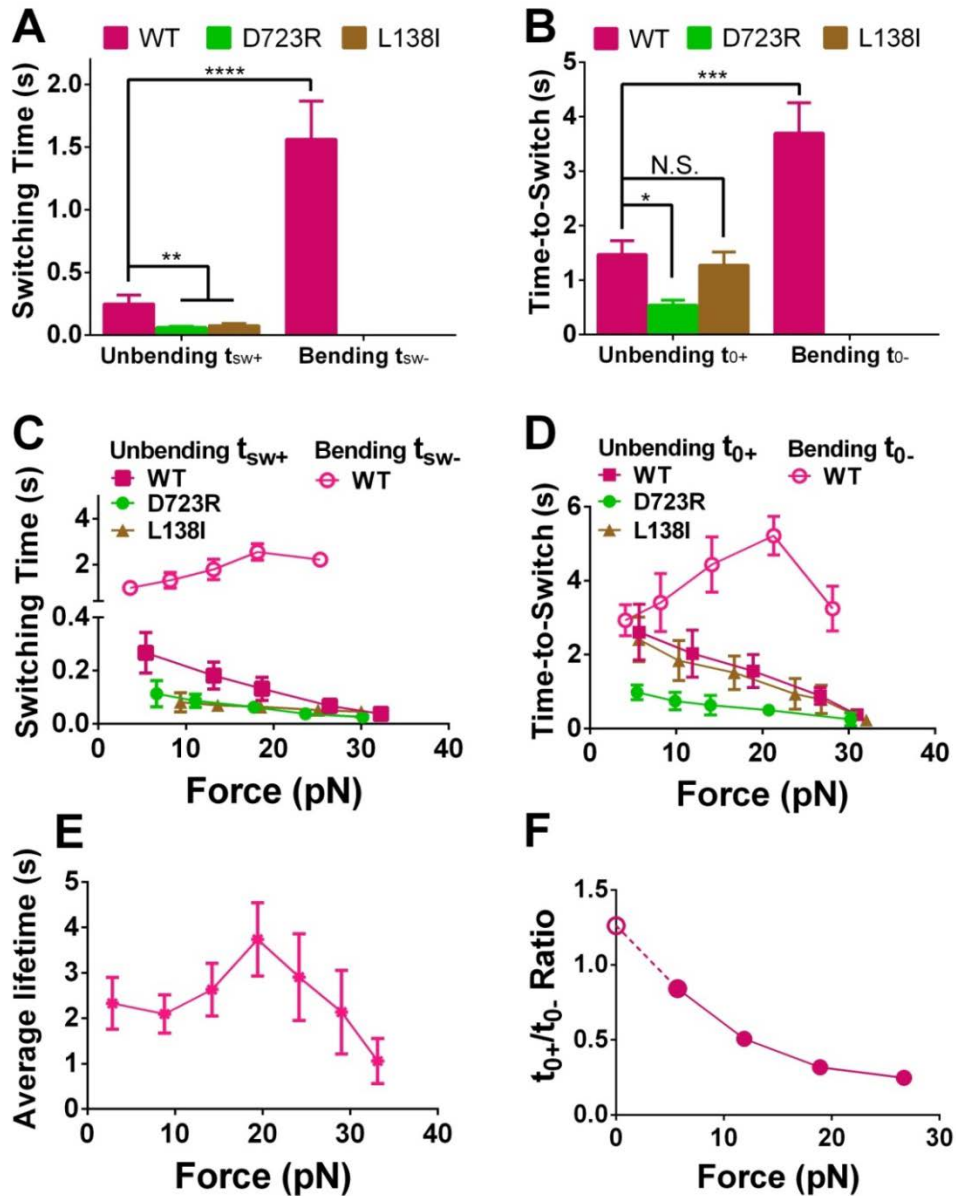


Figure 3-10. Analyzing the dynamics of the cell surface integrin conformational changes. (A,B) Mean \pm SEM of the switching time ($t_{sw\pm}$, A) or time-to-switch ($t_{0\pm}$, B) averaged over all clamping forces. (C,D) Bending (open symbols) and unbending (filled symbols) $t_{sw\pm}$ (C) or $t_{0\pm}$ (D) vs. pre-switch force curves for indicated integrins (Mean \pm SEM). In A-D, bending of D723R and L138I $\alpha_v\beta_3$ occurred too infrequently to obtain sufficient data for statistically stable characterization thus were not summarized. (E) WT $\alpha_v\beta_3$ -FN_{III7-10} lifetime vs. force data from measurements not containing bending and unbending events, to show the potential constraints of the receptor–ligand bond lifetime to the observable $t_{sw\pm}$ (C) and $t_{0\pm}$ (D). (F) Ratio of WT $\alpha_v\beta_3$ time-to-unbend t_{0+} to time-to-bend t_{0-} vs. clamping force, showing the force-dependent bent/extended state equilibrium. The solid circles were calculated from data in panel D. The value of the open circle was the ratio of the extended to bent integrin sub-populations estimated from Fig. 4E. N.S. = not significant; * = $p < 0.05$; ** = $p < 0.01$; *** = $p < 0.001$ **** = $p < 0.0001$, assessed by unpaired, two-tailed Student's *t*-test.

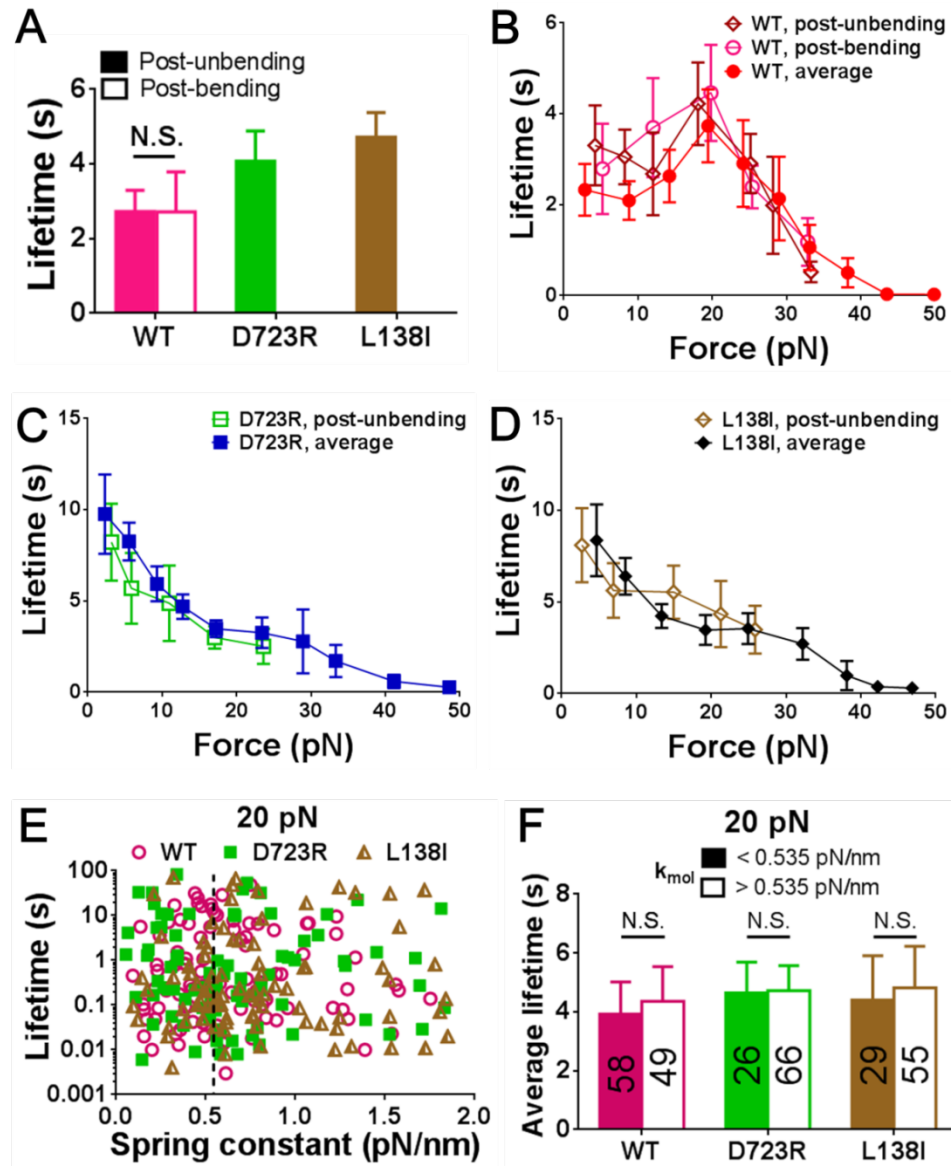


Figure 3-11. Lack of effect of cell surface $\alpha_v\beta_3$ bending/unbending on its ligand dissociation rate under force. (A) Mean \pm SEM of the post-unbending/bending lifetime averaged over all clamping forces. (B-D) Average, post-bending and post-unbending bond lifetime (mean \pm SEM) vs. force curves of WT (B), D723R (C) and L138I (D) $\alpha_v\beta_3$ integrin. The average lifetime was from measurements not containing bending/unbending events. The lower force regime (< 35 pN) fragment of the WT average lifetime curve (B, red filled circle) is identical to Fig. 5 F. Bending of D723R and L138I $\alpha_v\beta_3$ occurred too rarely to obtain sufficient data for statistically stable characterization. (E) Scatter plots of WT (magenta circle), D723R (green rectangle) and L138I (brown triangle) $\alpha_v\beta_3$ -FN_{III7-10} bond lifetime vs. molecular complex spring constant under 20 pN clamping force. The molecular complex spring constant was measured during the ramping phase as described in Fig. 4 A and B. (F) Average lifetimes of two subgroups of integrins with different molecular complex spring constants, $k_{mol} >$ and < 0.535 pN/nm (dashed line in panel (E)). The number of events is indicated in each bar. N.S. = not significant, assessed by unpaired, two-tailed Student's *t*-test.

To further confirm that the initial integrin conformation does not affect its bond dissociation, the lifetimes under 20 pN clamping force of all three genotypes were plotted against the molecular complex stiffness k_{mol} , given that the stiffness is an indicator of the integrin conformation, which showed no correlation at all (Fig. 3-11 E). Segregating the lifetime events according to $k_{mol} < \text{or} > 0.535$ pN/nm (the average of k_{bent} and $k_{extended}$), which acted as a rough method to separate bent and extended integrins, also showed no difference in the average lifetime (Fig. 3-11 F), suggesting that the lifetime is not dependent on k_{mol} .

This suggested that in the physiological cation condition $\text{Ca}^{2+}/\text{Mg}^{2+}$, the binding strength of integrin $\alpha_V\beta_3$ was not dependent on the extended/bent conformation or bending/unbending conformational changes, but rather probably some other conformational changes, like tail separation or hybrid-domain swing-out. However, to be noted, the bond lifetime is only a reflection of the off-rate, thus no prediction should be made on the on-rate or affinity of the binding.

3.2.2.5 Observation of fibrinogen-bound integrin $\alpha_V\beta_3$ bending/unbending conformational change

The fact that the probabilities of WT $\alpha_V\beta_3$ bending/unbending conformational changes reported by AP3 were much lower than by FN_{III7-10}, despite much higher lifetimes in most of the forces (compare Fig. 3-7 F, dark green curve with Fig. 3-11 B, red curve), raised the possibility that these conformational changes are ligand-discriminating. To test this hypothesis, fibrinogen, another ligand for $\alpha_V\beta_3$,

was used to interrogate the WT $\alpha_V\beta_3$. Both bending and unbending conformational change events were observed, the displacements of which distributed as single-peak Gaussians respectively (Fig. 3-12 A-D). The average bending and unbending displacements were both ~ 15 nm, which were identical to those of FN_{III7-10}-bound $\alpha_V\beta_3$ (Fig. 3-8 I). However, the frequency and probability of both bending and unbending of fibrinogen-bound WT $\alpha_V\beta_3$ were slightly lower as compared to FN_{III7-10}-bound (Fig. 3-8 J and Table 3-1), suggesting that fibrinogen may be unfavorable to the bending/unbending conformational changes.

The unbending t_{sw+} of fibrinogen-bound $\alpha_V\beta_3$ was comparable to FN_{III7-10}-bound (compared Fig. 3-10 C and Fig. 3-12 E, both curves with magenta solid squares), but t_{0+} appeared to be slightly longer under all forces (compared Fig. 3-10 D and Fig. 3-12 F, both curves with magenta solid squares), which may at least partially explain the lower probability of unbending. On the other hand, the bending t_{sw-} of fibrinogen-bound $\alpha_V\beta_3$ was longer than FN_{III7-10}-bound (compared Fig. 3-10 C and Fig. 3-12 E, both curves with magenta open circles), while the t_{0-} comparable at lower forces and shorter at higher forces (compared Fig. 3-10 D and Fig. 3-12 F, both curves with magenta open circles). To note, however, because the fibrinogen- $\alpha_V\beta_3$ lifetime is a slip bond (Fig. 3-12 G, solid red circles) while the FN_{III7-10}- $\alpha_V\beta_3$ lifetime is a catch-slip bond (Fig. 3-10 E), the lifetime of $\alpha_V\beta_3$ binding to fibrinogen was longer than FN_{III7-10} at low forces but became shorter when force is larger than 15 pN, which potentially brought more constraints to the observable $t_{0\pm}$ at higher forces.

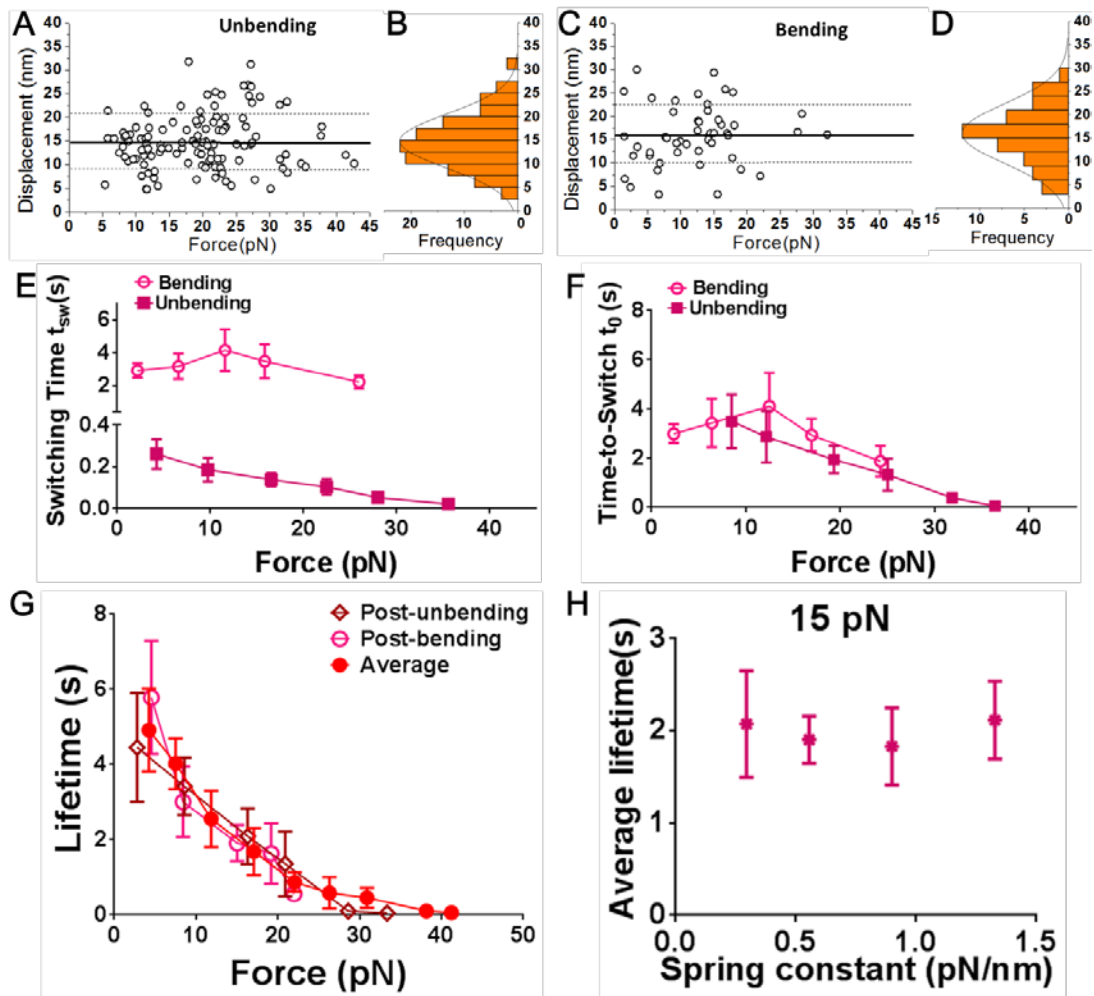


Figure 3-12. Observing bending/unbending conformational changes of fibrinogen-bound WT $\alpha_v\beta_3$ on cell surface. (A,C) Scatter plots of displacements vs. pre-switch forces of the unbending (A) and bending (C) events. Mean \pm SD of displacements are shown as solid and dashed lines. (B,D) Histograms (bars) and Gaussian fits (curves) of the data from A and C. (E,F) Bending and unbending switching t_{sw} (E) or t_0 (F) vs. pre-switch force curves (Mean \pm SEM). (G) Average, post-bending and post-unbending bond lifetime vs. force curves (Mean \pm SEM). The average lifetime was from measurements not containing bending/unbending events. (G) Mean \pm SEM, $\alpha_v\beta_3$ -fibrinogen average lifetime vs. molecular complex spring constant under 15 pN clamping force.

The post-bending, post-unbending and average lifetime curves of fibrinogen-bound $\alpha_v\beta_3$ all well overlapped under all forces (Fig. 3-12 G). Moreover, the average lifetime under 15 pN clamping force showed no correlation with the molecular complex spring constant (Fig. 3-12 H). These results indicated that, similar to FN_{III7-10} being the ligand, the bent/extended conformation or the

bending/unbending conformational change has negligible effects in the $\alpha_V\beta_3$ -fibrinogen dissociation rate under force.

3.2.3 Observation of integrin $\alpha_V\beta_3$ bending/unbending conformational change by High-Speed Atomic Force Microscopy (HS-AFM)

The dynamic process of integrin conformational changes has never been directly visualized. High-Speed Atomic Force Microscopy (HS-AFM) is an upgraded version of the conventional AFM setup, which was invented by Dr. Toshio Ando. It has a strong advantage in imaging high speed conformational and structural changes of macro-molecules^{110,111}. In collaboration with Dr. Peter Hinterdorfer lab at Johannes Kepler University (JKU) Linz, Austria, we employed a HS-AFM to directly image and characterize the real-time bending and unbending conformational changes of the recombinant integrin $\alpha_V\beta_3$. All the HS-AFM experimental results under this section were collected by Dr. Johannes Preiner, JKU, with my on-site help.

A mica surface pre-treated with 30 mM NiCl_2 was immersed by a working solution that contained physiological concentrations of Ca^{2+} and Mg^{2+} . Recombinant $\alpha_V\beta_3$ integrins were then seeded on to the surface. A high-speed super-resolution cantilever tip scanned over the surface of the mica with a spacial resolution of 1 nm and temporal resolution of 50 ms in a $20 \times 20 \text{ nm}^2$ area (Fig. 3-13 A). The topography of the scanned surface was reflected by the brightness in the image, with higher places indicated with a brighter color (Fig. 3-13 A). Both bent and extended integrins could

be visualized, with the positions of the headpiece and tailpiece easily recognizable based on the globular size and height (Fig. 3-13 B,C).

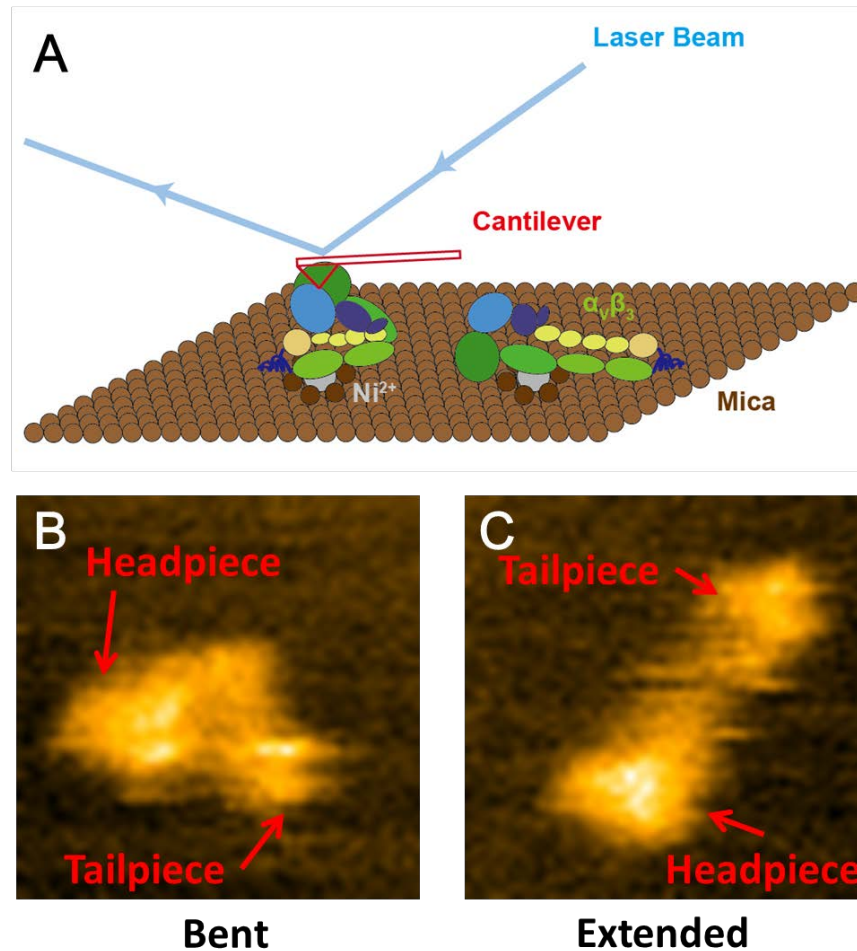


Figure 3-13. Imaging recombinant $\alpha_v\beta_3$ in bent and extended conformations using a HS-AFM (contributed by Dr. Johannes Preiner, JKU). (A) Sketch of the HS-AFM setup. Recombinant $\alpha_v\beta_3$ was seeded onto a mica surface in a Ni^{2+} -contain solution. A high-speed cantilever quickly scans the mica surface in the search of integrins and concurrently reflects the surface topography. (B) A HS-AFM image of a bent integrin. (C) A HS-AFM image of the same integrin in an extended conformation. (B,C) The positions of the headpiece and tailpiece were recognized by the size and shape, which were indicated on the panels.

By tracking a single integrin over time, we successfully captured the process of integrin bending/unbending conformational changes. Each integrin was undergoing highly dynamic conformational changes back-and-forth almost all the time, which agrees with the previous speculation of dynamic equilibrium (Fig. 3-14 A,B).

Interestingly, different than BFP observations, it appeared that in the absence of force, the integrin could reverse the direction of the conformational change in anywhere half-way, or temporarily oscillate within a small angle range.

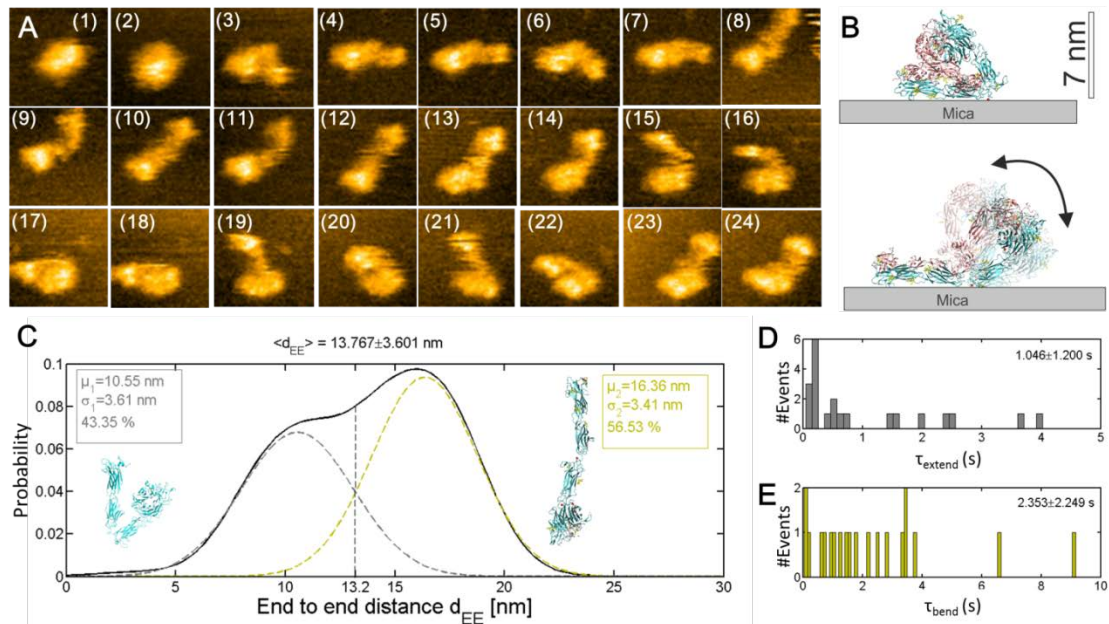


Figure 3-14. Imaging recombinant $\alpha_v\beta_3$ bending/unbending conformational changes using a HS-AFM (contributed by Dr. Johannes Preiner, JKU). (A) Images of a recombinant $\alpha_v\beta_3$ selected from a HS-AFM video, with a time interval of 3 seconds between two adjacent images. (B) A sketch of the postulated orientation of a bent (upper panel) and extended (upper panel) integrin. (C) Distribution and dual Gaussian fitting of the integrin end to end distance d_{EE} . The proportions and fitted means of d_{EE} of bent and extended integrins were indicated on the graph next to the corresponding conformation plot. (D,E) Scatter plots of time-to-extend (D) and time-to-bend (E). The averages (mean \pm SEM) were indicated at the right up corners.

The end to end distance d_{EE} of the integrin, measured as the linear distance from the ligand binding site of the head-piece to the C-terminus of the tail, of the bent and extended integrins distributed as a dual Gaussian, with the two means being 10.55 and 16.36 nm, which were presumably the d_{EE} of the integrin in bent and extended conformations. The difference, 5.79 nm, was much shorter than the average bending/unbending displacements measured on BFP (~ 13 nm in the purified system

and ~15 nm in the cell-surface system). We suspect this was due to that in BFP experiments the probe bead interrogated the integrin via ligand (FN_{III7-10} or fibrinogen) binding to the headpiece of the integrin, which increased the overall length of the rotating radius, and thus added up to the conformational change displacement.

The time-to-switch was then collected for both unbending and bending, which had the average of 1.046 s and 2.353 s, respectively (Fig. 3-14 D,E). The average time-to-extend was in agreement with the zero-force extrapolation of BFP results under the same condition, assuming that the time-to-extend exponentially decays with force (Fig. 3-5 B).

3.3 Discussion

The idea that integrins are undergoing reversible bending and unbending conformational changes in dynamic equilibrium has been speculated long time ago, but was confirmed only recently on a α I domain containing integrin, $\alpha_L\beta_2$ ⁶³. Based on the same technical approach, my study under this aim recapitulated this observation on a α I-absent integrin, $\alpha_V\beta_3$, both in a purified system and on cell surface. Moreover, we for the first time ever visualized these conformational changes with a HS-AFM.

Integrins can adopt multiple binding states against ligands. In the inactive state, integrins have a low affinity when binding to ligands, which will be drastically up-regulated upon activation (e.g., Mn^{2+} or talin head domain association). So far, this multi-binding-state property have been exhibited in integrin $\alpha_5\beta_1$, $\alpha_L\beta_2$, $\alpha_{IIb}\beta_3$ and $\alpha_M\beta_2$ in single molecular level^{26,27,29,57}, manifested by the change of dissociation rate

under different forces that does not follow Bell's model⁹⁶. Similarly, the lifetime of purified integrin $\alpha_V\beta_3$ -FN_{III7-10} in Mn^{2+} showed a catch-bond while in Ca^{2+}/Mg^{2+} manifesting a slip-bond (Fig. 3-6 C), suggesting the existence of multiple binding states. Compared with $\alpha_5\beta_1$ and $\alpha_L\beta_2$ whose catch-slip behavior was persistent in all tested cation conditions, $\alpha_V\beta_3$ possesses both catch- and slip-bond behaviors. In discrepancy with cell-free system, the lifetime of cell-surface WT $\alpha_V\beta_3$ -FN_{III7-10} binding was in the form of "slip-catch-slip" in Ca^{2+}/Mg^{2+} , which allows the bond to withstand a considerable level of force (Fig. 3-11 B). Nonetheless, all the lifetime curves of WT $\alpha_V\beta_3$ -FN_{III7-10} regardless of in the cell-free or cell-surface system, diminished at force $> \sim 40$ pN, which agreed with the previous quantification of the maximal force the cell could exert on a single $\alpha_V\beta_3$ -fibrinogen bond¹¹². Interestingly, the lifetime curves of D723R and L138I $\alpha_V\beta_3$ well overlapped, both manifesting a slip-bond which prolonged the lifetime under low forces but became identical to WT at force > 20 pN (Fig. 3-11 C,D).

Both bending and unbending can be observed on cell surface $\alpha_V\beta_3$ when interrogated by a RGD-containing fibronectin fragment FN_{III7-10}, fibrinogen or even antibody AP3 which targets on an epitope distal of the ligand bind site. Nonetheless, their occurring frequencies did show substantial differences, with FN_{III7-10} and fibrinogen higher than AP3 in both unbending and bending (Fig.3J). These data suggested that the dynamic bending/unbending switch is an interior attribute of the integrin, which is not relying on, but rather dependent on ligand association. This ligand dependency further extends to the kinetics characterizations of conformational

changes, exhibiting discrepancy between FN_{III7-10}- and fibrinogen-bound integrins in the t_{sw} and t_0 vs. force (Fig. 5C,D; Fig. 7E,F). We suspect that this ligand discrimination in bending and unbending is realized by the distinctive docking of the binding motifs of FN_{III7-10} (RGD) and fibrinogen (AGDV), which results in varied allosteric effects that propagate from the N-terminal ligand binding epitope to the overall structure of the integrin.

The criteria of distinguishing bending/unbending events from BFP lifetime signals is based on the stiffness difference in bent and extended conformations of the integrin. To confirm that, we measured the receptor-ligand molecular complex spring constants before bending and unbending events, which reflect the relative stiffness of the integrin in two conformations. Agreeing with the criteria and previous results on $\alpha_L\beta_2$ ⁶³, the integrin $\alpha_V\beta_3$ was measured to be softer in the bent conformation, and stiffer when extended (Fig. 3-4 B; Fig. 3-9 C). Taking advantage of these results, we employed Gaussian and dual Gaussian fittings and determined the initial fractions of bent and extended integrin sub-populations in the absence of force regulation (Fig. 3-4 C,D; Fig. 3-9 E-G).

Functional mutations have been utilized in the studies of integrin activity and signaling^{101,113}. The GOF mutation L138I results in a larger proportion of extended integrin than WT, which is in consistency with its reported function (Fig. 3-9 F)¹⁰¹. Interestingly, D723R, which causes tailpiece separation, also favored more extension, suggesting a allosteric relay between different categories of conformational changes

(Fig. 3-9 G)¹⁰¹. Moreover, as compared to WT, D723R significantly shortened the t_{sw} and t_0 of integrin unbending conformational change under force while L138I only shortened t_{sw} (Fig. 3-10 A-D), which should at least partially explain both MTs' sharp shift of the bent/extended fraction equilibrium towards extension.

Mechanical force regulates the conformational changes by providing a positive or negative work to the molecule when the headpiece travels along or against the direction of force pulling. Intuitively, one should assume that the tensile force exerted via ligand engagement should impede bending and favor unbending. Indeed, as reflected by t_{sw} and t_0 vs. force characterizations, force accelerates unbending and stabilizes the extended state, while decelerating bending and destabilizing the bent state (Fig. 3-5 B,C,E,F; Fig. 3-10 C,D). Calculation results also confirmed that force drastically tilted the equilibrium between bent and extended states towards unbending. $\alpha_v\beta_3$ was reported to initiate cell mechanotransduction via ligand engagement^{112,114}. However, the details of this process as well as how integrin conformational changes are aligned with transmembrane signaling still lack insights. The force-stimulated integrin extension could potentially serve as a manner of signaling initiation, considering that it may trigger certain deformations or rearrangements in the juxtamembrane domains¹⁹.

The relationship between integrin conformational states and binding capacity states has been implicated and confirmed in many different works, most of which provided only strong correlative but not causal evidences, so that in the inactive state,

integrins adopt a bent conformation and weak binding capacity, which undergo binding strength enhancement and ectodomain unbending upon activation^{40,46,47}. Agreeing with that, in this work, the correlation was also implicated by the two mutations that are associated with stronger binding and an obvious favor of unbending over bending. Chen et al used BFP to provide the first direct evidence that the bent/extended conformation by itself can have impact on the integrin binding, so that extended $\alpha_L\beta_2$ dissociated slower than bent⁶³. However, surprisingly, in $\alpha_V\beta_3$ this did not apply in the physiological $\text{Ca}^{2+}/\text{Mg}^{2+}$ cation condition: 1) bending and unbending had negligible effects on the post-switch lifetime (Fig. 3.6 C; Fig. 3-11 B-D; Fig. 3-12 G); 2) integrins in bent/extended conformations had comparable average lifetime (Fig. 3-11 E,F; Fig. 3-12 H). These evidences indicated that the bent/extended conformational states of integrin $\alpha_V\beta_3$ do not have direct correlation with the binding dissociation rate. In Mn^{2+} , however, the dependency showed up (Fig. 3.6 B). Nonetheless, considering that during unbending the upward movement and the re-orientation of the headpiece which should become more favorable for ligand binding, one may speculate that unbending increases the on-rate or affinity of integrin binding under all conditions, which obviously requires further investigations. For example, it was reported that ligand binding led to headpiece opening of $\alpha_{\text{IIb}}\beta_3$, which up-regulated its binding affinity for >200 folds, suggesting that ligand binding-induced integrin conformational changes can affect their binding¹¹⁵.

The fact that the dynamic switch of bending/unbending conformational changes can occur independent of cells, both under force (BFP) or without force (HS-AFM)

suggests that this reversible movement of integrins does not require external energy source, but may be fulfilled with the help of non-specific interactions like atom/molecule collision. However, considering that the bending could be observed in the presence of a considerable pulling force, e.g., 30 pN with a traveling distance (displacement) of ~15 nm, which applied a work of ~450 pN/nm, or $109.32 k_B T$, in which k_B is the Boltzmann constant and $T = 298.15$ K is the room temperature. It becomes intriguing and puzzling that how a single molecule could provide such a huge amount of energy.

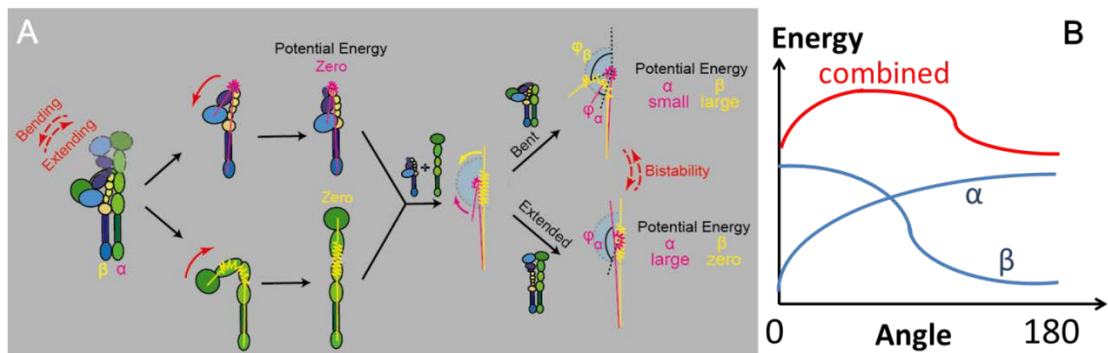


Figure 3-15. Integrin bistability model. (A) The integrin undergoes bending and unbending as an intact molecule. However, as postulated, when apart, the α and β subunits adopt extended and bent conformations respectively, where they can adopt a minimal energy. The two subunits act as two springs, so that when they are associated together, their elastic potential energies counteract with each other. The angle changes, φ_α and φ_β , were indicated in the graph. (B) A rough sketch demonstrating the energy vs. angle of the α and β subunits and the combined intact integrin. The energy of “combined” is the simple addition of “ α ” and “ β ”.

Inspired by the bistable behavior of certain mechanical structures realized by the counteraction of pre-stress inside the structure¹¹⁶, I proposed here a integrin bistability model (Fig. 3-15 A). In this model, the two subunits of the integrin, α and β , adopt an extended conformation and a bent conformation respectively when apart (for the ease of demonstration, assume that the α subunit is extended and β bent), where they reach

the minimum of their energy wells. As long as they are away from the default conformation (quantified by the angle change, φ_α and φ_β), work needs to be done to account for the energy increase, and presumably this energy keeps increasing with a larger deformation (Fig. 3-15 B). When the two subunits are forced to associate, in the bent conformation, the potential energy is small in α but large in β ; while in the extended conformation, the potential energy is small in β but large in α . Their elastic forces counteract with each other, which creates a energy pan-out with two energy wells surrounding the bent and extended conformations (Fig. 3-15 B). This realizes two stable conformational states of the integrin, bent and extended, and it will switch between them dynamics stimulated presumably by molecular vibration and collision. The validation of this model will definitely need further investigations.

CHAPTER 4: CHARACTERIZING GPIB-ALPHA-INITIATED PLATELET MECHANOSENSING IN SINGLE MOLECULAR LEVEL

**(This chapter of work was equally contributed by Dr. Lining Ju. No
conflict of interest is claimed.)**

4.1 Introduction

Platelets rapidly respond to changes in hydrodynamic forces and substrate stiffness^{2,117,118}, and its signaling pathways are substantially simplified due to the enucleated structure makes the investigations relatively easier. Previous studies have demonstrated the role of GPIb α as a mechanoreceptor for the process of platelet mechanosensing^{10,11,119}. As stated in Section 1.2.7, this mechanical-biochemical process can be broken down into four steps including mechanopresentation (ligand, VWF-A1), mechanoreception (GPIb α headpiece), mechanotransmission (GPIb α stalk region) and mechanotransduction (molecules currently unknown). A few biological or biomechanical evidences have been collected in the context of platelet GPIb α functionality and signaling: 1) GPIb α -mediated Ca²⁺ signaling is coupled to binding events, and the signaling intensity had a reverse relationship with platelet rolling velocity in the flow chamber system^{10,11}; 2) pulling force induces LRRD unfolding, which prolongs A1-GPIb bond lifetime⁸⁹; 3) force also unfolds the MSD, which has been implicated in platelet mechanosensing¹⁶; 4) GPIb α cytoplasmic domain is in direct association with a cytoplasmic protein 14-3-3 ζ , which is essential for its

signaling¹²⁰. However, how the inter-connected mechanosensing steps are orchestrated and associated with the conformational change of the molecule to enable the information encoded by force to be translated into biochemical signals is still poorly understood.

4.2 Results

4.2.1 Fluorescence BFP setup for studying GPIIb/IIIa-mediated Ca²⁺ signaling

The BFP system is a suitable approach to study VWF–GPIIb/IIIa interaction because its cycle-wise operation mimics the sequential formation, force loading, and dissociation of VWF–GPIIb/IIIa bonds during the translocation of a platelet on the sub-endothelium. In this BFP setup, the probe bead was functionalized with VWF-A1 or an anti-GPIIb monoclonal antibody (mAb), serving as a surrogate sub-endothelial surface (Fig. 4-1A,B). A platelet was aspirated by the target pipette to move in repetitive force-ramp or force-clamp cycles (Fig. 4-1 C,D) (Materials and Methods). Adhesion frequencies from these cycles were kept low (<20%) by adjusting the ligand or antibody density. Control experiments using beads lacking ligand showed no binding, and blocking with mAb AK2 (epitope mapped to LRR1-2 overlapping with the A1 binding site) eliminated GPIIb/IIIa binding to A1 but not mAb WM23 (epitope mapped to the MP below LRRD¹²¹) (Fig. 1D). This confirmed binding specificity and that the binding site of A1 is within LRRD but that of WM23 is outside¹⁶.

We then used the single-platelet calcium imaging by a fluorescence BFP (fBFP)^{91,104} (see Materials and Methods) to study how platelet signaling was triggered by GPIb α mechanoreception. Each platelet was interrogated by a sequence of intermittent single GPIb α bonding events in a 200-s observation time, and the resulted Ca²⁺ signal was collected.

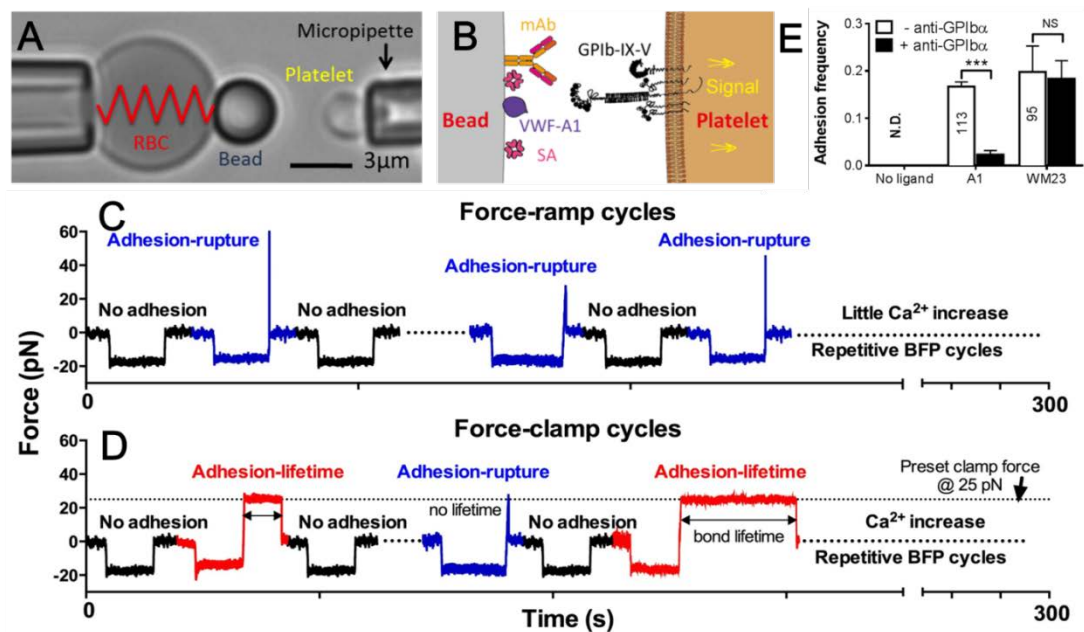


Figure 4-1. BFP analysis of ligand binding kinetics. (A) BFP micrograph. A micropipette-aspirated RBC with a probe bead attached to the apex (left) was aligned against a platelet held by an opposing micropipette (right). (B) BFP functionalization. The probe bead was coated with streptavidin (SA, for attachment to the biotinylated RBC) and VWF-A1 or mAb (left) for interaction with platelet GPIb α (right). (C,D) Representative force vs. time signals of repetitive force-clamp (C) and fore-ramp (D) cycles over a 200-s period. Cycles produced different results are color-coded (black: no bond; blue: bond-rupture; red: bond-lifetime). (E) Mean \pm s.e.m. of adhesion frequencies ($n \geq 3$) of platelets binding to beads functionalized with indicated proteins in the absence (open) or presence (closed) of 50 μ g/ml AK2. *** = $p < 0.001$ by t -test.

4.2.2 Identification of GPIb α -mediated Ca²⁺ signaling types

The Ca²⁺ signals over a 200-s observation time were classified into three types (Fig. 4-2 A): i) null-type, featured by a basal trace with a maximum Ca²⁺ intensity

increase (normalized by its initial value) $\Delta I_{\max} < 0.05$ (Fig. 4-2 B); ii) α -type, featured by an initial latent phase followed by a spike (mostly $\Delta I_{\max} > 0.5$) with a quick decay (Fig. 4-2 C); iii) β -type, featured by fluctuating signals around the baseline or gradually increasing signals to an intermediate level (mostly $\Delta I_{\max} < 0.5$) followed by a gradual decay to baseline (Fig. 4-2 D). The null type reflects background noise, while the α - and β -types match the previous characterization of Ca^{2+} signals triggered by VWF-GPIb α bonds measured in flow chamber-based population assays^{10,11}. For each platelet, the calcium trace was overlaid with the sequential binding events, bond lifetimes (if any), and their accumulation over the interrogation time was recorded (Figure 4-2C).

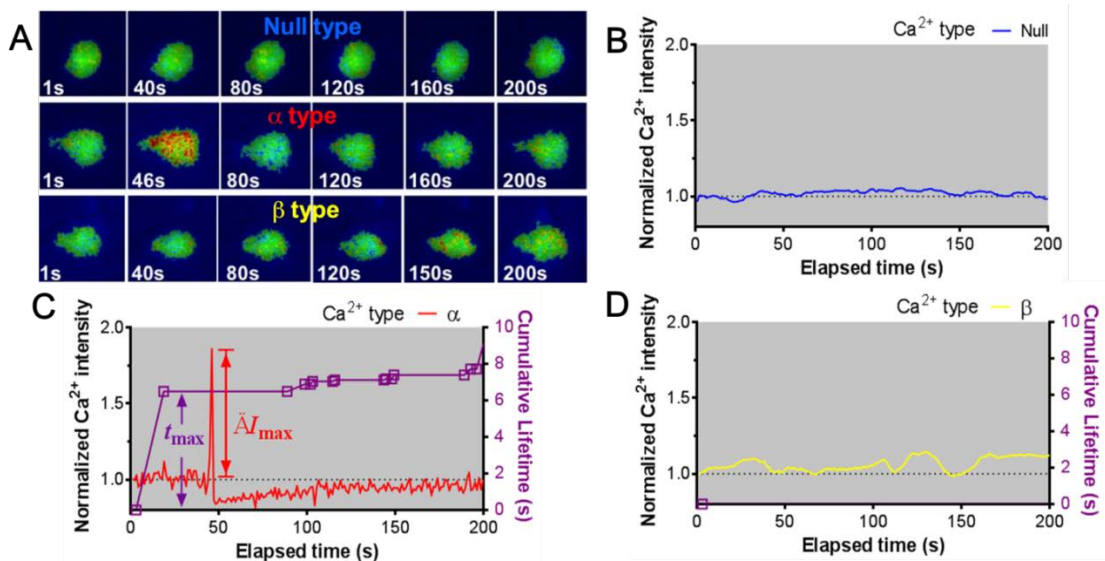


Figure 4-2. Concurrent analysis of single-platelet Ca^{2+} flux and GPIb-mediated single-bond binding at 25 pN clamped force. (A) Representative epi-fluorescence pseudo-colored images of intraplatelet Ca^{2+} of null (top row), α - (middle row), and β - (bottom row) types at indicated times. (B-D) Representative time courses of normalized Ca^{2+} intensity of the null (B), α (C) and β (D) types. In (C), the concurrent measurement of bond lifetime events (symbol) and the cumulative lifetime (curve) is overlaid. The pre- Ca^{2+} longest lifetime (t_{\max}) and the maximum intensity increase of the α -type Ca^{2+} (ΔI_{\max}) are indicated.

4.2.3 The necessity of durable bonds in GPIIb α -mediated mechanotransduction

We asked the question whether the mechanoreceptor GPIIb α is capable of sensing differences in the force waveform and in the ligand through which force is applied. We first performed force-ramp experiment using three ramping rates to generate a wide range of rupture forces: 100, 1,000 and 10,000 pN/s. However, only low levels of β -type and background level of null-type Ca²⁺ were resulted, which showed no correlation with the mean rupture force prior to calcium onset (Figure 4-3 B,D, right ordinate), regardless of whether platelets were tested by A1WT (Fig. 4-3A,B) or A1R1450E (Fig. 4-3C,D). In sharp contrast, pulled by a 25pN clamp force which realizes the highest average lifetime²³, A1WT-GPIIb α bonds triggered much higher ΔI_{\max} , showing 28, 42, and 30% of null-, α - and β -types, respectively (Fig. 4-3 E,F). A1R1450E which yielded much shorter lifetimes when binding to GPIIb α under 25 pN, on the other hand, resulted in much lower ΔI_{\max} and only 5% of α -type (Fig. 4-3 E,F). Moreover, we took advantage of the force-dependence of the binding kinetics²³, and manipulated the GPIIb α lifetime via changing the clamp forces (10, 25, 40, 60 pN). The ΔI_{\max} and the α -type Ca²⁺ ratio both elicited a strong correlation with the average lifetime for both A1WT and A1R1450E (This part of data has been thoroughly illustrated in the Ph.D. dissertation of my colleague and collaborator, Dr. Lining Ju¹²², and will not be reiterated here). All these results reflected the essential role of durable bonding to successfully trigger Ca²⁺ signaling.

As controls, merely holding aspirated platelets or contacting them using beads not coated with ligands showed null-type Ca^{2+} only (Fig. 4-3E,F). GPIb α pulled by an antibody AN51 resulted in robust Ca^{2+} signaling following durable binding events, with the ratio of null-, α - and β -types similar to A1WT (Fig. 4-3E,F). However, an antibody against GPIb β (LS-B3174) only induced low level Ca^{2+} although under the same clamp force and with similar average lifetime (Fig. 4-3E,F), despite that GPIb β is tightly connected with GPIb α and has been postulated to play a role in signaling through GPIb¹²³. These data demonstrated the necessity of GPIb α engagement to trigger intraplatelet Ca^{2+} , which agree with the previous report that α -type Ca^{2+} peaks occur when platelets are transiently arrested in the whole blood flow¹⁰.

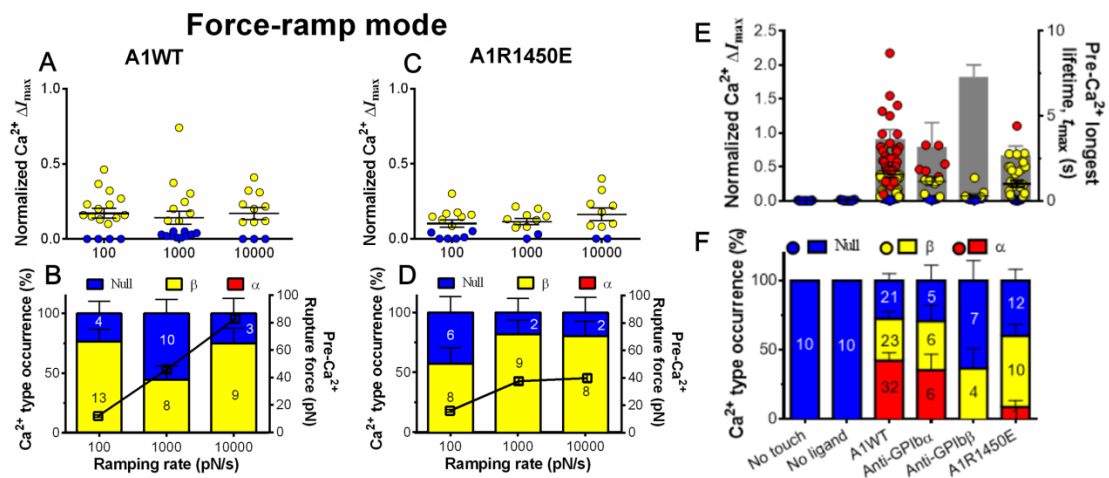


Figure 4-3. Robust platelet Ca^{2+} signal requires sustained bonding on GPIb α . (A-D) Individual ΔI_{\max} values and their mean \pm s.e.m. (A,C, points), Ca^{2+} types (B,D, stacked bars, left ordinate), and mean \pm s.e.m. of pre- Ca^{2+} average rupture force (B,D, black square, right ordinate) are plotted vs. force ramping rate for A1WT (A,B) or A1R1450E (C,D). (E, F) Individual ΔI_{\max} values and their mean \pm s.e.m. (points, left ordinate) and mean \pm s.e.m. t_{\max} (gray bar, right ordinate) (E) and fractions (F) of Ca^{2+} types triggered by different stimulations. Each point in (E) represents results from one platelet and the numbers of platelets in each column are indicated in the corresponding bar in (F), with matched colors indicating Ca^{2+} types.

4.2.4 A single durable bond mediating mechanism of GPIIb/IIIa mechanotransduction

The concurrently measurements of VWF–GPIIb/IIIa binding kinetics and intraplatelet Ca^{2+} allowed us to determine the pre- Ca^{2+} bond lifetimes (Fig. 4-2C), enabling single platelet correlative analysis of binding and signaling. Using the normalized maximum calcium intensity ΔI_{max} to represent the Ca^{2+} level, we compared its correlations with three statistics of A1WT–GPIIb/IIIa bond lifetime that occurred prior to Ca^{2+} onset. We found that ΔI_{max} correlates best with the pre- Ca^{2+} longest bond lifetime t_{max} (Fig. 4-4 A), similarly well with the pre- Ca^{2+} cumulative lifetime Σt_i (Fig. 4-4 B), but poorly with the pre- Ca^{2+} average lifetime $\langle t \rangle$ (Fig. 4-4C). Careful examination of many overlaid calcium and bond lifetime traces like that exemplified in Fig. 4-2C revealed that the Σt_i values are generally dominated by the t_{max} values, which are usually much longer than the rests of the pre- Ca^{2+} bond lifetimes and are immediately followed by the calcium onset before observing additional shorter bond lifetimes. In other words, for each platelet usually Σt_i could be approximated by t_{max} but $\langle t \rangle$ is of a smaller and variable value. This observation explains why calcium correlates equally well with t_{max} and Σt_i but not with $\langle t \rangle$. Importantly, this data also suggests that a single long-lived VWF–GPIIb/IIIa bond is sufficient to trigger Ca^{2+} in a platelet. This assertion has been further supported by the parallel analysis of the data for A1R1450E. Although for R1450E t_{max} was significantly shorter and α -type Ca^{2+} population was greatly reduced, the ΔI_{max} still

showed similar correlation with t_{\max} (Fig. 4-4D). Thus the pre- Ca^{2+} longest bond lifetime correlates the Ca^{2+} strength.

4.2.5 Cooperative unfolding of lucine-rich repeat domain (LRRD) and mechano-sensitive domain (MSD)

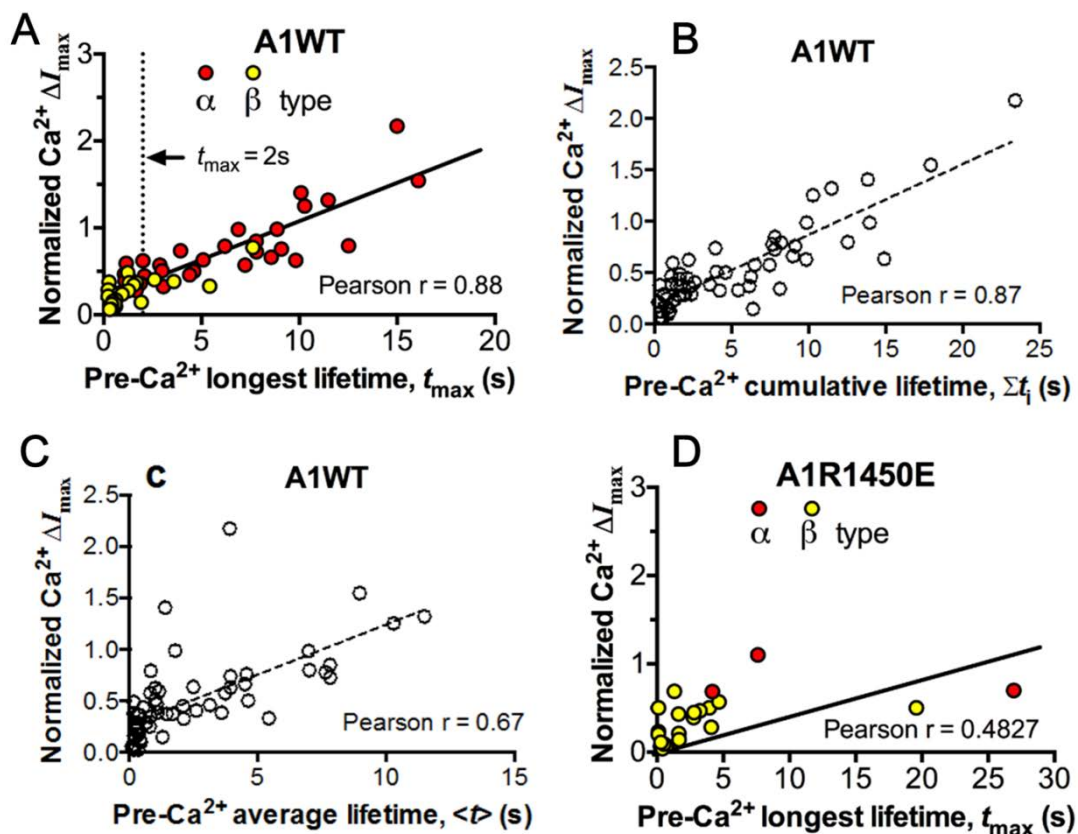


Figure 4-4. Quantitative correlation of GPIIb/IIIa lifetime and platelet Ca^{2+} signaling. (A,D) Scatter graphs of ΔI_{\max} vs. t_{\max} for A1WT (A) and A1R1450E (D). The solid lines are linear fits to respective data with corresponding Pearson coefficients indicated. The yellow and red colors of the dots indicate the observed Ca^{2+} signal type of corresponding platelets. (B,C) Scatter graphs of ΔI_{\max} vs. $\sum t_i$ (B) or $\langle t \rangle$ (C) for A1WT. The dashed lines are linear fits to respective data with corresponding Pearson coefficients indicated.

Using an optical trap, Zhang et al. observed force-induced MSD unfolding in purified recombinant full-length GPIIb-IX and a GPIIb α stalk region construct¹⁶. Using a BFP, we observed LRRD unfolding in glyocalicin (GC)⁸⁹, the extracellular segment of GPIIb α lacking the MSD (Liang et al., 2013) (Fig. 1-2B). The average

unfolding distance of MSD and LRRD was respectively determined to be 20 and 36 nm. Here we pulled GPIb α on platelets with ramped and clamped force waveforms and identified two corresponding unfolding signatures: a) ramped unfolding, featured by a sudden force kink at 5-20pN occurring in the ramping phase (Fig. 4-5A insert); b) clamped unfolding, featured by an abrupt force drop occurring in the clamping phase (Fig. 4-5 A,B). Unfolding lengths derived from both signatures were measured from the probe bead position vs. time data (Figure 4-5A insert and B), based on which, three subpopulations were segregated by Gaussians fit that respectively peaked at 20, 36 and 65 nm. Further experimental evidences showed that, the first two subpopulations were from single MSD and LRRD unfolding, while the last one were a combination of two domains unfolding concurrently (data not shown).

Interestingly, the two force waveforms induced unfolding of different GPIb α domains. Clamped forces unfolded only MSD as the unfolding lengths obtained by pulling platelet GPIb α via A1 or AN51 distribute as a single peak at 20nm. LRRD unfolding was observed in the ramping phase only. These results indicate that MSD can be unfolded by increasing forces as well as constant forces, while LRRD unfolding requires a force gradient. Some pulling cycles generated two consecutive unfolding events, one in the ramping and the other in the clamping phase, with respective unfolding lengths of 34-55nm and 13-25nm that total 47-80nm, agreeing with those of the LRRD, MSD, and MSD+LRRD subpopulations. Together, these results provide criteria to determine whether and which GPIb α domain(s) unfolded (Table 4-1).

To characterize responses of GPIIb α to mechanical cues it receives, we measured the frequency of LRRD and MSD unfolding induced by a range of clamped forces exerted on platelet GPIIb α via an engaged A1WT or a type 2B VWD mutant A1R1450E. The frequency of LRRD unfolding, which occurred in the ramping phase only, was undetectable at ≤ 10 pN but increased with the preset force at higher levels (Fig. 4-5 C). Interestingly, LRRD unfolded more frequently when pulled by A1WT than A1R1450E (Fig. 4-5 C).

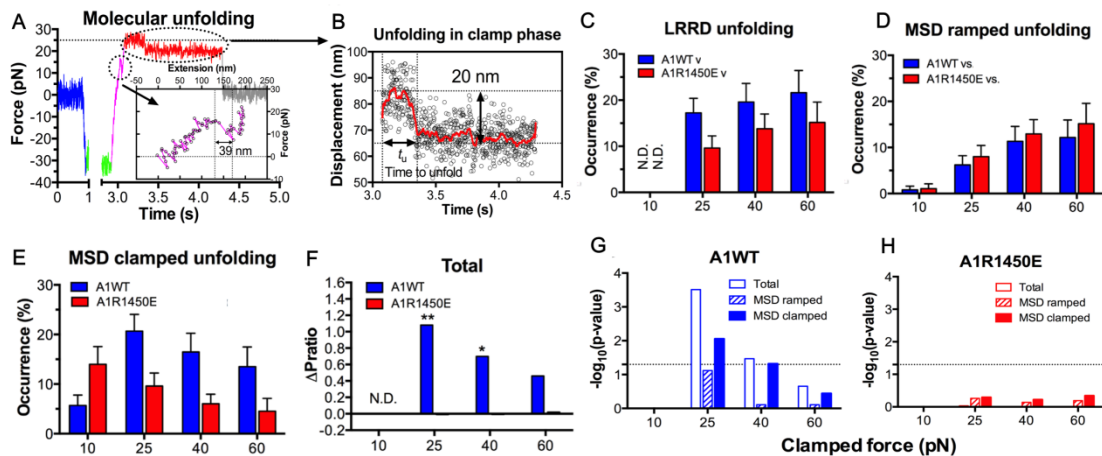


Figure 4-5. Force regulated and ligand-dependent cooperative unfolding of GPIIb α LRRD and MSD. (A) Force vs. time trace of a representative BFP cycle showing unfolding signatures in both ramping and clamping phases. The inset zooms in the ramped unfolding signature and indicates the unfolding distance. (B) Zoom-in view of the clamped unfolding signature in (A). Higher displacement resolutions were obtained after smoothing the raw data (points) by the Savitzky-Golay method (curves). Time to unfolding (t_u) is indicated. (C-E) Frequency of LRRD unfolding (C), MSD ramped unfolding (D) or MSD clamped unfolding (E) events by pulling via A1WT (blue) or A1R1450E (red) to the indicated clamped forces. (F) The degree of cooperativity, defined as $\Delta P/P = P(\text{MSD}, \text{LRRD})/[P(\text{MSD})P(\text{LRRD})] - 1$, is plotted vs. clamped force. $P(\text{LRRD})$, $P(\text{MSD})$ and $P(\text{LRRD}, \text{MSD})$ are the observed occurrence frequencies of unfolding events of LRRD alone, MSD alone and both LRRD and MSD, respectively. (G,H) Cooperativity assessment by (negative \log_{10} of) p-value of the χ^2 test of the null hypothesis H_0 : MSD unfolding and LRRD unfolding are independent. The χ^2 test was not performed at 10pN since under this force LRRD unfolding did not occur and hence no unfolding cooperativity.

By comparison, MSD ramped unfolding occurrence was indifferent to the ligand (Figure 4-5 D). Surprisingly, distinctive force-dependent trends of MSD clamped unfolding were observed when force was applied to platelet GPIb α via different ligands. When pulled by A1WT, the unfolding occurrence first increased with the clamped force, reached a maximum at 25pN, and decreased thereafter (Fig. 4-5 E, blue). When pulled by A1R1450E, by comparison, the MSD unfolding occurrence decreased monotonically with the clamped force (Fig. 4-5 E, red). These data provide evidence that the mechanoreceptor GPIb α may be able to interpret mechanical cues and discriminate ligands by responding to different force waveforms applied via different ligands with distinct LRRD and MSD unfolding frequencies.

The spatial separation of LRRD and MSD by the >30nm long MP region and the distinctive dependences of their unfolding on the force waveform would seem to favor these two GPIb α domains to unfold independently. This hypothesis predicts that the probability for LRRD and MSD to unfold concurrently should be equal to the product of the respective probabilities for LRRD and MSD to unfold separately. To test this hypothesis, we estimated these probabilities from the observed unfolding occurrence frequencies. At 25pN, the 34.5% of BFP force-clamp cycles with unfolding events consist of 7.6, 17.2, 6.9, and 2.8% of unfolding of LRRD alone, MSD alone, LRRD and MSD sequentially, and concurrently (Table 4-1). Significantly, the frequency of observing both LRRD and MSD unfolding in the same binding cycle, calculated by pooling together both cases of two domains unfolding sequentially and concurrently, $P(\text{MSD,LRRD}) = 9.7\%$, is much higher than the product of their respective

occurrence frequencies, $P(\text{MSD}) \times P(\text{LRRD}) = 4.65\%$, which is the joint probability for both to unfold assuming that they were independent (Table 4-2). Similar results were observed under higher forces as well for A1WT, but not A1R1450E (Table 4-2). These evidences suggest that the two domains may unfold cooperatively, i.e., one domain unfolding may increase the likelihood for the other to unfold. To quantify the degree of such cooperativity, we defined a relative probability difference, $\Delta P/P = [P(\text{MSD}, \text{LRRD}) - P(\text{MSD})P(\text{LRRD})]/[P(\text{MSD})P(\text{LRRD})]$. $\Delta P/P > 0$ indicates positive cooperativity between LRRD and MSD unfolding. No cooperativity was observed at 10pN, which is expected because this force is insufficient to induce appreciable LRRD unfolding. Pulled with A1WT by a 25pN clamped force generated high cooperativity, and further increase in force decreased cooperativity (Fig. 4-5 F). Remarkably, unfolding cooperativity was completely abolished at all forces when applied via the VWD mutant A1R1450E (Fig. 4-5 F). Furthermore, χ^2 test was used by our collaborator, Prof. Lingzhou Xue (The Pennsylvania State University) to determine if the hypothesis that MSD and LRRD unfolded independently should be rejected. Significant ($p < 0.05$) unfolding cooperativity was observed only for A1WT at 25 and 40pN. These data show that the cooperativity between LRRD and MSD unfolding is force-regulated and ligand-dependent.

4.2.6 Model for cooperativity between LRRD and MSD unfolding

To elucidate the mechanism underlying the force- and ligand-dependent unfolding cooperativity, we note that when the MSD unfolding events were separately

analyzed according to their occurrence in the ramping or clamping phase, MSD clamped, but not ramped, unfolding, was significantly ($p=8.79\times 10^{-3}$ vs. 0.076 at 25pN) enhanced by LRRD unfolding (Fig. 4-5 G), which occurred in the ramping phase only. This dominance of cooperativity by sequential rather than concurrent unfolding suggests a model for LRRD unfolding to impact MSD unfolding, which includes three ideas. The first idea has to do with the MSD time-to-unfold, t_u (cf. Fig. 4-5 B). Our force-clamp measurement revealed similar slip-bond trends for A1WT and A1R1450E (Fig. 4-6 C). The only exception is at 10pN where A1WT resulted in a shorter t_u than A1R1450E. This can be explained by their differential bond lifetimes with GPIb α (Fig. 4-6 A,B). Compared to A1R1450E, the much shorter GPIb α bond lifetime of A1WT at 10pN may result in underestimation of MSD clamped unfolding because early dissociation would have prevented the observation of slow MSD unfolding events. This reasoning provides the second idea for our model: MSD clamped unfolding should occur before VWF–GPIb α bond dissociation. The third idea comes from our previous observation⁸⁹ that LRRD unfolding significantly prolonged GPIb α bond lifetime with A1WT (Fig. 4-6 A) but not A1R1450E (Fig. 4-6 B). Combining these three ideas, our model proposes that the VWF–GPIb α bond lifetime, regulated by force and prolonged by LRRD unfolding in respective ligand-specific manners, determines the occurrence of MSD clamped unfolding, which, despite its ligand-independent unfolding kinetics, results in a cooperativity pattern that maximizes at the optimal force of 25pN for A1WT but shows no cooperativity for A1R1450E.

Table 4-1. Decision rules for and statistical summary of GPIIb/IIIa domain unfolding in force-clamp experiment mode. Criteria for deciding whether or not (+ or -) and which (LRRD, MSD, or both) GPIIb/IIIa domain(s) was (were) unfolded are based on BFP profile signatures and the unfolding length. YES = observed, NO = not observed. NA = not applicable.

	Clamped Force (pN)	Unfolding signatures		Decision rules		Number of observations and occurrence frequency	
		Ramping phase	Clamping phase	LRRD	MSD		
WT A1 vs. Platelet	10	NO	NO	-	-	115	93.50%
		<25nm	NO	-	+	1	0.81%
		NO	<25nm	-	+	7	5.69%
	25	NO	NO	-	-	95	65.52%
		25-56 nm	NO	+	-	11	7.59%
		<25nm	NO	-	+	5	3.45%
		NO	<25nm	-	+	20	13.79%
		<56nm	<25nm	+	+	10	6.90%
		>56nm	NO	+	+	4	2.76%
	40	NO	NO	-	-	60	61.86%
		25-56 nm	NO	+	-	10	10.31%
		<25nm	NO	-	+	8	8.25%
		NO	<25nm	-	+	10	10.31%
		<56nm	<25nm	+	+	6	6.19%
	60	>56nm	NO	+	+	3	3.09%
		NO	NO	-	-	45	60.81%
		25-56 nm	NO	+	-	10	13.51%
		<25nm	NO	-	+	7	9.46%
		NO	<25nm	-	+	6	8.11%
	R1450E vs. Platelet	10	<56nm	<25nm	+	+	3
>56nm			NO	+	+	3	4.05%
NO			NO	-	-	80	85.11%
25-56 nm			NO	+	-	0	0.00%
<25nm			NO	-	+	1	1.06%
25		NO	<25nm	-	+	13	13.83%
		<56nm	<25nm	+	+	0	0.00%
		>56nm	NO	+	+	0	0.00%
		NO	NO	-	-	93	74.40%
		25-56 nm	NO	+	-	10	8.00%
		<25nm	NO	-	+	8	6.40%
40		NO	<25nm	-	+	12	9.60%
		<56nm	<25nm	+	+	0	0.00%
		>56nm	NO	+	+	2	1.60%
		NO	NO	-	-	81	69.83%
		25-56 nm	NO	+	-	13	11.21%
		<25nm	NO	-	+	12	10.34%
60		NO	<25nm	-	+	7	6.03%
		<56nm	<25nm	+	+	0	0.00%
		>56nm	NO	+	+	3	2.59%
	NO	NO	-	-	45	68.18%	
	25-56 nm	NO	+	-	8	12.12%	
	<25nm	NO	-	+	8	12.12%	
60	NO	<25nm	-	+	3	4.55%	
	<56nm	<25nm	+	+	0	0.00%	
	>56nm	NO	+	+	2	3.03%	

To formulate the model mathematically, we multiplied the respective probability densities of the exponentially distributed MSD time-to-unfold (t_u) (Fig. 4-6 D) and

the dual-exponentially distributed lifetime (t_b) of GPIb α bonds with A1WT or A1R1450E (Tale 4-3)⁸⁸ to construct a joint probability density surface over the t_u - t_b plane (Fig. 4-6 E,F):

Step 1: Derive the parameters of lifetime and unfolding kinetics

The measured MSD time-to-unfold t_u distributed as a single exponential decay: $p_u(t_u) = k_u e^{-k_u t_u}$, where p_u is the probability density and k_u is the unfolding rate of MSD under a clamping force. By fitting the semi-log plotted experimental distribution with a straight line, the unfolding rate at 25pN was evaluated from the negative slope or the reciprocal average time-to-unfold, $k_u = 1/\langle t_u \rangle = 0.870 \text{ s}^{-1}$ (Figure 4-6 D). Modeling the force-dependent MSD unfolding kinetics by the Bell equation⁹⁶, we found the zero-force unfolding rate and the width of the energy barrier to be 0.26s^{-1} and 0.242nm for A1WT. For A1R1450E, the respective values are 0.31s^{-1} and 0.261nm .

We previously reported that the A1–GPIb α bond lifetime t_b distributed as a dual exponential decay with a fast- and a slow-dissociating off-rate⁸⁸. We also recently showed that unfolding of LRRD prolongs A1–GPIb α bond lifetime⁸⁹. These results were also observed in this work, which comprise individual measurements that gave rise to the averaged results in Fig. 4-6 A.

$$\text{For LRRD-: } p_1(t_b) = w_{11}k_{11}e^{-k_{11}t_b} + w_{12}k_{12}e^{-k_{12}t_b} \quad (\text{Equation 4-1})$$

$$\text{For LRRD+: } p_2(t_b) = w_{21}k_{21}e^{-k_{21}t_b} + w_{22}k_{22}e^{-k_{22}t_b} \quad (\text{Equation 4-2})$$

Table 4-2. Evaluation of LRRD and MSD unfolding cooperativity. All probabilities were calculated from occurrence data in Supplementary Table 1. Observed joint probabilities were compared to their predicted counterparts based on the assumption that LRRD and MSD unfolded independently. For example, in “WT A1 vs. Platelet” under 25 pN: The probability of LRRD unfolding is $P_{(LRRD)} = 3.4\% + 6.9\% + 2.76\% = 13.06\%$. The probability of MSD unfolding is $P_{(MSD)} = 7.6\% + 13.8\% + 6.9\% + 2.76\% = 31.06\%$. The probability of MSD ramped unfolding is $P_{(MSD, ramp)} = 7.6\% + 2.76\% = 10.36\%$. The probability of MSD clamped unfolding is $P_{(MSD, clamp)} = 13.8\% + 6.9\% = 20.7\%$.

	Clamped Force (pN)	Unfolding	Observed probability	Compared to	Predicted probability	Fold increase
WT A1 vs. Platelet	10	LRRD +, MSD +	0.00%	$P_{(MSD)} * P_{(LRRD)}$	0.00%	0
		LRRD +, MSD ramped +	0.00%	$\frac{P_{(MSD, ramp)}}{P_{(LRRD)}} *$	0.00%	0
		LRRD +, MSD clamped +	0.00%	$\frac{P_{(MSD, clamp)}}{P_{(LRRD)}} *$	0.00%	0
	25	LRRD +, MSD +	9.66%	$P_{(MSD)} * P_{(LRRD)}$	4.65%	1.1
		LRRD +, MSD ramped +	2.76%	$\frac{P_{(MSD, ramp)}}{P_{(LRRD)}} *$	1.07%	1.6
		LRRD +, MSD clamped +	6.90%	$\frac{P_{(MSD, clamp)}}{P_{(LRRD)}} *$	3.58%	0.9
	40	LRRD +, MSD +	9.28%	$P_{(MSD)} * P_{(LRRD)}$	5.45%	0.70
		LRRD +, MSD ramped +	4.12%	$\frac{P_{(MSD, ramp)}}{P_{(LRRD)}} *$	2.42%	0.70
		LRRD +, MSD clamped +	5.16%	$\frac{P_{(MSD, clamp)}}{P_{(LRRD)}} *$	3.03%	0.70
	60	LRRD +, MSD +	8.11%	$P_{(MSD)} * P_{(LRRD)}$	5.56%	0.46
		LRRD +, MSD ramped +	5.41%	$\frac{P_{(MSD, ramp)}}{P_{(LRRD)}} *$	3.21%	0.68
		LRRD +, MSD clamped +	2.70%	$\frac{P_{(MSD, clamp)}}{P_{(LRRD)}} *$	2.34%	0.15
R1450E vs. Platelet	10	LRRD +, MSD +	0.00%	$P_{(MSD)} * P_{(LRRD)}$	0.00%	0
		LRRD +, MSD ramped +	0.00%	$\frac{P_{(MSD, ramp)}}{P_{(LRRD)}} *$	0.00%	0
		LRRD +, MSD clamped +	0.00%	$\frac{P_{(MSD, clamp)}}{P_{(LRRD)}} *$	0.00%	0
	25	LRRD +, MSD +	1.60%	$P_{(MSD)} * P_{(LRRD)}$	1.69%	-0.05
		LRRD +, MSD ramped +	1.60%	$\frac{P_{(MSD, ramp)}}{P_{(LRRD)}} *$	0.77%	1.08
		LRRD +, MSD clamped +	0%	$\frac{P_{(MSD, clamp)}}{P_{(LRRD)}} *$	0.92%	-1.00
	40	LRRD +, MSD +	2.59%	$P_{(MSD)} * P_{(LRRD)}$	2.62%	-0.01
		LRRD +, MSD ramped +	2.59%	$\frac{P_{(MSD, ramp)}}{P_{(LRRD)}} *$	1.78%	0.45
		LRRD +, MSD clamped +	0.00%	$\frac{P_{(MSD, clamp)}}{P_{(LRRD)}} *$	0.83%	-1.00
	60	LRRD +, MSD +	3.03%	$P_{(MSD)} * P_{(LRRD)}$	2.98%	0.02
		LRRD +, MSD ramped +	3.03%	$\frac{P_{(MSD, ramp)}}{P_{(LRRD)}} *$	2.30%	0.32
		LRRD +, MSD clamped +	0.00%	$\frac{P_{(MSD, clamp)}}{P_{(LRRD)}} *$	0.69%	-1.00

where k_{ij} and w_{ij} ($w_{i1} + w_{i2} = 1$) denote, respectively, off-rates and associated fractions of bonds under a clamped force, with the first subscript indicating without

(Eq. 4-1) or with (Eq. 4-2) a prior LRRD unfolding and the second subscript indicating the fast (Eq. 4-1) or slow (Eq. 4-2) dissociation pathway. By fitting the above model to data⁸⁹, the parameters were calculated (Table 4-3).

Step 2: calculate the unfolding probability using the model

Assuming that MSD unfolding and A1–GPIb α unbinding are independent events, the joint probability density for MSD unfolding at time t_u and A1–GPIb α unbinding at time t_b is $p(t_u, t_b) = p_u(t_u)p_i(t_b)$ where $i = 1, 2$ depending on whether LRRD unfolding occurs. This joint probability is depicted as a surface in Fig. 4-6 E,F using respective A1WT and A1R1450E data measured at 25pN clamped force. The condition for observing MSD clamped unfolding is that the A1–GPIb α bond lifetime t_b lasts longer than the time-to-unfold t_u . Thus, the probability of observing MSD unfolding in the clamping phase P_{ui} is the volume under the probability density surface over the region $0 < t_u < t_b < \infty$, which is marked by the vertical red planes in Fig. 4-6 E,F. For instance, in the absence of LRRD unfolding, the probability of observing MSD unfolding in the clamping phase of 25pN is:

$$P_{u1} = \int_0^{+\infty} \left[p_1(t_b) * \int_0^{t_b} p_u(t_u) dt_u \right] dt_b = \frac{w_{11}k_u}{k_u+k_{11}} + \frac{w_{12}k_u}{k_u+k_{12}} = 21.5\% \quad (\text{Equation 4-3})$$

Similarly, in the presence of LRRD unfolding,

$$P_{u2} = \frac{w_{21}k_u}{k_u+k_{21}} + \frac{w_{22}k_u}{k_u+k_{22}} = 46.2\% \quad (\text{Equation 4-4})$$

The model was applied to predict the MSD clamped unfolding probability under different clamped forces pulled by A1R1450E as well. In these conditions, the

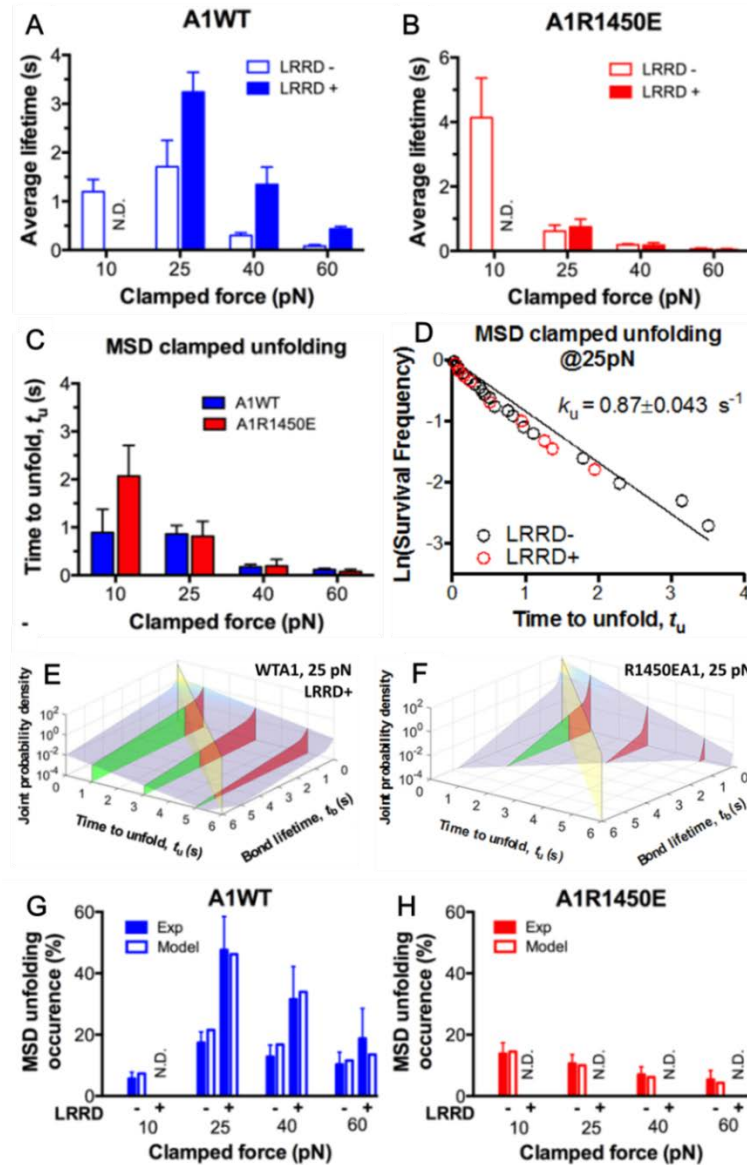


Figure 4-6. LRRD unfolding prolongs VWF–GPIIb bond lifetime and facilitates MSD clamped unfolding. (A–C) Mean \pm s.e.m. GPIIb bond lifetimes (t_b , A,B) and MSD time-to-unfold (t_u , A) with A1WT (blue) or A1R1450E (red) were measured in the clamping phase at different forces in the absence (-) or presence (+) of LRRD unfolding in the same BFP cycle. No LRRD unfolding occurred at 10pN; hence no bond lifetime was measured under this condition. (D) Time-to-unfold (t_u) distributions of MSD clamped unfolding with (red) and without (black) a preceding LRRD unfolding at 25pN clamped force. The unfolding rate k_u were calculated from the slope of $\ln(\text{survival frequency})$ vs. time-to-unfold overlaid plot and the error were estimated from the 95% confident interval. (E,F) 3D plot of the surface of joint probability density (z -axis) of A1WT (E) or A1R1450E (F) to dissociate from GPIIb at t_b (x -axis) and MSD to unfold at t_u (y -axis). (G, H) Measured (solid bar) and predicted (open bar) frequency of MSD unfolding events occurred in the clamping phase induced by A1WT (G) and A1R1450E (H) at indicated forces in the presence (+) or absence (-) of LRRD unfolding in the same BFP cycle. N.D. = not detected. Error bar = s.e.m. estimated by the multinomial distribution of events.

ensemble MSD clamped unfolding events were no longer segregated into LRRD- and LRRD+ groups, because few MSD clamped unfolding events occurred following LRRD unfolding due to the reduced bond lifetime.

Table 4-3. MSD unfolding rates (k_u) and the fraction (w_1) and off-rates (k_1 , k_2) of GPIba binding to A1WT or A1R1450E under different forces. w_1 represents the fraction of binding events that dissociate with the off-rate k_1 . The fraction of events that dissociate with the off-rate of k_2 is simply calculated as $w_2 = 1 - w_1$. NA = not applicable.

Force (pN)	MSD unfolding k_u (s^{-1})	A1-GPIba bond kinetic parameters by model fitting.			
		LRRD unfolding	w_1	k_1 (s^{-1})	k_2 (s^{-1})
WT					
10	0.705	-	0.712	71.33	2.711
25	0.870	-	0.703	23.80	0.486
		+	0.263	8.430	0.597
40	2.952	-	0.665	70.56	3.826
		+	0.448	25.67	1.764
60	9.992	-	0.910	75.42	6.236
		+	0.775	88.10	3.178
R1450E					
10	0.362	-	0.8354	10.14	0.144
25	1.693	-	0.8416	22.60	1.776
40	3.183	-	0.9336	44.88	5.827
60	8.887	-	1	160.85	NA

When the model was tested against experiment, not only did the calculated force-dependent MSD unfolding frequency match the biphasic pattern for A1WT (Fig. 4-6 G) and the monophasic pattern for A1R1450E (Fig. 4-6 H), but it also compared well with the observed occurrence frequencies numerically at all forces. Remarkably, the model predicts both the quantitative enhancement of MSD unfolding by LRRD unfolding for A1WT and the lack of enhancement for A1R1450E. The excellent

agreement between theory and experiment has provided strong support to our model and explained the data in Fig. 4-6 G,H.

4.2.7 LRRD unfolding strengthens signaling by prolonging the lifetime while MSD unfolding is key to determining Ca²⁺ type

The findings that durable force is important to both MSD unfolding and Ca²⁺ triggering prompted us to investigate the relation between GPIIb/IIIa domain unfolding and platelet signal initiation. We segregated the Ca²⁺ data generated by a 25pN clamped force on A1WT bonds according to whether and which domain(s) was (were) unfolded prior to calcium onset. Platelets whose tests contained without unfolding events showed short t_{\max} and low calcium of β - and null-types (Fig. 4-7A). Platelets whose tests contained at least one pre-Ca²⁺ MSD unfolding event but no LRRD unfolding showed slightly longer t_{\max} and higher calcium of mostly α -type. By comparison, only β -type Ca²⁺ was observed in the rare (2.6%) cases where LRRD but not MSD unfolded despite the much longer t_{\max} , excluding t_{\max} as the direct determining parameter for the Ca²⁺ type. Remarkably, the group with both a LRRD and a MSD unfolding event exhibited long t_{\max} and high post-unfolding calcium of mostly α -type. Consistent results were obtained using WM23 to pull GPIIb/IIIa to bypass LRRD unfolding, showing significantly longer t_{\max} and higher calcium for platelets with than without a MSD unfolding event and a clear α - vs. β -type signal distinction between them (Fig. 4-7B). The data in Figure 4-7 A,B indicate that at least one MSD unfolding event is required for triggering α -type Ca²⁺. Interestingly, regardless of

strong pulling represented by bond rupture forces (Fig. 4-7C,D, right ordinate), the force-ramp experiments that triggered only null/ β -type but not α -type Ca^{2+} (Fig. 4-3 B,D and 4-7 C,D, left ordinate) generated very infrequent MSD unfolding events for both A1WT and WM23 cases (Fig. 4-7 C,D). This indicates that both force-induced MSD unfolding and bond lifetime are necessary for triggering α -type Ca^{2+} . In 83% of the cases only a single MSD unfolding event was observed. Of these, 43% showed only one bond with lifetime prior to Ca^{2+} onset. Thus, platelet signaling can be induced by a single A1-GPIIb α bond.

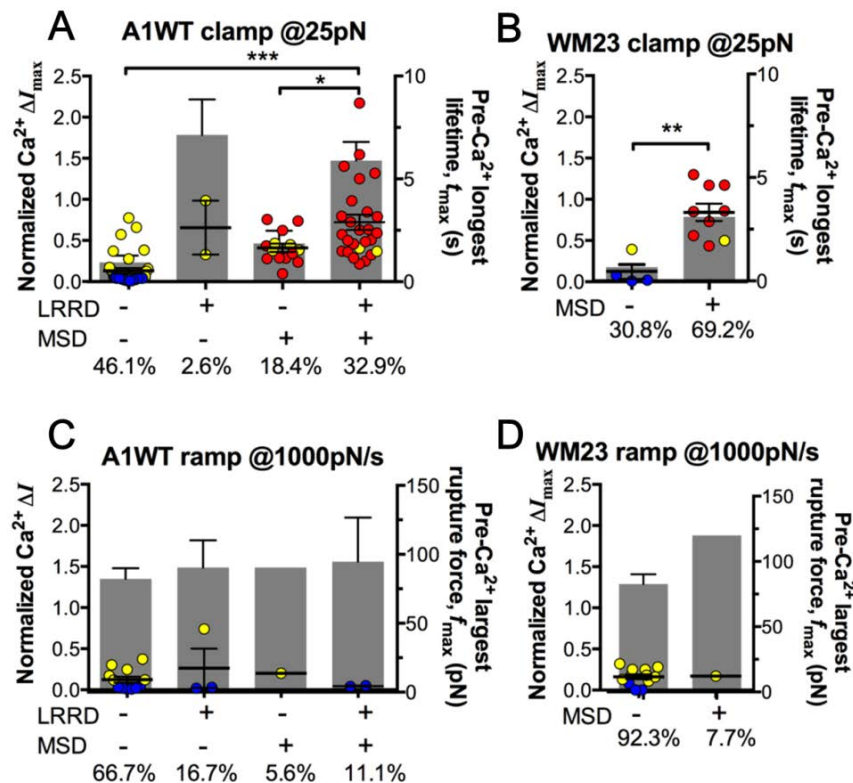


Figure 4-7. Correlation between GPIIb domain unfolding and Ca^{2+} triggering at 25pN clamped force. Individual ΔI_{\max} values and their mean \pm s.e.m. (points, left ordinate) in platelets triggered by A1 (A,C) or WM23 (B, D) binding were plotted, which were from events with (+) or without (-) unfolding of LRRD and/or MSD. Each point represents measurement from a platelet. The frequency of each unfolding combination to occur was indicated. (A,B) Data obtained from 25pN force-clamp experiments. Corresponding t_{\max} (gray bars, right ordinate) were overlaid with ΔI_{\max} . (C,D) Data obtained from 1,000pN/s force-ramp experiments. Corresponding pre- Ca^{2+} largest rupture force f_{\max} (gray bars, right ordinate) were overlaid with ΔI_{\max} .

Furthermore, using a sensitivity-specificity analysis that slides a putative threshold through the t_{\max} vs. Ca^{2+} type data, Prof. Xue found $t_{\max} > 2\text{s}$ to be the best predictor for A1WT to trigger α -type Ca^{2+} (Fig. 4-4 A, dashed line). Thus, a longer-lived bond favors MSD unfolding, thereby triggering α -type Ca^{2+} ; otherwise, it tends to trigger β -type Ca^{2+} . Together, our data suggest separate roles of LRRD and MSD unfolding in GPIb α signaling, with the former intensifying the Ca^{2+} level and the latter determining the Ca^{2+} type digitally.

4.2.8 Perturbing cytoplasmic association of GPIb α with 14-3-3 ζ inhibits mechanoreception

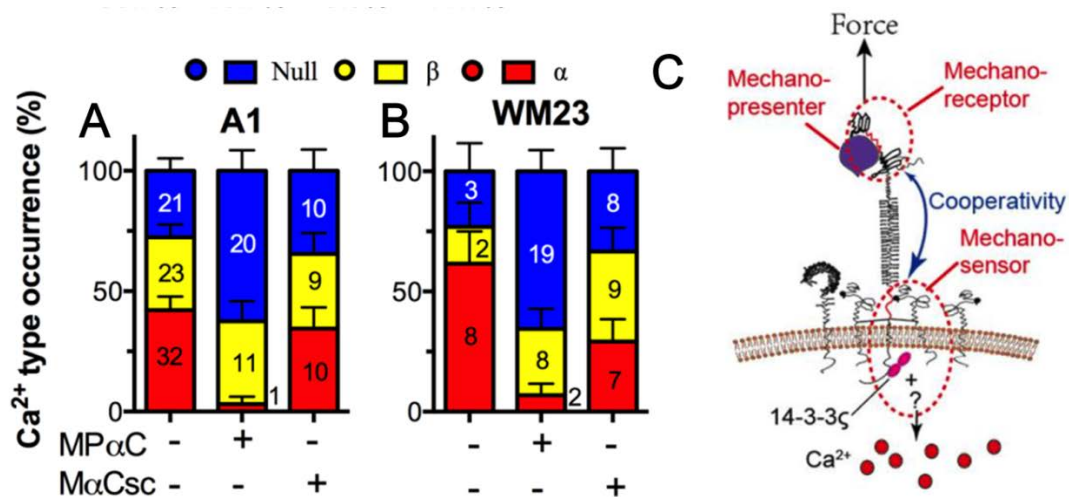


Figure 4-8. The effect of 14-3-3 ζ blockade to platelet Ca^{2+} signaling and a proposed model. (A) Percentage of total events of three Ca^{2+} types in platelets in the same experiments as in Fig. 4-7 (A) and (B) (left bars) as well as additional experiments performed in the presence of MP α C (middle bars) or M α Csc (right bars). Error bar = s.e.m. estimated from the multinomial distribution of events. (C) A postulated model of GPIb α -mediated mechanosensing. Force applied via VWF-A1 induces GPIb α LRRD and MSD unfolding. GPIb β head domain binds to the unfolded MSD and causes the dissociation of its cytoplasmic tail from GPIb α -associated 14-3-3 ζ , which transduces signals across the platelet membrane and further downstream, finally leading to α -type Ca^{2+} . Component names of the mechanotransduction system are indicated.

To understand GPIb α -mediated mechanotransduction requires analysis of not only ligand binding and domain unfolding in the extracellular segment of GPIb α but also events in its cytoplasmic region. 14-3-3 ζ is a cytoplasmic protein that has direct association with both GPIb α and GPIb β at C-terminus¹⁴ and regulates their signaling¹²⁴. To investigate the role of 14-3-3 ζ in GPIb α -mediated Ca²⁺ signaling, we perturbed the system with a myristoylated peptide (MP α C) that blocks the association of GPIb cytoplasmic terminus to 14-3-3 ζ . MP α C mimics the 14-3-3 ζ binding sequence of GPIb α ; a scramble peptide (M α Csc) was used as control. Consistent with the previously reported signaling inhibition effect^{124,125}, MP α C reduced the fraction of α -type Ca²⁺ from 34 to 3% without affecting β -type Ca²⁺, whereas M α Csc had no effect (Fig. 4-8A). Similar results were obtained by pulling GPIb α via WM23 (Fig. 4-8B). Thus, GPIb–14-3-3 ζ association, a biochemical event, is crucial for the transduction of MSD unfolding, a mechanical event, into intracellular signals. These observations indicate that GPIb–14-3-3 ζ serves, at least in part, as a mechanosensor. Incorporating previous discoveries, I proposed that this mechanosensor works in the following way: a durable binding of the headpiece of GPIb α induces LRRD unfolding, which prolongs the lifetime and cooperatively favors MSD unfolding. The unfolding of MSD exposes a domain for the headpiece of GPIb β to bind, which causes the motion and rotation of the whole GPIb β and the dissociation of its cytoplasmic tail from GPIb α -associated 14-3-3 ζ . This dissociation exposes certain domains in the GPIb β or 14-3-3 ζ that may act as a catalytic domain to facilitate further chemical reactions and finally leads to acute and robust intraplatelet granule Ca²⁺ release

(α -type) (Fig. 4-8C, 4-9 C). If the bond is not lasting, no time is given to allow MSD unfolding, which fails to trigger the above Ca^{2+} signaling. However, the transient engagement of GPIIb α via ligand binding under force should still lead to certain intraplatelet reactions which adopt an alternative signaling pathway, resulting in β -type Ca^{2+} (Fig. 4-9 B). To note, β -type Ca^{2+} was regarded in previous publications as a more trivial signal because of its low intensity. If no bond is form at all, then only null-type Ca^{2+} should be observed as a result of no signal transduction at all (Fig. 4-9 C).

4.3 Discussion

The mechanoreception of GPIIb α has been supported by direct observations of transient intracellular Ca^{2+} spike (termed type α/β peak) upon platelet translocation on VWF under shear, with Ca^{2+} intensity reversely proportional to the platelet translocation velocity^{10,11}. Our observation of similar α/β type Ca^{2+} signals that increased with the A1WT–GPIIb α bond lifetime suggests that, despite their isolated, aglycosylated and monomeric nature, recombinant A1 domains may be used as a valid model for studying force-dependent dissociation of GPIIb α bonds and unfolding of GPIIb α domains. However, many questions remain unresolved. Using fBFP real-time single-molecule, single-platelet analysis of ligand binding kinetics, receptor mechanical unfolding and intraplatelet calcium imaging, we have: 1) identified, characterized and mathematically modeled the force regulated and ligand-dependent cooperativity between LRRD and MSD unfolding; 2) defined an optimal magnitude and a threshold duration of clamped force for platelet signal initiation via a single

A1WT–GPIb α bond; 3) uncovered mechanopresentation defects in a type 2B VWD mutant A1R1450E; 4) delineated the interplay among ligand engagement, GPIb α domain unfolding and signal induction; and 5) revealed inhibition of GPIb α mechanoreception by perturbing its cytoplasmic association with 14-3-3 ζ .

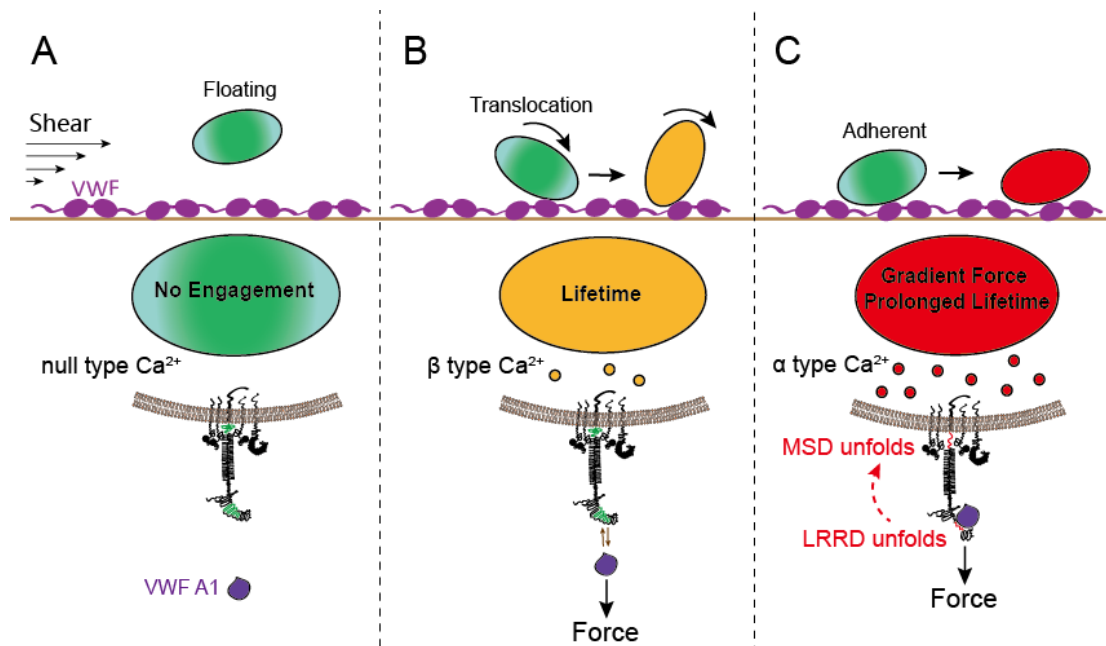


Figure 4-9. Model of GPIb-mediated platelet mechanotransduction. For a circulating platelet above an injured site without physical contact, its GPIb α signaling will not be triggered (A). Upon interacting with VWF, platelets tether and translocate on the sub-endothelial surface via sequential intermittent A1–GPIb α bonds that provide adhesive forces. Having relatively short lifetimes, these forces unlikely induce MSD unfolding on GPIb α , hence only trigger β -type Ca $^{2+}$ (B). LRRD unfolding under a ramped force prolongs bond lifetime to result in temporary platelet attachment, providing a higher chance for MSD unfolding, which triggers α -type Ca $^{2+}$ (C).

It is an interesting yet challenging problem to define the minimum mechanical stimulation for inducing mechanotransduction. We demonstrated that pulling a single GPIb α by a 25pN force of >2s to unfold MSD once is necessary and sufficient to induce α -type Ca $^{2+}$ signals. By comparison, to trigger calcium in a naïve CD8 $^{+}$ T lymphocyte requires a sequence of intermittent bonds with a total of >10s lifetimes

under 10pN accumulated in the first 60s of contacts between T cell receptors and agonist peptide-major histocompatibility complex molecules¹⁰⁴. In both cases durable forces are required, as ramped forces without a clamp phase are unable to trigger appreciable levels of α -type Ca^{2+} regardless of its magnitude (Fig. 4-3 A-D).

The binding defects of VWF-A1 with type 2B VWD mutations have long been recognized¹²⁶. A recent study has shown one such mutation, V1316M, also causes signaling defects¹²⁷. We showed that another mutation, A1R1450E, also has signaling defect. Interestingly, the defect to induce calcium has the same root as the binding defect, namely, the conversion of the wild-type catch-slip bond to the mutant slip-only bond²³. Consequently, force exerted on GPIIb α by A1R1450E is less able to unfold LRRD (Fig. 4-5 C), lasts shorter at 25pN to unfold MSD less frequently (Fig. 4-5 E), does not generate unbinding cooperativity between the LRRD and MSD (Fig. 4-6 G,H, Table 4-2), and induces lower level and frequency of α -type Ca^{2+} at 25 pN (Fig. 4-3 E,F, 4-4 D). Thus, the mechanical requirements for signal induction result in force-dependent patterns of VWF–GPIIb α bond lifetimes, MSD unfolding frequencies, unfolding cooperativities, and Ca^{2+} levels/types that are similar for the same A1 construct but distinct between A1WT and A1R1450E. These findings show that the GPIIb α mechanoreceptor can discriminate ligands and shed light to the biophysical mechanisms of type 2B VWD.

Our new data on the interplay among VWF binding, GPIIb α unfolding, and Ca^{2+} signaling have provided new insights into the inner workings of the A1–GPIIb–

14-3-3 ζ molecular assembly (Fig. 4-8). By residing in the juxtamembrane stalk region, the MSD has been suggested to play a role in mechanosensing, hence termed mechanosensitive domain¹⁶. In the present work, we found that MSD unfolding is required to trigger α -type Ca^{2+} (Fig. 4-7 A,B), showing that this extracellular mechanical event is transduced into intracellular biochemical signals via the 14-3-3 ζ connection. By overlapping with the ligand-binding site, the LRRD can feel the structural change in the A1 and respond with an altered unfolding frequency and changed bond lifetime with and without unfolding its tertiary structure. Further, LRRD unfolding increased the frequency of α -type Ca^{2+} and its level (Fig. 4-7 A). Our findings have broad implications since LRRD is a common structure shared by many adhesion and signaling receptors, e.g., toll-like receptors. Thus, our study has elucidated part of a mechanosensor that includes three components: 1) a MSD in the juxtamembrane region whose conformational change leads to a binary decision of Ca^{2+} type, 2) a LRRD in the ligand-binding region whose conformational change leads to continuous alterations in ligand-binding, signal level and fractions of different signal types, and 3) a MP region that transmits force over a distance and provides coupling between the two domains. Such a delicate mechanosensing system may be important for the platelet to balance its functions between the hemostasis and thrombosis. Future studies will further define these synthetic biology design principles for a generic mechanosensing machine.

CHAPTER 5: GPIB-ALPHA

MECHANOTRANSDUCTION PRIMES PLATELETS INTO AN INTERMEDIATE ACTIVATION STATE

5.1 Introduction

Platelet functioning requires activation by soluble agonists (e.g., ADP and thrombin) or via surface receptor mechanotransduction (e.g., through GPIb α and GPVI), which leads to granule release, P-selectin expression, phosphatidylserine exposure, and the up-regulation of integrin $\alpha_{IIb}\beta_3$ ^{44,74,128-131}.

Previous works demonstrated that platelet $\alpha_{IIb}\beta_3$ could be activated by 1) inside-out signaling, which involves binding of talin and kindlin to the β_3 cytoplasmic domain and the integrin tail separation^{36,40-44,132,133}; and 2) outside-in signaling, which requires ligand association at its headpiece and the downward signal transmission in a structurally allosteric fashion¹³⁴. Inhibition of $\alpha_{IIb}\beta_3$ activation by talin blockage and mutation caused bleeding disorders *in vivo*^{10,11,81,135,136}.

P-selectin expression is a key step in platelet activation, because it is originally stored in the α -granule and will only be available on the cytoplasmic membrane surface upon granule release. P-selectin expression was found on platelets downstream of *in vivo* intracoronary stenosis, suggesting a correlation between stenosis and platelet activation^{69,117,137}. PS exposure allows coagulant activity of platelets, which mainly contributes to the later stages of hemostasis. PS exposure was originally regarded as a sign of platelet apoptosis. But recently it was discovered that

platelet activation could result in PS exposure in a non-apoptotic manner^{71,138}.

Interestingly, shear force played a critical role in both above observations.

However, important questions remain unanswered. Exactly how is the platelet integrin activity regulated on the single-molecular and populational scales? Can platelets discriminate different stimulating signals with regard to integrin activation? Is there a receptor that mediates P-selectin expression and PS exposure under shear force, if so, which one? Is platelet activation reversible in the physiological context?

To answer these questions, we invented the switch BFP approach and measured integrin binding kinetics on the single-cell level, the results of which was complemented by a populational flow-chamber assay (not included in this thesis). Our results provide a conceptual advance to the current model which regards the $\alpha_{\text{IIb}}\beta_3$ activation as a binary result, and demonstrated four related and hierarchical adhesiveness states following different stimulations (inactive; intermediate, following GPIb α mechanotransduction; active, following ADP or thrombin activation, or realized by a cooperation of GPIb α and $\alpha_{\text{IIb}}\beta_3$ mechano-signaling; and hyperactive, following ADP and $\alpha_{\text{IIb}}\beta_3$ cooperative signaling); each state is associated with distinct signaling pathways and integrin conformations. On the other hand, I for the first demonstrated that GPIb α —A1 interaction can trigger low level P-selectin expression and PS exposure.

My work for the first time provides mechanistic insights of integrin activity regulation on live cell surface. Moreover, the low-level up-regulation of integrin

$\alpha_{IIb}\beta_3$, together with moderate level of P-selectin expression and PS exposure, defines an intermediate activation state of platelets following GPIb α mechanotransduction.

5.2 Results

5.2.1 Bidirectional signals drive multi-state transition of integrin $\alpha_{IIb}\beta_3$ on platelets

In this project, we are curious about how inside-out and outside-in signaling regulate integrin $\alpha_{IIb}\beta_3$ activity on live platelets. The conformational dynamics and binding activities of integrin $\alpha_{IIb}\beta_3$ on platelets were characterized by BFP.

5.2.1.1 Single durable adhesion through GPIb α triggers platelet integrin up-regulation

Platelet integrin $\alpha_{IIb}\beta_3$ can be activated through GPIb α -mediated mechano-signaling⁹⁻¹¹. To study this process in the single-cell level, a freshly isolated human platelet was gently aspirated by a micropipette and served as the target. Plasma VWF, which interacts with both GPIb α and integrins $\alpha_{IIb}\beta_3$ ¹³⁹, was coated onto a streptavidin (SA)-coupled glass bead that served as the probe. Adhesion frequency experiments were performed, and adhesion events were enumerated over 50 and 100 cycles of touch (see Materials and Methods) to yield adhesion frequencies. The reason to trace the adhesion frequency for two different numbers of cycles is considering that the integrin up-regulation might be a gradual process. Surprisingly, the adhesion frequencies were comparable to control which blocked β_3 integrins binding by integrilin¹⁴⁰, indicating negligible integrin activity (Fig. 5-1A *left*). In

sharp contrast, force-clamp experiments which allowed durable binding (see Materials and Methods) drastically up-regulated the adhesion frequency to ~2-fold (Fig. 5-1A *right*).

To rule out the possibility that the binding strengthening was due to conformational changes of the VWF by force stretching, two separate platelet ligands, mA1 and FN_{III7-10} were instead used as a dual ligand setup to repeat the experiments. The Arg-Gly-Asp (RGD) sequence FN_{III7-10} contains in domain 10 is shared by VWF^{15,141-143}. To note, the synergy site contained in fibronectin domain 9 is important in $\alpha_5\beta_1$ binding¹⁴⁴, but secondary for $\alpha_{IIb}\beta_3$ and trivial for $\alpha_v\beta_3$ ¹⁴⁵. After blocking one of the dual receptor-ligand interactions with 6G1 (mA1 blocking Ab)¹⁴⁶ or integrilin ($\alpha_{IIb}\beta_3$ antagonist), the adhesion frequency exhibited no difference over touches and between the lifetime-absent/-present conditions, confirming the stability of sole GPIIb α -mA1 and $\alpha_{IIb}\beta_3$ -FN_{III7-10} interactions (Fig. 5-1B). Overlaying the sole GPIIb α -mA1 and $\alpha_{IIb}\beta_3$ -FN_{III7-10} interactions yielded an adhesion frequency (Fig. 5-1B, dashed line) that was comparable to the lifetime-absent dual-receptor interaction, suggesting no receptor inter-talk in the absence of durable binding. In comparison, allowing durable binding substantially elevated the adhesion frequency to >1.5-fold, which (50%) was much higher than the overlay of the two sole interactions (26% + 4%) (Fig. 5-1B). As controls, adenosine diphosphate (ADP)-activated platelets yielded a high adhesion frequency even after 6G1 blockade that reflected a strong integrin activity, which was nearly eliminated by integrilin and soluble RGDS¹³⁵ (Fig. 5-1C).

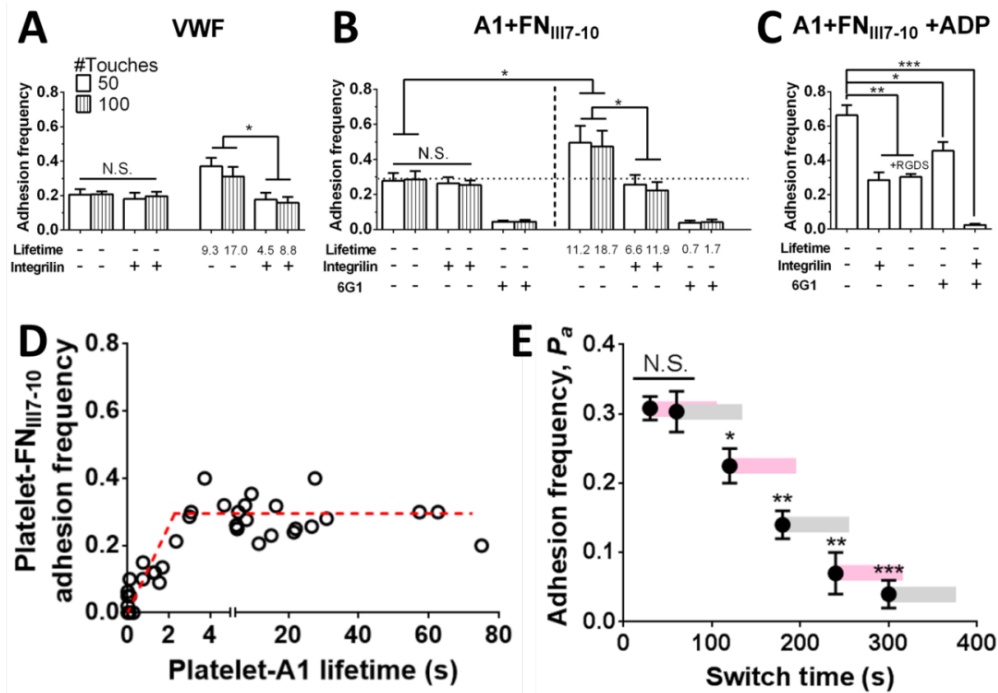


Figure 5-1. Identification of β_3 integrin up-regulation following GPIIb mechanotransduction. (A-C) Adhesion frequencies of platelets vs. plasma VWF (A) or dually-coated A1+ FN_{III7-10} (B,C). Each platelet-bead pair was tested repeatedly for 50 and 100 cycles to estimate two separate adhesion frequencies. Four pairs were tested to obtain mean \pm SEM. 10 μ g/ml integrilin and 2 μ M 6G1 were used to respectively block β_3 integrins and GPIIb binding. The permission of lifetime events was decided by pre-setting the experimental mode to force-ramp (lifetime -) or force-clamp (lifetime +). The average number of lifetime events, if permitted, was indicated under each bar. (B) Horizontal dashed line: overlay of the averaged sole GPIIb α -mA1 (P_1) and $\alpha_{IIb}\beta_3$ -FN_{III7-10} (P_2) adhesion frequencies by $P_{1+2} = 1 - (1 - P_1) * (1 - P_2)$. (C) Platelets were treated with ADP for activation. (D) Scatter plot of platelet-A1 lifetime vs. platelet-FN_{III7-10} adhesion frequency. Each point represented one platelet under interrogation. The two dashed red lines were linear fittings of the data in lifetime regimes of [0~5 s] and [5~80 s]. Each platelet-bead pair was tested repeatedly for 30 cycles with a 1 s contact time to estimate the adhesion frequency. (E) Post-switch platelet-FN_{III7-10} adhesion frequency vs. switch time, showing instability of integrin up-regulation. The switch time was defined as the interval between the end of the platelet touching Probe I and the beginning of it touching Probe II. Magenta and gray stripes marked the time range that each adhesion frequency data point was summarized from (30 cycles = 75 seconds). N.S. = not statically significant; * = $p < 0.05$; ** = $p < 0.01$; *** = $p < 0.001$; assessed by unpaired, two-tailed Student's *t*-test.

To look into more details of GPIIb mechanotransduction and the dual-receptor inter-talk process, we upgraded our BFP system to perform a switch BFP assay, in which two probes were assembled to sequentially interrogate a single platelet (see Materials and Methods). The beads of Probe I and II were respectively functionalized

with mA1 and FN_{III7-10} (or Fg in following experiments). A platelet was first aligned and repeatedly touched with Probe I in force-clamp mode allowing durable binding under ~25 pico-Newton (pN), the force that realized peak lifetime in GPIb α -mA1 catch-bond (Fig. 2-4A)^{23,89,105,146}. Once a lifetime event was observed, the platelet-holding micropipette would be quickly maneuvered to move upward and align with Probe II and began repeated touches to test integrin activity (Fig. 2-4B).

Using this newly built dual BFP system, we investigated the temporal requirements for integrin activation by GPIb α -induced inside-out signaling. In the first experiment, once a bond lifetime event with the A1-bearing Probe I was observed, the platelet was switched to the FN_{III7-10}-bearing Probe II to test integrin binding. It took ~30 s to switch the platelet from Probe I to II. The integrin-FN_{III7-10} binding frequency, estimated from 30 repetitive touches that took ~75 s to complete, was plotted vs. the GPIb α -A1 bond lifetime both measured using the same platelet (Fig. 5-1D). The reason to use 30 instead of 50 or 100 touches here was to avoid the contamination of the data by further integrin up-regulation via its outside-in signaling. Platelet adhesion to FN_{III7-10} increased with GPIb α -A1 bond lifetime initially but reached a steady-state of ~30% at 2 s (Fig. 5-1D, red dashed line). These data demonstrate the necessity of a durable force for GPIb α mechanotransduction and the sufficiency of a single GPIb α bond for upregulation of platelet integrins. The 2-s threshold also agreed well with the lifetime threshold defined in Chapter 4 that triggers mostly α -type Ca²⁺ (Fig. 4-4A), further confirming the central role of α -type Ca²⁺ in platelet activation.

In the second experiment, we prolonged the time to switch from Probe I to II to examine the sustainability of integrin activation. The result was plotted on Fig. 5-1E, showing that, once triggered by a >2-s GPIIb α -A1 bond lifetime event, platelet integrins remained activated for ~130 s, but were downregulated gradually with further increase in switch time, and eventually returned to the low activity state. This reversal of integrin activation coincided with the cease of active shape changes in platelets, which were often observed in our BFP experiments when they were repeatedly touched by GPIIb α -bearing beads. The return to their discoid shape suggested that platelet and integrin activation triggered by GPIIb α mechanotransduction is reversible¹¹.

5.2.1.2 GPIIb α mechanotransduction primed platelet $\alpha_{IIb}\beta_3$ into an intermediate state

Platelet $\alpha_{IIb}\beta_3$ can be chemically activated by soluble agonists like ADP and thrombin, which is in parallel with mechanotransduction by adhesions^{37,44,135}. We wondered whether the mechano-activation and chemo-activation of platelets lead to distinct integrin up-regulations. To test that, we conducted adhesion frequency experiments between platelets and FN_{III7-10} beads. Non-treated platelets exhibited very weak binding of ~5% adhesion frequency (Fig. 5-2A, green non-patterned bar). Agreeing with their activating roles, pre-treatment of ADP and thrombin drastically promoted the adhesion frequency over all contact times (Fig. 5-2A, red and brown bars). The adhesion frequency data were fitted to a Poisson distribution to evaluate the equilibrated average number of receptor-ligand bonds that form between the two

surfaces at contact (see Materials and Methods for details), which was then normalized by the $FN_{III7-10}$ site density to derive $\langle n \rangle_{total}/m_1^{92,95}$, which revealed a >10-fold difference between non-treated and ADP-/thrombin-activated groups (Fig. 5-2C). To note, because a low adhesion frequency may compromise the accuracy of fitting, beads with a higher site density ($60 / \mu m^2$ vs. $28 / \mu m^2$) were used to repeat the experiments for the non-treated group, the results of which were normalized based on the site density to derive the average number of bonds (Fig. 5-2A).

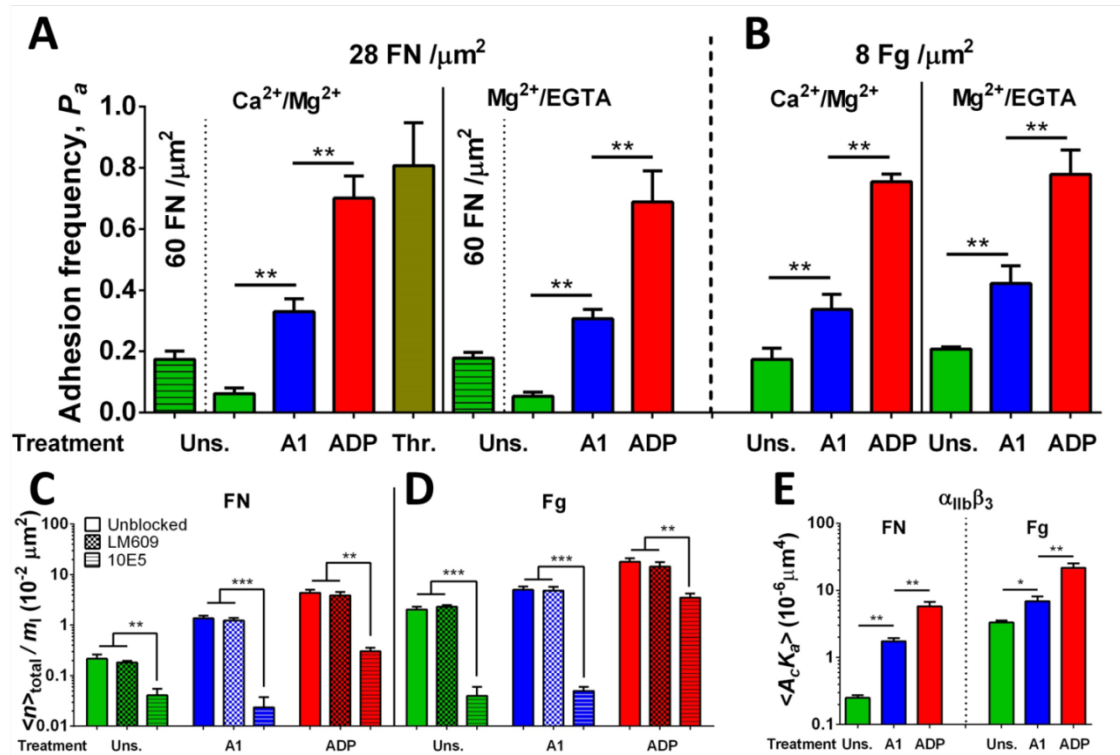


Figure 5-2. Characterization of platelet binding kinetics against $FN_{III7-10}$ and fibrinogen. (A,B) Adhesion frequency of platelets binding to $FN_{III7-10}$ (A) and fibrinogen (B) at 5-s contact time. The platelets were without pre-treatment (green curves), triggered by durable mA1 binding (blue curves) or incubated with $100 \mu M$ ADP (red curves) or $0.1 U/ml$ thrombin (brown curve in panel A). The experiments were performed both in Ca^{2+}/Mg^{2+} and $Mg^{2+}/EGTA$. Each platelet-bead pair was tested repeatedly for 30 cycles to estimate the adhesion frequency; four pairs were tested under each contact time to obtain mean \pm SEM. (C,D) Mean \pm SEM of average number of bonds normalized by ligand site density ($\langle n \rangle_{total}/m_1$) of platelet binding to $FN_{III7-10}$ (C) or fibrinogen (D), with and without $\alpha_{IIb}\beta_3$ -blocking antibody 10E5 and $\alpha_{V}\beta_3$ -blocking antibody LM609. (E) $\alpha_{IIb}\beta_3$ - $FN_{III7-10}$ and $\alpha_{IIb}\beta_3$ -Fg average effective affinity.

*N.S. = not statically significant; ** = $p < 0.01$; assessed by unpaired, two-tailed Student's t -test.*

Remarkably, mA1 triggering realized an intermediate level of adhesion frequency which resided between the non-treated and ADP-/thrombin-activated groups (Fig. 5-2A). The $\langle n \rangle_{\text{total}}/m_1$ was 5-fold more than the non-treated group but 2.5-fold less than ADP-/thrombin-activated groups (Fig. 5-2C). Substituting mA1 with dimeric VWF A1 to allow *cis*-crosslinking of GPIb α molecules did not make any difference to the adhesion frequency (Fig. 5-3, dark blue bar). Priming ADP-activated platelets with mA1 does not further elevate the adhesion level, suggesting that the effects of ADP and mA1 are not cooperative (Fig. 5-3, black bar).

Despite the predominant abundance of $\alpha_{\text{IIb}}\beta_3$ on platelet surface, the contribution of other two integrins, $\alpha_{\text{V}}\beta_3$ and $\alpha_5\beta_1$, to the binding may still need to be reckoned with. The addition of integrilin eliminated all binding of both mA1-triggered and ADP-activated platelets to FN_{III7-10}, ruling out the involvement of $\alpha_5\beta_1$ (Fig. 5-3). On the other hand, 10E5, an Ab that specifically blocks $\alpha_{\text{IIb}}\beta_3$ but not $\alpha_{\text{V}}\beta_3$ ¹⁴⁷, eliminated almost all binding of mA1-triggered platelets, whereas ADP-activated platelets still maintained a considerable level of binding (Fig. 5-2C). Consistent with that, LM609, a $\alpha_{\text{V}}\beta_3$ -specific blocking Ab¹⁴⁸, caused negligible effects to mA1-triggered platelets, but slightly weakened the binding of ADP-activated platelets (Fig. 5-2C). Fitting the two ADP-activated adhesion frequency data suggested that the average number of bonds formed by $\alpha_{\text{IIb}}\beta_3$ was ~8-fold of $\alpha_{\text{V}}\beta_3$. As a control, pre-incubating the platelets with a T-cell receptor antibody which is non-specific to this system yielded no effect

at all (Fig. 5-3). All these results indicated that ADP-activated strong adhesiveness was co-contributed by $\alpha_{IIb}\beta_3$ and $\alpha_v\beta_3$ activation in which $\alpha_{IIb}\beta_3$ played the dominant role, while the mA1-triggered intermediate adhesiveness was solely from $\alpha_{IIb}\beta_3$.

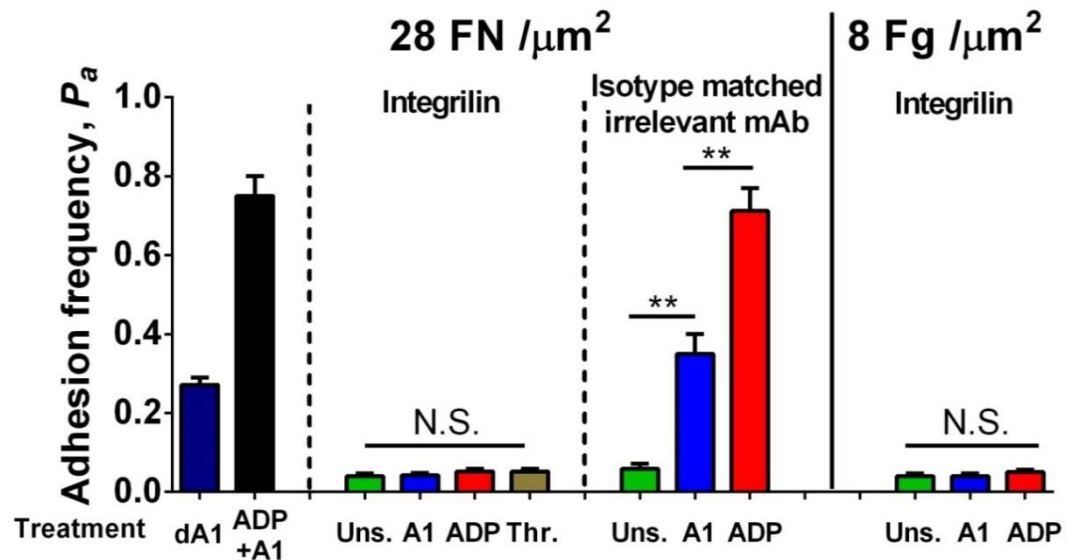


Figure 5-3. Platelet–FN (left) and –Fg (right) adhesion frequency after different treatments (indicated in the figure). Each platelet–bead pair was tested repeatedly for 30 cycles to estimate the adhesion frequency; four pairs were tested under each contact time to obtain mean \pm SEM.

The $\langle n \rangle_{\text{total}}/m_1$ with LM609 blockade was then divided by m_r to derive three distinctive average effective affinities of $\alpha_{IIb}\beta_3$ – binding capacity averaged over all $\alpha_{IIb}\beta_3$ population – following no treatment, mA1 triggering and ADP activation (Fig. 5-2E). These results defined three populational states of platelet surface $\alpha_{IIb}\beta_3$ – inactive, intermediate and active.

Remarkably, platelets also exhibited three distinct states against another major β_3 ligand, fibrinogen, following no treatment, mA1 triggering and ADP activation (Fig. 5-2B). Blockade by integrilin, LM609 and 10E5 further confirmed that these three adhesivenesses were again predominantly realized by $\alpha_{IIb}\beta_3$ (Fig. 5-2, 5-3). $\alpha_v\beta_3$ had

no activity on inactive and A1-triggered platelets, but was up-regulated on ADP-activated platelets. To note, much stronger binding was observed from non-treated platelet $\alpha_{\text{IIb}}\beta_3$ against fibrinogen than $\text{FN}_{\text{III7-10}}$, consistent with the fact that non-activated platelets could attach onto surfaces with immobilized fibrinogen (Fig. 5-2E, compare two green bars)¹⁴⁹. Chelating the extracellular Ca^{2+} by EGTA slightly strengthened the binding with no statistical significance under all conditions, indicating that extracellular Ca^{2+} was unessential in these activation pathways (Fig. 5-2 A,B). Remember that Mg^{2+} is a weak integrin activator and moderately activates cell surface integrins^{29,150,151}, it becomes puzzling that $\text{Mg}^{2+}/\text{EGTA}$ failed to make any difference in this context. We postulate that this was owing to the strong platelet regulation on the integrins, which overrode the cation interference.

5.2.1.3 Progression and recession of the intermediate state

Integrins could transduce signals bi-directionally, namely, inside-out and outside-in signaling^{135,152}. Binding of $\alpha_{\text{IIb}}\beta_3$ to immobilized VWF was shown to induce robust Ca^{2+} influx (γ -type signaling) following $\text{GPIIb}\alpha$ -triggered transient Ca^{2+} (α/β -type signaling)^{10,11}. To investigate how this outside-in signaling changes the activity of $\alpha_{\text{IIb}}\beta_3$, repeated touches of $\text{FN}_{\text{III7-10}}$ were applied to the post-switch platelets over 200 cycles, considering that the signal transduction should consume time. After ~50 cycles' of relatively stable activity, the slide frequency (adhesion frequency within a 30-cycle sliding window) started to gradually increase, which eventually stabilized at a much higher level after ~80 cycles, indicating a

second-stage up-regulation of the integrins (Fig. 5-4 A,C, magenta). In sharp contrast, chelating extracellular Ca^{2+} by EGTA deprived the integrins' capability to be primed, and instead caused a gradual recession that reached minimum after ~ 100 cycles (Fig. 5-4 A,C, cyan). As controls, non-treated platelets exhibited a low level of binding throughout the 200 cycles in both $\text{Ca}^{2+}/\text{Mg}^{2+}$ and $\text{Mg}^{2+}/\text{EGTA}$ (Fig. 5-4B). Substituting $\text{FN}_{\text{III7-10}}$ with PAC-1, a ligand-mimicking Ab specifically targeting the active binding epitope, also yielded similar results of binding progression in $\text{Ca}^{2+}/\text{Mg}^{2+}$ (Fig. 5-4F). However, the anticipated recession in $\text{Mg}^{2+}/\text{EGTA}$ was not observed (Fig. 5-4G).

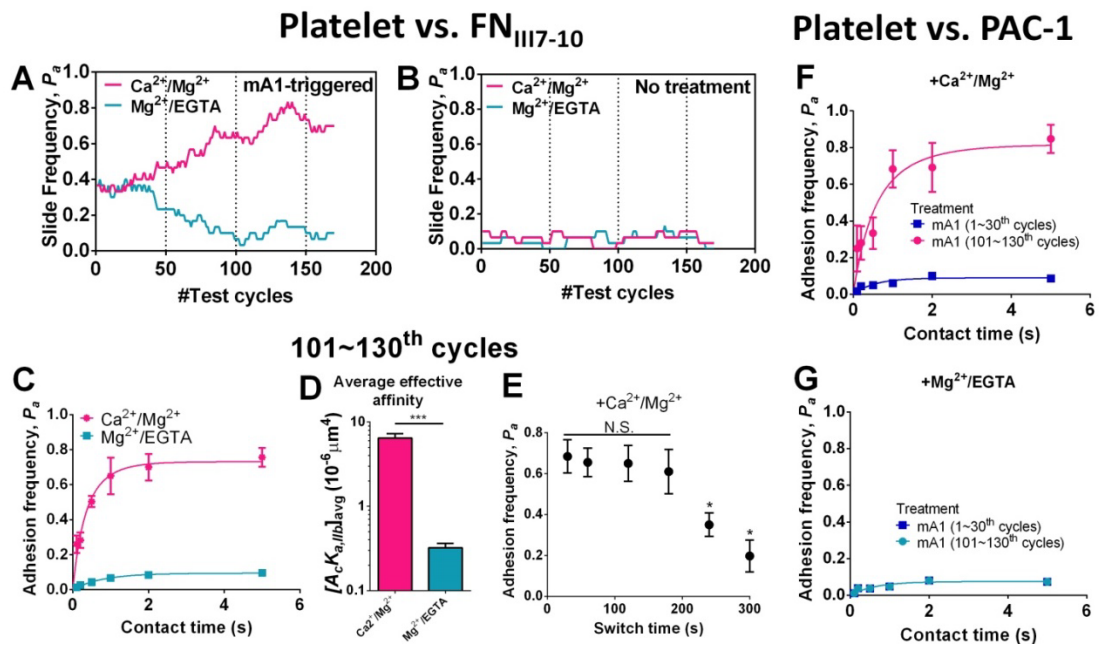


Figure 5-4. Progression and recession of intermediate state. LM609 was added in all experiments to block $\alpha_v\beta_3$. (A,B) Representative platelet- $\text{FN}_{\text{III7-10}}$ binding slide frequency (window size: 30) vs. #test cycles after mA1 triggering (A) or without pre-treatment (B). The experiments were performed in $\text{Ca}^{2+}/\text{Mg}^{2+}$ (magenta curves) or $\text{Mg}^{2+}/\text{EGTA}$ (cyan curves). (C) Adhesion frequency vs. contact time of mA1-triggered platelets binding to $\text{FN}_{\text{III7-10}}$ after 100 cycles in $\text{Ca}^{2+}/\text{Mg}^{2+}$ (magenta curve) or $\text{Mg}^{2+}/\text{EGTA}$ (cyan curve). (D) Mean \pm SEM of average effective 2-D affinity ($\langle A_c K_a \rangle$) calculated from fitting Equation 1 in Materials and Methods to the adhesion frequency data in (C) followed by applying Equation 9. (E) Adhesion frequency vs. switch time of mA1-triggered platelets binding to $\text{FN}_{\text{III7-10}}$ after 100 cycles in $\text{Ca}^{2+}/\text{Mg}^{2+}$. (F,G) Adhesion frequency vs. contact time of mA1-triggered platelets binding to

*FN_{III7-10} in Ca²⁺/Mg²⁺ (F) or Mg²⁺/EGTA (G) (blue curves: first 30 cycles; magenta (F) or cyan (G) curves: 101~130th cycles). In panels C, E, F and G, each platelet–bead pair was tested repeatedly for 30 cycles to estimate the adhesion frequency; four pairs were tested under each contact time to obtain mean ± SEM. N.S. = not statically significant; * = p < 0.05; *** = p < 0.001; assessed by unpaired, two-tailed Student’s t-test.*

The $\alpha_{\text{IIb}}\beta_3$ -FN_{III7-10} adhesion frequency vs. contact time curves (Fig. 5-4C) were fitted to the 2D kinetics model to evaluate $\langle A_c K_a \rangle$ after 100 cycles of touch. Intriguingly, the affinity of platelets under Ca²⁺/Mg²⁺ condition was comparable to ADP-activated platelets, while that under Mg²⁺/EGTA condition similar to non-treated (compare Fig. 5-4D and 5-2F).

All the above evidences, together with the aforementioned “post-switch adhesion frequency vs. switch time” results (Fig. 5-1E), implicated that the intermediate but not inactive state will progress into the active state upon $\alpha_{\text{IIb}}\beta_3$ outside-in signaling, which requires both ligand priming and extracellular Ca²⁺. Or else, it will fast recess back to the weak adhesiveness state.

5.2.1.4 Identification of three bond dissociating states

Integrins may adopt more than one conformational state and affinity state, which reach different equilibriums on the populational level under different environmental, cellular and mechanical conditions^{27,29,47,153}. We hypothesized that the observed distinct adhesiveness states of $\alpha_{\text{IIb}}\beta_3$ were a collective effect of the state equilibrium shifts of individual integrins. To test this hypothesis, bond lifetimes were measured using BFP force-clamp assay to collect bond kinetics information on the single-molecular level. Plotting average lifetime *versus* clamping force revealed that

the non-treated platelet $\alpha_{IIb}\beta_3$ binding to $FN_{III7-10}$ manifested a “slip-bond” behavior¹⁰⁵, with the lifetime monotonically decreasing with force increase and eventually diminishing at 30 pN (Fig. 5-5A, green). ADP-activated platelets realized a robust catch-bond that ranged from 0 to 30 pN, reaching a peak of 18 s¹⁰⁵; afterwards, it started to decrease and eventually approached zero at 85 pN (Fig. 5-5A, red). Interestingly, the lifetime of the mA1-triggered group again resided in between of these two groups (Fig. 5-5A, blue). The curve exhibited a subtle “catch” behavior below 6 pN, and the force range was 0-37 pN, broader than non-treated but narrower than ADP-treated platelets (Fig. 5-5A, blue). The distinction among the three curves suggested that at least three bond states were involved. To confirm this postulation and gain more insights into the force regulation on the binding kinetics, we fit the lifetime data with a multi-state model, assuming a mixture of several subpopulations of bonds, each of which follows first-order dissociation kinetics that governs an exponential distribution of lifetimes under any constant force (see Materials and Methods). The semi-log survival frequency vs. lifetime curves (Fig. 5-6) were well-fitted by a three-state model (Table 5-1, setting $R^2 > 0.90$ as the criteria of good fitting), which yielded the off-rates and subpopulation fractions of each state – fast-, intermediate- and slow-dissociating states – under forces (Fig. 5-5 B-E). Remarkably, when the off-rates of the three states were superimposed onto the same semi-log plot against force, they beautifully aligned with three linear fittings, indicating that the off-rates of the three states decreased exponentially with increasing force (Fig. 5-5B), in agreement with the Bell’s model⁹⁶ (see Materials and Methods). The three fitting

lines thus defined the off-rates of the three bond states under all forces (Table 5-2). The subpopulation composition of non-treated group was simple: all integrins adopted the fast-dissociating state (Fig. 5-5C). A mixture of fast- and intermediate-dissociating bonds formed in the mA1-triggered group, with the respective fractions of subpopulation monotonically decreasing and increasing along force increase, suggesting a force-activating mechanism (Fig. 5-5C). ADP-activated group, on the other hand, formed bonds from all three dissociating states. The fractions of fast- and slow-dissociating bonds monotonically increased along force increase, while that of intermediate-dissociating bonds appeared to be oscillatory (Fig. 5-5D). To note, under the maximal force of non-treated, mA1-triggered and ADP-activated groups, the bond composition was respectively dominated by the fast-, intermediate- and slow-dissociating state.

Different than FN_{III7-10}, all three $\alpha_{IIb}\beta_3$ -Fg lifetime curves exhibited evident “catch-slip” signatures, but with step-wise developmentally broadened catch-bond regime, higher peak lifetime amplitude and wider force range (Fig. 5-5F). To note, the non-treated lifetime curve showing a catch-bond was in discrepancy with the previous results collected in a purified system⁵⁸, which we speculated was owing to the cellular regulation of the platelet. Further analysis revealed that the Fg binding also followed a three-state model, each of the states again benignly following the Bell’s model (Fig. 5-5G, Table 5-1, 5-2). However, the composition of bond states became more complicated: besides fast-dissociating bonds, non-treated platelets also formed intermediate-dissociating bonds under force priming, whereas mA1-triggered and

ADP-activated platelets realized all three bond states under certain forces (Fig. 5-5 H-J). These results indicated a ligand-discriminative mechanism in the force-regulation of $\alpha_{IIb}\beta_3$ binding. Nonetheless, in consistency with FN_{III7-10} binding, increase of force again monotonically increased the fraction of slower-dissociating states, and decreased the fraction of faster-dissociating states in all Fg binding (Fig. 5-5 H-J). All these results identified three bond states of $\alpha_{IIb}\beta_3$ binding to both FN_{III7-10} and Fg, which reach different equilibriums under different conditions; both force and platelet activation shifted the equilibrium towards more stronger and less weaker bonds.

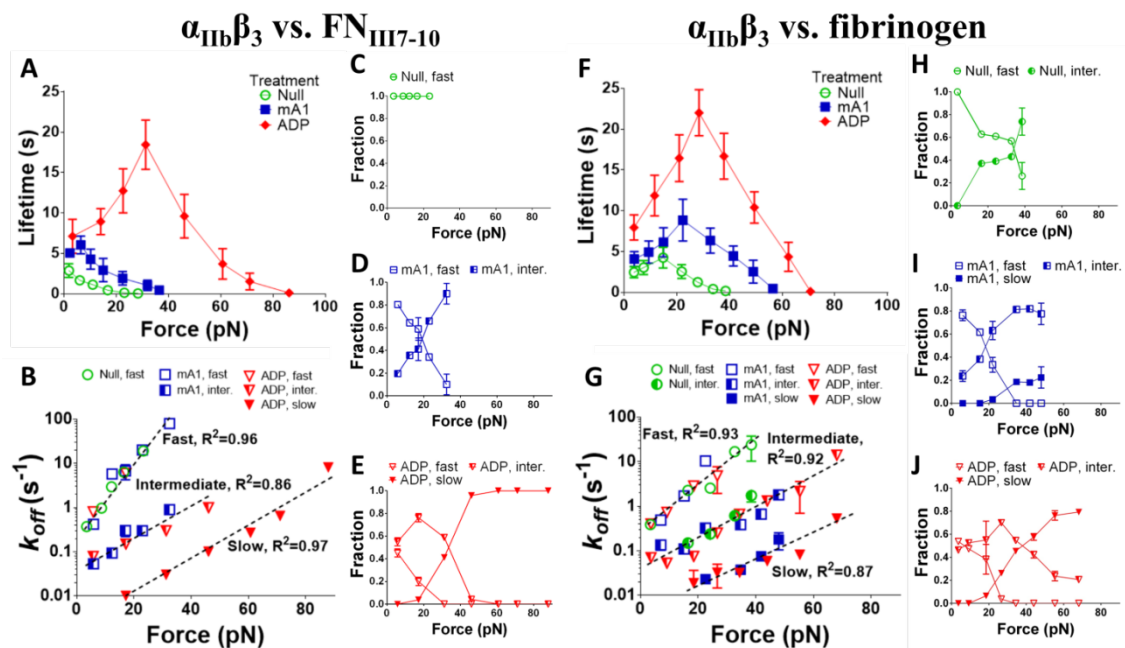


Figure 5-5. Characterization and three-state model of $\alpha_{IIb}\beta_3$ -ligand bond dissociation under forces. LM609 was added in all experiments to block $\alpha_v\beta_3$. (A,F) Mean \pm SEM of lifetime vs. force of non-treated (green curves), mA1-triggered (blue curves) and ADP-activated (red curves) platelets binding to FN_{III7-10} (A) or fibrinogen (F) in Ca²⁺/Mg²⁺. (B,G) Plots of off-rates (k_{off}) of the fast- (open symbols), intermediate- (half-filled symbols), and slow-dissociating states evaluated from fitting a three-state model to the $\alpha_{IIb}\beta_3$ -FN_{III7-10} or $\alpha_{IIb}\beta_3$ -fibrinogen lifetime survival frequency (Supplemental Fig. 4; Materials and Methods, Equation 10). (C-E,H-J) Fraction of $\alpha_{IIb}\beta_3$ -FN_{III7-10} (C-E) or $\alpha_{IIb}\beta_3$ -fibrinogen (H-J) bonds in fast- (open symbols), intermediate- (half-filled symbols), and slow-dissociating states. (B,G) The points in fast-, intermediate- and slow-dissociating states were fitted by the Bell's model

respectively (dashed lines; Materials and Methods, Equation 11). The platelets were non-treated (C,H), mA1-triggered (D,I), or ADP-activated (E,J). Error bars: SEM.

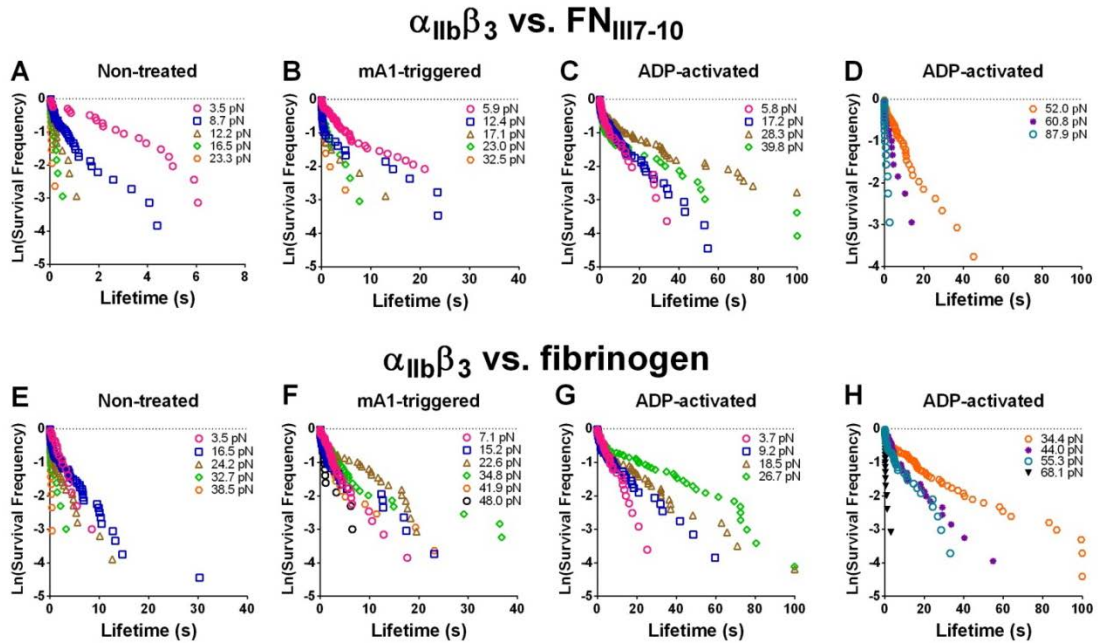


Figure 5-6. Semi-log survival frequency vs. lifetime of platelet $\alpha_{IIb}\beta_3$ binding to $FN_{III7-10}$ (A-D) and fibrinogen (E-H) under different forces. The platelets were non-treated (A,E), mA1-triggered (B,F), or ADP-activated (C,D,G,H). A linear distribution indicates one bond dissociating state, while a kink in the curve indicates a mixture of multiple states.

When force approached zero, non-treated platelets only formed fast-dissociating bonds, whereas mA1 and ADP promoted a fraction of the bonds to the intermediate-dissociating state (Fig. 5-5 C-E, H-J). This information, together with the enhanced adhesiveness of mA1-triggered and ADP-activated platelets observed from adhesion frequency enhancement, suggested that activations primed a proportion of the integrins into a higher affinity state with an intermediate off-rate. However, one should not assume that the affinity states of individual integrins have one-to-one correspondence to the bond states. For example, the 6-fold increase in the $FN_{III7-10}$ binding $\langle A_c K_a \rangle$ following mA1 triggering meant that the average number of bonds formed by these platelets were 6-fold more than non-treated (Fig. 5-2F), suggesting

that the up-regulated integrins contributed most of the bonds; however, based on lifetime fitting results, the intermediate-dissociating state only contributed ~1/5 of the total bond number (Fig. 5-5D), exhibiting a huge discrepancy. Remember that affinity is the ratio of on-rate and off-rate, it is likely that a considerable fraction of the integrin population had their affinity substantially elevated, but still remained in the fast-dissociating bond state, realizing an intermediate-affinity state with high on-rate and high off-rate.

Table 5-1. Goodness-of-fit of one-, two- or three-state model fitting to the survival frequency vs. lifetime of platelet $\alpha_{IIb}\beta_3$ binding to FN_{III7-10} and fibrinogen under different forces (Fig. 5-6).

		Goodness-of-fit (R^2)			Goodness-of-fit (R^2)			
#States		1	2	3		1	2	3
Ligand		FN _{III7-10}			Fg			
Condition	Force (pN)				Force (pN)			
Non-treated	3.5	0.93	0.93	0.95	3.5	0.98	0.99	0.99
	8.7	0.90	0.99	0.99	16.5	0.74	0.96	0.99
	12.2	0.92	0.98	0.98	24.2	0.72	0.97	0.99
	16.5	0.95	0.98	0.98	32.7	0.63	0.99	0.99
	23.3	0.90	0.94	0.94	38.5	0.87	0.99	0.99
mA1-triggered	5.9	0.77	0.99	0.99	7.1	0.81	0.99	0.99
	12.4	0.53	0.97	0.98	15.2	0.69	0.98	0.98
	17.1	0.36	0.99	0.997	22.6	0.41	0.83	0.97
	23	0.80	0.99	0.99	34.8	0.54	0.99	0.99
	32.5	0.43	0.94	0.97	41.9	0.61	0.99	0.99
				48	0.62	0.95	0.95	
ADP-activated	5.8	0.87	0.98	0.98	3.7	0.78	0.99	0.99
	17.2	0.87	0.89	0.99	9.2	0.75	0.92	0.996
	28.3	0.74	0.99	0.99	18.5	0.58	0.81	0.99
	39.8	0.88	0.98	0.99	26.7	0.65	0.82	0.97
	52	0.92	0.98	0.996	34.4	0.86	0.98	0.98
	60.8	0.96	0.97	0.97	44	0.88	0.99	0.99
	87.9	0.98	0.99	0.99	55.3	0.87	0.98	0.98
				68.1	0.22	0.99	0.99	

5.2.1.5 Signaling pathway and integrin conformation of the intermediate and active states

Physiological activation of integrins involves talin binding to the β -subunit cytoplasmic tail, which disrupts the clasping and causes separation of the two subunits in the tailpiece, and subsequently enhances integrin binding activity via allosteric effects^{40,44,46,132,154}. Two recent works further demonstrated that soluble platelets agonists triggers two opposite yet sequential waves of talin and $G\alpha_{13}$ binding to $\alpha_{IIb}\beta_3$, which are respectively involved in inside-out and outside-in signaling^{135,155}. To investigate the relation of these signaling events with the adhesiveness states defined above, platelets were treated with two β_3 cytoplasmic sequence mimicking peptides mP₁₃ (blocking both talin and $G\alpha_{13}$) and mP₆ (blocking $G\alpha_{13}$)¹³⁵. mP₁₃ drastically weakened the binding of both mA1-triggered and ADP-/thrombin-activated platelets to the level indistinguishable from the non-treated group (Fig. 5-7A), reflecting an indispensable role of talin binding to realizing both the intermediate and active states. On the other hand, mP₆ had no effect on the mA1-triggered platelets, but lowered the binding of ADP-/thrombin-activated platelets to the same level as mA1-triggered, indicating that $G\alpha_{13}$ binding is respectively necessary and superfluous for the intermediate and active states. As controls, two scrambled control peptides exhibited no effect to ADP and thrombin activation at all (Fig. 5-7 A,B)¹³⁵, and DMSO alone also showed no difference to all states (Fig. 5-3E).

Integrins could adopt multiple global conformations, including a bent or extended ectodomain, a joined or separated tailpiece and a close or opened β subunit hybrid domain; integrin signaling and activation are accompanied by conformational changes^{47,108,152,153,156,157}. To identify the conformations of $\alpha_{IIb}\beta_3$ under the different

adhesiveness states, we coated several conformation-sensitive Abs onto probe beads, and measured their binding to platelets. PAC-1 manifested minimal binding to both non-treated and mA1-triggered platelets, but strongly bound to ADP-activated platelets, indicating that the active ligand binding epitope was not exposed by GPIIb α mechanotransduction (Fig. 5-7C, magenta). This also explained the lack of recession of platelet intermediate state under the interrogation of PAC-1 (Fig. 5-4G), because the intermediate state is specific to ligands but not PAC-1. Similarly, AP5, an Ab that reports β_3 hybrid domain swing-out¹⁵⁸, only bound to platelets after ADP activation but not mA1 stimulation. On the other hand, LIBS-2 (ab62), which reports ectodomain extension, exhibited similarly high binding to mA1-triggered and ADP-activated platelets.

Table 5-2, parameters of fast-, intermediate- and slow-dissociating states of platelet $\alpha_{IIb}\beta_3$ binding to FN_{III7-10} or Fg, fitted by Bell's model (Governing Equation).

Governing Equation		$k(f) = k_0 \exp (af/k_B T)$					
Ligand		FN _{III7-10}			Fg		
Parameter		k_0 (s ⁻¹)	$a/k_B T$ (pN ⁻¹)	a (nm)	k_0 (s ⁻¹)	$a/k_B T$ (pN ⁻¹)	a (nm)
Bond state	fast-diss.	0.240	0.190	0.780	0.256	0.122	0.503
	inter.-diss.	0.049	0.072	0.295	0.037	0.080	0.331
	slow-diss.	0.0017	0.090	0.370	0.0051	0.062	0.256

Integrins act as a spring under a tensile force, with the stiffness dependent on the conformation. Previous studies reported that integrins $\alpha_L\beta_2$ ⁶³ and $\alpha_4\beta_1$ ¹⁵⁹ were softer and stiffer when the ectodomain was respectively bent and extended. The molecular stiffness thus provides an alternative approach to inspect the integrin conformation.

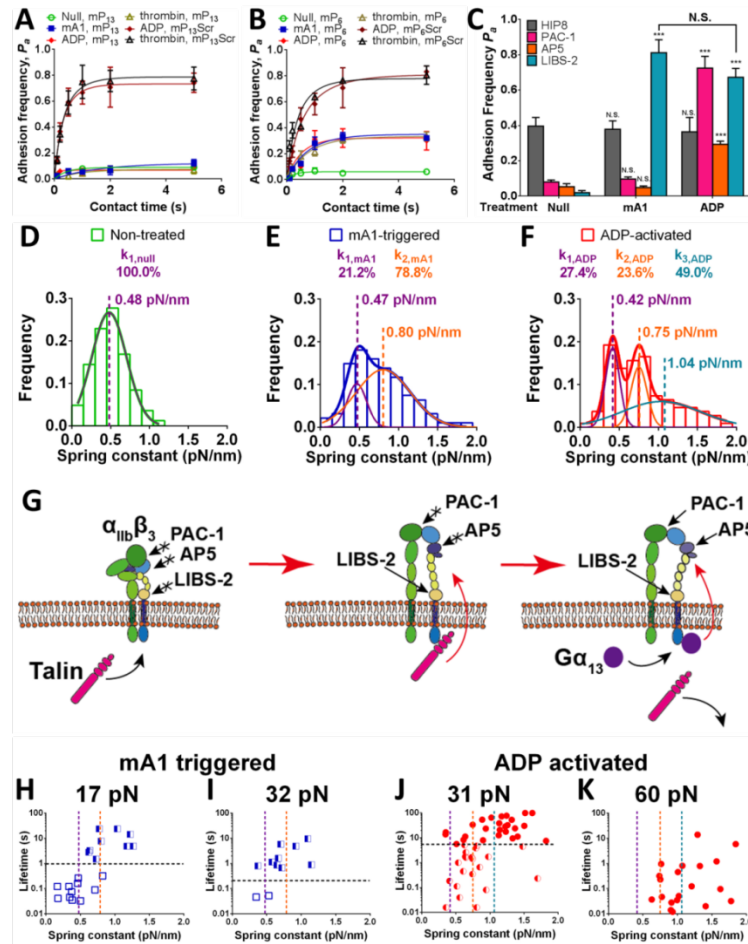


Figure 5-7. $\alpha_{IIb}\beta_3$ inside-out signaling pathway and conformational changes following up-regulation. (A,B) Mean \pm SEM, adhesion frequency vs. contact time of non-treated (green), mA1-triggered (blue), and ADP- (red) and thrombin- (brown) activated platelets binding to FN_{III7-10} after treatment of mP₁₃ (A) and mP₆ (B). Scrambled peptides (A: mP₁₃Scr or B: mP₆Scr) treated platelets were activated by ADP (dark red) or thrombin (black) as control. (C) Mean \pm SEM of adhesion frequency of non-treated, mA1-triggered, and ADP-activated platelets binding to HIP8- (gray), PAC-1- (magenta), AP5- (orange), and LIBS-2- (cyan) coated beads. N.S. = not statically significant; *** = p < 0.001; assessed by unpaired, two-tailed Student's t-test. (D-F) Histograms (bars) and single (D), dual (E), or triple (F) Gaussian fits (purple, orange and cyan curves were respectively fits to the first, second and third sub-population; color-matched curves were fits to the whole populations) of k_{mol} for non-treated (D, $k_{1,null}$), mA1-triggered (E, $k_{1,mA1}$ and $k_{2,mA1}$) and ADP-activated (F, $k_{1,ADP}$, $k_{2,ADP}$ and $k_{3,ADP}$) platelets pulled by FN_{III7-10}. The calculated fractions of each sub-population were indicated. (G) Hypothetical model of $\alpha_{IIb}\beta_3$ sequential association with talin and Gα₁₃ and the concomitant conformational changes. The accessibility of LIBS-2, PAC-1 and AP5 to the integrin was indicated. (H-K) k_{mol} vs. lifetime of mA1-triggered (H,I; clamping force: 17, 32 pN) and ADP-activated (J,K; clamping force: 31, 60 pN) platelets binding to FN_{III7-10}. Horizontal dashed lines: lifetime threshold for different bond dissociating states. Open, half-filled, and filled symbols indicate lifetimes categorized in fast-, intermediate- and slow-dissociating states respectively. Vertical dashed lines: means of Gaussian fits on the spring constant distribution from panel E (H and I) or F (J and K), with the colors matched.

By using a stretch method (see Materials and Methods) to analyze the lifetime events data mentioned above which ensured predominant single-molecular binding, we measured the stiffness of single $\alpha_{IIb}\beta_3$ -FN_{III7-10} molecular complex, k_{mol} from all three conditions. The stiffness distribution from non-treated platelets obeyed a single Gaussian fitting with the mean at $k_{1,null} = 0.48$ pN/nm (Goodness-of-fit: $R^2 = 0.99$), confirming the existence of only one bent conformation (Fig. 5-7D). The distribution from mA1-triggered platelets, however, was better fitted by a dual Gaussian with two means at $k_{1,mA1} = 0.47$ and $k_{2,mA1} = 0.80$ pN/nm ($R^2 = 0.98$; single-Gaussian: $R^2 = 0.89$), indicating the appearance of a higher stiffness subpopulation corresponding to the extended integrins, agreeing with $\alpha_L\beta_2$ ⁶³ and $\alpha_4\beta_1$ ¹⁵⁹. Interestingly, fitting of the data from ADP-activated platelets required three Gaussians, with means at $k_{1,ADP} = 0.42$, $k_{2,ADP} = 0.75$ and $k_{3,ADP} = 1.04$ pN/nm ($R^2 = 0.997$; single Gaussian: $R^2 = 0.73$; dual Gaussian: $R^2 = 0.83$). The first two agreed with the respective stiffness of bent and extended integrins, while the stiffest subpopulation could be explained by hybrid domain swing-out. Fraction calculations revealed that mA1 and ADP stimulated the extension of more than 70% integrins, while ADP also resulted in 49% hybrid domain swing-out.

The above results indicated that, the intermediate state triggered by GPIIb α mechanotransduction is associated with a conformation of $\alpha_{IIb}\beta_3$ that adopts an extended ectodomain, a closed hybrid domain and a ligand-binding epitope unrecognizable by PAC-1; while the active state, triggered by ADP activation, is associated with a conformation with an extended ectodomain, an open hybrid domain

and a PAC-1 recognizable ligand-binding epitope. This, together with the correlation of talin and $G\alpha_{13}$ with the adhesiveness states, suggested a two-step inside-out signaling model: the first wave of binding by talin caused the unclasping of the cytoplasmic tails, which allosterically triggered integrin ectodomain extension, and primed the integrins into the intermediate state; the second wave of binding by $G\alpha_{13}$ which substituted talin association, furthermore realized hybrid domain swing-out and activated the integrins into the active state (Fig. 5-7G). GPIb α mechanotransduction could only trigger the recruitment of talin and thus realized the intermediate state; whereas ADP (and presumably thrombin as well, considering its stronger stimulating function) induced both talin and $G\alpha_{13}$ association, and thus was capable to realize the active state.

To test the relation between integrin activation and conformational change, we measured the k_{mol} from lifetime events of mA1-triggered and ADP-activated groups. Lifetimes were roughly segregated into different dissociating states using the kink in the semi-log survival frequency vs. lifetime plots (Fig. 5-6) as a threshold. Remarkably, in the mA1-triggered group, k_{mol} corresponding to fast- and intermediate-dissociating lifetimes was respectively distributed like the bent and extended conformations (Fig. 5-7 H,I). Similarly, k_{mol} corresponding to intermediate- and slow-dissociating lifetimes in the ADP-activated group was respectively distributed like the [ectodomain extended, hybrid domain swung-in] and [ectodomain extended, hybrid domain swung-out] conformations (Fig. 5-7 J,K). This evidence

linked the three integrin conformations characterized in this work with the three bond states.

5.2.1.6 Synergy of chemical inside-out and mechanical outside-in signaling realize a fourth, hyperactive state

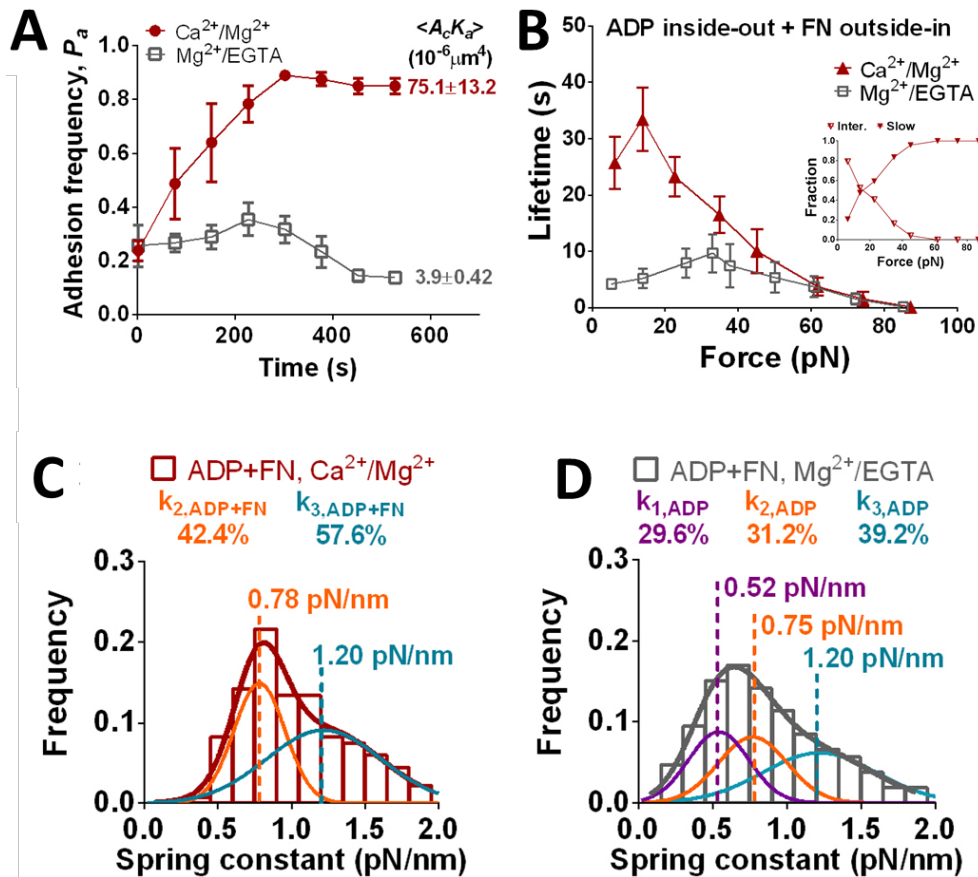


Figure 5-8. $\alpha_{IIb}\beta_3$ outside-in mechanical signaling following ADP activation. (A) Adhesion frequency vs. time of ADP-activated platelets binding to $\text{FN}_{III7-10}$ over repeated contacts in $\text{Ca}^{2+}/\text{Mg}^{2+}$ (dark red) and $\text{Mg}^{2+}/\text{EGTA}$ (gray). The adhesion frequency was calculated every 30 cycles. Four pairs were tested under each contact time to obtain mean \pm SEM. (B) Mean \pm SEM, lifetime vs. force curves of ADP-activated platelets after 210 cycles of contact with $\text{FN}_{III7-10}$ in $\text{Ca}^{2+}/\text{Mg}^{2+}$ (dark red) and $\text{Mg}^{2+}/\text{EGTA}$ (gray). Inset: fitted fractions of bonds of the intermediate- (half-filled symbols) and slow-dissociation (filled symbols) states of ADP+ $\text{FN}_{III7-10}$ -activated platelets in $\text{Ca}^{2+}/\text{Mg}^{2+}$. (C,D) Histograms (bars) and dual (C) or triple (D) Gaussian fits (purple, orange and cyan curves were respectively fits to the first, second and third sub-population; color-matched curves were fits to the whole populations) of k_{mol} for ADP-activated platelets after 210 cycles of contact with $\text{FN}_{III7-10}$ in $\text{Ca}^{2+}/\text{Mg}^{2+}$ (C) and $\text{Mg}^{2+}/\text{EGTA}$ (D). The calculated fractions of each sub-population were indicated. Ab LM609 was added in all experiments to block $\alpha_V\beta_3$.

The fact that GPIIb α mechanotransduction and ADP stimulation could only activate a portion of the integrins into the intermediate-dissociating bond state in the absence of force suggests a huge potential of further improvement. Remember from above that integrin outside-in signaling realized the progression of mA1-triggered intermediate state, we asked whether an ensuing outside-in signaling could also realize the progression of ADP-triggered active state.

To test this hypothesis, ADP-activated platelets were interrogated by a low site density FN_{III7-10} bead ($3/\mu\text{m}^2$). The adhesion frequency was first at a relatively low level (20%), but promptly increased after ~50 contacts and finally reached a plateau with slight oscillation (Fig. 5-8A, dark red). Fitting the adhesion frequency vs. contact time data prior to and after this progression revealed a 13.5-fold increase in the average effective affinity (Fig. 5-8A). On the other hand, post-progression bond lifetime measurement by the switch assay using a 0.1X FN_{III7-10} bead and an even more sparsely coated FN_{III7-10} bead yielded a distinct lifetime vs. force curve as well: the catch-bond regime substantially shrank leftwards to 0-14 pN; average lifetimes over the lower force regime (<35 pN) were all elongated while the higher force regime (>35 pN) remained similar to ADP-activated platelets (Fig. 5-8B). Multi-state analysis reflected that the lifetime events in this context was composed of bonds in intermediate- and slow-, but not fast-dissociating state (Fig. 5-8B, insert). Again, the increase of force monotonically enhanced and declined the fraction of slow- and intermediate-dissociating states, respectively. Spring constant analysis revealed that only two stiffer subpopulations remained while the softest disappeared, indicating that

the mechanical outside-in signaling following ADP activation primed all integrins to extend (Fig. 5-8C). All the above results indicated the existence of a fourth, hyperactive state, which was overwhelmingly more powerful than, and was reached by the progression of, the ADP-induced active state. This progression was again realized by the state equilibrium shift of the integrin subpopulations.

In comparison, chelating Ca^{2+} by EGTA eliminated this progression: the adhesion frequency only elicited a temporary and moderate elevation during the repeated touches, but eventually dropped to even lower than the initial value (Fig. 5-8, gray). Agreeing with the affinity decrease, the lifetime in $\text{Mg}^{2+}/\text{EGTA}$ was also shorter than the ADP activated group, especially at ~ 35 pN where the peak of the catch-bond was reached; but at low and high forces, the difference became less distinguishable. Spring constant analysis revealed that, $\text{FN}_{\text{III7-10}}$ priming ADP activated platelets in $\text{Mg}^{2+}/\text{EGTA}$ caused a slight decrease of the fractions of extended subpopulations and an increase of that of bent (Fig. 5-8D). These data suggested that extracellular Ca^{2+} is necessary to the mechanical outside-in signaling of $\alpha_{\text{IIb}}\beta_3$ following ADP activation.

5.2.2 GPIIb α -triggered signal primes low-level P-selectin expression on platelet surface

I used two probe proteins to detect the P-selectin expression of platelets, AK4, a monoclonal Ab against P-selectin¹⁶⁰, and 2GSP6, a binding epitope bearing fragment of the P-selectin ligand PSGL-1¹⁶¹. Unstimulated platelets exhibited very low level of adhesion frequency against both AK4 and 2GSP6, confirming that they do not express

P-selectin (Fig. 5-9A). ADP-activated platelets manifest a dose-dependent behavior, so that a higher concentration of ADP would induce a higher level of P-selectin expression; while a low dosage (0.1 U/ml) of thrombin was already sufficient to trigger 100% adhesion frequency against AK4 and 70% against 2GSP6, even higher than the 1000 μ M ADP group (Fig. 5-9A). Compared with above, mA1-triggered platelets bound to AK4 and 2GSP6 beads with an adhesion frequency of ~65% and ~40%, respectively, comparable to the 1000 μ M ADP group (Fig. 5-9A). These results indicated that GPIb α -triggered signal primes low-level P-selectin expression, which is comparable to extremely high dosage ADP treatment, but weaker than thrombin.

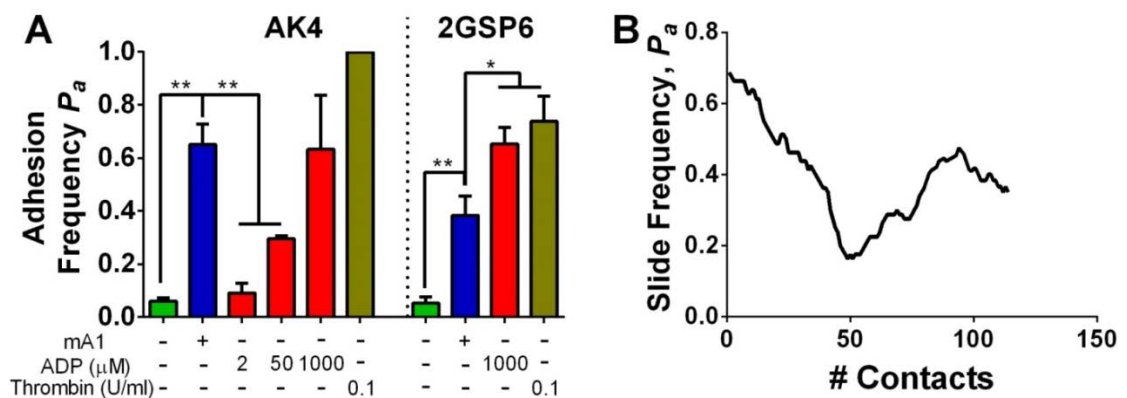


Figure 5-9. Platelet P-selectin expression after different treatments. (A) Detection of platelet P-selectin expression after no treatment, mA1 stimulation and ADP or thrombin activation, as probed by AK4 and 2GSP6 coated beads. * = $p < 0.05$; ** = $p < 0.01$; assessed by unpaired, two-tailed Student's *t*-test. (B) Slide frequency (window size: 20 contacts) of A1-triggered platelets binding to AK4 coated beads over repeated contacts, averaged over four platelet–bead pairs.

We then looked into the time dependency of the AK4 binding frequency after mA1 triggering. Surprisingly, the slide frequency decreased from ~65% to <40% over 100 contacts, with a considerable oscillation in the middle (Fig. 5-9B). Considering that P-selectin is a membrane surface expressed receptor, it becomes puzzling why the

AK4 binding would weaken over time. A possible explanation is the functional suppression by the platelet due to a lack of further hemostatic stimulation; alternatively, it could be also due to the internalization of P-selectin.

5.2.3 GPIb α -triggered signal primes PS exposure in platelet outer membrane layer

Annexin V was used to detect the PS exposure of platelets¹³⁸. Unstimulated platelets exhibited very low level of adhesion frequency against Annexin V, confirming that they barely have PS exposed to the exterior surface (Fig. 5-10A). ADP-activated platelets manifest a dose-dependent behavior similar to what was observed in P-selectin expression (Fig. 5-9A); however, even with an extremely high ADP concentration the detected PS exposure was still low, manifested by a 20% adhesion frequency (Fig. 5-10A). A low dosage (0.1 U/ml) of thrombin only triggered a moderate level of PS exposure, but increasing the dosage to 1 U/ml remarkably enhanced the adhesion frequency to a much higher level (Fig. 5-10A). These agreed with previously published observation that soluble agonists did not have strong effects in stimulating PS exposure¹³⁸. Compared with above, mA1-triggered platelets bound to Annexin V beads with an adhesion frequency of ~45%, even higher than the 1000 μ M ADP group but slightly lower than the 1 U/ml thrombin group (Fig. 5-10A). These results indicated that GPIb α -triggered signal primes low-level PS exposure.

Different to the decay of P-selectin detection over time (Fig. 5-9B), the slide frequency of Annexin V binding to mA1-triggered platelets was relatively stable over

a total of 150 contacts, equaling to ~6 min (Fig. 5-10B). This suggested that the PS exposure stimulated by GPIIb α mechanotransduction is persistent, even without further stimulation from GPIIb α .

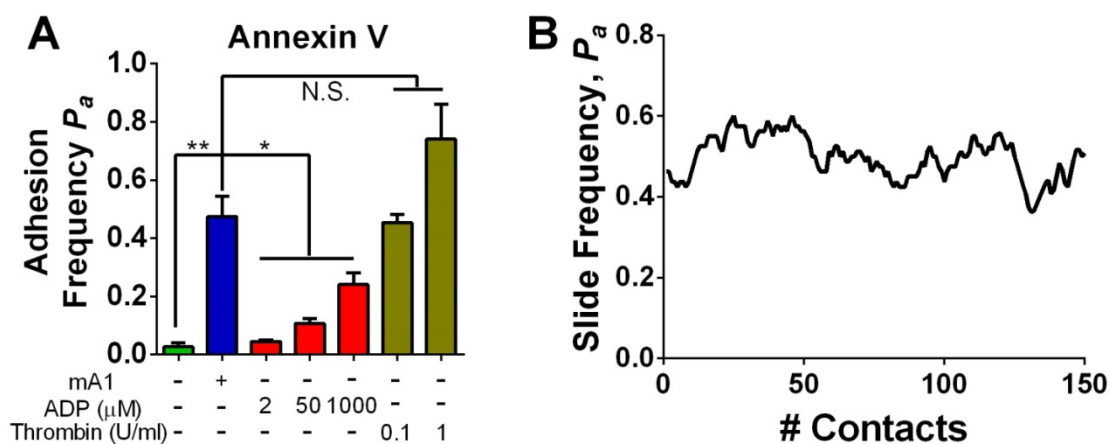


Figure 5-10. Platelet PS exposure after different treatments. (A) Detection of platelet PS exposure after no treatment, mA1 stimulation and ADP or thrombin activation, as probed by Annexin V coated beads. N.S. = not statically significant; * = $p < 0.05$; ** = $p < 0.01$; assessed by unpaired, two-tailed Student's t -test. (B) Slide frequency (window size: 20 contacts) of A1-triggered platelets binding to Annexin V coated beads over repeated contacts, averaged over four platelet—bead pairs.

5.3 Discussion

$\alpha_{IIb}\beta_3$, as the first defined member of the integrin superfamily, has been studied for decades¹⁶². Integrins mediate cell adhesion and transduce signals bidirectionally, allowing the cells to communicate with the extracellular environment. Especially, integrin $\alpha_{IIb}\beta_3$ which is primarily expressed on platelet surface, plays a critical role in platelet activation, adhesion and mechanosensing^{11,117,135,149,163}. A good amount of works have substantially characterized $\alpha_{IIb}\beta_3$ in three aspects: 1) structure and conformation^{43,46,47,147,158,164}; 2) adhesion activity^{28,57,58,165,166}; and 3) signaling pathways^{10,11,81,135,149,167}. However, the study of platelet surface $\alpha_{IIb}\beta_3$ activity

regulation still remains in its infancy. For example, the detection of integrin activation, by either ligand or PAC-1 binding, was still limited to a binary resolution⁸².

GPIb α triggers mechano-signaling through ligand binding and in turn up-regulates $\alpha_{IIb}\beta_3$ by inside-out signaling^{9,10}. Due to technical difficulties, the mechanism of this mechano-signaling process has never been thoroughly figured out. Our results indicated a lifetime-dependence of GPIb α mechanotransduction, and a lifetime threshold mechanism for β_3 integrin up-regulation (Fig. 5-1 D), which as confirmed by further investigation was realized by $\alpha_{IIb}\beta_3$ alone (Fig. 5-2 D-F). Comparing this with another way of inside-out signaling, namely, via stimulation of soluble agonists, revealed a remarkable weakness in the binding kinetics, defining two distinct adhesiveness states of $\alpha_{IIb}\beta_3$ – intermediate and active – on top of the inactive state seen on unstimulated platelets (Fig. 5-2). This intermediate state associated with GPIb α mechanotransduction appeared not to be a middle-stage product in the proceeding of $\alpha_{IIb}\beta_3$ to the active state, because even extremely long-duration GPIb α -ligand associations and crosslinking of GPIb α receptors by dimeric A1 cannot further enhance the binding (Fig. 5-1E, 5-3B). To note, ADP but not mA1 triggering can up-regulate integrin $\alpha_V\beta_3$ to realize feeble binding, which suggests its auxiliary role in the later but not earlier stages of arterial hemostasis (Fig. 5-2D). The intermediate state is highly transient, so that when repeatedly primed by ligands or a ligand-mimicking Abs in the presence of extracellular Ca²⁺, the integrins will progress to the active state within minutes, indicating integrin up-regulation by outside-in

signaling. On the contrary, without sufficient stimulations, it would recess to the weak adhesiveness state (Fig. 5-4).

The developmental inhibitory effects of mP₆ and mP₁₃ suggested a two-stage integrin up-regulation procedure which sequentially requires talin-integrin and Gα₁₃-integrin associations (Fig. 5-7 A,B). To note, the inhibitory effect of mP₆ on integrin activation was not observable in the original work that invented this peptide, which reported positive fluorescence staining of both Fg and PAC-1¹³⁵. We suspect this was due to the co-incubation of platelets with thrombin and Fg/PAC-1 over time, which allowed a cooperative inside-out and outside-in signaling that overcome the inhibition. The conformations of integrins, as detected by two mutually complementary approaches, revealed a [ectodomain bent, hybrid domain swung-in] -> [ectodomain extended, hybrid domain swung-in] -> [ectodomain extended, hybrid domain swung-out] shift following the two-wave talin and Gα₁₃ association, the proceeding of adhesiveness states (Fig. 5-7 C-F) and also the bond dissociating states (Fig. 5-7 H-K). This is in consistency with previous works demonstrating that both ectodomain extension and hybrid domain swing-out are associated with integrin activation^{45,47,98,168,169}. Models of talin binding leading to integrin tailpiece separation and ectodomain extension have been proposed in previous studies^{46,170}; the point that Gα₁₃ binding triggers hybrid domain swing-out, as suggested by this work, requires further confirmation.

The fact that PAC-1 cannot distinguish the intermediate state suggested that it is not sensitive enough to detect low-level integrin activations. Remember that previous studies prevalingly relied on PAC-1 staining as a canonical marker of integrin activation, this result implicates that the conclusion of integrin activation based on PAC-1 staining should be drawn with more caution.

Inspired by the progression of the intermediate state, we wondered whether the ADP –activated integrins still possess the potential to be further up-regulated. Indeed, repeated ligand priming triggered outside-in signaling to boost the progression of the active state to a hyperactive state, which defined the fourth state (Fig. 5-8A).

The discovery of the distinct and relative independent active states on the populational scale gave rise to two alternative hypotheses: 1) agreeing with the conventional binary model, the individual $\alpha_{\text{IIb}}\beta_3$ molecules could only adopt either an inactive state with low affinity or an active state with high affinity, and the equilibrium shift of the two subpopulations realized all different adhesiveness states; and 2) individual $\alpha_{\text{IIb}}\beta_3$ molecules could adopt multiple affinity states, which add up to a more complicated equilibrium model. By measuring bond dissociation rates, we gained in-depth insights of the integrin activity on single-molecular level, which reflected the existence of three dissociating states. The transitions between adhesiveness states closely correlated with a shift of the equilibrium between the dissociating states towards larger slower-dissociating subpopulations and smaller faster-dissociating subpopulations, while an increase in the pulling force also induced

a similar effect (Fig. 5-5, 5-8B). Further analysis argues that the number of $\alpha_{\text{IIb}}\beta_3$ affinity states should be at least 4, with the fast-dissociating bond state associated with two, and the intermediate- and slow-dissociating bond states each associated with one, which we artificially name as low-, intermediate-, high- and hyper-affinity states. We suspect that the evolution of intermediate-affinity state from low-affinity state was realized by the ectodomain extension, which realizes a more accessible orientation of the ligand binding site in the integrin headpiece, but does not guarantee an intermediate-dissociating bond state, that is more related to the local conformation of the ligand binding epitope. To note, the lifetime results and multi-state analysis reflected a remarkable discrimination over the two ligands despite their overlapping binding epitope (Fig. 5-5, compare A-E with F-J). We suspect that this is caused by the distinctive docking of the binding motifs of FN_{III7-10} and Fg¹⁷¹, which produces different allosteric effects that propagate from the N-terminal ligand binding epitope to the overall integrin structure.

Integrins adopting multiple bond states has been known for long^{26,150}, but conventionally it is believed that a three-state bond dissociating model can only be realized by αI -domain bearing integrins, taking advantage of the cooperation between the αI and βI -domains. Agreeing with that, $\alpha_{\text{L}}\beta_2$ was found to bear three bond states when binding to its ligand ICAM-1²⁹, while purified $\alpha_{\text{IIb}}\beta_3$ -Fg only contained two^{57,58}. However, our work for the first time demonstrated the three-state model in the platelet surface $\alpha_{\text{IIb}}\beta_3$, disputing the necessity of αI - βI cooperation. The discrepancy in

$\alpha_{IIb}\beta_3$ -Fg association between the purified system and platelet surface system is also intriguing and informative.

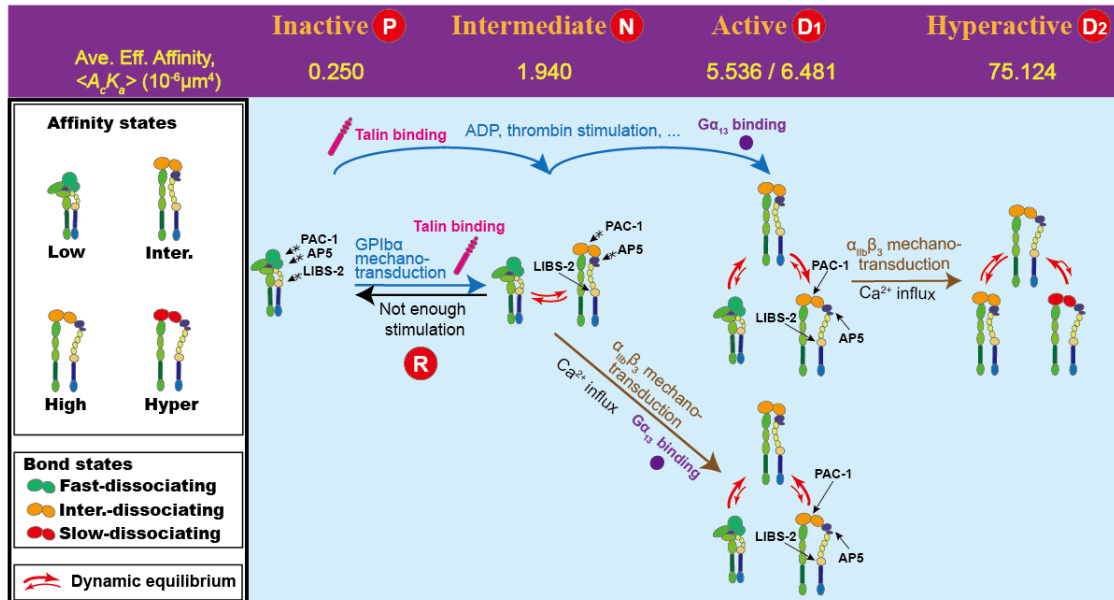


Fig. 5-11. Shifts between multiple states of individual $\alpha_{IIb}\beta_3$ realized four populational states: inactive, intermediate, active and hyperactive. The average effective affinity ($\langle A_c K_a \rangle$) of each state was annotated. The conformational states and bond states the integrins switch among under each state were indicated, which in combination define the four affinity states (left). Three colors of the headpiece represented three bond states: fast- (green), intermediate- (orange) and slow- (red) dissociating (left). The required conditions/stimulations to transit between states were indicated besides the corresponding arrowheads. Inside-out and outside-in signaling pathways were marked by cyan and brown respectively. The coupled reversely directional red arrowheads indicated dynamic equilibrium between different integrin states, with the relative thickness indicating the dominant state. The car transmission gear positions as a metaphor of $\alpha_{IIb}\beta_3$ activity were annotated by the representing letters (P, park; R, reverse; N, neutral; D₁, drive₁; D₂, drive₂).

To better illustrate the discoveries in this work, I summarized them as a model of platelet $\alpha_{IIb}\beta_3$ regulation by bidirectional signaling events. On inactive platelets, $\alpha_{IIb}\beta_3$ integrins reside in the low-affinity state, and thus realize a weak adhesiveness state of the platelet (Fig. 5-11, *Weak*). Upon GPIIb/IIIa mechanotransduction, most of the integrins extend and adopt the intermediate-affinity state, a portion of which further adopts the intermediate-dissociating bond state and evolves into the high-affinity state.

The mixture of these three affinity states defines the intermediate state (Fig. 5-11, *Intermediate*), and also the ADP/thrombin-stimulated active state with fractional differences (Fig. 5-11, *Active*). Under the active state, a portion of integrins undergoes hybrid domain swing-out conformational change, which probably does not affect their affinity but enables them to enter the slow-dissociating bond state under force (Fig. 5-11, *Active*). The hyperactive state is realized by only the high- and hyper-affinity states (Fig. 5-11, *Hyperactive*). Integrins under all adhesiveness states are capable of reacting to force which promotes their bond states to manifest a catch-bond behavior (Fig. 5-11, *lower row*). This enables the platelets to resist the high shear under arterial environments. To note, part of this model, e.g., the reversibility of the intermediate state and the correspondence between single integrin affinity states and populational adhesiveness states, specifically applies to the interaction with RGD-bearing ligands VWF and fibronectin. The regulation of platelet-fibrinogen interaction is more complicated, and requires further investigations.

The four adhesiveness states of platelet $\alpha_{IIb}\beta_3$ indicate a multi-step mechanism of platelet activation instead of the one-step “suicidal attack” model, which we believe reflects the realistic situation. It was probably because in physiological condition, all of the stimulations to platelets appear within such a very short period of time, that it becomes difficult to beware of each step of platelet activation. We figured that this highly mimics the operation of a transmission that controls the movement of a car, considering that integrin activation to some extent “drives” the proceeding of hemostasis. The weak adhesiveness state “locks” the integrins to remain inert, which

is similar to the gear “P” (Park). The intermediate state prepares the integrins for adhesion and progression, similar to the gear “N” (Neutral). The active and hyperactive states realize different levels of strong adhesion, which are similar to different gears of Drive, “D1” and “D2”. Importantly, recession of the intermediate state in the absence of further stimulation provides the system with an opportunity to dissipate the activation, which is similar to reversing a car using the gear “R” (Reverse). This discovery for the first time suggests a reversibility of the platelet activation through a physiological pathway instead of inhibitor/drug interference, which should be important in maintaining the balance between hemostasis and thrombosis. In conclusion, this transmission-mimicking mechanism ensures developmentally appropriate responses of $\alpha_{IIb}\beta_3$ integrins at distinct stages of platelet (de)activation.

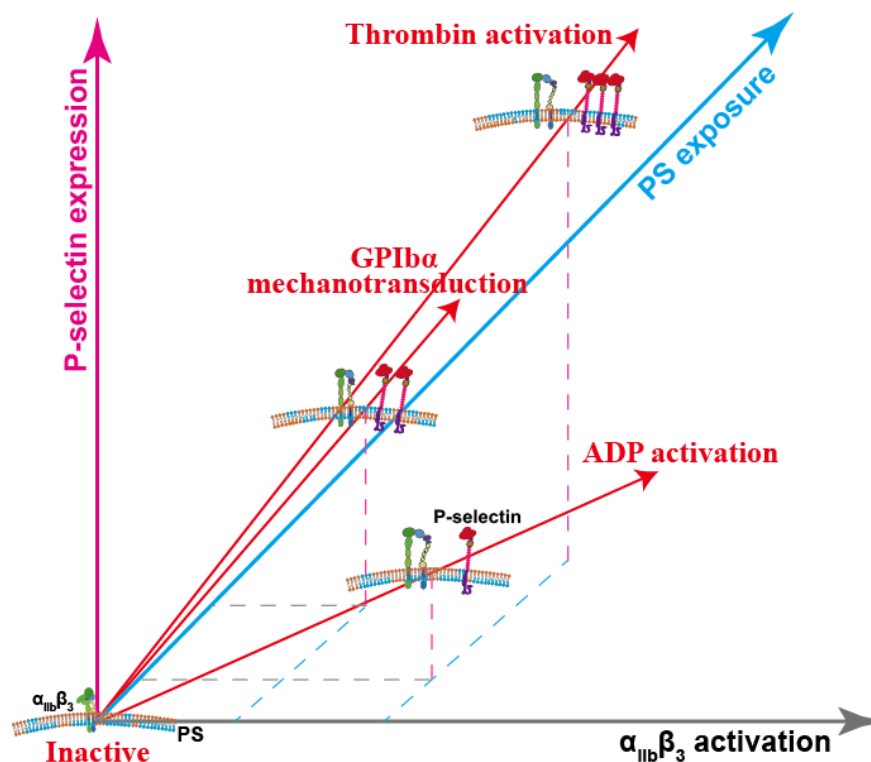


Fig. 5-12. Multi-dimensional model of platelet activation. The three axis's represent the extent of integrin $\alpha_{IIb}\beta_3$ activation, P-selectin expression and PS exposure, respectively. Red arrowheads indicate the direction of the platelet activation under this coordinate triggered respectively by GPIb α mechanotransduction, ADP and thrombin.

In addition to up-regulating $\alpha_{IIb}\beta_3$, GPIb α mechanotransduction also stimulates moderate levels of P-selectin expression, a marker of platelet granule release, and PS exposure, a sign of platelets gaining procoagulant activities (Figs. 6-9, 6-10). Remember from a recent publication that shear force is critical to trigger platelet PS exposure in cooperation with soluble agonists' treatment¹³⁸, my results further illustrated that mechanical force alone suffices independent of soluble agonists, and specifically, the mecano-receptor involved is GPIb α .

Conventionally, GPIb α 's role in initiating platelet activation signaling was believed to be secondary, while more focus was put on soluble agonists and also GPVI (more important in low-shear vascular environment). However, my studies provide an enormous amount of evidences to dispute and argue that, GPIb α mechanotransduction plays an important and indispensable role in platelet activation and activity: 1) GPIb α up-regulates the integrin $\alpha_{IIb}\beta_3$ into an intermediate state, which gains a considerable binding activity and prepares it ready to be further activated; and 2) GPIb α mechanotransduction has similar effects to ADP and thrombin activation with regard to inducing P-selectin expression and PS exposure indicate. To note, the mismatch of GPIb α , ADP and thrombin in triggering $\alpha_{IIb}\beta_3$ activation (GPIb α < ADP \approx thrombin), P-selectin expression (ADP \leq GPIb α < thrombin) and PS

exposure (ADP < GPIb α \leq thrombin) is suggestive that, platelet activation by different stimulus may not only differ in the extent of activation, but can rather lead to distinctive directions on a multi-dimensional coordinate of activation. With that said, one single gauge of “platelet activation” will never exist anymore.

CHAPTER 6: CONCLUSIONS

6.1 Summary

Mechanosensing is a complicated yet intriguing problem for biologists and biophysicists, which acts as a symbolic example of mechanical regulation in biology. Mechanosensing is of extreme importance in the functionality of platelets, because changes in the vascular hydraulic environment is a critical result of vascular injuries, which has to be perceived by platelet surface receptors to initiate hemostasis. On the other hand, in thrombosis the pathological environment — like stenosis and high blood pressure, also causes certain changes to the mechanical properties of the blood, which is likely associated with the reported platelet hyperreactivity. This is related to severe diseases including obesity, diabetes, high blood pressure and coronary and peripheral arterial disease. In this context, an important, yet incompletely understood, question in hemostasis and thrombosis is: how platelet adhesion leads to signaling and activation?

Cell signal transduction is accomplished by the cooperation of a number of molecules in a sequential fashion. However, before studying the cooperation, it is important to understand these molecules by themselves first, especially the

mechano-receptors. My previous colleague and collaborator, Dr. Lining Ju, focused his Ph.D. research on the molecule GPIb α . I, on the other hand, selected integrins. Integrins have a highly flexible structure, so that they can adopt multiple conformational and affinity states, which regulate and are regulated by cellular and environmental mechano-signals. In Chapter 3, I characterized the integrin $\alpha_v\beta_3$ bending and unbending conformational changes. I found:

- 1) The bending and unbending conformational changes can occur both on purified integrin molecules and on those expressed on cell surface, both with and without ligand, indicating that they are spontaneous molecular dynamic processes that do not require cellular support and ligand engagement.
- 2) Mechanical force favors unbending and suppresses bending, presumably by providing and consuming mechanical energy, suggesting an activating role of mechanical force in β_3 integrin regulation.
- 3) The dynamics of bending and unbending are also regulated by the cation condition, mutation and the engaged ligand.
- 4) Bending and unbending conformational changes do not affect the lifetime of the integrin binding to its ligands in $\text{Ca}^{2+}/\text{Mg}^{2+}$, but in Mn^{2+} unbending facilitates the lifetime prolongation while bending shortens the lifetime.

Furthermore, in Chapter 4 I started to collaborate with Dr. Ju and investigated the platelet GPIb α mechanosensing. Similar to integrins, GPIb α can also undergo conformational changes, specifically, LRRD and MSD unfolding. But unlike integrin

bending unbending, these two domains' unfolding appears to be irreversible under constant force pulling. Further study revealed that:

- 1) A single durable GPIIb/IIIa bonding is necessary and also sufficient to trigger platelet intracellular calcium signaling, manifested as an acute pulse of calcium flux. The signal intensity is linearly correlated with the bond lifetime duration.
- 2) The LRRD and MSD unfolding is cooperative, so that LRRD unfolding should facilitate MSD unfolding.
- 3) LRRD unfolding increases the calcium signal intensity by prolonging the bond lifetime, while the MSD unfolding digitally determines the α/β type of the signal.
- 4) A type 2B VWD mutant R1450E has mechanotransduction defect because of the lifetime shortening under higher forces.
- 5) Inhibition of GPIIb/IIIa mechanoreception by perturbing its association with 14-3-3 ζ .

This work developed novel biophysical methods and analyses (fBFP) to visualize in real-time a chain of coordinated single-molecular events on a living cell, enabling us to elucidate the inner workings of a mechanoreceptor important to platelet biology. Our findings have defined the minimum mechanical stimulation for inducing mechanotransduction, which should be of broad interests to scientists working in cell and molecular biology, single-molecule biophysics, and hematology. Because LRRD

and MSD are common structures shared by many receptors, the mechanosensory system we described may represent a general mechanism in mechanobiology. The design principles elucidated herein may serve as guidelines for synthetic biology approaches to a generic mechanosensing machine.

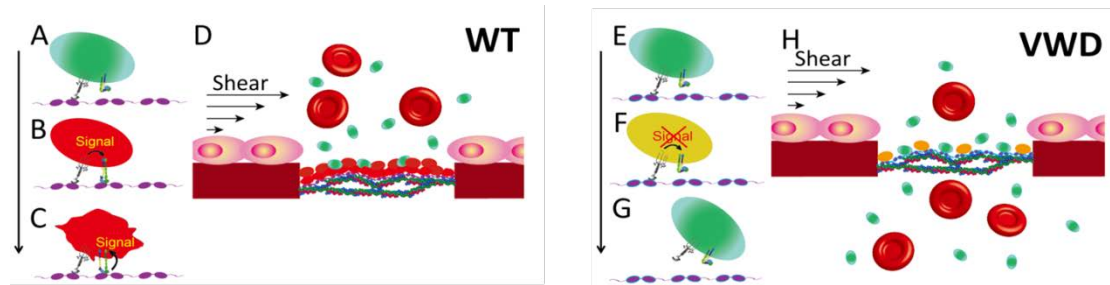


Figure 6-1. Hypothesized model of normal and defected hemostasis from humans that have WT (A-D) and R1450E VWD MT (E-H) plasma VWF. Robust calcium of platelet via binding to WT VWF (B) triggers integrin activation (C) and in turn the platelet aggregate formation which stops bleeding (D). R1450E does not trigger robust calcium (F) and thus fails to induce integrin activation (G) and the bleeding becomes excessive (H).

VWD was conventional regarded as an adhesion deficiency disease. Until recently it was discovered that a type 2B VWD mutant, V1316M, inhibits activation of integrin $\alpha_{IIb}\beta_3$ and facilitates thrombocytopeny¹²⁷, which for the first time demonstrated a signal deficiency caused by VWD. Agreeing with that, we found that another type 2B VWD mutant, R1450E, also failed to trigger robust calcium signal under high forces. Based on this, I postulate that unlike WT VWF that triggers platelet calcium signaling under high shear rates in arterial environments and lead to integrin activation (Fig. 6-1A-D), R1450E cannot initiate calcium signal and integrin activation and thus compromises the platelet firm adhesion and aggregation, resulting in excessive bleeding (Fig. 6-1E-H).

Continuing from above, in Chapter 5 I followed the signaling pathway to downstream and investigated the integrins activation, P-selectin expression and PS

exposure induced by GPIb α mechanotransduction, as well as the mechanotransduction of activated integrin $\alpha_{IIb}\beta_3$. It is found that:

- 1) GPIb α mechanotransduction up-regulates $\alpha_{IIb}\beta_3$ into a transient intermediate activity state, which is in between of the inactive state and ADP or thrombin triggered active state.
- 2) In both the intermediate and active states but not the inactive state, $\alpha_{IIb}\beta_3$ can initiate outside-in mechanical signaling by repeatedly binding to its ligand so as to further promote its binding capacity. This process does not require durable binding as GPIb α but requires extracellular calcium.
- 3) The different states of $\alpha_{IIb}\beta_3$ adopt distinctive compositions of subpopulations with different binding affinities, bond strengths, as well as molecular conformations.
- 4) The intermediate state requires talin binding to β_3 tail, whereas the active state requires the binding of both talin and $G\alpha_{13}$.
- 5) GPIb α mechanotransduction triggers low-level P-selectin expression and PS exposure.

This work developed a novel approach to study *cis*-crosstalk of heterogeneous receptors on the same living cell, realizing a step forward in the field of biomechanics and platelet mechano-biology. Our scientific findings refine the understanding of $\alpha_{IIb}\beta_3$ regulation and platelet activation, revealing that both involve multiple serial

steps and can be finely controlled. Our work should also be of broad interests to mechano-biologists, since integrins form a big family of adhesion molecules and are expressed on almost all cells as mechano-receptors.

A bioengineer needs to think about scientific questions in two completely different mindsets: “bio” and “engineer”. Being a biologist, one has to investigate unknown and unclear biological phenomena and invent new approaches to fight against inabilities and diseases, which serves to improve the physical health of human. On the other hand, a qualified engineer not only has to develop tools and techniques to accommodate new projects, but also need the ability to solve scientific problems that are associated with engineering, like mechanics, electronics and more. In my Ph.D. career, with honor, I accomplished a series of projects that were contributed by both the biologist and engineer inside me. In Chapter 2, I helped in the assembly of the fluorescence function of BFP, and solely improved the BFP system with a temperature controlling system, which were both used in the study in Chapter 4, where we investigated the mechanisms of GPIIb α mechanosensing. I also built the dual-probe system which is used in the “switch BFP” assay, a new approach that can investigate the receptors’ *cis*-cross-talk. This assay became the core technique of Chapter 5, where we studied the mechanical signal transduction between GPIIb α and integrin $\alpha_{IIb}\beta_3$. Moreover, my training in mechanical engineering also helped me tremendously in addressing the scientific questions. For example, the lifetime multi-state analysis originated from biomechanics. Also, when characterizing integrin

bending and unbending conformational changes, I calculated the energy generation and consumption.

To summarize, I used and invented several single-cell biomechanical techniques and certain engineering skills, and studied the molecular dynamics of β_3 integrins and GPIb α and the mechanosensing mechanisms of platelets. I investigated how the conformational changes of β_3 integrins and GPIb α are regulated mechanically, chemically and biologically, and related them to their roles of adhesion and mechanotransduction. I deciphered how platelets interpret mechanical signals and convert them to chemical signals accordingly through those mechano-receptors, and gained insights into the related signaling pathways.

6.2 Future works

Like two sides of a coin, the subsequent adhesion and signal transduction of platelets lead to platelet activation/aggregation and normal hemostasis; however, an exaggerated platelet activation response can result in acute thrombotic events, leading to arterial thrombotic events such as ischemic stroke and myocardial infarction, which claim 2,200 American lives every day¹⁷². Platelets in patients with thrombotic diseases could transiently or persistently become hyperreactive, achieving robust activation with the stimulation of sub-threshold concentrations of agonists¹⁷³⁻¹⁷⁵, which is often associated with pathological conditions including obesity, diabetes, hypertension and peripheral artery disease (PAD)¹⁷⁶⁻¹⁷⁸. Insulin resistance, hyperglycemia and inflammation were reported to be the major contributors to

platelet hyperreactivity in both type I and II diabetes. Unfortunately, our knowledge on platelet hyperreactivity is still superficial, which is reflected from the fact that, all the current commercialized anti-coagulant agents have a severe side-effect of causing excessive bleeding, making even small traumas fatal for patients who take them. Especially, due to the limitations in instrumentation and methodology, the relation of diabetes -associated platelet hyperreactivity with platelet adhesion and mechano-activation remains unclear.

Continuing from Chapter 3-5, which majorly target on the platelet physiology, in this section I will describe my tentative works on the study of platelet pathology, specifically, platelet mechanical hyperreactivity in diabetes. This work has not been finished yet, and will be one of the future research directions for the younger fellows.

6.2.1 Type I Diabetes – a preliminary study in platelet biomechanical thrombosis

In collaboration with Dr. Eric Felner from Emory University, we had stable access to blood samples of diabetic and healthy adolescents.

Remember from Chapter 5 that, inactive platelet $\alpha_{IIb}\beta_3$ from healthy donors have low binding ability to its ligands fibronectin and fibrinogen, which was re-confirmed here on healthy adolescents, 5% against FN_{III7-10} and 10% against Fg (Fig. 6-2A,B, green). In contrast, however, platelets purified from diabetic patients' blood had much stronger binding, which reached 20% against both FN_{III7-10} and Fg (Fig. 6-2A,B, green), which mimics the intermediate state of healthy platelet $\alpha_{IIb}\beta_3$. Moreover, in

Chapter 5 I demonstrated that healthy platelet $\alpha_{IIb}\beta_3$ cannot trigger outside-in mechanical signaling to up-regulate itself from the inactive state by binding to $FN_{III7-10}$, which is also reflected here by data from healthy adolescents (Fig. 6-2C, green). But in the diabetic group this signaling pathway appeared to be open, so that over repeated touches the binding frequency was elevated from 20% to ~80% (Fig. 6-2C, blue). These results suggested that, on the inactive diabetic platelets, the $\alpha_{IIb}\beta_3$ integrins already adopt an intermediate or similar activity state, which broke the self-suppressive mechanism observed in healthy platelets.

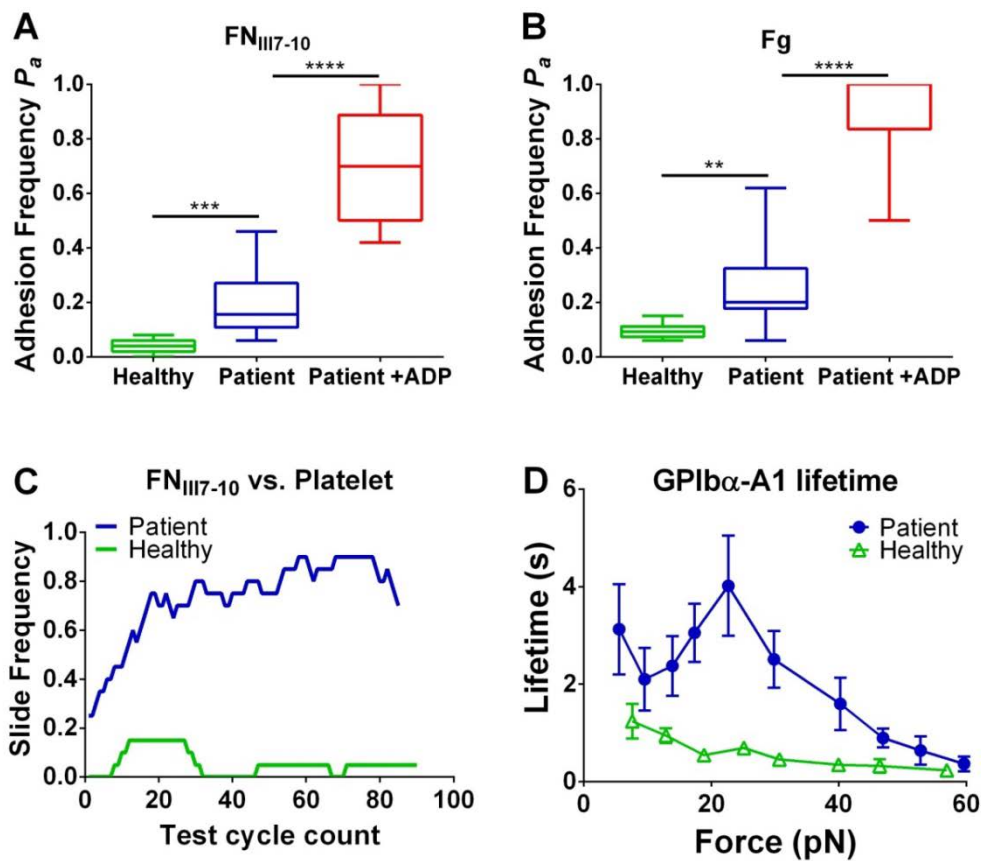


Figure 6-2. Adhesion and signaling abnormality of Type I diabetic GPIIb α and $\alpha_{IIb}\beta_3$. (A,B) adhesion frequency of healthy and patient (with and without ADP activation) platelets binding to $FN_{III7-10}$ (A) and Fg (B) coated beads. (C) Slide frequency of healthy and patient platelets binding to $FN_{III7-10}$ over repeated contacts. (D) Mean \pm SEM, lifetime vs. force of healthy and patient GPIIb α binding to VWF A1. ** = $p < 0.01$; *** = $p < 0.001$; **** = $p < 0.0001$; assessed by unpaired, two-tailed Student's t -test.

On the other hand, the lifetime of diabetic platelet GPIIb/IIIa was much longer than healthy group under all forces. Especially, the catch-slip-catch signature became much more sound, so that at ~25 pN where both lifetime curves peaked, the maximal lifetime was prolonged from <1 s to 4 s (Fig. 6-2D).

6.2.2 Type II Diabetes – a preliminary study in platelet biomechanical thrombosis

I investigated the Type II Diabetic GPIIb/IIIa adhesion and signaling and compared it with healthy control. The lifetime of patient group GPIIb/IIIa was significantly elevated (Fig. 6-3A). The linear correlation between pre-Ca²⁺ longest lifetime and Ca²⁺ signal intensity still stands for the diabetic group; however, compared with the healthy group, its linear fitting was upward shifted in parallel, indicating a higher trigger efficiency (Fig. 6-3B). As an additive result of these two effects, the overall Ca²⁺ triggered in diabetic platelet was much higher than healthy (Fig. 6-3C).

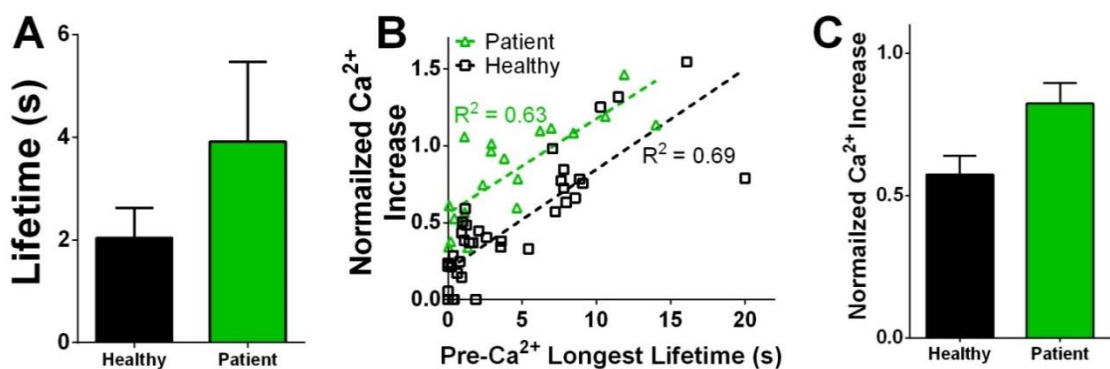


Figure 6-3. Adhesion and signaling abnormality of Type II diabetic GPIIb/IIIa. (A) Mean \pm SEM, lifetime of healthy and patient GPIIb/IIIa binding to VWF A1 under 25 pN. (B) Scatter graphs of ΔI_{max} vs. t_{max} for Healthy (black) and Patient (green) groups derived from platelet–A1 clamped binding under 25 pN. The dashed lines are linear fits to respective data with corresponding Pearson coefficients indicated. (C) Mean \pm SEM, average Ca²⁺ increase triggered by healthy and patient GPIIb/IIIa mechanotransduction.

6.2.3 Summary

These tentative works indicated that, platelets from diabetes patients are mechanically hyperreactive, so that both adhesion and mechano-signaling of their GPIb α and $\alpha_{IIb}\beta_3$ are pathologically exaggerated. As a result, diabetic platelets are more adhesive, and also more responsive to adhesion initiated mechano-signaling to realize activation, which we postulate will ease the process of platelets adhering to unwounded blood vessels and attracting more cells and proteins to massively aggregate, leading to thrombosis.

To make this work more clinically relevant, the next step will be to study the molecular mechanism of these abnormalities. It is speculated that they were due to the disturbance of the internal activation-suppressing signaling pathways of platelets by the diabetic pathological environments, which 1) activates the two receptors GPIb α and $\alpha_{IIb}\beta_3$ to become more adhesive; and 2) reinforces the functioning of certain signaling proteins like PI3 kinase.

CHAPTER 7: MISCELLANEOUS PROJECTS

Regulation of Mac-1 (integrin $\alpha_M\beta_2$) affinity and conformational states by a lupus-associated mutation

This work was part of a collaboration project with Dr. Tanya Mayadas lab from Harvard Medical School. It has been published in 2015 as a research report²⁷.

Systemic lupus erythematosus (SLE) is an auto-immune disease that lacks cure. ~5 million people are suffering from SLE worldwide. In healthy humans, leukocytes are only immuno-active to pathogens. However, leukocytes in SLE patients can be activated by and attack autologous cells, causing multi-organ damages like heart inflammation and kidney failure. Genetic studies identified a SLE-associated variant of the *ITGAM* gene, which poses a R77H mutation in the α -subunit of integrin $\alpha_M\beta_2$, a critical adhesion receptor on leukocytes' surface¹⁷⁹. $\alpha_M\beta_2$ is involved in the activation of leukocytes, and mediates their crawling on and infiltration through the vascular wall. However, how R77H affects the function of $\alpha_M\beta_2$, and why it is correlated to high susceptibility of SLE is unclear.

To address the above questions, Mayadas lab used a flow chamber technique and found that R77H $\alpha_M\beta_2$ has a weakened adhesion capability under flow, but has similar binding behavior to WT in a static environment, suggesting that the impact of R77H is force-related.

Following that, I used BFP to measure the adhesion of cell surface $\alpha_M\beta_2$ and the impact of R77H on the single cell and single molecular level. It was discovered that: 1)

R77H reduces both the binding affinity and binding strength of $\alpha_M\beta_2$, compromising the catch-bond behavior of WT integrin under high forces; 2) The defects in binding resulted by R77H could be rescued by an activating antibody (CBR LFA-1/2) and certain artificial mutations (Δ GFFKR, V124A). This work characterized the $\alpha_M\beta_2$ binding kinetics in single-molecular level, and shed more light on the SLE-associated mutation R77H. Interestingly, this was the first work that described that a mutation in a binding epitope distal domain, the α -subunit β -propeller domain, could have substantial impacts on the binding of an integrin, which provides valuable information to the future studies of integrin structure.

Based on these results and results from previous works, we hypothesized that R77H, by weakening the binding of $\alpha_M\beta_2$, suppresses its mechano-signaling function, and in turn facilitates leukocyte over-activation and SLE development. Obviously, this requires further investigations, which are still undergoing. The activating antibody CBR LFA-1/2 and mutations Δ GFFKR and V124A which were demonstrated to have rescuing effects to the R77H mutation may inspire new biomedical approaches in the future to fight against SLE.

REFERENCE

- 1 Rodvien, R. & Mielke, C. H., Jr. Role of platelets in hemostasis and thrombosis. *West J Med.* **125** (3), 181-186 (1976).
- 2 Jackson, S. P. Arterial thrombosis--insidious, unpredictable and deadly. *Nat Med.* **17** (11), 1423-1436, doi:10.1038/nm.2515, (2011).
- 3 Broos, K., Feys, H. B., De Meyer, S. F., Vanhoorelbeke, K. & Deckmyn, H. Platelets at work in primary hemostasis. *Blood Rev.* **25** (4), 155-167, doi:10.1016/j.blre.2011.03.002, (2011).
- 4 Thrombosis: a major contributor to the global disease burden. *J Thromb Haemost.* **12** (10), 1580-1590, doi:10.1111/jth.12698, (2014).
- 5 Kaplan, Z. S. & Jackson, S. P. The role of platelets in atherothrombosis. *Hematology Am Soc Hematol Educ Program.* **2011** 51-61, doi:10.1182/asheducation-2011.1.51, (2011).
- 6 Nuyttens, B., Thijs, T., Deckmyn, H. & Broos, K. Platelet adhesion to collagen. *Thrombosis research.* **127 Suppl 2** 9, doi:10.1016/s0049-3848(10)70151-1, (2011).
- 7 Pugh, N. *et al.* Synergism between platelet collagen receptors defined using receptor-specific collagen-mimetic peptide substrata in flowing blood. *Blood.* **115** (24), 5069-5079, doi:10.1182/blood-2010-01-260778, (2010).
- 8 Huang, J., Roth, R., Heuser, J. E. & Sadler, J. E. Integrin alpha(v)beta(3) on human endothelial cells binds von Willebrand factor strings under fluid shear stress. *Blood.* **113** (7), 1589-1597, doi:10.1182/blood-2008-05-158584, (2009).

- 9 Kasirer-Friede, A. *et al.* Signaling through GP Ib-IX-V activates alpha IIb beta 3 independently of other receptors. *Blood*. **103** (9), 3403-3411, doi:10.1182/blood-2003-10-3664, (2004).
- 10 Mazzucato, M., Pradella, P., Cozzi, M. R., De Marco, L. & Ruggeri, Z. M. Sequential cytoplasmic calcium signals in a 2-stage platelet activation process induced by the glycoprotein Ibalpha mechanoreceptor. *Blood*. **100** (8), 2793-2800, doi:10.1182/blood-2002-02-0514, (2002).
- 11 Nesbitt, W. S. *et al.* Distinct glycoprotein Ib/V/IX and integrin alpha IIbbeta 3-dependent calcium signals cooperatively regulate platelet adhesion under flow. *J Biol Chem*. **277** (4), 2965-2972, doi:10.1074/jbc.M110070200, (2002).
- 12 McEwan, P. A. *et al.* Quaternary Organization of GPIb-IX Complex and Insights Into Bernard-Soulier Syndrome Revealed by the Crystal Structures of GPIb beta Ectodomain and a GPIb beta/GPIX Chimera. *Blood*. **118** (21), 958-958 (2011).
- 13 Mo, X., Liu, L., Lopez, J. A. & Li, R. Transmembrane domains are critical to the interaction between platelet glycoprotein V and glycoprotein Ib-IX complex. *J Thromb Haemost*. **10** (9), 1875-1886, doi:10.1111/j.1538-7836.2012.04841.x, (2012).
- 14 Calverley, D. C., Kavanagh, T. J. & Roth, G. J. Human signaling protein 14-3-3zeta interacts with platelet glycoprotein Ib subunits Ibalpha and Ibbeta. *Blood*. **91** (4), 1295-1303 (1998).
- 15 Humphries, J. D., Byron, A. & Humphries, M. J. Integrin ligands at a glance. *Journal of Cell Science*. **119** (19), 3901-3903, doi:Doi 10.1242/Jcs.03098, (2006).

- 16 Zhang, W. *et al.* Identification of a juxtamembrane mechanosensitive domain in the platelet mechanosensor glycoprotein Ib-IX complex. *Blood*. **125** (3), 562-569, doi:10.1182/blood-2014-07-589507, (2015).
- 17 Ware, J., Russell, S. & Ruggeri, Z. M. Generation and rescue of a murine model of platelet dysfunction: the Bernard-Soulier syndrome. *Proc Natl Acad Sci U S A*. **97** (6), 2803-2808, doi:10.1073/pnas.050582097, (2000).
- 18 Bergmeier, W. *et al.* The role of platelet adhesion receptor GPIb α far exceeds that of its main ligand, von Willebrand factor, in arterial thrombosis. *Proc Natl Acad Sci U S A*. **103** (45), 16900-16905, doi:10.1073/pnas.0608207103, (2006).
- 19 Deng, W. & Li, R. Juxtamembrane contribution to transmembrane signaling. *Biopolymers*. doi:10.1002/bip.22651, (2015).
- 20 Dong, J. F. *et al.* ADAMTS-13 rapidly cleaves newly secreted ultralarge von Willebrand factor multimers on the endothelial surface under flowing conditions. *Blood*. **100** (12), 4033-4039, doi:10.1182/blood-2002-05-1401, (2002).
- 21 Lisman, T. *et al.* A single high-affinity binding site for von Willebrand factor in collagen III, identified using synthetic triple-helical peptides. *Blood*. **108** (12), 3753-3756, doi:10.1182/blood-2006-03-011965, (2006).
- 22 Doggett, T. A. *et al.* Selectin-like kinetics and biomechanics promote rapid platelet adhesion in flow: the GPIb α -vWF tether bond. *Biophys J*. **83** (1), 194-205, doi:10.1016/S0006-3495(02)75161-8, (2002).

- 23 Yago, T. *et al.* Platelet glycoprotein Ibalpha forms catch bonds with human WT vWF but not with type 2B von Willebrand disease vWF. *J Clin Invest.* **118** (9), 3195-3207, doi:10.1172/JCI35754, (2008).
- 24 Doggett, T. A. *et al.* Alterations in the intrinsic properties of the GPIIb/IIIa-VWF tether bond define the kinetics of the platelet-type von Willebrand disease mutation, Gly233Val. *Blood.* **102** (1), 152-160, doi:10.1182/blood-2003-01-0072, (2003).
- 25 Juliano, R. L. Signal transduction by cell adhesion receptors and the cytoskeleton: functions of integrins, cadherins, selectins, and immunoglobulin-superfamily members. *Annu Rev Pharmacol Toxicol.* **42** 283-323, doi:10.1146/annurev.pharmtox.42.090401.151133, (2002).
- 26 Kong, F., Garcia, A. J., Mould, A. P., Humphries, M. J. & Zhu, C. Demonstration of catch bonds between an integrin and its ligand. *J Cell Biol.* **185** (7), 1275-1284, doi:10.1083/jcb.200810002, (2009).
- 27 Rosetti, F. *et al.* A Lupus-Associated Mac-1 Variant Has Defects in Integrin Allosteric and Interaction with Ligands under Force. *Cell Rep.* doi:10.1016/j.celrep.2015.02.037, (2015).
- 28 Litvinov, R. I., Shuman, H., Bennett, J. S. & Weisel, J. W. Binding strength and activation state of single fibrinogen-integrin pairs on living cells. *Proc Natl Acad Sci U S A.* **99** (11), 7426-7431, doi:10.1073/pnas.112194999, (2002).
- 29 Chen, W., Lou, J. & Zhu, C. Forcing switch from short- to intermediate- and long-lived states of the alphaA domain generates LFA-1/ICAM-1 catch bonds. *J Biol Chem.* **285** (46), 35967-35978, doi:10.1074/jbc.M110.155770, (2010).

- 30 Fiore, V. F., Ju, L., Chen, Y., Zhu, C. & Barker, T. H. Dynamic catch of a Thy-1-alpha5beta1+syndecan-4 trimolecular complex. *Nat Commun.* **5** 4886, doi:10.1038/ncomms5886, (2014).
- 31 Aplin, A. E., Howe, A., Alahari, S. K. & Juliano, R. L. Signal transduction and signal modulation by cell adhesion receptors: the role of integrins, cadherins, immunoglobulin-cell adhesion molecules, and selectins. *Pharmacol Rev.* **50** (2), 197-263 (1998).
- 32 Springer, T. A. & Dustin, M. L. Integrin inside-out signaling and the immunological synapse. *Curr Opin Cell Biol.* **24** (1), 107-115, doi:10.1016/j.ceb.2011.10.004, (2012).
- 33 Zarbock, A., Polanowska-Grabowska, R. K. & Ley, K. Platelet-neutrophil-interactions: linking hemostasis and inflammation. *Blood Rev.* **21** (2), 99-111, doi:10.1016/j.blre.2006.06.001, (2007).
- 34 McCaffery, P. J. & Berridge, M. V. Expression of the leukocyte functional molecule (LFA-1) on mouse platelets. *Blood.* **67** (6), 1757-1764 (1986).
- 35 Diacovo, T. G., deFougerolles, A. R., Bainton, D. F. & Springer, T. A. A functional integrin ligand on the surface of platelets: intercellular adhesion molecule-2. *J Clin Invest.* **94** (3), 1243-1251, doi:10.1172/JCI117442, (1994).
- 36 Estevez, B., Shen, B. & Du, X. Targeting integrin and integrin signaling in treating thrombosis. *Arterioscler Thromb Vasc Biol.* **35** (1), 24-29, doi:10.1161/ATVBAHA.114.303411, (2015).

- 37 McCarty, O. J. *et al.* Evaluation of the role of platelet integrins in fibronectin-dependent spreading and adhesion. *J Thromb Haemost.* **2** (10), 1823-1833, doi:10.1111/j.1538-7836.2004.00925.x, (2004).
- 38 Philippeaux, M. M., Vesin, C., Tacchini-Cottier, F. & Pigué, P. F. Activated human platelets express beta2 integrin. *Eur J Haematol.* **56** (3), 130-137 (1996).
- 39 Bennett, J. S., Berger, B. W. & Billings, P. C. The structure and function of platelet integrins. *Journal of Thrombosis and Haemostasis.* **7** 200-205, doi:DOI 10.1111/j.1538-7836.2009.03378.x, (2009).
- 40 Shattil, S. J., Kim, C. & Ginsberg, M. H. The final steps of integrin activation: the end game. *Nat Rev Mol Cell Biol.* **11** (4), 288-300, doi:10.1038/nrm2871, (2010).
- 41 Lau, T. L., Kim, C., Ginsberg, M. H. & Ulmer, T. S. The structure of the integrin alphaIIb beta3 transmembrane complex explains integrin transmembrane signalling. *EMBO J.* **28** (9), 1351-1361, doi:10.1038/emboj.2009.63, (2009).
- 42 Kahner, B. N. *et al.* Kindlins, integrin activation and the regulation of talin recruitment to alphaIIb beta3. *PLoS One.* **7** (3), e34056, doi:10.1371/journal.pone.0034056, (2012).
- 43 Ye, F., Kim, C. & Ginsberg, M. H. Reconstruction of integrin activation. *Blood.* **119** (1), 26-33, doi:10.1182/blood-2011-04-292128, (2012).
- 44 Ma, Y. Q., Qin, J. & Plow, E. F. Platelet integrin alpha(IIb)beta(3): activation mechanisms. *J Thromb Haemost.* **5** (7), 1345-1352, doi:10.1111/j.1538-7836.2007.02537.x, (2007).

- 45 Cosemans, J. M., Iserbyt, B. F., Deckmyn, H. & Heemskerk, J. W. Multiple ways to switch platelet integrins on and off. *J Thromb Haemost.* **6** (8), 1253-1261, doi:10.1111/j.1538-7836.2008.03041.x, (2008).
- 46 Ye, F. *et al.* Recreation of the terminal events in physiological integrin activation. *J Cell Biol.* **188** (1), 157-173, doi:10.1083/jcb.200908045, (2010).
- 47 Takagi, J., Petre, B. M., Walz, T. & Springer, T. A. Global conformational rearrangements in integrin extracellular domains in outside-in and inside-out signaling. *Cell.* **110** (5), 599-511 (2002).
- 48 Kim, M., Carman, C. V. & Springer, T. A. Bidirectional transmembrane signaling by cytoplasmic domain separation in integrins. *Science.* **301** (5640), 1720-1725, doi:10.1126/science.1084174, (2003).
- 49 Gawaz, M. P. *et al.* Ligand bridging mediates integrin alpha IIb beta 3 (platelet GPIIB-IIIa) dependent homotypic and heterotypic cell-cell interactions. *J Clin Invest.* **88** (4), 1128-1134, doi:10.1172/JCI115412, (1991).
- 50 Rooney, M. M., Farrell, D. H., van Hemel, B. M., de Groot, P. G. & Lord, S. T. The contribution of the three hypothesized integrin-binding sites in fibrinogen to platelet-mediated clot retraction. *Blood.* **92** (7), 2374-2381 (1998).
- 51 Charo, I. F., Nannizzi, L., Smith, J. W. & Cheresch, D. A. The vitronectin receptor alpha v beta 3 binds fibronectin and acts in concert with alpha 5 beta 1 in promoting cellular attachment and spreading on fibronectin. *J Cell Biol.* **111** (6 Pt 1), 2795-2800 (1990).

- 52 Rout, U. K., Wang, J., Paria, B. C. & Armant, D. R. Alpha5beta1, alphaVbeta3 and the platelet-associated integrin alphaIIbbeta3 coordinately regulate adhesion and migration of differentiating mouse trophoblast cells. *Dev Biol.* **268** (1), 135-151, doi:10.1016/j.ydbio.2003.12.010, (2004).
- 53 Garcia, A. J., Schwarzbauer, J. E. & Boettiger, D. Distinct activation states of alpha5beta1 integrin show differential binding to RGD and synergy domains of fibronectin. *Biochemistry.* **41** (29), 9063-9069 (2002).
- 54 Makogonenko, E., Tsurupa, G., Ingham, K. & Medved, L. Interaction of fibrin(ogen) with fibronectin: further characterization and localization of the fibronectin-binding site. *Biochemistry.* **41** (25), 7907-7913 (2002).
- 55 Ni, H. *et al.* Plasma fibronectin promotes thrombus growth and stability in injured arterioles. *Proc Natl Acad Sci U S A.* **100** (5), 2415-2419, doi:10.1073/pnas.2628067100, (2003).
- 56 Cho, J. & Mosher, D. F. Impact of fibronectin assembly on platelet thrombus formation in response to type I collagen and von Willebrand factor. *Blood.* **108** (7), 2229-2236, doi:10.1182/blood-2006-02-002063, (2006).
- 57 Litvinov, R. I. *et al.* Resolving two-dimensional kinetics of the integrin alphaIIbbeta3-fibrinogen interactions using binding-unbinding correlation spectroscopy. *J Biol Chem.* **287** (42), 35275-35285, doi:10.1074/jbc.M112.404848, (2012).

- 58 Litvinov, R. I. *et al.* Dissociation of bimolecular alphaIIb beta3-fibrinogen complex under a constant tensile force. *Biophys J.* **100** (1), 165-173, doi:10.1016/j.bpj.2010.11.019, (2011).
- 59 Xie, C. *et al.* Structure of an integrin with an alphaI domain, complement receptor type 4. *EMBO J.* **29** (3), 666-679, doi:10.1038/emboj.2009.367, (2010).
- 60 Nishida, N. *et al.* Activation of leukocyte beta2 integrins by conversion from bent to extended conformations. *Immunity.* **25** (4), 583-594, doi:10.1016/j.immuni.2006.07.016, (2006).
- 61 Beglova, N., Blacklow, S. C., Takagi, J. & Springer, T. A. Cysteine-rich module structure reveals a fulcrum for integrin rearrangement upon activation. *Nat Struct Biol.* **9** (4), 282-287, doi:10.1038/nsb779, (2002).
- 62 Humphries, M. J., Symonds, E. J. & Mould, A. P. Mapping functional residues onto integrin crystal structures. *Curr Opin Struct Biol.* **13** (2), 236-243 (2003).
- 63 Chen, W., Lou, J., Evans, E. A. & Zhu, C. Observing force-regulated conformational changes and ligand dissociation from a single integrin on cells. *J Cell Biol.* **199** (3), 497-512, doi:10.1083/jcb.201201091, (2012).
- 64 Van de Walle, G. *et al.* Activation of alphaIIb beta3 is a sufficient but also an imperative prerequisite for activation of alpha2 beta1 on platelets. *Blood.* **109** (2), 595-602, doi:10.1182/blood-2005-11-011775, (2007).
- 65 Zhang, D. *et al.* Two disparate ligand-binding sites in the human P2Y1 receptor. *Nature.* **520** (7547), 317-321, doi:10.1038/nature14287, (2015).

- 66 Hollopeter, G. *et al.* Identification of the platelet ADP receptor targeted by antithrombotic drugs. *Nature*. **409** (6817), 202-207, doi:10.1038/35051599, (2001).
- 67 Coughlin, S. R. How the protease thrombin talks to cells. *Proc Natl Acad Sci U S A*. **96** (20), 11023-11027 (1999).
- 68 Bennett, J. S. & Vilaire, G. Exposure of platelet fibrinogen receptors by ADP and epinephrine. *J Clin Invest*. **64** (5), 1393-1401, doi:10.1172/JCI109597, (1979).
- 69 Yong, A. S. *et al.* Intracoronary shear-related up-regulation of platelet P-selectin and platelet-monocyte aggregation despite the use of aspirin and clopidogrel. *Blood*. **117** (1), 11-20, doi:10.1182/blood-2010-04-278812, (2011).
- 70 Suzuki, J., Umeda, M., Sims, P. J. & Nagata, S. Calcium-dependent phospholipid scrambling by TMEM16F. *Nature*. **468** (7325), 834-838, doi:10.1038/nature09583, (2010).
- 71 Yang, H. *et al.* TMEM16F forms a Ca²⁺-activated cation channel required for lipid scrambling in platelets during blood coagulation. *Cell*. **151** (1), 111-122, doi:10.1016/j.cell.2012.07.036, (2012).
- 72 Bevers, E. M., Comfurius, P. & Zwaal, R. F. Changes in membrane phospholipid distribution during platelet activation. *Biochim Biophys Acta*. **736** (1), 57-66 (1983).
- 73 Rosing, J. *et al.* The role of activated human platelets in prothrombin and factor X activation. *Blood*. **65** (2), 319-332 (1985).
- 74 Lentz, B. R. Exposure of platelet membrane phosphatidylserine regulates blood coagulation. *Prog Lipid Res*. **42** (5), 423-438 (2003).

- 75 Zwaal, R. F., Comfurius, P. & Bevers, E. M. Scott syndrome, a bleeding disorder caused by defective scrambling of membrane phospholipids. *Biochim Biophys Acta*. **1636** (2-3), 119-128, doi:10.1016/j.bbaliip.2003.07.003, (2004).
- 76 Kuijpers, M. J. *et al.* Facilitating roles of murine platelet glycoprotein Ib and alphaIIb beta3 in phosphatidylserine exposure during vWF-collagen-induced thrombus formation. *J Physiol*. **558** (Pt 2), 403-415, doi:10.1113/jphysiol.2004.062414, (2004).
- 77 Springer, T. A. von Willebrand factor, Jedi knight of the bloodstream. *Blood*. **124** (9), 1412-1425, doi:10.1182/blood-2014-05-378638, (2014).
- 78 Fox, J. E., Aggerbeck, L. P. & Berndt, M. C. Structure of the glycoprotein Ib/IX complex from platelet membranes. *J Biol Chem*. **263** (10), 4882-4890 (1988).
- 79 Kasirer-Friede, A., Ruggeri, Z. M. & Shattil, S. J. Role for ADAP in shear flow-induced platelet mechanotransduction. *Blood*. **115** (11), 2274-2282, doi:10.1182/blood-2009-08-238238, (2010).
- 80 Yap, C. L. *et al.* Synergistic adhesive interactions and signaling mechanisms operating between platelet glycoprotein Ib/IX and integrin alpha IIb beta 3. Studies in human platelets and transfected Chinese hamster ovary cells. *J Biol Chem*. **275** (52), 41377-41388, doi:10.1074/jbc.M005590200, (2000).
- 81 Nesbitt, W. S. *et al.* Intercellular calcium communication regulates platelet aggregation and thrombus growth. *J Cell Biol*. **160** (7), 1151-1161, doi:10.1083/jcb.200207119, (2003).

- 82 Li, A., Guo, Q., Kim, C., Hu, W. & Ye, F. Integrin alphaII b tail distal of GFFKR participates in inside-out alphaII b beta3 activation. *J Thromb Haemost.* **12** (7), 1145-1155, doi:10.1111/jth.12610, (2014).
- 83 Feral, C. C. *et al.* CD98hc (SLC3A2) mediates integrin signaling. *Proc Natl Acad Sci U S A.* **102** (2), 355-360, doi:10.1073/pnas.0404852102, (2005).
- 84 Wang, N., Butler, J. P. & Ingber, D. E. Mechanotransduction across the cell surface and through the cytoskeleton. *Science.* **260** (5111), 1124-1127 (1993).
- 85 Hudspeth, A. J. Hair-bundle mechanics and a model for mechanoelectrical transduction by hair cells. *Soc Gen Physiol Ser.* **47** 357-370 (1992).
- 86 Gillespie, P. G. & Walker, R. G. Molecular basis of mechanosensory transduction. *Nature.* **413** (6852), 194-202, doi:10.1038/35093011, (2001).
- 87 Orr, A. W., Helmke, B. P., Blackman, B. R. & Schwartz, M. A. Mechanisms of mechanotransduction. *Dev Cell.* **10** (1), 11-20, doi:10.1016/j.devcel.2005.12.006, (2006).
- 88 Ju, L., Dong, J.-f., Cruz, M. A. & Zhu, C. The N-terminal Flanking Region of the A1 Domain Regulates the Force-dependent Binding of von Willebrand Factor to Platelet Glycoprotein Ib *Journal of Biological Chemistry.* **288**, doi:10.1074/jbc.M113.504001, (2013).
- 89 Ju, L., Lou, J., Chen, Y., Li, Z. & Zhu, C. Force-Induced Unfolding of Leucine-Rich Repeats of Glycoprotein Ibalpha Strengthens Ligand Interaction. *Biophys J.* **109** (9), 1781-1784, doi:10.1016/j.bpj.2015.08.050, (2015).

- 90 Cruz, M. A., Handin, R. I. & Wise, R. J. The interaction of the von Willebrand factor-A1 domain with platelet glycoprotein Ib/IX. The role of glycosylation and disulfide bonding in a monomeric recombinant A1 domain protein. *J Biol Chem.* **268** (28), 21238-21245 (1993).
- 91 Chen, Y. *et al.* Fluorescence Biomembrane Force Probe: Concurrent Quantitation of Receptor-ligand Kinetics and Binding-induced Intracellular Signaling on a Single Cell. *J Vis Exp.* (102), doi:10.3791/52975, (2015).
- 92 Chesla, S. E., Selvaraj, P. & Zhu, C. Measuring two-dimensional receptor-ligand binding kinetics by micropipette. *Biophys J.* **75** (3), 1553-1572, doi:10.1016/S0006-3495(98)74074-3, (1998).
- 93 Zarnitsyna, V. I. & Zhu, C. Adhesion frequency assay for in situ kinetics analysis of cross-junctional molecular interactions at the cell-cell interface. *J Vis Exp.* (57), e3519, doi:10.3791/3519, (2011).
- 94 Chen, W., Evans, E. A., McEver, R. P. & Zhu, C. Monitoring receptor-ligand interactions between surfaces by thermal fluctuations. *Biophys J.* **94** (2), 694-701, doi:10.1529/biophysj.107.117895, (2008).
- 95 Jiang, N. *et al.* Two-stage cooperative T cell receptor-peptide major histocompatibility complex-CD8 trimolecular interactions amplify antigen discrimination. *Immunity.* **34** (1), 13-23, doi:10.1016/j.immuni.2010.12.017, (2011).
- 96 Bell, G. I. Models for the specific adhesion of cells to cells. *Science.* **200** (4342), 618-627 (1978).

- 97 Schurpf, T. & Springer, T. A. Regulation of integrin affinity on cell surfaces. *EMBO J.* **30** (23), 4712-4727, doi:10.1038/emboj.2011.333, (2011).
- 98 Chen, X. *et al.* Requirement of open headpiece conformation for activation of leukocyte integrin $\alpha X\beta 2$. *Proc Natl Acad Sci U S A.* **107** (33), 14727-14732, doi:10.1073/pnas.1008663107, (2010).
- 99 Zhang, C. *et al.* Modulation of integrin activation and signaling by $\alpha 1/\alpha 1'$ -helix unbending at the junction. *J Cell Sci.* **126** (Pt 24), 5735-5747, doi:10.1242/jcs.137828, (2013).
- 100 Hughes, P. E. *et al.* Breaking the integrin hinge. A defined structural constraint regulates integrin signaling. *J Biol Chem.* **271** (12), 6571-6574 (1996).
- 101 Pines, M., Fairchild, M. J. & Tanentzapf, G. Distinct regulatory mechanisms control integrin adhesive processes during tissue morphogenesis. *Dev Dyn.* **240** (1), 36-51, doi:10.1002/dvdy.22488, (2011).
- 102 Luo, B. H., Karanicolas, J., Harmacek, L. D., Baker, D. & Springer, T. A. Rationally designed integrin $\beta 3$ mutants stabilized in the high affinity conformation. *J Biol Chem.* **284** (6), 3917-3924, doi:10.1074/jbc.M806312200, (2009).
- 103 Chen, W. *et al.* Molecular dynamics simulations of forced unbending of integrin $\alpha(v)\beta(3)$. *PLoS Comput Biol.* **7** (2), e1001086, doi:10.1371/journal.pcbi.1001086, (2011).
- 104 Liu, B., Chen, W., Evavold, B. D. & Zhu, C. Accumulation of dynamic catch bonds between TCR and agonist peptide-MHC triggers T cell signaling. *Cell.* **157** (2), 357-368, doi:10.1016/j.cell.2014.02.053, (2014).

- 105 Marshall, B. T. *et al.* Direct observation of catch bonds involving cell-adhesion molecules. *Nature*. **423** (6936), 190-193, doi:10.1038/nature01605, (2003).
- 106 Manibog, K., Li, H., Rakshit, S. & Sivasankar, S. Resolving the molecular mechanism of cadherin catch bond formation. *Nat Commun*. **5** 3941, doi:10.1038/ncomms4941, (2014).
- 107 Du, X. *et al.* Long range propagation of conformational changes in integrin alpha IIb beta 3. *J Biol Chem*. **268** (31), 23087-23092 (1993).
- 108 Choi, W. S., Rice, W. J., Stokes, D. L. & Collier, B. S. Three-dimensional reconstruction of intact human integrin alphaIIbeta3: new implications for activation-dependent ligand binding. *Blood*. **122** (26), 4165-4171, doi:10.1182/blood-2013-04-499194, (2013).
- 109 Pampori, N. *et al.* Mechanisms and consequences of affinity modulation of integrin alpha(V)beta(3) detected with a novel patch-engineered monovalent ligand. *J Biol Chem*. **274** (31), 21609-21616 (1999).
- 110 Kodera, N., Yamamoto, D., Ishikawa, R. & Ando, T. Video imaging of walking myosin V by high-speed atomic force microscopy. *Nature*. **468** (7320), 72-76, doi:10.1038/nature09450, (2010).
- 111 Sutter, M. *et al.* Visualization of Bacterial Microcompartment Facet Assembly Using High-Speed Atomic Force Microscopy. *Nano Lett*. doi:10.1021/acs.nanolett.5b04259, (2015).
- 112 Wang, X. & Ha, T. Defining single molecular forces required to activate integrin and notch signaling. *Science*. **340** (6135), 991-994, doi:10.1126/science.1231041, (2013).

- 113 Flevaris, P. *et al.* A molecular switch that controls cell spreading and retraction. *J Cell Biol.* **179** (3), 553-565, doi:10.1083/jcb.200703185, (2007).
- 114 Roca-Cusachs, P., Gauthier, N. C., Del Rio, A. & Sheetz, M. P. Clustering of alpha(5)beta(1) integrins determines adhesion strength whereas alpha(v)beta(3) and talin enable mechanotransduction. *Proc Natl Acad Sci U S A.* **106** (38), 16245-16250, doi:10.1073/pnas.0902818106, (2009).
- 115 Zhu, J., Zhu, J. & Springer, T. A. Complete integrin headpiece opening in eight steps. *J Cell Biol.* **201** (7), 1053-1068, doi:10.1083/jcb.201212037, (2013).
- 116 Guo, Q., Zheng, H., Chen, W. & Chen, Z. Modeling bistable behaviors in morphing structures through finite element simulations. *Biomed Mater Eng.* **24** (1), 557-562, doi:10.3233/BME-130842, (2014).
- 117 Warwick, S. N. *et al.* A shear gradient-dependent platelet aggregation mechanism drives thrombus formation. *Nature Medicine.* **15**, doi:10.1038/nm.1955, (2009).
- 118 Qiu, Y., Ciciliano, J., Myers, D. R., Tran, R. & Lam, W. A. Platelets and physics: How platelets "feel" and respond to their mechanical microenvironment. *Blood Rev.* doi:10.1016/j.blre.2015.05.002, (2015).
- 119 Ruggeri, Z. M. Platelet GPIb: sensing force and responding. *Blood.* **125** (3), 423-424, doi:10.1182/blood-2014-12-610642, (2015).
- 120 Gu, M., Xi, X., Englund, G. D., Berndt, M. C. & Du, X. Analysis of the roles of 14-3-3 in the platelet glycoprotein Ib-IX-mediated activation of integrin alpha(IIb)beta(3) using a reconstituted mammalian cell expression model. *J Cell Biol.* **147** (5), 1085-1096 (1999).

- 121 Dong, J. F. *et al.* Ristocetin-dependent, but not botrocetin-dependent, binding of von Willebrand factor to the platelet glycoprotein Ib-IX-V complex correlates with shear-dependent interactions. *Blood*. **97** (1), 162-168 (2001).
- 122 Ju, L. *Single-molecule study on GPIb-alpha and von Willebrand factor mediated platelet adhesion and signal triggering* Ph.D. thesis, Georgia Institute of Technology, (2013).
- 123 Strassel, C. *et al.* Synthesis of GPIb beta with novel transmembrane and cytoplasmic sequences in a Bernard-Soulier patient resulting in GPIb-defective signaling in CHO cells. *J Thromb Haemost.* **4** (1), 217-228, doi:10.1111/j.1538-7836.2005.01654.x, (2006).
- 124 Dai, K., Bodnar, R., Berndt, M. C. & Du, X. A critical role for 14-3-3zeta protein in regulating the VWF binding function of platelet glycoprotein Ib-IX and its therapeutic implications. *Blood*. **106** (6), 1975-1981, doi:10.1182/blood-2005-01-0440, (2005).
- 125 Yin, H. *et al.* Role for platelet glycoprotein Ib-IX and effects of its inhibition in endotoxemia-induced thrombosis, thrombocytopenia, and mortality. *Arterioscler Thromb Vasc Biol.* **33** (11), 2529-2537, doi:10.1161/ATVBAHA.113.302339, (2013).
- 126 Ruggeri, Z. M. Type IIB von Willebrand disease: a paradox explains how von Willebrand factor works. *J Thromb Haemost.* **2** (1), 2-6 (2004).
- 127 Casari, C. *et al.* von Willebrand factor mutation promotes thrombocytopeny by inhibiting integrin alphaIIb beta3. *J Clin Invest.* **123** (12), 5071-5081, doi:10.1172/JCI69458, (2013).

- 128 Du, X. Signaling and regulation of the platelet glycoprotein Ib-IX-V complex. *Curr Opin Hematol.* **14** (3), 262-269, doi:10.1097/MOH.0b013e3280dce51a, (2007).
- 129 Rendu, F. & Brohard-Bohn, B. The platelet release reaction: granules' constituents, secretion and functions. *Platelets.* **12** (5), 261-273, doi:10.1080/09537100120068170, (2001).
- 130 Manon-Jensen, T., Kjeld, N. G. & Karsdal, M. A. Collagen-mediated hemostasis. *J Thromb Haemost.* **14** (3), 438-448, doi:10.1111/jth.13249, (2016).
- 131 Ferroni, P. *et al.* Biomarkers of platelet activation in acute coronary syndromes. *Thromb Haemost.* **108** (6), 1109-1123, doi:10.1160/TH12-08-0550, (2012).
- 132 Kim, C. *et al.* Basic amino-acid side chains regulate transmembrane integrin signalling. *Nature.* **481** (7380), 209-213, doi:10.1038/nature10697, (2012).
- 133 Watanabe, N. *et al.* Mechanisms and consequences of agonist-induced talin recruitment to platelet integrin alphaIIb beta3. *J Cell Biol.* **181** (7), 1211-1222, doi:10.1083/jcb.200803094, (2008).
- 134 Du, X. P. *et al.* Ligands "activate" integrin alpha IIb beta 3 (platelet GPIIb-IIIa). *Cell.* **65** (3), 409-416 (1991).
- 135 Shen, B. *et al.* A directional switch of integrin signalling and a new anti-thrombotic strategy. *Nature.* **503** (7474), 131-135, doi:10.1038/nature12613, (2013).
- 136 Stefanini, L. *et al.* A talin mutant that impairs talin-integrin binding in platelets decelerates alphaIIb beta3 activation without pathological bleeding. *Blood.* **123** (17), 2722-2731, doi:10.1182/blood-2013-12-543363, (2014).

- 137 Stalker, T. J. *et al.* Hierarchical organization in the hemostatic response and its relationship to the platelet-signaling network. *Blood*. **121** (10), 1875-1885, doi:10.1182/blood-2012-09-457739, (2013).
- 138 Delaney, M. K. *et al.* Agonist-induced platelet procoagulant activity requires shear and a Rac1-dependent signaling mechanism. *Blood*. **124** (12), 1957-1967, doi:10.1182/blood-2014-03-560821, (2014).
- 139 Ruggeri, Z. M. & Mendolicchio, G. L. Adhesion mechanisms in platelet function. *Circ Res*. **100** (12), 1673-1685, doi:10.1161/01.RES.0000267878.97021.ab, (2007).
- 140 Okada, Y., Nishikawa, J., Semma, M. & Ichikawa, A. Induction of integrin beta3 in PGE(2)-stimulated adhesion of mastocytoma P-815 cells to the Arg-Gly-Asp-enriched fragment of fibronectin. *Biochem Pharmacol*. **81** (7), 866-872, doi:10.1016/j.bcp.2011.01.010, (2011).
- 141 Zhou, Y. F. *et al.* Sequence and structure relationships within von Willebrand factor. *Blood*. **120** (2), 449-458, doi:10.1182/blood-2012-01-405134, (2012).
- 142 Pankov, R. & Yamada, K. M. Fibronectin at a glance. *J Cell Sci*. **115** (Pt 20), 3861-3863 (2002).
- 143 Petrie, T. A. *et al.* Multivalent integrin-specific ligands enhance tissue healing and biomaterial integration. *Sci Transl Med*. **2** (45), 45ra60, doi:10.1126/scitranslmed.3001002, (2010).
- 144 Redick, S. D., Settles, D. L., Briscoe, G. & Erickson, H. P. Defining fibronectin's cell adhesion synergy site by site-directed mutagenesis. *J Cell Biol*. **149** (2), 521-527 (2000).

- 145 Bowditch, R. D. *et al.* Identification of a novel integrin binding site in fibronectin. Differential utilization by beta 3 integrins. *J Biol Chem.* **269** (14), 10856-10863 (1994).
- 146 Ju, L. *et al.* Von Willebrand factor-A1 domain binds platelet glycoprotein Ibalpha in multiple states with distinctive force-dependent dissociation kinetics. *Thromb Res.* **136** (3), 606-612, doi:10.1016/j.thromres.2015.06.019, (2015).
- 147 Mitchell, W. B. *et al.* Mapping early conformational changes in alphaIIb and beta3 during biogenesis reveals a potential mechanism for alphaIIbbeta3 adopting its bent conformation. *Blood.* **109** (9), 3725-3732, doi:10.1182/blood-2006-11-058420, (2007).
- 148 Kaul, D. K. *et al.* Monoclonal antibodies to alphaVbeta3 (7E3 and LM609) inhibit sickle red blood cell-endothelium interactions induced by platelet-activating factor. *Blood.* **95** (2), 368-374 (2000).
- 149 Qiu, Y. *et al.* Platelet mechanosensing of substrate stiffness during clot formation mediates adhesion, spreading, and activation. *Proc Natl Acad Sci U S A.* **111** (40), 14430-14435, doi:10.1073/pnas.1322917111, (2014).
- 150 Li, N. *et al.* Distinct binding affinities of Mac-1 and LFA-1 in neutrophil activation. *J Immunol.* **190** (8), 4371-4381, doi:10.4049/jimmunol.1201374, (2013).
- 151 Shamri, R. *et al.* Lymphocyte arrest requires instantaneous induction of an extended LFA-1 conformation mediated by endothelium-bound chemokines. *Nat Immunol.* **6** (5), 497-506, doi:10.1038/ni1194, (2005).

- 152 Arnaout, M. A., Mahalingam, B. & Xiong, J. P. Integrin structure, allostery, and bidirectional signaling. *Annu Rev Cell Dev Biol.* **21** 381-410, doi:10.1146/annurev.cellbio.21.090704.151217, (2005).
- 153 Luo, B. H. & Springer, T. A. Integrin structures and conformational signaling. *Curr Opin Cell Biol.* **18** (5), 579-586, doi:10.1016/j.ccb.2006.08.005, (2006).
- 154 Kim, C., Ye, F., Hu, X. & Ginsberg, M. H. Talin activates integrins by altering the topology of the beta transmembrane domain. *J Cell Biol.* **197** (5), 605-611, doi:10.1083/jcb.201112141, (2012).
- 155 Gong, H. *et al.* G protein subunit Galpha13 binds to integrin alphaIIb beta3 and mediates integrin "outside-in" signaling. *Science.* **327** (5963), 340-343, doi:10.1126/science.1174779, (2010).
- 156 Xiong, J. P. *et al.* Crystal structure of the extracellular segment of integrin alpha Vbeta3. *Science.* **294** (5541), 339-345, doi:10.1126/science.1064535, (2001).
- 157 Xiong, J. P. *et al.* Crystal structure of the complete integrin alpha Vbeta3 ectodomain plus an alpha/beta transmembrane fragment. *J Cell Biol.* **186** (4), 589-600, doi:10.1083/jcb.200905085, (2009).
- 158 Peterson, J. A., Nelson, T. N., Kanack, A. J. & Aster, R. H. Fine specificity of drug-dependent antibodies reactive with a restricted domain of platelet GPIIIA. *Blood.* **111** (3), 1234-1239, doi:10.1182/blood-2007-09-112680, (2008).
- 159 Choi, Y. I. *et al.* Dynamic control of beta1 integrin adhesion by the plexinD1-sema3E axis. *Proc Natl Acad Sci U S A.* **111** (1), 379-384, doi:10.1073/pnas.1314209111, (2014).

- 160 Liu, Z. *et al.* Differential regulation of human and murine P-selectin expression and function in vivo. *J Exp Med.* **207** (13), 2975-2987, doi:10.1084/jem.20101545, (2010).
- 161 Leppanen, A., White, S. P., Helin, J., McEver, R. P. & Cummings, R. D. Binding of glycosulfopeptides to P-selectin requires stereospecific contributions of individual tyrosine sulfate and sugar residues. *J Biol Chem.* **275** (50), 39569-39578, doi:10.1074/jbc.M005005200, (2000).
- 162 Hynes, R. O. The emergence of integrins: a personal and historical perspective. *Matrix Biol.* **23** (6), 333-340, doi:10.1016/j.matbio.2004.08.001, (2004).
- 163 Bledzka, K., Smyth, S. S. & Plow, E. F. Integrin α IIb β 3: from discovery to efficacious therapeutic target. *Circ Res.* **112** (8), 1189-1200, doi:10.1161/CIRCRESAHA.112.300570, (2013).
- 164 Xiao, T., Takagi, J., Collier, B. S., Wang, J. H. & Springer, T. A. Structural basis for allostery in integrins and binding to fibrinogen-mimetic therapeutics. *Nature.* **432** (7013), 59-67, doi:10.1038/nature02976, (2004).
- 165 Litvinov, R. I., Farrell, D. H., Weisel, J. W. & Bennett, J. S. The Platelet Integrin α IIb β 3 Differentially Interacts with Fibrin Versus Fibrinogen. *J Biol Chem.* doi:10.1074/jbc.M115.706861, (2016).
- 166 Agnihotri, A., Soman, P. & Siedlecki, C. A. AFM measurements of interactions between the platelet integrin receptor GPIIbIIIa and fibrinogen. *Colloids Surf B Biointerfaces.* **71** (1), 138-147, doi:10.1016/j.colsurfb.2009.01.019, (2009).

- 167 Hynes, R. O. Integrins: bidirectional, allosteric signaling machines. *Cell*. **110** (6), 673-687 (2002).
- 168 Luo, B. H., Carman, C. V. & Springer, T. A. Structural basis of integrin regulation and signaling. *Annu Rev Immunol*. **25** 619-647, doi:10.1146/annurev.immunol.25.022106.141618, (2007).
- 169 Luo, B. H., Springer, T. A. & Takagi, J. Stabilizing the open conformation of the integrin headpiece with a glycan wedge increases affinity for ligand. *Proc Natl Acad Sci U S A*. **100** (5), 2403-2408, doi:10.1073/pnas.0438060100, (2003).
- 170 Luo, B. H., Springer, T. A. & Takagi, J. A specific interface between integrin transmembrane helices and affinity for ligand. *PLoS Biol*. **2** (6), e153, doi:10.1371/journal.pbio.0020153, (2004).
- 171 Springer, T. A., Zhu, J. & Xiao, T. Structural basis for distinctive recognition of fibrinogen gammaC peptide by the platelet integrin alphaIIb beta3. *J Cell Biol*. **182** (4), 791-800, doi:10.1083/jcb.200801146, (2008).
- 172 Mozaffarian, D. *et al.* Heart Disease and Stroke Statistics-2016 Update: A Report From the American Heart Association. *Circulation*. **133** (4), e38-e360, doi:10.1161/CIR.0000000000000350, (2016).
- 173 Kisucka, J. *et al.* Elevated levels of soluble P-selectin in mice alter blood-brain barrier function, exacerbate stroke, and promote atherosclerosis. *Blood*. **113** (23), 6015-6022, doi:10.1182/blood-2008-10-186650, (2009).

- 174 Htun, P. *et al.* Course of platelet activation and platelet-leukocyte interaction in cerebrovascular ischemia. *Stroke*. **37** (9), 2283-2287, doi:10.1161/01.STR.0000236638.75591.61, (2006).
- 175 Razmara, M., Hjemdahl, P., Ostenson, C. G. & Li, N. Platelet hyperprocoagulant activity in Type 2 diabetes mellitus: attenuation by glycoprotein IIb/IIIa inhibition. *J Thromb Haemost.* **6** (12), 2186-2192, doi:10.1111/j.1538-7836.2008.03185.x, (2008).
- 176 Jacopo, G. *et al.* Identification of platelet hyper-reactivity measured with a portable device immediately after percutaneous coronary intervention predicts in stent thrombosis. *Thromb Res.* **121** (3), 407-412, doi:10.1016/j.thromres.2007.04.009, (2007).
- 177 Smith, T., Dhunoo, G., Mohan, I. & Charlton-Menys, V. A pilot study showing an association between platelet hyperactivity and the severity of peripheral arterial disease. *Platelets.* **18** (4), 245-248, doi:10.1080/09537100601078091, (2007).
- 178 Anfossi, G. *et al.* Impaired synthesis and action of antiaggregating cyclic nucleotides in platelets from obese subjects: possible role in platelet hyperactivation in obesity. *Eur J Clin Invest.* **34** (7), 482-489, doi:10.1111/j.1365-2362.2004.01370.x, (2004).
- 179 Han, S. Z. *et al.* Evaluation of imputation-based association in and around the integrin-alpha-M (ITGAM) gene and replication of robust association between a non-synonymous functional variant within ITGAM and systemic lupus erythematosus (SLE). *Human Molecular Genetics.* **18** (6), 1171-1180, doi:10.1093/hmg/ddp007, (2009).

CURRICULUM VITAE

Qualifications

Sep. 2006 – Jun. 2010

B.S., Theoretical and Applied Mechanics, Peking University, China. GPA: 3.68/4.0

B.S., Major in Economics (Double Major), Peking University, China. GPA: 3.16/4.0

Aug. 2010 – current

Ph.D. Candidate, Bioengineering, advised by Prof. Cheng Zhu, Georgia Institute of Technology, USA. GPA: 3.91/4.0

- Use a Biomembrane Force Probe to study the binding and conformation dynamics of single integrins.
- Investigate dysregulation of leukocyte integrin Mac-1 adhesion and signaling by a lupus-associated mutation.
- Upgrade the Biomembrane Force Probe to study adhesion and mechanotransduction of platelet surface receptors GPIIb α and integrin $\alpha_{IIb}\beta_3$.
- Investigate the biomechanical dysregulation of platelet adhesion and activation in diabetes-related atherothrombosis.

Jan. – Feb. 2014

Visiting scholar, advised by Prof. Peter Hinterdorfer, Johannes Kepler University, Austria

- Use a High Speed Atomic Force Microscopy to observe and characterize integrin bending/extending conformational changes.

Jan. – Feb. 2016

Visiting scholar, advised by Prof. Shaun Jackson, The University of Sydney, Australia

- Learn platelet biology, platelet mechanotransduction and mouse Type I Diabetes model and stroke models.

Current Position

Aug. 2010-now

Graduate Research Assistant in Prof. Cheng Zhu's lab, Coulter Department of Biomedical Engineering, Georgia Institute of Technology, USA

Peer Reviewed Publications

1. **Chen Y.**, Lee H., Schwartz M., Zhu C., *Force regulated conformational change of integrin $\alpha_V\beta_3$* . (Accepted by Matrix Biology). Impact Factor: 4.47
2. Elosegui-Artola A., Oria R., **Chen Y.**, Kosmalka A., Pérez-González C., Castro N., Zhu C., Trepas X., Roca-Cusachs P., *Mechanical regulation of a molecular clutch defines force transmission and transduction in response to matrix rigidity*. Nature Cell Biology. doi:10.1038/ncb3336. (2016). Impact Factor: 19.68
3. Ju L., Lou J., **Chen Y.**, Zhu C., *Force-induced unfolding of leucine-rich repeats of*

- glycoprotein Iba prolongs bond lifetime with von Willebrand factor*. Biophysical Journal 109(9):1781-4. doi: 10.1016/j.bpj.2015.08.050. (2015). Impact Factor: 3.97
4. Ju L., **Chen Y.**, Zhou F., Lu H., Cruz M., Zhu C., *Von Willebrand factor-A1 domain binds platelet glycoprotein Iba in multiple states with distinctive force-dependent dissociation kinetics*. Thrombosis research 136(3):606-12. doi: 10.1016/j.thromres.2015.06.019. (2015). Impact factor: 2.45
5. **Chen Y.***, Liu B.*, Ju L.*, Hong, J.*, Ji Q., Chen W., Zhu C., *Fluorescence Biomembrane Force Probe: Concurrent Quantitation of Receptor-Ligand Kinetics and Binding-induced Intracellular Signaling on a Single Cell*. Journal of Visualized Experiments (102), e52975, doi:10.3791/52975. (2015) (***Co-first authors**). Impact factor: 1.33
6. Rosetti F.*, **Chen Y.***, Sen M., Thayer E., Azcutia V., Herter J. M., Lusinskas F. W., Cullere X., Zhu C., Mayadas T.N., *A Lupus-Associated Mac-1 Variant Has Defects in Integrin Allostery and Interaction with Ligands under Force*. Cell Reports 10, 1655-1664, doi:10.1016/j.celrep.2015.02.037. (2015) (***Co-first authors**). Impact factor: 8.36
7. Fiore V. F., Ju L., **Chen Y.**, Zhu C., Barker T. H., *Dynamic catch of a Thy-1- $\alpha 5\beta 1$ +syndecan-4 trimolecular complex*. Nature Communications 12;5:4886, doi: 10.1038/ncomms5886. (2014). Impact Factor: 11.47

Book Chapter Publications

1. Ju L., **Chen Y.**, Rushdi M., Chen W., Zhu C., *Two-dimensional analysis of cross-junctional molecular interaction by force probes*. Book Title: *The Immune Synapse: Methods and Protocols*. Edited by: Cosima T. Baldari, PhD and Michael L. Dustin, PhD.

Abstract Publications

1. **Chen Y.**, Ju L., Zhu C., *Identification and Characterization of Integrin α IIb β 3 Intermediate Affinity State Induced By GpIb α Mechanotransduction*. Blood: 126 (23). (2015).
2. Xu X., Spring C., Ju L., Wang Y., Reheman A., Yang H., Jin J., Lei X., Yang Yan., Reddy E., **Chen Y.**, Chen P., Zhu G., Marchese P., Zarpellon A., Zhang H., She Y., Cyr T., Zhu C., Freedman J., Tso P., Sean D., Ruggeri Z. M., Ni H., *Apolipoprotein A-IV Is a Novel Ligand of Platelet α IIb β 3 Integrin and an Endogenous Thrombosis Inhibitor: Measurement of Single-Molecular Interactions By Biomembrane Force Probe*. Blood: 124 (21). (2014)

Publications in Preparation

1. **Chen Y.**, Zhu C., *Observing force-regulated purified integrin bending/extending conformational changes*. (Manuscript in preparation)

2. Ju L.*, **Chen Y.***, Xue L., Du X., Zhu C., *Cooperative unfolding of distinctive mechanoreceptor domains transduces force into signals. (*Co-first authors)*. (Under review by *Elife*)

3. **Chen Y.**, Ju L., Zhou F., Zhu C., *Mechanical Inside-out and Outside-in Signaling of Integrin $\alpha_{IIb}\beta_3$* . (Manuscript in preparation)

4. Xu X., Wang Y., Reheman A., Ju L., Spring C. M., Jin J. W., Yang H., Chen P., Yang Yan., Lei X., **Chen Y.**, Zhang H., Song J., Zhang D., Carrim N., Zhu G., She Y., Cyr T., Liu G., Connelly P. W., Freedman J., Tso P., Marchese P., Zhu C., Davidson W. S., Ruggeri Z. M., Ni H., *Apolipoprotein A-IV is a novel ligand of platelet $\alpha_{IIb}\beta_3$ integrin and an endogenous inhibitor of thrombosis*. (Manuscript in preparation)

Inventions and Technology Upgrades

1. **Mar. 2016**, **Chen Y.**, Ju L., Chen W., Zhu C., *Micro-space Heater and Temperature Controller*. (Georgia Tech Invention Disclosure No. 7219)

2. **Mar. 2016**, Ju L., Chen W., Liu B., **Chen Y.**, Zhu C., *Fluorescence Biomembrane Force Probe*. (Georgia Tech Invention Disclosure No. 7232)

Awards

- **Oct. 2015**, ASH (American Society of Hematology) Abstract Achievement Award

- **2013-2014**, Molecular Biophysics Senior Student Award, Georgia Institute of Technology
- **Nov. 2009**, Outstanding Student Award, Peking University
- **Nov. 2009**, Sinopec Scholarship, Peking University
- **Dec. 2008**, Fuqing Yang&Yangyuan Wang Academician Scholarship, Peking University
- **Nov. 2007**, Baosteel Scholarship, Peking University

Attended Meetings

- **07/22-07/27/2012**, 2012 Gordon Research Conferences (Hemostasis), Waterville Valley, USA.

Poster presentation, Chen, Y., Ju, L., Liu, B., Cruz, M., and Zhu, C., "Two-stage Adhesion Kinetics of Single Platelet to VWF and Fibronectin".

- **10/24-10/27/2012**, 2012 Biomedical Engineering Society Meeting, Atlanta, USA.

Poster presentation, Chen, Y., Chen, W., and Zhu, C., "Observing Real-time Bending/unbending Conformational Changes of a Single Integrin in a Cell-free System".

- **01/31-02/03/2014**, XVIth Linz Winter Workshop, Linz, Austria.

Oral presentation, Chen, Y. and Zhu, C., "Observing Real-time Bending/unbending Conformational Changes of a Single Integrin in a Cell-free System".

- **07/27-08/01/2014**, 2014 Gordon Research Conferences (Hemostasis), Waterville Valley, USA.

Poster presentation, Chen, Y., Ju, L., and Zhu, C., "Identify an Intermediate Affinity State of Integrin $\alpha_{IIb}\beta_3$ Induced by GPIIb Mechanotransduction".

- **06/30-07/03/2015**, 2015 Society for Mathematical Biology Conference. Atlanta, USA.

Mini symposium talk, Chen, Y., Ju, L., Jackson, S. and Zhu, C., "Identification and Characterization of an Intermediate State of Integrin $\alpha_{IIb}\beta_3$ ".

- **11/07-11/11/2015**, American Heart Association Scientific Session 2015. Orlando, USA.
- **12/05-12/08/2015**, 57th American Society of Hematology Annual Meeting. Orlando, USA.

Oral presentation, Chen, Y., Ju, L., Jackson, S. and Zhu, C., "Identification of Integrin $\alpha_{IIb}\beta_3$ Intermediate Affinity State Induced by GPIIb Mechanotransduction".

(Abstract Achievement Award Winner)

Poster presentation, Chen, Y., Ju, L., Lou, J. and Zhu, C., "Force-induced cooperative unfolding of two distinctive domains in a single GPIIb molecule".

Professional Associations

- **Student Member of American Heart Association**
- **Student Member of American Society of Haematology**

Activities

- **Invited talk, Charles Perkins Centre, The University of Sydney, Australia, Jan. 20th, 2016**
- **The student speaker of Immunoengineering Seminar Series, Georgia Tech and Emory, 2015**
- **The student speaker of Immunoengineering Seminar Series, Georgia Tech and Emory, 2014**
- **The student speaker of Molecular Biophysics Seminar Series, Georgia Tech, 2014**
- **The student speaker of Biomechanics Meeting, Georgia Tech, 2013**

Teaching Experience

- **Teaching Practicum, BMED 3400, *Introduction of Biomechanics*, advised by Prof. Lena Ting, Georgia Tech, 2014**